$Ca_V2.2$ Channels in Brain Development and Synaptic Plasticity

Kjara Sophia Pilch

Doctor of Philosophy

2022

Department of Neuroscience, Physiology and Pharmacology
Division of Biosciences
University College London
Gower Street
London WC1E 6BT

Declaration

I, Kjara Sophia Pilch confirm that the work presented in this thesis is my own. Where information has been derived from other sources, I confirm that this has been indicated in this thesis.

Kjara Sophia Pilch

Acknowledgements

I would first like to thank Annette Dolphin for letting me carry out this research project. I consider myself very lucky for the guidance and support I have received for the duration of this project. I will forever be grateful for this.

I would also like to thank all my wonderful colleagues from the Dolphin lab for their collaboration and for their friendship. A particular thank you to Dr Krishma Ramgoolam, who has become such a close friend and is the kind of scientist I aspire to be. Another special mention to Dr Shehrazade Dahimene, Dr Laurent Ferron, Dr Ivan Kadurin and Dr Manuela Nieto-Rostro. You have not only helped me with setting up experiments but have also become trusted friends.

Finally, a huge thank you to my family who has taught me to always be curious. Thank you for your unconditional support and for always being there for me!

Dolphin lab members (past and present) in no particular order:

Annette C Dolphin, Krishma Ramgoolam, Laurent Ferron, Ivan Kadurin, Shehrazade Dahimene, JF Otto Meyer, Wendy Pratt, Manuela Nieto-Rostro, Karen Page, Kanchan Chaggar, Stuart Martin.

Kjara S Pilch

Publications

1. **Pilch KS**, Ramgoolam KH, Dolphin AC. Involvement of CaV2.2 channels and α2δ-1 in hippocampal homeostatic synaptic plasticity. bioRxiv [Internet]. 2022.06.27.497782.

2. Dahimene S., Elsner L. von, Holling T., Mattas L. S., Pickard J., Lessel D., **Pilch KS**., Kadurin, I., Pratt, WS., Zhulin, IB., Dai, H., Hempel, M., Ruzhnikov, MRZ., Kutsche, K., Dolphin, AC. **(2022)** Biallelic CACNA2D1 loss-of-function variants cause early-onset developmental epileptic encephalopathy. Brain, awac081.

3. **Pilch KS***., Bertin E*., Deluc T*., Martinez A., Pougnet JT, Doudnikoff E, Allain AE, Bergmann P, Russeau M, Toulmé E, Bezard E, Koch-Nolte F, Séguéla P, Lévi S, Bontempi B, Georges F, Bertrand SS, Nicole O, Boué-Grabot E. **(2021)** Increased surface P2X4 receptor regulates anxiety and memory in P2X4 internalization-defective knock-in mice. Mol Psychiatry. 2021 Feb;26(2):629-644. PMID: 31911635. *co-first

4. Walker KT., Donora M., Thomas A., Phillips AJ., Ramgoolam K., **Pilch KS.**, Oberacker P., Jurkowski TP., Gosman RM., Fleiss A., Perkins A., MacKenzie N., Zuckerman M., Danovi D., Steiner H., & Meany T. **(2020)**. CONTAIN: An open-source shipping container laboratory optimised for automated COVID-19 diagnostics. BioRxiv, 2020.05.20.106625.

5. Ferron L., Novazzi CG., **Pilch KS**., Moreno C., Ramgoolam K., & Dolphin AC. **(2020)**. FMRP regulates presynaptic localization of neuronal voltage gated calcium channels. Neurobiol Dis. 2020 May; 138:104779. PMID: 31991246.

6. Wang S., Millward JM., Hanke-Vela L., Malla B., **Pilch K**., Gil-Infante A., Waiczies S., Mueller S., Boehm-Sturm P., Guo J., Sack I., & Infante-Duarte C. **(2020)**. MR Elastography-Based Assessment of Matrix Remodeling at Lesion Sites Associated With Clinical Severity in a Model of Multiple Sclerosis. Front Neurol. 2020 Jan 13; 10:1382. PMID: 31998225.

7. Gomez-Sanchez JA., **Pilch KS**., Van Der Lans M., Fazal SV., Benito C., Wagstaff LJ., Mirsky R., & Jessen KR. **(2017)**. After nerve injury, lineage tracing shows that myelin and Remak Schwann cells elongate extensively and branch to form repair Schwann cells, which shorten radically on remyelination. J Neurosci. 2017 Sep 13;37(37):9086-9099. PMID: 28904214.

8. **Pilch KS**., Spaeth PJ., Yuki N., & Wakerley BR. **(2017)**. Therapeutic complement inhibition: a promising approach for treatment of neuroimmunological diseases. Expert Rev Neurother. 2017 Jun;17(6):579-591. PMID: 28092989.

Abstract

In the mammalian brain, presynaptic $Ca_V2.2$ channels play a pivotal role for synaptic transmission by mediating fast neurotransmitter exocytosis via influx of Ca^{2+} into the active zone at the presynaptic terminal. The distribution and activity of $Ca_V2.2$ channels at different synapses and maturity stages in the brain remains to be elucidated. In this study, I first show high levels of $Ca_V2.2$ channels in mouse cortex and hippocampus throughout development, persisting into adulthood. In contrast, $Ca_V2.2$ channels in the cerebellum and brain stem decreased as the brain matured. I thereafter assessed $Ca_V2.2$ channels during homeostatic synaptic plasticity, a compensatory form of homeostatic control preventing excessive or insufficient neuronal activity during which extensive active zone remodelling has been described. In this work I show that chronic silencing of neuronal activity in mature hippocampal cultures resulted in elevated presynaptic Ca^{2+} transients, mediated by a 30 % increase in $Ca_V2.2$ channel levels at the presynapse. Next, this work focussed on $\alpha_2\delta$-1 subunits, important regulators of synaptic transmission and $Ca_V2.2$ channel abundance at the presynaptic membrane. Here, I show that $\alpha_2\delta$-1-overexpression reduces the contribution of $Ca_V2.2$ channels to total Ca^{2+} flux without altering the amplitude of the Ca^{2+} transients. Finally, levels of endogenous $\alpha_2\delta$-1 decreased during homeostatic synaptic plasticity, whereas the overexpression of $\alpha_2\delta$-1 prevented homeostatic synaptic plasticity in hippocampal neurons. Together, this study reveals a key role for $Ca_V2.2$ channels and novel roles for $\alpha_2\delta$-1 during plastic synaptic adaptation.

Impact statement

Since the discovery of $Ca_V2.2$ channels in the 1980s, numerous studies have examined their biophysical properties. However, due to the lack of antibodies targeting extracellular epitopes of $Ca_V2.2$, many questions regarding their distribution at different synapses in the brain remain unanswered. In this work, I present a novel $Ca_V2.2\_HA^{KI/KI}$ mouse model which will be a useful tool for studying endogenous $Ca_V2.2$ channels at the plasma membrane. In hippocampal neurons from this mouse I show the endogenous distribution of $Ca_V2.2$ channels for the first time. I also show that during a developmental switch period in the neonatal brain, $Ca_V2.2$ channel levels decrease in the brain stem and cerebellum but remain elevated in the cortex and hippocampus. This has been a matter of debate with contradicting results published previously. Results presented here also provide the first evidence of an involvement of $Ca_V2.2$ channels and its auxiliary subunit $\alpha_2\delta$-1 in homeostatic synaptic plasticity after chronic network silencing in mature hippocampal neurons. These findings are a crucial step towards an improved understanding of presynaptic function in different brain areas, at different ages and different synaptic activity levels. This work therefore uncovers novel ways of presynaptic homeostatic adaptations which might eventually contribute to translational approaches for the treatment of synaptic dysfunction. Indeed, $Ca_V2.2$ channels are potential therapeutic targets as their aberrant function might be involved in neuropathic pain and in fragile X syndrome and analgesic drugs inhibiting $\alpha_2\delta$-1 subunits are already used clinically for pain treatment.

Table of Contents

List of Figures

List of tables

Abbreviations

AF	Alexa Fluor
AMPA	α-amino-3-hydroxy-5-methyl-4-isoxazolepropionic acid
ANOVA	Analysis of variance
AP	Action potential
AP-1	Activator protein-1
AP5	DL-2-amino-5-phosphonovaleric acid
Bs	Brain stem
BSA	Bovine serum albumin
CA	Cornu ammonis
CaM	Calmodulin
Ca_V	Voltage-gated Ca^{2+} channels
Cb	Cerebellum
CCK	Cholecystokinin
CDI	Ca^{2+} dependant inactivation
Cdk5	Cyclin-dependent kinase 5
cDNA	Complementary DNA
CNQX	6-cyano-7-nitroquinoxaline-2,3-dione
CNS	Central nervous system
ConTx	ω-conotoxin GVIA
cpGFP	circularly permuted GFP
CRMP	Collapsin response mediator protein
C_T	Cycle threshold
Cx	Cortex
DAPI	4,6-diamidino-2- phenylindole
DG	Dentate gyrus
DHP	Dihydropyridine
DIV	Days *in vitro*
DMEM	Dulbecco's Modified Eagle Medium
DNA	Deoxyribonucleic acid
DRG	Dorsal root ganglion
EC	Extracellular
ER	Endoplasmic reticulum
EV	Empty vector
FBS	Fetal bovine serum

Fig.	Figure
FMRP	Fragile mental retardation protein
FXS	Fragile X syndrome
GABA	Gamma aminobutyric acid
GAPDH	Glyceraldehyde 3-phosphate dehydrogenase
GFP	Green fluorescent protein
GK	Guanylate kinase
GPCR	G-protein coupled receptor
GPI	Glycosylphosphatidylinositol
GS	Goat serum
HA	Haemagglutinin
HBSS	Hank's Balanced Salt Solution
Hc	Hippocampus
Hprt1	Hypoxanthine-phosphoribosyl transferase 1
Hr	Hours
HR	Homologous recombination
HRP	Horseradish peroxidase
HSP	Homeostatic plasticity
HVA	High-voltage activated
IC	Intracellular
K_V	voltage-gated K^+ channels
LTD	Long-term depression
LTP	Long-term potentiation
LVA	Low-voltage-activated
MAP2	microtubule-associated protein 2
MEM	Minimum Essential Medium
MIDAS	Metal ion-dependent adhesion site
Min	Minutes
mRNA	Messenger RNA
Na_V	Voltage-gated Na^+ channels
NMDA	N-methyl-D-aspartate
N-type	Neuronal type
P	Postnatal
PBS	Phosphate buffered saline
PCR	Polymerase chain reaction
PDZ	PSD-95-DLG-ZO-1

PFA	Paraformaldehyde
PKC	Protein kinase C
PNS	Peripheral nervous system
PV	Parvalbumin
PVDF	Polyvinylidene difluoride
RBP	RIM binding protein
RIM	Rab3A-interacting molecule
RNA	Ribonucleic acid
ROI	Region of interest
RT	Room temperature
SC	Schaffer collateral
SDS-PAGE	Sodium dodecyl sulfate polyacrylamide gel electrophoresis
SEM	Standard error of the mean
SH3	Src homology 3
SM	Sec1/Munc-18 like protein
SNAP	Synaptosomal-Associated Protein
SNARE	Soluble NSF attachment receptor proteins
Sy-GCaMP6f	Synaptophysin-green fluorescent protein-calmodulin protein
Synprint	Synaptic protein interaction
TTX	Tetrodotoxin
VAMP-mOr2	Vesicle-associated membrane protein mOrange2
VD	Voltage-dependent
VDI	Voltage-dependent inhibition
vGAT	Vesicular GABA transporter
VGCC	Voltage-gated calcium channel
vGluT	vesicular Glutamate transporter
VSD	Voltage-sensing domain
VWA	Von-Willebrand-A
WT	Wild type

Chapter 1. Introduction

1.1 Biological membrane organisation and cellular signalling

Communication between cells and their environment is vital for the functioning of organs and organisms. The basis for this is the highly organised and specialised plasma membrane. Surrounding every living cell, the plasma membrane functions as a barrier between intra- and extracellular compartments and as a gate for the selective uptake and secretion of molecules and ions via embedded transmembrane proteins.

1.1.1. The plasma membrane

The plasma membrane is a 6-12 nm thick, lipid bilayer mainly composed of phospholipids. Amphipathic phospholipids are specifically arranged to form an inner hydrophobic region, with hydrophilic heads pointing towards the outside of the bilayer. Glycolipids can be found embedded and attached to the membrane along with integral and peripheral proteins. One of the key features of the plasma membrane is their semi-permeability, which allows certain molecules to pass through by diffusion, whilst most molecules require specialised facilitated transport. This provides a mechanism by which cells keep their intracellular content separated from the extracellular environment and permits specific signalling via transmembrane proteins, such as ion channels, transporters and receptors.

1.1.2. Ions and their distribution

The differential distribution of ions inside and outside of cells generates the membrane potential which provides the basis for cellular signalling. The principal ions involved are potassium (K^+), sodium (Na^+), chloride (Cl^-) and calcium (Ca^{2+}), where each ion has a different equilibrium potential (E_{ion}) at which no net ions move across the membrane (Table 1.1). The equilibrium potentials determine the resting membrane potential, calculated with the Goldman-Hodgkin-Katz equation (Goldman 1943; Hodgkin and Keynes 1955) taking into consideration the cell membrane potential, temperature and the charge of the ions.

	[Extracellular] (mM)	[Intracellular] (mM)	E_{ion} at 37°C (mV)
K^+	5	100	-80
Na^+	150	15	62
Cl^-	150	13	-65
Ca^{2+}	2	< 0.0002	123

Table 1. 1. Ion concentration inside and outside of excitable cells (here: neurons).

Electrochemical gradients of ions are the basis for signal transmission. The equilibrium potential (E_{ion}) is the potential at which there is no net flux of ions from one side to the other and is calculated using the Nernst equation (Bear *et al.* 2007).

When an ion is not at its electrochemical equilibrium, an electrochemical driving force would cause the ion to move according to its electrochemical gradient. At rest, the plasma membrane is most permeable for K^+ which are actively concentrated inside the cell, largely determining the intracellular resting potential (approximately -70 mV in neurons). In contrast, Na^+, Cl^- and Ca^{2+} are actively extruded to maintain low intracellular concentrations.

1.1.3. Ion channels and ion pumps

The transmission of signals in the nervous system relies on ions moving along their electrochemical gradients trying to reach their equilibrium potential. For this, ion channels inserted into the plasma membrane allow ionic movement from one side to the other. The resting membrane potential is principally determined by a constant passive efflux of K^+ through abundantly distributed resting K^+ channels. Na^+/K^+-ATPase pumps are important for the maintenance of the resting potential (Brodie *et al.* 1987). These pumps are electrogenic and use adenosine triphosphate to actively transport two K^+ into the cell and extrude three Na^+ from the cell. Broadly, there are three main groups of ion channels which are gap junctions, voltage-gated- and ligand-gated ion channels.

1.1.4. The action potential

In excitable cells, such as neurons, action potentials (APs) are changes in the membrane potential through which information is propagated in the nervous system. First described by Hodgkin and Huxley in the giant squid axon, these membrane changes are mediated by increased inward Na^+ and outward K^+ conductance (Hodgkin and Huxley 1945; Hodgkin and Huxley 1952a; Hodgkin and Huxley 1952b; Hodgkin and Huxley 1952c). Later, the importance of coordinated activity of ion channels was determined with tetrodotoxin (TTX), a voltage-gated Na^+ channels (Na_V) blocker. While TTX application suppressed Na^+ conductance and blocked APs, the resting potential and K^+ flux were not affected (Narahashi *et al.* 1964).

As determined by Hodgkin and Huxley (Hodgkin and Huxley 1952d), a neuronal AP sequence consists of a cycle of membrane depolarization, hyperpolarization and repolarisation lasting 1-2 milliseconds (ms) (Fig. 1.1).

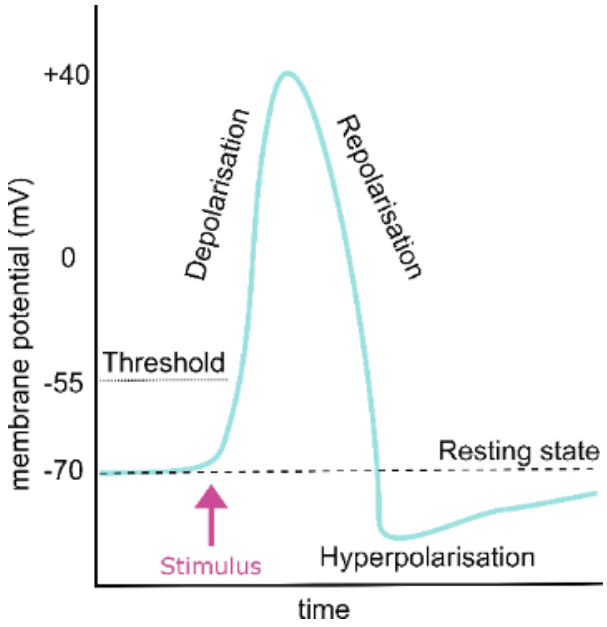

Figure 1. 1. AP curve in a neuron with a resting potential of -70 mV. When a stimulus depolarizes the membrane to a certain threshold (here -55 mV) the membrane depolarizes until it reaches a peak. The membrane then repolarizes to negative potentials and is hyperpolarized briefly. During this phase (refractory period), no new AP can be elicited.

The changes in membrane potential result from increases in the permeability of a region of the membrane to different ions, mainly Na^+ and K^+. Upon stimulation, Na_V channels open and Na^+ influx into the cell reduces the resting potential of the plasma membrane. If the stimulus is sufficient to depolarise the membrane to the threshold voltage of ~-55 mV, an AP is generated. More Na_V channels open and further Na^+ enters the cell until the membrane potential reaches approximately 40 mV. During this depolarization peak, Na_V channels inactivate themselves and voltage-gated K^+ channels (K_V) open, allowing K^+ to diffuse into the extracellular space following their concentration gradient and their equilibrium potential of -90 mV. This phase is called the repolarisation phase. For a brief period, the membrane potential reaches values more negative than the resting potential which is referred to as the hyperpolarisation phase during which no new AP can be generated. This is due to inactivated Na_V channels and opened K_V channels. As K^+ channels close, the resting membrane potential is locally re-established by the activity of the Na^+/K^+-ATPase pump. As each AP follows an *all-or-none* principle, the strength of the stimulus is encoded in the frequency of incoming APs. The local depolarisation during an AP spreads passively triggering Na_V channels to open and more APs to be elicited.

1.1.5. Neurons

Neurons are the main signalling units of the central nervous system (CNS: brain and spinal cord) and the peripheral nervous system (PNS: sensory and motor neurons outside the CNS). Neurons are polarised and highly specialised cells that generate APs to transmit information throughout the body. Most neurons have three functional domains: a cell body, dendrites and an axon (Fig. 1.2). The cell body (soma) is the main metabolic centre of the neuron which orchestrates the biosynthesis and trafficking of proteins into the various processes that extend from the soma. Dendrites extend from the cell body and allow a neuron to receive and process incoming information (input stimuli).

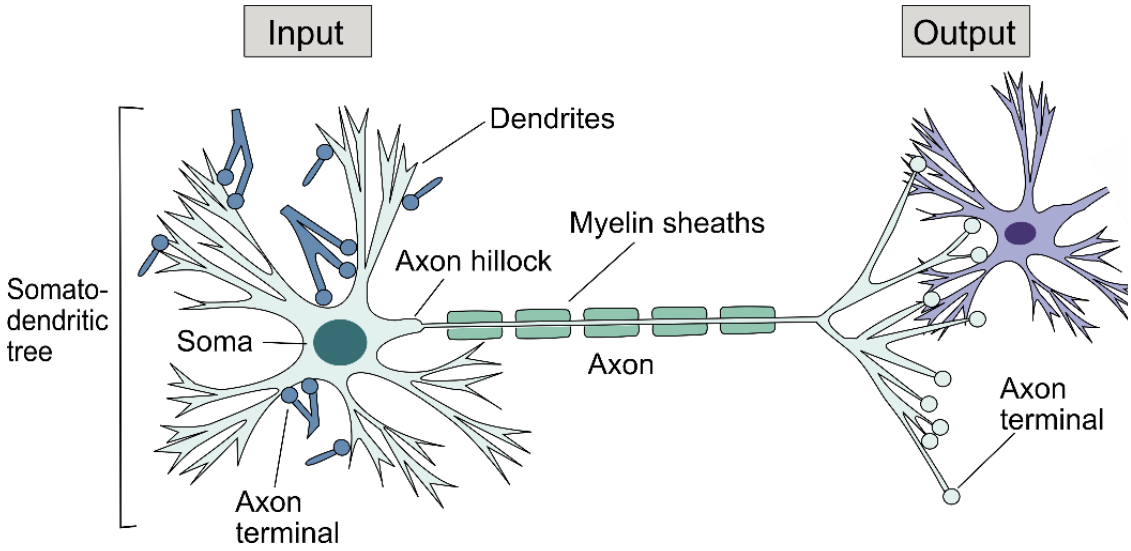

Figure 1. 2. Myelinated multipolar neuron of the CNS.
Information is received at the somatodendritic tree (input), integrated at the axon hillock and sent down the axon to the axon terminals (output; adapted from (Hammond 2015).

The sum of excitatory and inhibitory inputs, increasing or decreasing the likelihood of a postsynaptic AP, is integrated at the initial segment of the axon (axon hillock). Once the threshold is reached, APs are generated and propagate down the axon. The axon may either split up into terminal axonal boutons or boutons *en-passant* are formed along the axon. Both types of axon terminals synapse onto postsynaptic dendrites, somata or other axons.

Contrary to dendrites, axons are usually uniform in diameter. Some axons are ensheathed by myelin, allowing for rapid saltatory conduction of signals along the nodes of Ranvier. An immense variety of neuronal morphology depending on their function and location within the nervous system has been described. Neurons can be classified based on the number of axons and dendrites (unipolar, bipolar, multipolar), the shape of their dendritic tree (stellate, pyramidal), connections (motor, sensory), axon length (projection, local circuit neurons) or based on the neurotransmitters they release (excitatory or inhibitory). Notably, every aspect of neuronal function is supported by glial cells such as oligodendrocytes, astrocytes, microglia, ependymal-, Schwann-, and satellite cells.

1.1.6. Chemical synaptic transmission is quantal

In the brain, approximately 100 trillion synapses connect neurons, forming a vast and complex network. Synapses are close connections between neurons where signals are transmitted from the presynaptic region to the postsynaptic region of the target neuron or other effector cells like muscular and glandular cells. In the mammalian brain, the majority of fast interneuronal communication is via chemical synapses (Fig. 1.3). Other mechanisms of neuronal communication include electrical gap junctions and autocrine, paracrine and long-range signalling involving numerous molecules.

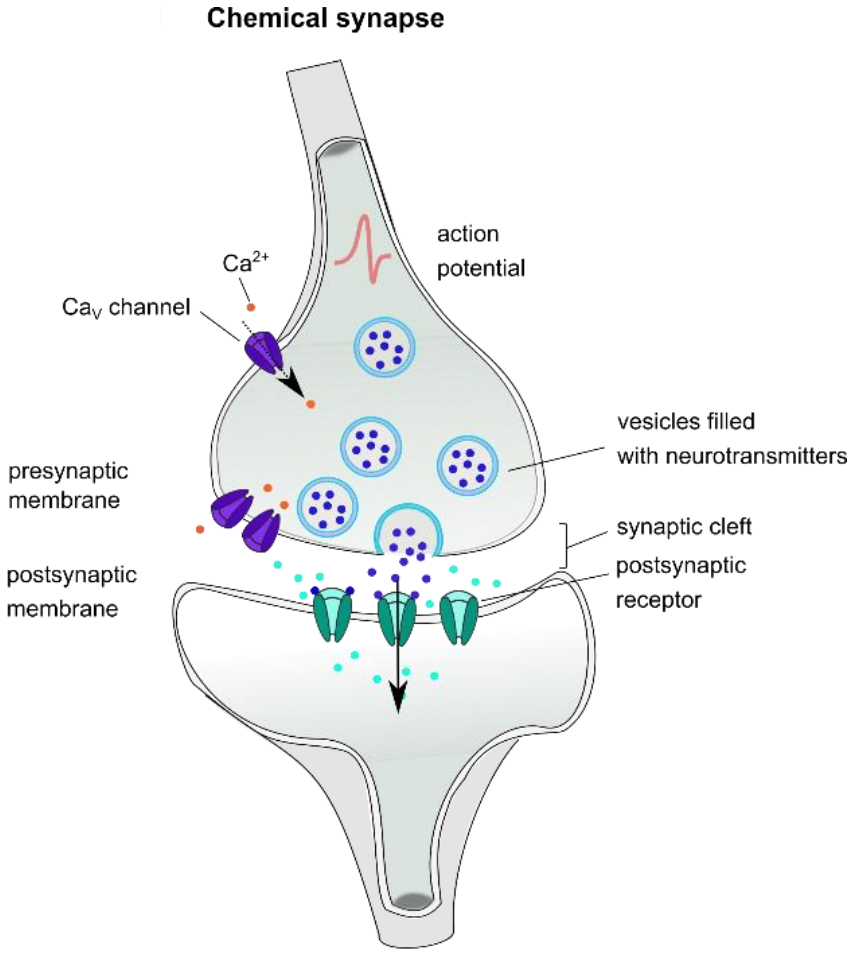

Figure 1. 3. Chemical synaptic transmission.
The chemical presynapse releases neurotransmitters in quanta from synaptic vesicles that bind and open specific postsynaptic receptors. Upon opening, these enable an influx of ions into the postsynapse and thereby the transmission of the signal.

Chemical synapses are characterized by the presence of a synaptic cleft between a highly specialised presynaptic membrane, containing mitochondria and synaptic vesicles that store neurotransmitters, and a precisely aligned postsynaptic membrane.

In general, neurotransmitters are released in quanta (one quantum referring to the content of one synaptic vesicle) with three main modes of exocytosis. Neurotransmitters can be released (i) spontaneously and random in the absence of a stimulus, usually triggering miniature postsynaptic potentials (Fatt and Katz 1952). AP-dependent release is either (ii) synchronous (milliseconds after an AP invaded the presynaptic terminal) or (iii) asynchronous (depending on the stimulation, can last tens of milliseconds to several seconds). During synchronous release, an AP briefly synchronises the opening of presynaptic voltage-gated Ca^{2+} (Ca_V) channels and the subsequent Ca^{2+} influx increases the rate of synaptic vesicle exocytosis allowing the secretion of an integral multiple of a quanta instantaneously (del Castillo and Katz 1954). Released neurotransmitters bind to specific receptors anchored in the postsynaptic density of the postsynaptic membrane, which can result in an influx of ions into the postsynaptic neuron which generates excitatory or inhibitory postsynaptic currents. Afterwards, neurotransmitters are quickly degraded or recycled back into the presynaptic terminal. Initially, chemical synapses were classified as excitatory or inhibitory, based on the basis of neurotransmitter stored in the presynapse. However, in recent years it has become clear that synapses exhibit more complex functional and molecular diversity (O'Rourke *et al.* 2012). A single presynaptic terminal may use a combination of spontaneous, synchronous and asynchronous neurotransmitter release while others may rely on one type exclusively. This provides a means for modulation of different synaptic inputs, for example during synaptic plasticity.

1.1.7. Neurotransmitter release at central synapses

Most transmission at central synapses relies on the opening of Ca_V channels in the presynaptic terminal in response to an AP, which results in a highly localised Ca^{2+} influx.

Synaptic vesicles docked at the presynaptic active zone fuse with the plasma membrane to release quanta of neurotransmitters into the synaptic cleft. This multistep process is mediated by a cycle of assembly and disassembly of SNARE (soluble NSF attachment receptor proteins) and SM (Sec1/Munc-18-like) proteins (Hata *et al.* 1993).

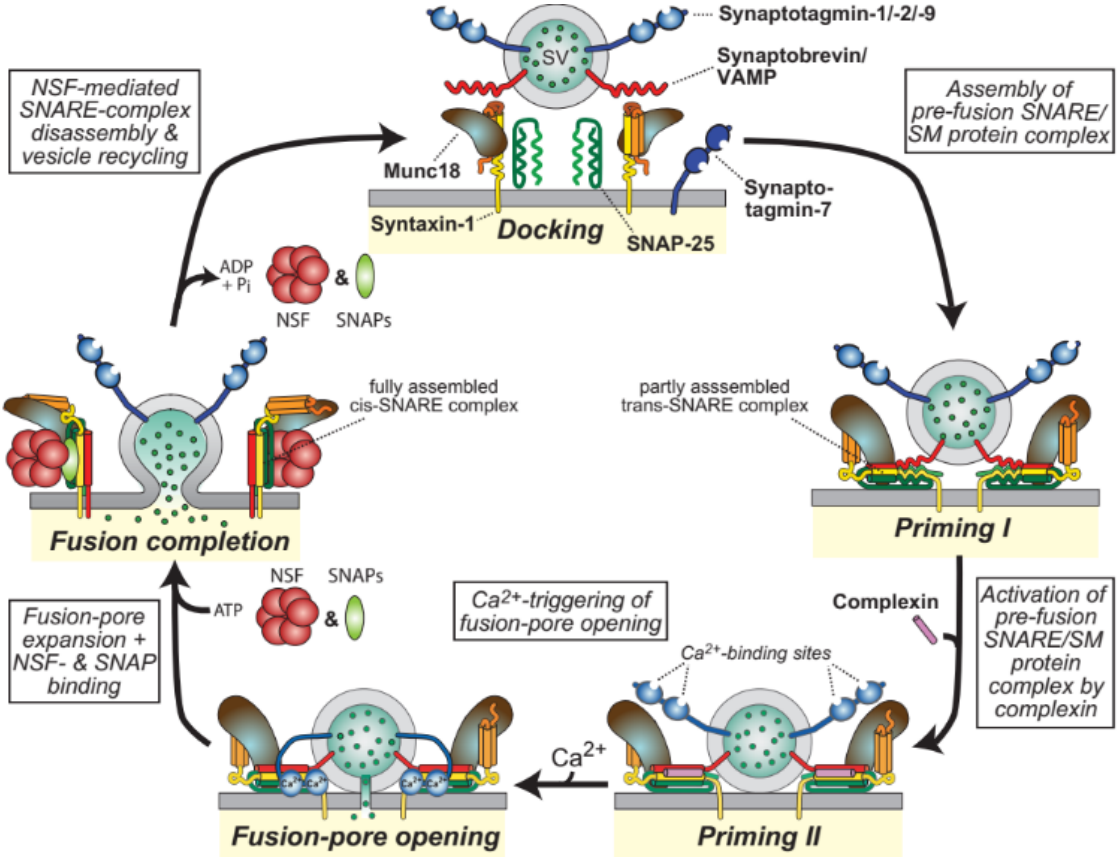

Figure 1. 4. Multistep process of fast neurotransmitter release.
Prior to neurotransmitter release, SNARE proteins VAMP, SNAP-25 and syntaxin assemble to form the SNARE/SM protein complex. Superprimed by complexin, Ca^{2+} influx into the active zone via Ca_V channels initiates the fusion of the synaptic vesicle membrane with the plasma membrane and the release of neurotransmitters. This is followed by the disassembly of the SNARE-complex and vesicle recycling (Südhof 2013).

For fast neurotransmitter release, a subpopulation of synaptic vesicles is docked at the active zone close to the release site via vesicular protein synaptobrevin (or vesicle-associated membrane protein (VAMP)) interacting with SNAP-25 (synaptosomal-associated protein 25) and syntaxin on the plasma membrane (Söllner *et al.* 1993).

Prior to vesicle exocytosis, cytoplasmic domains of synaptobrevin, SNAP-25 and syntaxin assemble into a helix bundle (*trans*-SNARE complex) tethering the vesicle to the plasma membrane.

SV fusion is regulated by two proteins: Ca^{2+} sensor synaptotagmin, located on the SV surface, and complexin, a cytoplasmic protein regulating SNARE assembly (Südhof 2013). Recent work revealed the crystal structure of the primed SNARE complex prior to neurotransmitter exocytosis (Zhou *et al.* 2017). This work suggests two interfaces of synaptotagmin. A primary interface between synaptotagmin and SNAREs tethering SV to the plasma membrane required for fast neurotransmitter release, and a tripartite interface between synaptotagmin, SNARE proteins and complexin. This tripartite complex is thought to present a pre-fusion state in which SV are prevented to fuse with the membrane in the absence of Ca^{2+} (Brunger *et al.* 2019). When an AP depolarises the membrane of the presynaptic terminal, highly localised, rapid influx of Ca^{2+} ions through Ca_V2 channels creates a local Ca^{2+} elevation. The close proximity of synaptotagmin to presynaptic Ca_V2 channels allows sub millisecond SV release. Ca^{2+} binding to synaptotagmin in the tripartite complex results in conformational changes, release of complexin and progressive zipping of the helical SNARE complex. This brings the fusing membranes into close proximity resulting in a destabilisation of their hydrophilic surfaces and of full merging of the plasma membrane with the synaptic vesicle (Hanson *et al.* 1997). The expansion of the pore converts the initial *trans*-SNARE complex into *cis*-SNARE complex that is dissociated by the ATPase NSF and components of the release complex are recycled for the next neurotransmitter release event (Söllner *et al.* 1993).

1.1.8. Organisation of the active zone

At the presynapse, fast synchronous neurotransmitter release requires the close proximity of Ca_V channels and primed synaptic vesicles at the active zone. Three distinct pools of synaptic vesicles have been described, (i) the readily releasable pool (RRP), available immediately during stimulation and rapidly depleted during high frequency

stimulation, (ii) the recycling pool, which maintains release during moderate stimulation and (iii) the reserve pool which contains the majority of vesicles and constitutes a depot of vesicles. At the active zone, the docking and priming of synaptic vesicles and the recruiting and tethering of Ca_V channel clusters are mediated by a protein complex whose central components consist of three multidomain proteins called RIM (Rab3-interacting protein), RIM-BP (Rim-binding protein) and Munc-13. RIM docks synaptic vesicles by binding Ras-related protein Rab3 and Rab27 GTP-binding proteins on the synaptic vesicle membrane. This brings them in close proximity to Ca_V channels, which RIM binds via its PSD-95-DLG-ZO-1 (PDZ) domain, and indirectly via RIM-BP (Kaeser *et al.* 2011). Munc-13 contributes to Ca_V channel tethering by binding RIM and the SNARE fusion machinery, acting as a linker that brings Ca_V channel clusters and primed synaptic vesicles together. Other scaffolding proteins at the active zone include α-liprins, and ELK proteins.

1.2. Ca_V channels

Ca_V channels mediate many key functions in the body. They are multiprotein channels that are found in the plasma membrane of all excitable cells including neurons. In response to changes in the membrane potential, Ca_V channels activate and allow the influx of Ca^{2+} into the cell. Entrant Ca^{2+} initiates a multitude of cellular events such as synaptic vesicle release, muscle contraction and regulation of gene expression. Ca_V channels are a complex group of hetero-oligomeric ion channels containing ten different subtypes, each with distinct pharmacological properties and distribution (Dolphin 2016). The pore-forming α_1 subunit, encoded by the *CACNA1x* genes, is the major determinant of channel function (Westenbroek *et al.* 1992) and can be classified into three families: Ca_V1, Ca_V2 and Ca_V3 channels (Fig. 1.5).

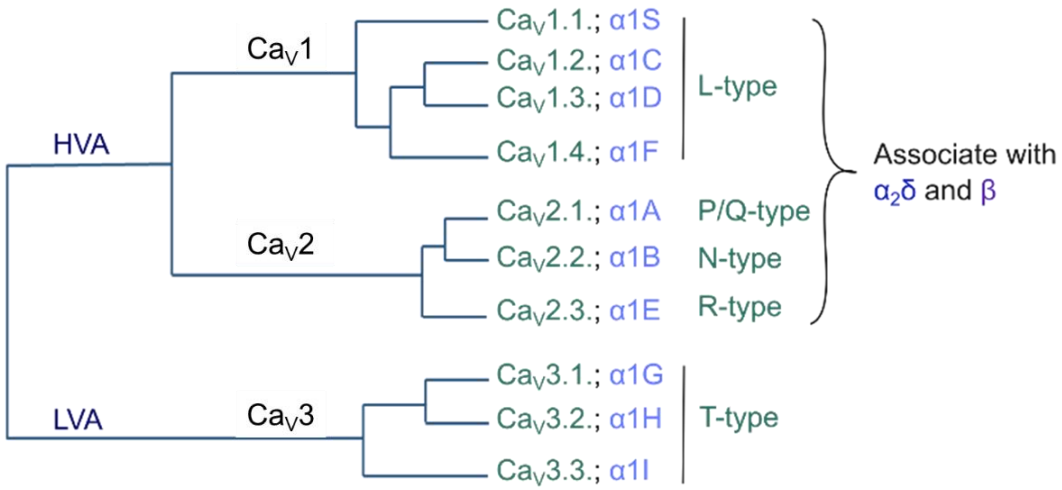

Figure 1. 5. Classification of Ca_V channel types.

Traditionally, Ca_V subtypes have been classified into high-voltage activated (HVA; Ca_V1 and Ca_V2) and low-voltage activated (LVA; Ca_V3), though it is now accepted that there is a continuum of activation thresholds.

Channel diversity is further increased by auxiliary subunits $\alpha_2\delta$ and β that associate with Ca_V1 and Ca_V2 channels to modulate their function. Moreover, all subunits can be alternatively spliced, providing further functional diversity. General roles of Ca_V channels include excitation-contraction coupling, excitation-transcription-coupling, and secretion processes (Catterall 2011).

1.2.1. Distribution and physiological function of Ca_V channels

The different members of the Ca_V channels family are widely distributed throughout the body and exert a myriad of functions summed up in Table 1.2.

Current type	Channel	Tissue distribution	Physiological function	Blockers
L	**$Ca_V1.1$**	Skeletal muscle	Excitation-contraction coupling; Ca^{2+} homeostasis; gene regulation	Dihydropyridine (DHP)
	$Ca_V1.2$	Cardiac and vascular smooth muscle, endocrine and neuronal cells	Excitation-contraction coupling; cardiac, smooth muscle contraction; neuronal excitability, synaptic plasticity, Ca^{2+} homeostasis, gene regulation	DHP, Verapamil (phenylalkylamine), Diltiazem (benzothiazepine)
	$Ca_V1.3$	Cardiac nodes, endocrine and neuronal cells, auditory hair cells	Pacemaking; hormone secretion; gene regulation; tonic neurotransmitter release	DHP
	$Ca_V1.4$	Retinal synapse	Neurotransmitter release; synapse formation at photoreceptors	DHP (low affinity)
P/Q	**$Ca_V2.1$**	CNS: presynaptic terminals, dendrites, soma, neuroendocrine cells, neuromuscular junction	Neurotransmitter release; dendritic Ca^{2+} transients	ω-agatoxin IVA
N	**$Ca_V2.2$**	CNS and PNS: presynaptic terminals, dendrites, soma, neuroendocrine cells	Neurotransmitter release; dendritic Ca^{2+} transients	ω-conotoxin GVIA; MVIIA
R	**$Ca_V2.3$**	CNS and PNS: presynaptic terminals, dendrites, soma	Neurotransmitter release	SNX-482
T	**$Ca_V3.1$**	Cardiac and skeletal muscle, neuronal soma, dendrites	Pacemaking; subthreshold oscillations	TTA-P2
	$Ca_V3.2$	Cardiac and smooth muscle, neuronal soma, dendrites, endocrine cells	Pacemaking; subthreshold oscillations	TTA-P2, Ni^{2+}
	$Ca_V3.3$	Neuronal soma, dendrites	Pacemaking; subthreshold oscillations	TTA-P2

Table 1. 2. Distribution and physiological function of the different Ca_V channels.

1.2.2. Topology of Ca_V channels

Ca_V channels are large heteromeric complexes consisting of various subunits (Fig. 1.6). α_1 is a large protein (175-225 kDa) that constitutes the main and the pore-forming subunit and determines the Ca^{2+} channel subtype. Ca_V1 and Ca_V2 channels co-assemble with auxiliary subunits β and $\alpha_2\delta$ and sometimes γ (Ca_V1 channels).

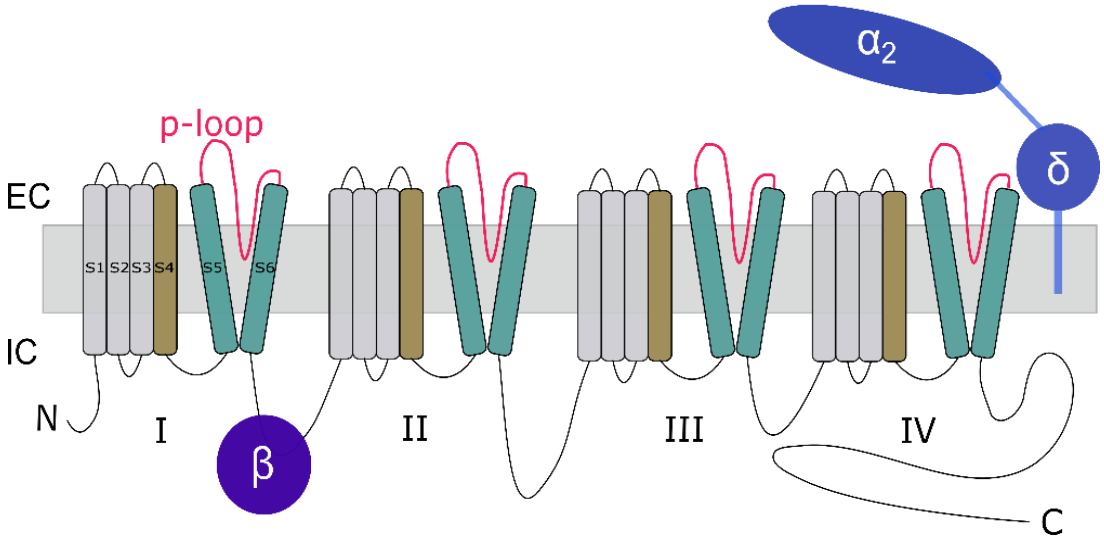

Figure 1. 6 Schematic of the different subunits of Ca_V channels.
The four domains of α_1 contain 6 transmembrane segments each (grey, ochre, blue cylinders) with S4 domains as voltage sensors (ochre) and S5 and S6 as pore forming domains (blue). Segments are connected by cytoplasmic loops and bracketed by an N-terminus and a large C-terminal domain. Ca_V1 and Ca_V2 channels are associated with auxiliary subunits β, binding the intracellular I-II linker of α_1, and auxiliary subunit $\alpha_2\delta$, largely extracellular and glycosylphosphatidylinositol (GPI)-anchored to the plasma membrane. EC = extracellular IC = intracellular.

α_1 consists of four homologous repeated domains (I-IV), each of which contains six transmembrane segments (S1-S6) and a large cytoplasmic C-terminal domain. The S1-S4 unit of each domain comprises the voltage-sensing domain (VSD), with S4 being the voltage sensor, and S5-S6 comprises the connecting p-loop that forms the Ca^{2+}-selective pore.

1.2.3. Pore selectivity

Ca_V channels are highly selective for divalent cations such as Ca^{2+}, allowing rapid influx into cells at a rate of 10^6 ions/s. Notably, in the experimental context, barium and strontium can permeate Ca_V channels. The central pore conducting Ca^{2+} is formed in the centre of the four domains of the α_1 subunit with S5 and S6 lining the pore and the S5-S6 linker forming a re-entrant p-loop that contributes to the selectivity filter (Fig. 1.6). The molecular basis of the channel selectivity has been elucidated by analysis of its structural determinants (Wu *et al.* 2016). The p-loop lines the extracellular side of the channel and contains a set of four negatively charged glutamate residues, with one glutamate from each subunit, essential for the selective interaction with Ca^{2+} (Tang *et al.* 2014; Ellinor *et al.* 1995). The architecture of the pore suggests three consecutive binding sites for Ca^{2+} with different affinities, allowing unidirectional flow of hydrated Ca^{2+} through the channel in a stepwise process (Tang *et al.* 2014; Wu *et al.* 2016).

1.2.4. Voltage sensor

The voltage-sensor in each domain of α_1 consists of several positively charged amino acid residues (arginines or lysines) in S4. During resting states, these residues form pairs with negatively charged amino acid residues of neighbouring transmembrane segments. The electrostatic attraction to the negative intracellular potential keeps them locked in a *downstate*, sealing the pore. During depolarisation of the membrane, the electrostatic force is relieved and the S4 segments move outwards into an *activated up-state* as proposed by the *sliding helix* model (Catterall 2010). This conformational change exerts a pulling force on S5 which bends the S6 segment, forming an activation gate that opens the pore and allows the inward flux of Ca^{2+}.

1.2.5. Voltage- and Ca^{2+}-dependent inactivation of Ca_V channels

Ca_V channels undergo conformational changes in response to changes in membrane potential, such as channel opening during membrane depolarisation. This is followed by

channel closing and a short inactivation period. Two major mechanisms, voltage- and Ca^{2+}-dependent inactivation (VDI and CDI, respectively) provide quick feedback inhibition by inactivating Ca_V channels in response to prolonged depolarisation or increasing intracellular Ca^{2+} levels (Fig. 1.7).

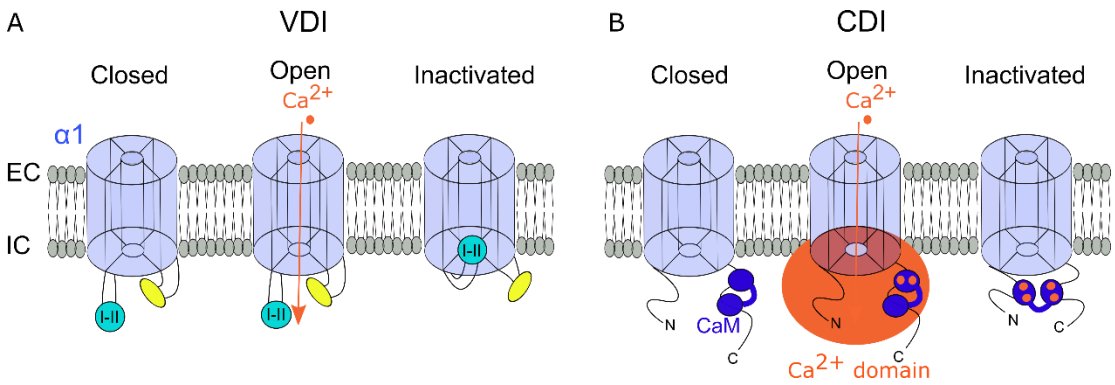

Figure 1. 7. Schematic of voltage- and Ca^{2+}-dependent inactivation.
(A) Upon prolonged membrane depolarisation the I-II linker occludes the pore preventing further Ca^{2+} influx **(B)** During CDI, increased levels of intracellular Ca^{2+} cause a conformational change in Calmodulin (CaM, dark blue) which in turn results in a movement of N- and C- termini, inactivating the channel (adapted from Simms & Zamponi, 2014) EC = extracellular IC = intracellular.

VDI of Ca_V channels is an important mechanism preventing excitotoxicity caused by intracellular accumulation of toxic Ca^{2+} levels (Fig. 1.7 A). Using a series of chimeric channels expressed in cell lines, a model for VDI has emerged in which the I-II linker region forms a hinged lid structure. In response to prolonged membrane depolarisation, S6 segments undergo conformational changes, exposing a docking site for the I-II linker, allowing channel occlusion (Stotz *et al.* 2000; Stotz *et al.* 2004).

CDI is triggered by increased levels of cytosolic Ca^{2+} and transduced via Calmodulin (CaM) (Fig. 1.7 B). During resting states, CaM is pre-associated with the C-terminal of certain subtypes of Ca_V channels (Liu *et al.* 2010). Ca^{2+}-binding to CaM upon channel opening causes a conformational change in the C-terminus/CaM-complex that inactivates the channel. Notably, CDI mechanisms differ between the different Ca_V

channel isoforms. In Ca_V1 channels, local rises in Ca^{2+} near the pore are sufficient to mediate CDI. In contrast, Ca_V2 channels are inactivated in a Ca^{2+}-dependent manner in response to global rises in intracellular Ca^{2+}, usually mediated by several Ca_V channels opening simultaneously (Dick *et al.* 2008). $Ca_V1.4$ and Ca_V3 channels lack CDI and are exclusively inactivated by VDI, in $Ca_V2.2$ there is very little CDI.

1.2.6. Auxiliary subunits

Ca_V1 and Ca_V2 channels co-assemble with at least two auxiliary subunits: cytoplasmic β and extracellular $\alpha_2\delta$ subunits. $Ca_V1.1$ channels in the vertebrate skeletal muscle additionally associate with a γ subunit.

1.2.6.1. Auxiliary subunit $\alpha_2\delta$

Auxiliary $\alpha_2\delta$ subunits are crucial for the function of Ca_V channels (Dolphin 2013). Of the four isoforms, $\alpha_2\delta$-1 is ubiquitously expressed, including in presynaptic terminals in the CNS and PNS, particularly of excitatory neurons (Klugbauer *et al.* 1999; Cole *et al.* 2005). $\alpha_2\delta$-2 expression is more restricted, but also found at the presynapse, predominantly of inhibitory neurons in the cerebellum (Barclay *et al.* 2001; Cole *et al.* 2005). $\alpha_2\delta$-3 is found throughout the brain with a strong presence in the caudate putamen, auditory system and retina (Cole *et al.* 2005). $\alpha_2\delta$-4 is exclusively distributed in endocrine tissues and the retina (Wycisk *et al.* 2006). All $\alpha_2\delta$ genes encode for a single precursor protein which is posttranslationally cleaved into α_2 and δ. α_2 is entirely extracellular but remains attached to δ via disulphide bonds with δ anchored to the plasma membrane via a C-terminal GPI anchor. The von-Willebrand-A (VWA) domain in $\alpha_2\delta$ contains a metal-ion-dependent adhesion site motif that was shown to be essential for trafficking of Ca_V channels (Cantí *et al.* 2005; Wu *et al.* 2016). Additionally, Cache domains, C-terminal to the VWA domain, have also been demonstrated to interact with the α_1 subunit of $Ca_V1.1$ (Wu *et al.* 2016) and $Ca_V2.2$ channels (Dahimene *et al.* 2018).

The roles of $\alpha_2\delta$ for Ca_V channel function are highly diverse and the precise mechanisms of interaction remain to be fully elucidated. It is clear however, that the presence of $\alpha_2\delta$ is essential for Ca_V channel function, as $\alpha_2\delta$ serves as a checkpoint for the trafficking and activation of Ca_V channels (Hoppa *et al.* 2012; Kadurin *et al.* 2016). $\alpha_2\delta$ subunits, together with β, also increase the number of Ca_V channels inserted into the plasma membrane (Cassidy *et al.* 2014). Moreover, in hippocampal mouse neurons it was shown that $\alpha_2\delta$-1 specifically facilitates Ca^{2+} transients through $Ca_V2.1$ channels via a specific interaction with neurexin1α, a presynaptic cell-adhesion molecule binding postsynaptic neuroligin-1 (Brockhaus *et al.* 2018).

$\alpha_2\delta$ is a multifunctional protein with accumulating evidence emerging for its role for neuronal functioning independent from Ca_V channels. This includes key functions in synaptogenesis and synaptic function in the adult. It has been shown that postsynaptic $\alpha_2\delta$-1 interacts with thrombospondin receptors mediating excitatory synaptogenesis (Eroglu *et al.* 2009). In the context of synaptic plasticity, $\alpha_2\delta$-1 was reported to enhance excitatory neurotransmission by direct interaction with glutamatergic N-methyl-D-aspartate (NMDA) receptors in the spinal cord (Chen *et al.* 2018) and during corticostriatal long-term potentiation (Zhou *et al.* 2018). Moreover, $\alpha_2\delta$-1 and $\alpha_2\delta$-2 contain binding sites for anti-epileptic and neuropathic pain drugs pregabalin and gabapentin (Field *et al.* 2006) and mutations have been implied in diseases including epilepsies, paroxysmal dyskinesia, night blindness, neuropsychiatric, cardiac and endocrine dysfunction (Ablinger *et al.* 2020).

1.2.6.2. Auxiliary subunit β

The β subunit is a 55 kDa cytoplasmic protein important for trafficking, biophysical and pharmacological properties of HVA Ca_V channels. Of the four mammalian isoforms, β1 associates with Ca_V channels in skeletal muscles cells (β1a) (Ruth *et al.* 1989), neurons (β1b) and cardiac cells. β2 and β3 are also found in cardiac and smooth muscle cells, whereas β4 is widely expressed in the brain. The β subunit belongs to the membrane-

associated guanylate kinase (GK) family consisting of Src-homology 3 and GK domains, the latter binding to the proximal cytoplasmic linker between domain I and II of α_1 (α-interaction domain) (Pragnell *et al.* 1994). The key function of β subunits is to increase the current density for HVA Ca_V channels (Dolphin 2003a; Dolphin 2012), largely mediated by increasing numbers of functional Ca_V channels inserted into the plasma membrane and by shifting the activation curve of channels to more hyperpolarized potentials thus increasing channel open probability. It was shown that β supports the functional expression of Ca_V channels by protecting them from proteasomal degradation thus enabling more channels to reach the plasma membrane (Waithe *et al.* 2011; Altier *et al.* 2011). Furthermore, simultaneous binding of Ca_Vβ and Ca^{2+} to the pore promotes correct folding and trafficking of α_1 to the plasma membrane (Liu *et al.* 2020; Meyer *et al.* 2019).

1.3. $Ca_V2.2$ channels

$Ca_V2.2$ channels, also termed neuronal (N)-type channels, are HVA channels that are expressed in combination with different isoforms of $Ca_V\beta$ and $Ca_V\alpha_2\delta$. Their currents are characterized by an intermediate activation at membrane potentials around -20 mV, peaking at approximately +10 mV in medium containing Ca^{2+} (Bleakman *et al.* 1995). A conductance hierarchy of $Ca_V1 > Ca_V2 > Ca_V3$ is assumed, determined in the presence of high barium concentrations. However, single-channel patch-clamp recordings with physiological extracellular Ca^{2+} concentrations, revealed $Ca_V2.2$ channels to carry the largest current (Weber *et al.* 2010). N-type currents were first described in sensory neurons of chick dorsal root ganglia (DRG) (Nowycky *et al.* 1985) by their insensitivity to inhibition by DHP. Now, $Ca_V2.2$ channels are distinguished from other channels by the use of selective inhibitors ω-conotoxin-GVIA (ConTx) and ω-conotoxin-MVIIA.

1.3.1. Expression and distribution of $Ca_V2.2$ channels in the brain

$Ca_V2.2$ channels are widely distributed throughout the PNS and CNS (Westenbroek *et al.* 1992). Somatic Ca^{2+} influx through $Ca_V2.2$ channels in central neurons for example, contributes to excitation-transcription coupling (Weber *et al.* 2010) and dendritic $Ca_V2.2$ channels regulate cellular excitability. The most important role of $Ca_V2.2$ channels in the brain is fast neurotransmitter release from the presynaptic terminal, where channels are in close association with the synaptic vesicle release machinery (Muller *et al.* 2010). This has been described for the release of most neurotransmitters including glutamate (Luebke *et al.* 1993), gamma aminobutyric acid (GABA) (Horne and Kemp 1991), acetylcholine (Wessler *et al.* 1990), dopamine (Herdon and Nahorski 1989; Turner *et al.* 1993; Woodward *et al.* 1988), serotonin (Foehring 1996) and noradrenaline (Dooley *et al.* 1988). In sympathetic (Murakami *et al.* 2001) and DRG neurons (Hirning *et al.* 1988), $Ca_V2.2$ channels were found to be the dominant Ca_V channels at the presynapse, where

they mediate the release of norepinephrine from sympathetic terminals and of glutamate during nociceptive transmission from DRG primary afferent terminals.

In the brain, $Ca_V2.2$ channels have been detected in most regions, with a uniform messenger ribonucleic acid (mRNA) expression in the murine cortex, hippocampus and cerebellum (Schlick *et al.* 2010). Further studies, mostly using selective toxins, electrophysiology or polymerase-chain-reaction (PCR), demonstrated the presence of $Ca_V2.2$ channels in neuronal cultures from the hippocampus (Nimmervoll *et al.* 2013), the cerebellum (Falk *et al.* 1999; Mintz *et al.* 1995) and in brain stem slices containing the Calyx of Held (Iwasaki and Takahashi 1998). However, the distribution of $Ca_V2.2$ channels in the brain is likely to be heterogeneous with most synaptic transmission mediated by the joint action of $Ca_V2.1$ and $Ca_V2.2$ channels, and $Ca_V2.3$ to a lesser extent, each with distinct properties (Takahashi and Momiyama 1993; Ariel *et al.* 2012; Wheeler *et al.* 1996). This enables the diversification and fine-tuning of synaptic signalling allowing dynamic adaptation to changing neuronal network activity, for example during synaptic plasticity.

The number and type of presynaptic Ca_V channels is an important determinant of vesicle release probability, however few generalities can be made regarding which subtype distribution is predominant in which synaptic context. Studies suggest the involvement of $\alpha_2\delta$ subunits for the trafficking and accumulation of both subtypes at the synapse (Hoppa *et al.* 2012). Overall, the Ca_V2 channel repertoire at central synapses varies substantially and the precise mechanisms governing the preference of one subtype or of a joint activity remain to be elucidated. Numerous studies have been performed aiming to dissect the different contributions of $Ca_V2.1$ and Ca_V 2.2 channels in different mammalian brain areas. The first studies were performed on the Calyx of Held, a large auditory relay synapse in the brain stem. Here it was shown that the synaptic transmission before hearing onset during development is mediated by loosely coupled $Ca_V2.1$ and $Ca_V2.2$ channels (microdomain coupling with a mean coupling

distance between Ca_V2 and release sensor of more than 40-50 nm), whereas the mature synapse exclusively relies on tightly coupled $Ca_V2.1$ channels (nanodomain coupling with a mean coupling distance of less than 40 nm) (Iwasaki and Takahashi 1998; Iwasaki *et al.* 2000; Fedchyshyn and Wang 2005; Bornschein *et al.* 2019). The nanodomain coupling of $Ca_V2.1$ channels allows rapid and temporally precise glutamate release, required for auditory processing. This developmental switch from $Ca_V2.2$ to $Ca_V2.1$ channels during synaptic maturation has been described in other brain areas as well (Miki *et al.* 2013; Scholz and Miller 1995).

In contrast, many central synapses rely on variable stimulus-response properties depending on synapse type. Synaptic transmission at highly plastic hippocampal synapses for example, is mediated by joint activities of $Ca_V2.1$ and $Ca_V2.2$ channels, with the distinct contribution of each type depending on the synapse and factors such as developmental stage and neuronal activity. At hippocampal mossy fibre boutons between *cornu ammonis* (CA) 3 and dentate gyrus (DG) neurons, $Ca_V2.1$ channels mediate most synaptic vesicle release during a low stimulation of 1 AP, with an increasing contribution of $Ca_V2.2$ and $Ca_V2.3$ channels upon stronger stimulation, proposing the expression of all three Ca_V2 channel types at these synapses (Li *et al.* 2007). In contrast, inhibitory synapses formed with DG neurons rely on either $Ca_V2.1$ or $Ca_V2.2$ channels for GABA release from parvalbumin (PV) or cholecystokinin (CCK) positive neurons, respectively (Goswami *et al.* 2012). Further evidence proposed the sole reliance of DG basket and granule cells on $Ca_V2.1$ channels for neurotransmitter exocytosis (Bucurenciu *et al.* 2010). There is no consensus yet, if a certain Ca_V2 channel subtype is preferred depending on excitatory or inhibitory neurotransmitters and if so, what implications this would have on synaptic function. Some findings indicate a preference of $Ca_V2.2$ channels for inhibitory signalling in the rat hippocampus (Potier *et al.* 1993). Together, this indicates a high variability and plasticity of the expression of the

two main presynaptic Ca_V2 channels, providing a way of terminal-specific modulation of synaptic function.

1.3.2. Trafficking of $Ca_V2.2$ channels

Trafficking of proteins to their subcellular location is a multi-step process. Briefly, after the transcription of DNA in the nucleus, mRNA is translated into proteins that are then modified and subsequently transported to their destination (Fig. 1.8). Transcription of DNA occurs in the nucleus. mRNA is then exported into the cytosol through nuclear pores where it associates with ribosomes that translate mRNA into proteins. Non-cytosolic proteins are translocated across the membranes of the endoplasmic reticulum (ER) where proteins are assembled, folded and post-translationally modified. After the ER, proteins are carried to the Golgi-complex in transport vesicles where they are further modified and finally transported to their subcellular localisation. For proteins of the presynaptic active zone, this involves anterograde transport in vesicles along microtubules with a kinesin motor.

Two main mechanisms regulate Ca^{2+} influx into the presynapse, the first is via regulation of the number of active Ca_V2 channels inserted into the membrane and the other is via regulation of channel activity. For both processes, auxiliary subunits β and $\alpha_2\delta$ are key players. The synthesis of α_1 occurs on ER-associated ribosomes. In the ER, α_1 associates with $Ca_V\beta$. Studies knocking down the β subunit show a significant reduction in the expression of HVA channels on the plasma membrane in DRG neurons (Berrow et al., 1995). Later, it was demonstrated that β prevents the polyubiquitination of $Ca_V2.2$ α_1 subunit thus protecting it from proteasomal degradation (Waithe *et al.* 2011). Mutagensis of the I-II linker of $Ca_V2.2$ channels abolished β-binding and thereby the protection of $Ca_V2.2$ channels from degradation.

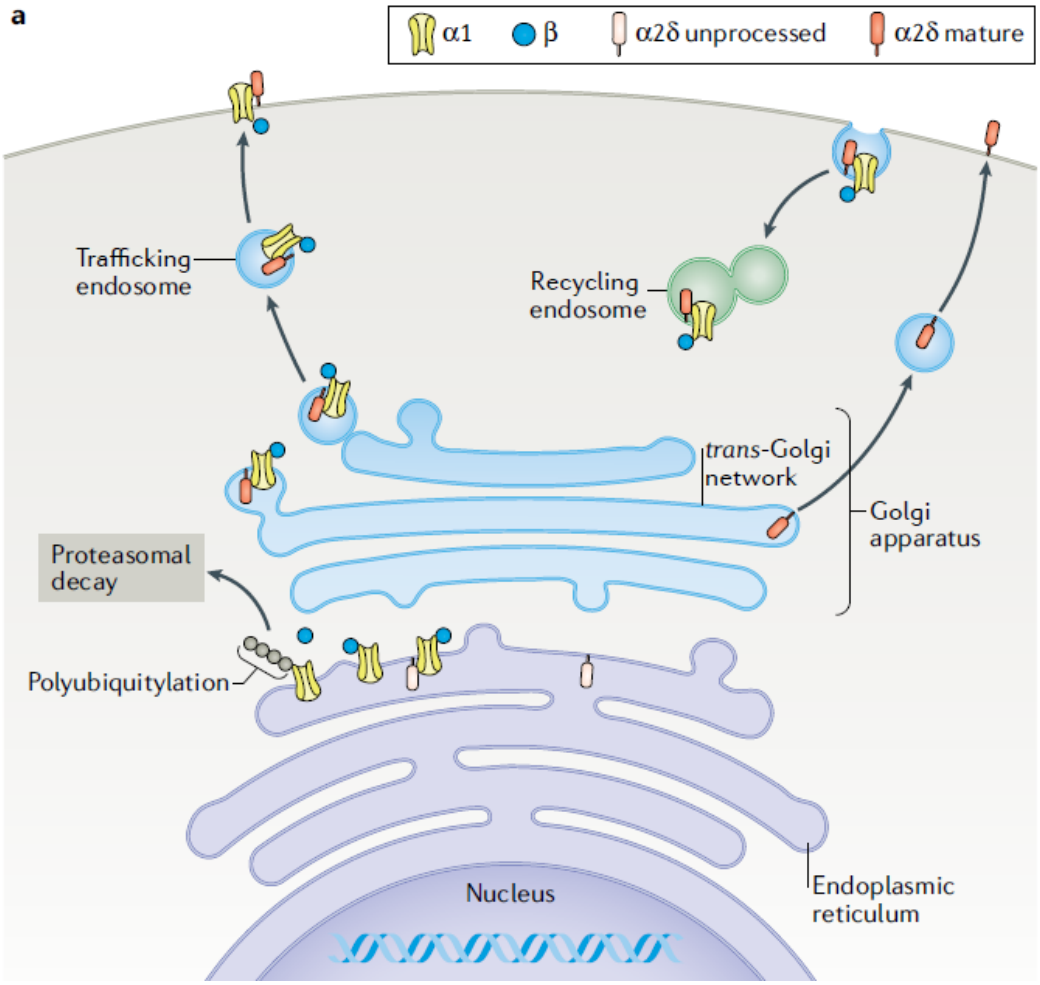

Figure 1. 8. Synthesis of Ca_V2 channels and trafficking to the presynaptic terminal.

Synthesis and assembly of Ca_V2 channels is a multistep process starting with the transcription in the nucleus and subsequent translation by ribosomes, which are associated with the ER in the case of membrane proteins. Channels are post-translationally modified and assembled as they progress through the ER and the trans-Golgi network. During this process, auxiliary subunits β and $\alpha_2\delta$ associate with α_1 to promote folding and trafficking of the Ca_V2 channel complex. Notably, $\alpha_2\delta$ can travel to the plasma membrane alone, whereas α_1 trafficking is strongly promoted by both β and $\alpha_2\delta$ (Dolphin and Lee 2020).

Recenty, it has also been shown that Ca^{2+} binding within the selectivity filter of the to α_1 pore promotes the correct folding of α_1 (Meyer *et al.* 2019). Besides β, $\alpha_2\delta$ plays a key role in promoting folding and assembly of α_1 in the ER and the Golgi. It was shown

that uncleaved $\alpha_2\delta$ does not promote Ca^{2+} influx through Ca_V2 channels, a mechanism that may prevent immature Ca_V2 channels from leaking Ca^{2+} from the ER into the cytosol (Kadurin *et al.* 2016). In the *trans*-Golgi network, Ca_V2 channels are packaged into trafficking endosomes for sorting to their destination. For optimal trafficking to the presynapse, Ca_V2 channels require the presence of $\alpha_2\delta$ (Nieto-Rostro *et al.* 2018; Ferron *et al.* 2018; Kadurin *et al.* 2016; Macabuag and Dolphin 2015). Proteolytic cleavage of $\alpha_2\delta$ in the Golgi exposes the adaptor protein (AP)-1 binding motif in the channel, enhancing the exit of Ca_V2 channels from the *trans*-Golgi into trafficking endosomes (Macabuag and Dolphin 2015). The importance of $\alpha_2\delta$ for Ca_V2 channel trafficking becomes clear when looking at the effect of gabapentin, shown to inhibit $Ca_V2.2$ forward trafficking (Hendrich *et al.* 2008). Notably, the total number of active Ca_V2 channels at the plasma membrane is not only determined by trafficked channels from the soma, but also by their turnover at the plasma membrane. Ca_V2 channels are subject to endocytosis and recycling (Tran-Van-Minh and Dolphin 2010; Macabuag and Dolphin 2015; Meyer and Dolphin 2021). Furthermore, different splicing variants of $Ca_V2.2$ channels as well as other interacting molecules alter the channels' predisposition to internalization (Raingo *et al.* 2007).

1.3.3. Alternative splicing of $Ca_V2.2$ channels

Each mammalian *Cacna1x* gene (encoding α_1) can potentially generate thousands of different Ca_V channels by alternative splicing. Controlled by cell-specific splicing factors, this process enables mRNA to direct the synthesis of different isoforms with distinct cellular functions and expression levels. The *Cacna1b* gene (encoding α_1B of $Ca_V2.2$ channels) has four cell-specific sites of alternative splicing, three cassette exons (18a, 24a and 31a), that are either spliced out or retained in the primary transcript, and a pair of mutually exclusive exons (37a/37b), as shown in Figure 1.9. Sites of alternative splicing are mainly located in intracellular C-termini and the II-III linker of $Ca_V2.2$ channels which impacts on the biophysical properties of $Ca_V2.2$ channels including the VD

activation and inactivation, channel kinetics, CDI and modulation by other proteins. Of special interest are the two mutually exclusive exons, e37a and e37b, encoding sequences in the C-terminus of $Ca_V2.2$ channels.

It was shown that 37a is mainly expressed in a subpopulation of DRG neurons, where channels regulate nociception and morphine-mediated analgesia (Bell *et al.* 2004; Andrade *et al.* 2010).

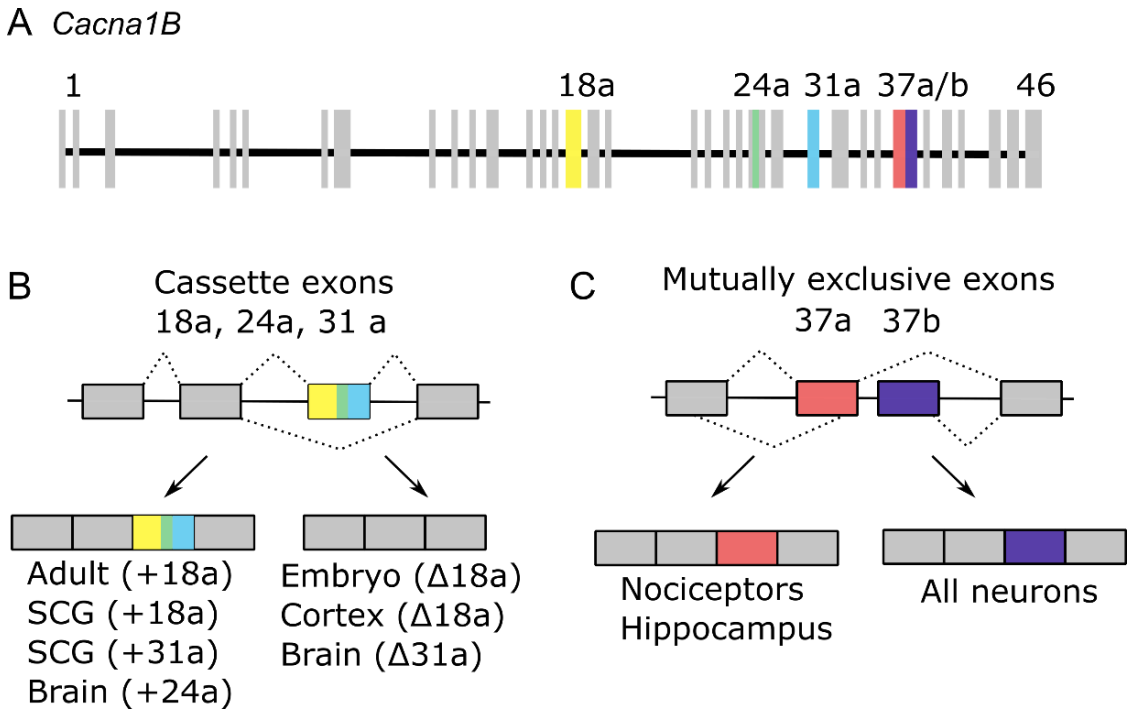

Figure 1. 9. Alternative splicing of *Cacna1b*.

(A) The four cell-specific sites of *Cacna1b* alternative splicing altering channel function are cassette exons 18a (yellow), 24a (green) and 31a (blue) and mutually exclusive 37a/37b (red and purple, respectively). **(B and C)** All splice variants show a specific tissue distribution depending on developmental stage and region within the nervous system. Adapted from (Lipscombe *et al.* 2013).

Recently, $Ca_V2.2e37a$ was also detected in excitatory projection neurons orchestrating neurotransmitter release in the entorhinal cortex-DG pathway (Bunda *et al.* 2019). Generally, compared to $Ca_V2.2e37b$, $Ca_V2.2.e37a$ channels exhibit a hyperpolarized shift in voltage-dependence, larger whole cell currents and a higher expression on the cell surface (Castiglioni *et al.* 2006; Bell *et al.* 2004; Macabuag and

Dolphin 2015). The latter is mediated by AP-1 binding to the C-terminus of $Ca_V2.2$e37a thereby increasing trafficking of the channel to the plasma membrane (Macabuag and Dolphin 2015). Moreover, the inclusion of e37a is required for optimal G-protein-mediated voltage-independent inhibition of $Ca_V2.2$ channels in sensory neurons (Raingo *et al.* 2007). Using splice isoform specific-small interfering RNA, it was also shown that only $Ca_V2.2$e37a-containing channels play a role for synaptic transmission of thermal nociception during normal signalling and during neuropathic pain, implying important therapeutic implications for isoform-specific $Ca_V2.2$ channel inhibition (Altier *et al.* 2007). In contrast, $Ca_V2.2$.e37b expression is abundant throughout the nervous system and is usually associated with smaller current densities and a lower susceptibility to G-protein inhibition (Bell *et al.* 2004; Castiglioni *et al.* 2006). Moreover, e37b is more prone to ubiquitination and subsequent degradation by the ubiquitin-proteasome system, reducing the number of $Ca_V2.2$e37b channels at the cell surface (Marangoudakis *et al.* 2012). Overall, alternative splicing of *Cacna1b* is another mechanism of fine-tuning neurotransmitter release by allowing cells to regulate the sensitivity of presynaptic $Ca_V2.2$ channels to G-protein mediated inhibition by adjusting the ratio of $Ca_V2.2$e37a to $Ca_V2.2$e37b (Lipscombe and Raingo 2007).

1.3.4. Organisation and function of $Ca_V2.2$ channels at the brain presynaptic terminal

Ca^{2+} influx through $Ca_V2.1$ and $Ca_V2.2$ channels coordinates synchronous neurotransmitter release at fast synapses in the CNS and PNS, therefore channels are concentrated at the active zone at presynaptic terminals. APs induce a depolarisation of the presynaptic membrane resulting in the opening of Ca_V2 channels and a highly localised fast influx of Ca^{2+} into the presynapse. This leads to conformational changes in the SNARE/SM complex and to neurotransmitter exocytosis (see also 1.1.7).

However, synapses are highly diverse regarding their activity and protein composition, which includes different distributions of $Ca_V2.1$ and $Ca_V2.2$ channels. It has

been shown that Ca^{2+} influx triggers synaptic fusion in less than 100 µs, enabled by the close proximity of Ca_V2 channels to docked and primed synaptic vesicles. To facilitate effective fast coupling between the synaptic vesicle release machinery and Ca^{2+} entry, Ca_V2 channels are arranged in micro- or nanodomains, tethered by presynaptic proteins (Eggermann *et al.* 2011; Bornschein *et al.* 2019) (Fig. 1.10). RIM, one key regulator of neurotransmitter release, directly binds to the C-terminal of $Ca_V2.2$ channels via its PDZ domain, recruiting and tethering $Ca_V2.2$ channels to the active zone in close proximity to docked vesicles (Han *et al.* 2011; Kaeser *et al.* 2011) (Fig. 1.10). RIM has also been shown to indirectly interact with $Ca_V2.2$ channels via RIM-BP, binding the C-terminal of Ca_V2. Recently the role of liquid-liquid phase separation, the formation of molecular assemblies within aqueous solutions, has emerged as a crucial mechanism of active zone organisation at the synapse (Chen *et al.* 2020). Using an *in vitro* reconstitution approach, it was shown that RIM and RIM-BPs drive this phase separation and, via binding the C-terminal of Ca_V2 channels, organise and cluster channels to the active zone in proximity to calcium sensors and synaptic vesicles (Wu *et al.* 2019). Their findings suggest that these RIM and RIM-BP clusters also mediate the Ca_V2 micro- and nanodomains. Additionally, both RIM and RIM-BP have been demonstrated to bind $Ca_V\beta$, suppressing channel inactivation and prolonging Ca^{2+} currents which results in increased neurotransmitter release (Kiyonaka *et al.* 2012; Kiyonaka *et al.* 2007).

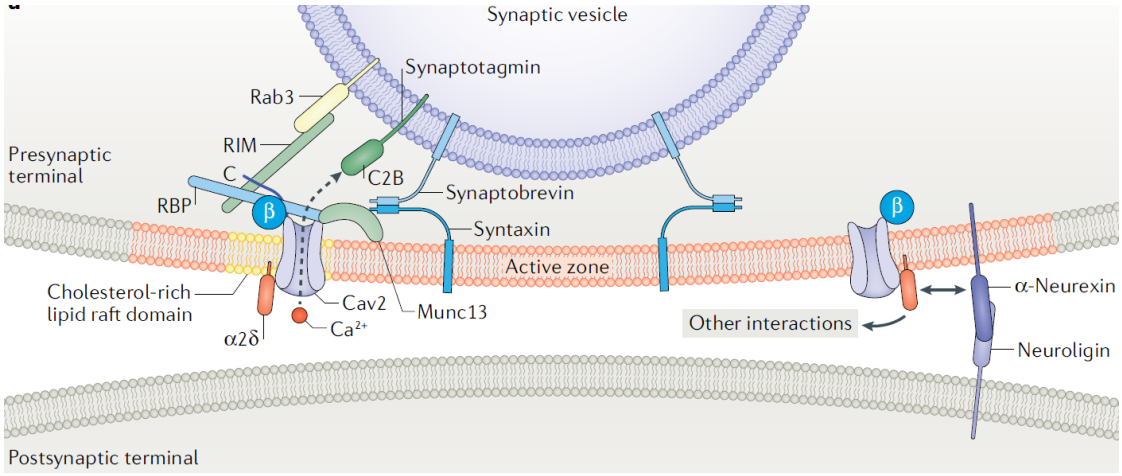

Figure 1. 10. Molecular model of Ca_V2 channel organisation at the active zone.

Ca_V2 channels are tethered close to primed synaptic vesicles by a tripartite complex composed of cytosolic RIM, RIM-BP and the C-terminal of the Ca_V2 channel. Synaptic vesicle proteins Rab3, synaptotagmin and plasma membrane-anchored proteins Munc13 and Syntaxin interact with components of the tripartite complex ensuring close proximity of vesicles to the plasma membrane and Ca_V2 channels. Presynaptic $\alpha_2\delta$ can act trans-synaptically on postsynaptic proteins, for example via interaction with the α-neurexin-neuroligin complex. From (Dolphin and Lee 2020).

1.3.5. Regulation of $Ca_V2.2$ channels

Modulation of Ca^{2+} entry through $Ca_V2.2$ channels into the presynapse is one of the key mechanisms by which neurotransmitter release is regulated and is therefore tightly controlled by several mechanisms (Fig. 1.11).

Spatially, Ca^{2+} buffer systems at the active zone, such as CaM attached to presynaptic proteins (Faas *et al.* 2011; Eggermann *et al.* 2011), restrict the diffusion of Ca^{2+} thereby generating a local Ca^{2+} elevations, able to trigger vesicular fusion. Temporal characteristics of Ca_V2 channel opening are determined by gating properties of the channels. Several molecules interact with intracellular loops of $Ca_V2.2$, precisely controlling channel gating properties and thereby cellular excitability and synaptic plasticity (Muller *et al.* 2010). Most of the mechanisms described in the following section apply for all Ca_V2 channels, however the focus will be on studies performed on $Ca_V2.2$

channels. The role of VDI and CDI as well as the modulation by auxiliary subunits has been covered in 1.2.5. and 1.2.6.

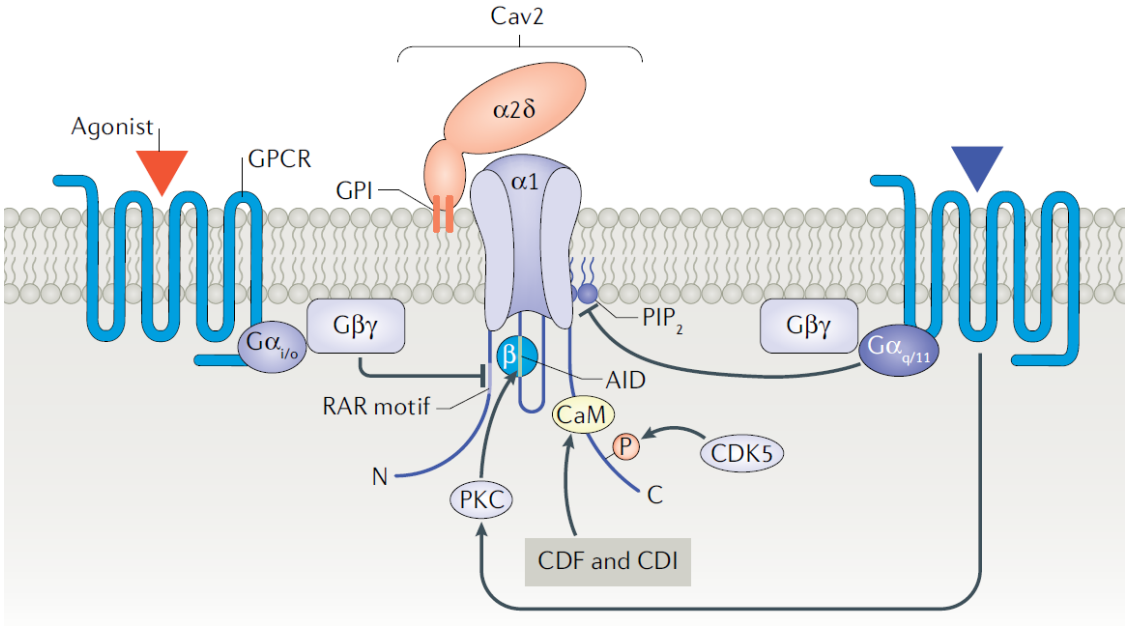

Figure 1. 11. Fine tuning of neurotransmitter release by modulation of $Ca_V2.2$ channels at the presynapse.

Many proteins interact with and modulate $Ca_V2.2$ channel distribution and activity. G-protein coupled receptors (GPCRs) inhibit $Ca_V2.2$ channel activity via binding the N-terminus or by activating protein kinase C (PKC) which phosphorylates the synprint site and the I-II linker. C-terminal interactions involve CDI (described in 1.2.5.) and phosphorylation by cyclin-dependent kinase 5 (CDK5). CDI = Ca^{2+}-dependent inactivation and CDF = Ca^{2+}-dependent facilitation. From (Dolphin and Lee 2020).

1.3.5.1. Inhibition by G-proteins

Numerous neurotransmitters that have been released into the synaptic cleft, activate presynaptic GPCRs, providing negative feedback through inhibition of $Ca_V2.2$ channels, crucial for fine-tuning synaptic activity. GPCRs are seven transmembrane-spanning surface receptors that couple to various heterotrimeric G-proteins, classified into four major families G_s, G_i, G_q and G_{12}. Agonist-binding leads to the dissociation of two functional units, G_α and $G_{\beta\gamma}$, both initiating numerous intracellular signalling cascades.

The most prominent form of $Ca_V2.2$ channel inhibition is VDI via $G_{i/o}$-derived $G_{\beta\gamma}$, first shown in sympathetic ganglion neurons (Herlitze *et al.* 1996; Ikeda 1996). This interaction occurs via $G_{\beta\gamma}$ dimers directly binding the I-II linker on α_1, resulting in a conformational change that slows current activation kinetics of the channel and shifts the voltage-dependence of activation to more depolarized potentials. Notably, upon strong membrane depolarisation, $G_{\beta\gamma}$ uncouples from α_1. Essential for the VD dissociation of $G_{\beta\gamma}$ is the presence of $Ca_V\beta$, binding to similar regions in the I-II linker (Meir *et al.* 2000; Currie 2010). Besides binding to the I-II linker, further binding sites for $G_{\beta\gamma}$ were identified on the N-terminus (Page *et al.* 1998; Canti *et al.* 1999) and on the C-terminus of α_1B.

Whereas VDI is a widespread mechanism throughout the nervous system, voltage-independent inhibition of $Ca_V2.2$ channels by GPCR has also been described. In sympathetic neurons, G_q-mediated secondary messenger cascades initiate $Ca_V2.2$ channel inhibition through phospholipase C-induced phosphatidylinositol 4,5-bisphosphate hydrolysis (Castro *et al.* 2020; Vivas *et al.* 2013). Another mechanism of voltage independent inhibition is PKC antagonising $G_{\beta\gamma}$ inhibition by phosphorylating $Ca_V2.2$ channels at multiple sites (Doering *et al.* 2004).

Additionally, GPCRs have also been shown to directly interact with $Ca_V2.2$ channels. In DRG neurons, δ- and μ-opioid (Heinke *et al.* 2011) GPCRs mediate $Ca_V2.2$ channel cell surface expression and internalisation, a mechanism used to treat analgesia after spinal cord injury, for example. Similarly, GPCR dopamine 1 directly interacts with $Ca_V2.2$ channels in dendrites of the rat prefrontal cortex, facilitating trafficking into the membrane and internalisation of the Ca^{2+} channel (Kisilevsky *et al.* 2008; McCarthy *et al.* 2020). In dorsal horn synapses, $GABA_B$ receptors inhibit $Ca_V2.2$ channel activity (Huynh *et al.* 2015). Finally, recent studies also suggest the endocannabinoid GPCR CB_1 suppresses GABA release from axon terminals by inhibiting $Ca_V2.2$ channel function (Szabo *et al.* 2014). This inhibitory modulation of $Ca_V2.2$ channels has also been shown at granule to Purkinje cell synapses in the cerebellum (Brown *et al.* 2004).

1.3.5.2. Phosphorylation by protein kinases

Kinases are enzymes that regulate the activity of proteins by phosphorylating hydroxyl groups of serine and threonine amino acid residues. Several kinases have been implicated in the modulation of $Ca_V2.2$ channels including PKC and cyclin-dependent kinase 5 (CKD5). Balanced antagonistic activities of kinases and phosphatases at the presynapse modulate $Ca_V2.2$ channel function and thereby contribute to fine-tuning neurotransmitter release.

PKC was shown to directly modulate $Ca_V2.2$ channel function in neuronal growth cones in *Aplysia* (Zhang *et al.* 2008). Here, PKC activation was demonstrated to activate downstream signalling cascades that ultimately result in an increased translocation of $Ca_V2.2$ channels to the membrane, resulting in presynaptic potentiation in these neurons. Additionally, PKC also interferes with G-protein mediated inhibition of $Ca_V2.2$ channels by phosphorylating the I-II linker thereby disrupting the interaction with Gβγ and $Ca_V\beta$ (Zhu and Ikeda 1994; Zamponi *et al.* 1997).

CDK5, activated by two neuronal-specific activators p35 and p39 (Ko *et al.* 2001), has been found to be a central regulator of brain synaptic function, generally inhibiting neurotransmitter release and controlling synaptic vesicle pools (Kim and Ryan 2010). CDK5 has also been implicated in regulating presynaptic Ca_V2 channels by phosphorylating the C-terminal of $Ca_V2.2$ channels leading to enhanced channel opening probabilities and increased neurotransmitter release (Su *et al.* 2012). It was furthermore shown that CDK5-mediated phosphorylation is required for the interaction of $Ca_V2.2$ channels and RIM1, allowing the docking of more synaptic vesicles to the active zone with direct implications for synaptic function and adaptations during synaptic plasticity. This was demonstrated by diminished synaptic field excitatory postsynaptic potentials upon mutation of phosphorylation sites in $Ca_V2.2$ channels. However, using an optical approach to study the influence of CDK5 on $Ca_V2.2$ channels at the rat hippocampal synapse revealed a potentiation of Ca^{2+} influx when suppressing CDK5 activity (Kim and

Ryan 2013). Similarly, $Ca_V2.1$ channels phosphorylated by CDK5 showed diminished activity and this resulted in overall reduced neurotransmitter release at the synapse (Tomizawa *et al.* 2002). Though results are discrepant, phosphorylation by CDK5 undoubtedly regulates $Ca_V2.2$ channel function, furthermore highlighting the importance of kinases interacting with $Ca_V2.2$ channels.

1.3.5.3. Regulation of $Ca_V2.2$ channel trafficking by CRMP-2

Collapsin response mediator protein 2 (CRMP-2) has recently emerged as a $Ca_V2.2$ channel-interacting protein. CRMP-2 is a cytosolic phosphoprotein regulating axonal growth by modulating microtubule dynamics (Arimura *et al.* 2005). Co-immunoprecipitation studies showed that CRMP-2 associates with $Ca_V2.2$ channels in DRG neurons and that overexpression of CRMP-2 in sensory neurons results in increased $Ca_V2.2$ channel surface expression and increased Ca^{2+} currents (Chi *et al.* 2009). This provides another pathway of modulating presynaptic $Ca_V2.2$ channel activity and thereby neurotransmitter release.

1.3.5.4. Fragile X mental retardation protein

Fragile X mental retardation protein (FMRP) is an important inhibitor of mRNA translation, crucial for many aspects of synaptic organization in the context of synaptogenesis, synaptic plasticity and normal neuronal functioning (Sidorov *et al.* 2013). In Fragile X syndrome, silencing of the *FMR1* gene results in severe neurodevelopmental deficits and intellectual impairment. FMRP knock-down in cultured DRG neurons resulted in synaptic dysfunction due to increased levels of somatic and presynaptic $Ca_V2.2$ channels. Furthermore, the C-terminus of FMRP is likely to directly interact with the C-terminus and the II-III linker of $Ca_V2.2$, targeting the channel for proteasomal degradation (Ferron *et al.* 2014). These findings were recently complemented by optophysiological studies in DRG and hippocampal neurons which showed elevated levels of $Ca_V2.2$ channels due to increased forward trafficking from the ER to the plasma membrane when FMRP was silenced (Ferron *et al.* 2020a).

1.3.5.6. Pharmacological inhibitors

There are several selective inhibitors available for studying $Ca_V2.2$ channels and one inhibitory drug clinically approved for alleviation of severe chronic pain. The most potent inhibitor widely used for experimental purposes is the highly selective ConTx, derived from the cone snail *Conus geographus*. The small peptide can potently block the pore of $Ca_V2.2$ channels, providing nearly irreversible inhibition (Reynolds *et al.* 1986). A synthetic version of the related toxin, ω-conotoxin MVIIA, named ziconotide (SNX-111, Prialt) is in use as an analgesic for the amelioration of severe pain conditions (McGivern 2007). Notably, ziconotide is injected intrathecally, as it cannot be absorbed orally or cross the blood-brain-barrier. Both toxins act via binding S5-S6 in the domain III region, resulting in pore occlusion (Ellinor *et al.* 1994; Gao *et al.* 2021). There are several other selective $Ca_V2.2$ channel peptide blockers derived from marine snails, all acting in a similar way by blocking the pore and therefore the influx of Ca^{2+} into cells (Zamponi *et al.* 2015). Gabapentin (Neurontin) and pregabalin (Lyrica) are anticonvulsants used to treat epileptic seizures and neuropathic pain. Initially developed as $GABA_A$ receptor activators, both were found to instead bind $\alpha_2\delta$-1 and -2 with high affinity, indirectly reducing forward trafficking and thereby cell surface expression of $Ca_V2.2$ channels (Tran-Van-Minh and Dolphin 2010; Cassidy *et al.* 2014).

1.3.6. Neuropathophysiology of $Ca_V2.2$ channels

$Ca_V2.2$ channels have diverse roles in the nervous system, orchestrating aspects of neurotransmission, synaptic plasticity and neuronal development. Hence, alterations in channel expression and alterations in channel activity due to mutations can result in neuronal dysfunction and disease. $Ca_V2.2$ knockout mice have a mild phenotype, possibly due to compensatory upregulation of $Ca_V2.1$ and $Ca_V2.3$ channels. The most important observed deficiencies include impaired nociception with reduced pain hypersensitivity in models of neuropathic pain (Hatakeyama *et al.* 2001; Kim *et al.* 2001; Saegusa *et al.* 2001). Furthermore, mice are hyperactive (Beuckmann *et al.* 2003;

Nakagawasai *et al.* 2010), less anxious (Saegusa *et al.* 2001) and show reduced voluntary alcohol intake (Newton *et al.* 2004).

1.3.6.1. Clinical presentation of $Ca_V2.2$ channelopathies

Only few genetic mutations of *CACNA1B* have been detected in patients. Recently, a gain-of-function point mutation was found in a family that resulted in a myoclonus-dystonia phenotype, with involuntary muscle twitching in the upper body, dystonia and psychological symptoms (Groen *et al.* 2015). The mutation was identified to affect the third p-loop of $Ca_V2.2$, crucial for Ca^{2+} conductance. Transfection of tsA-201 cells with $Ca_V2.2$ channels carrying the same mutation revealed larger whole-cell Ca^{2+} currents. However, these findings were challenged (Mencacci *et al.* 2015) and demand further evidence for a genetic involvement of $Ca_V2.2$ channels in myoclonus-dystonia.

In six children from three unrelated families, a bi-allelic loss-of-function of *CACNA1B* was identified, leading to severe neurodevelopmental delays, progressive epilepsy-dyskinesia and death before reaching adulthood (Gorman *et al.* 2019).

Finally, there is evidence for autoimmune responses against $Ca_V2.2$ channels. Targeted disruption of $Ca_V2.2$ channels by auto-antibodies could alter Ca^{2+} conduction of the channels and alter or abolish channel function. Patients with anti-$Ca_V2.2$ channel antibodies were diagnosed with autoimmune autonomic ganglionopathy and encephalitis (Kimpinski *et al.* 2009; Finkel and Koh 2013).

1.3.6.2. $Ca_V2.2$ channels in neuropathic pain

Neuropathic pain is characterized by nociceptor sensitization, allodynia (pain due to stimulus that usually does not provoke pain) and hyperalgesia (increased pain sensation from a stimulus that usually provokes pain) with multiple underlying causes. One common mechanism is an altered function of $Ca_V2.2$ channels and $\alpha_2\delta$ subunits in primary sensory DRG neurons (nociceptors), where $Ca_V2.2$ channels play a dominant role in neurotransmitter release from the afferent terminals in the spinal dorsal horn. Thus, specific inhibition of $Ca_V2.2$ channels is a promising therapeutic approach for

treatment of pain. The pharmacological inhibition or ablation of $Ca_V2.2$ channels has already been shown to decrease pain responses in animal models of neuropathic pain (Hatakeyama *et al.* 2001; Kim *et al.* 2001; Saegusa *et al.* 2001) and ziconotide is used clinically for the treatment of severe chronic pain. Finally, morphine-induced analgesia is likely to be in part mediated by inhibition of primary afferent $Ca_V2.2$ channels (Lipscombe and Raingo 2007; Currie 2010).

Gabapentin and pregabalin target $\alpha_2\delta$-1 and -2 and are more widely used for the treatment of neuropathic pain than ziconotide. These drugs were shown to also indirectly act on $Ca_V2.2$ channels, by inhibiting $\alpha_2\delta$-mediated trafficking of Ca_V channels to the plasma membrane and thereby reducing synaptic transmission of pain signals (Field *et al.* 2006). Genetic ablation of $\alpha_2\delta$-1 in a knockout mouse model abolishes $Ca_V2.2$ channels on the cell surface of DRG neurons (Nieto-Rostro *et al.* 2018). All these findings give an indication of the crucial role of $Ca_V2.2$ channel activity in the pain pathway and the implications for selective targeting of these channels. For example, the ability to specifically target $Ca_V2.2$e37a, the dominant isoform in nociceptors, would allow for selective inhibition while sparing channels expressed elsewhere in the nervous system.

1.4. The role of $Ca_V2.2$ channels in synaptic plasticity

1.4.1. $Ca_V2.2$ channels and synaptogenesis in the brain

1.4.1.1. Role of $Ca_V2.2$ channels for neuronal migration and synapse organisation during development

The development of the CNS is a tightly controlled process, where Ca^{2+} is one of the key molecules mediating neuronal migration, synaptogenesis and the formation of networks (Scheiffele 2003). During development, neuronal migration is guided by repulsive and attractive signalling molecules. Upon development of initial axon-target interactions, signalling molecules, such as neurexins recruit scaffolding proteins that support the differentiation of pre- and postsynaptic specialisations, required for synapse formation (Scheiffele *et al.* 2000; Biederer and Südhof 2000). With Ca^{2+} as an important mediator of most steps from neuronal migration to synaptic network refinement, $Ca_V2.2$ channels may orchestrate some processes during synaptogenesis (Su *et al.* 2012).

The activity-dependent changes of intracellular Ca^{2+} that regulate neuronal migration as well as neuronal outgrowth during early postnatal development (Kater and Mills 1991) were shown to be mediated by Ca^{2+} influx through $Ca_V2.2$ channels (Komuro and Rakic 1996). In the developing cerebellum, it was shown that inhibition of $Ca_V2.2$ channels results in decreased migration of granule cells, thereby demonstrating the importance of $Ca_V2.2$ channels (Komuro and Rakic 1992). More evidence for the role of $Ca_V2.2$ channels for neurite outgrowth was provided by experiments using cultured *Xenopus* neurons to show the interaction of laminin β2 with $Ca_V2.2$ channels controlling neurite outgrowth and sensory innervation in a Ca^{2+}-dependent manner (Sann *et al.* 2008). Moreover, at the neuromuscular junction in the PNS, the interaction of $Ca_V2.2$ channels with laminin β2 is involved in $Ca_V2.2$ channel clustering and the establishment of further presynaptic specialisations required for the assembly of the neurotransmitter release site (Nishimune *et al.* 2004). Studying synaptic targeting of epitope-tagged $Ca_V2.2$ channels in rat hippocampal cultures, showed that this recruitment was

dependent on the interaction of $Ca_V2.2$ with adaptor molecules Mint1 and CASK (Maximov *et al.* 1999; Maximov and Bezprozvanny 2002). However, more recently, the idea of $Ca_V2.2$ regulating synapse development was challenged (Held *et al.* 2020). By genetic ablation of different Ca_V2 channel subtypes in cultured hippocampal neurons and neurons from the Calyx of Held, it was shown that presynaptic formation did not rely on Ca_V2 channels (Held *et al.* 2020).

Notably, there is evidence that $\alpha_2\delta$ is crucial for neuronal development and synaptogenesis independent from its association with Ca_V channels. It was recently discovered, for example, that $\alpha_2\delta$-1 is involved in excitatory synaptogenesis. Binding of postsynaptic $\alpha_2\delta$-1 to astrocyte-secreted extracellular matrix protein thrombospondin promotes both synaptogenesis and spinogenesis in the mouse cortex (Eroglu *et al.* 2009; Risher *et al.* 2018). A recent study found $\alpha_2\delta$-1 (here acting presynaptically) to specifically drive the formation of excitatory networks in hippocampal cultures (Bikbaev *et al.* 2020), although a role for thrombospondin was not invoked here. $\alpha_2\delta$-2 was found to limit axon growth as inhibition of $\alpha_2\delta$-2 in DRG neurons resulted in increased axon growth and stronger synaptic transmission (Tedeschi *et al.* 2016). Lastly, $\alpha_2\delta$-3 was also found to play a role in synaptogenesis, as knockout of the $\alpha_2\delta$-3 homologue in *Drosophila melanogaster* resulted in failed motor terminal development (Dickman *et al.* 2008; Kurshan *et al.* 2009). Recent studies showed that contrary to $\alpha_2\delta$-1, $\alpha_2\delta$-3 specifically drives inhibitory network development in rat hippocampal cultures (Bikbaev *et al.* 2020), a process that may be mediated by an activity-dependent bone morphogenetic protein signalling pathway, as shown at the neuromuscular junction in *Drosophila* (Hoover *et al.* 2019).

1.4.1.2. $Ca_V2.2$ channels at the immature and mature synapse

As neurons and neuronal networks mature during CNS and PNS development, the distribution of $Ca_V2.2$ channels is likely to change depending on developmental stage and neuronal activity. In rat hippocampal neurons it was shown that $Ca_V2.2$ channels are

diffusely distributed in somatodendritic and axonal compartments in the immature neuron, but form discrete clusters at the presynapse as postsynaptic contacts are made and neurons mature (Maximov and Bezprozvanny 2002). In the mammalian brain, both $Ca_V2.1$ and $Ca_V2.2$ channels provide the main sources of Ca^{2+} influx at the presynapse. However, the composition of Ca_V2 channels at the presynapse depends on specific synapse needs (Dolphin and Lee 2020). There is evidence for a developmental shift from a predominant expression of $Ca_V2.2$ channels in some immature terminals whereas $Ca_V2.1$ might dominate at fully mature terminals (Reid *et al.* 2003). This has been functionally shown using selective toxins at different developmental stages targeting either $Ca_V2.1$ or $Ca_V2.2$ channels in hippocampal cultures (Scholz and Miller 1995; Scholz and Miller 1996), at the rat brain stem auditory synapse formed by the calyx of Held (Iwasaki and Takahashi 1998; Fedchyshyn and Wang 2005), at thalamic and cerebellar synapses (Iwasaki *et al.* 2000) and in striatal interneurons (Momiyama 2003). This certainly does not hold true for adult synapses in general, as terminals have been observed to express a combination of $Ca_V2.1$ and $Ca_V2.2$ channels or exclusively one or the other (as discussed in 1.3.1). Moreover, at some synapses the expression of all Ca_V2 channels declines as neurons mature, as shown in cultures from the rat cerebellar cortex (Falk *et al.* 1999).

However, the developmental regulation of presynaptic channel sorting has important implications for neuronal function, providing each terminal with the required composition of Ca_V2 channels. Developmentally immature terminals with a greater complement of $Ca_V2.2$ channels are more prone to G-protein-mediated modulation (see also 1.3.5.1). This has been demonstrated both in striatal brain slices and in hippocampal neurons, where a decline in contribution of $Ca_V2.2$ channels to Ca^{2+} flux was paralleled by a decrease of dopamine 1- (Momiyama 2003) and adenosine 1-receptor- (Scholz and Miller 1996) mediated inhibition, respectively. This predominance of $Ca_V2.2$ channels at the immature synapse could thus be part of a modulatory process by which excessive

excitation of immature terminals can be rapidly downregulated by presynaptic inhibition, or to keep immature synapses in a *reserve* state.

1.4.1.3. Changes in coupling efficiencies between Ca_V channels and Ca^{2+} sensors at the maturing synapse

Synaptic transmission occurs with great spatial and temporal precision. Modulation of presynaptic Ca_V2 channels is a powerful mean to regulate neurotransmitter release as a 2-fold change in Ca^{2+} currents results in an 8-16 fold change in synaptic vesicle exocytosis (Catterall and Few 2008). Ca_V2 channels are arranged in nano- or microdomains around a vesicle release site (Eggermann *et al.* 2011), implying a more or less tight coupling to the vesicle release site, respectively (Bornschein *et al.* 2019). In the case of nanodomain-coupling, fewer channels are needed for a Ca^{2+} influx sufficient to trigger neurotransmitter release whereas in the case of a microdomain, a larger number of channels is required to contribute to sufficient Ca^{2+} flux triggering vesicle release (Rebola *et al.* 2019). The predominance of $Ca_V2.1$ channels at some mature synapses is related to its nanodomain coupling at the presynaptic terminal providing faster, more precise and more energy-efficient synaptic transmission (Bucurenciu *et al.* 2008; Eggermann *et al.* 2011). This form of release may be advantageous at fast synapses that require reliable signalling, for example at the adult auditory Calyx of Held synapse (Fedchyshyn and Wang 2005). Nanocoupling has also been shown to be present at central inhibitory synapses (Eggermann *et al.* 2011) and excitatory synapses in the brain stem (Nakamura *et al.* 2015) and neocortex (Bornschein *et al.* 2019). Synapses with loose coupling properties typically exhibit large short-term facilitation, as described at the mossy fibre synapse, a system widely studied in the context of presynaptic plasticity (Vyleta and Jonas 2014).

It has been shown that Ca_V2 coupling distances change during neuronal development. Several studies suggest that $Ca_V2.2$ channels are more loosely coupled at the immature terminal and that this coupling undergoes substantial developmental

tightening (Vyleta and Jonas 2014). Studies at the mature parallel fibre-Purkinje cell synapse in the cerebellum suggest that this developmental tightening is mediated by Munc13-1 (Kusch *et al.* 2018). Furthermore, the immature calyx of Held for example relies on microdomain Ca^{2+} elevations for exocytosis by loosely coupled $Ca_V2.1$ and $Ca_V2.2$ channels, whereas after hearing onset the mature synapse signals via tight $Ca_V2.1$ nanodomains (Fedchyshyn and Wang 2005).

1.4.2. $Ca_V2.2$ channels during synaptic plasticity at central synapses

Intracellular Ca^{2+} elevation via presynaptic Ca_V2 channels is crucial for coupling membrane depolarization to synaptic transmission. Ca^{2+} is also a key second messenger for dynamic adaptations in synaptic strength in response to a constantly changing environment. These adaptations are termed synaptic plasticity and encompass all changes to pre- and postsynaptic loci to strengthen or weaken synaptic connections in response to changes in activity. Because of the pivotal role of Ca^{2+}, presynaptic Ca_V2 channel modulation has an important impact on synaptic strength and on the expression of presynaptic plasticity. The three types of Ca_V2 channels mediate fast vesicle release at most synapses in the brain, each with distinct biophysical properties allowing precise fine-tuning of synapses. There are different forms of synaptic plasticity, and their interplay is crucial for information processing and proper functioning of the brain.

Generally, synaptic strength is determined by (i) the number of synaptic connections, (ii) the postsynaptic sensitivity to quantal release of neurotransmitters and (iii) the probability of neurotransmitter release (P_r). The latter is heavily influenced by Ca_V2 channels, especially during repetitive stimulation (Dittman and Ryan 2019). Modulation of P_r plays an important role in short-term synaptic plasticity which usually occurs within milliseconds to minutes (Zucker and Regehr 2002). Short-term adaptations reflect changes in presynaptic neurotransmitter release after recent bursts of activity that have led to residual accumulation of Ca^{2+} (Zucker and Regehr 2002). Depending on

recent synaptic activity and type of stimulus, synapses either exhibit facilitation or depression. Synapses with an initial high P_r are more likely to exhibit short-term depression during spike trains, because their RRP of vesicles will be rapidly used up. In contrast, synapses with a low P_r will likely show short-term synaptic facilitation during fast spike stimulation, due to Ca^{2+} triggering exocytosis of vesicles that were not used during prior synaptic activity (Schlüter *et al.* 2006). Many studies have investigated the involvement of presynaptic Ca_V2 channels in short-term plastic changes (Few 2009; Sheng *et al.* 2012; Catterall *et al.* 2013; Inchauspe *et al.* 2004). $Ca_V2.1$ channels, which exhibit both CaM-mediated facilitation and inactivation, were reported to mediate facilitation or depression in the rodent hippocampus (Nanou *et al.* 2016), cerebellum (Weyrer *et al.* 2019), cortex (Ali and Nelson 2006; Yamamoto and Kobayashi 2018) and superior cervical ganglion neurons (Scheuber *et al.* 2004; Mochida *et al.* 2008). Notably, $Ca_V2.2$ channels have been shown to contribute to short-term plasticity (Mochida 2019), mostly in the context of activity-dependent relief of G-protein inhibition (Scheuber *et al.* 2004) or for short-term synaptic adaptations in the rat cortex (Ali and Nelson 2006; Yamamoto and Kobayashi 2018).

Long-term plasticity encompasses long-lasting changes in synaptic efficacy that generally include Hebbian long-term potentiation (LTP) and long-term depression (LTD), which dynamically regulate information flow in neural circuits. To avoid excessive or insufficient firing potentially leading to pathological states of the neuronal networks, homeostatic mechanisms counteract perturbations in synaptic activity and restrain it within a dynamic, but physiological range. These compensatory adaptations are termed homeostatic synaptic plasticity (HSP). The balance between stability and flexibility is fundamental for proper functioning of the brain, and $Ca_V2.2$ channels may be among the many molecular players that are involved in both processes. This is due to the importance of $Ca_V2.2$ channels for (i) synaptic vesicle release, (ii) their expression at synapses known to be highly plastic, for example in the hippocampus, (iii) their G-protein

inhibition and (iv) due to their interaction with numerous proteins crucial for presynaptic function and plasticity.

1.4.2.1. Role of $Ca_V2.2$ channels for long-term synaptic plasticity

1.4.2.1.1. Role of $Ca_V2.2$ channels for Hebbian plasticity

Hebbian plasticity is a form of long-term plasticity which involves long-lasting modifications of synaptic strength, widely considered to be the mechanism by which information is encoded and retained in the brain. The prototypic form of Hebbian plasticity is NMDA receptor-dependent LTP or LTD, often studied in the tri-synaptic loop of the hippocampus, believed to represent cellular correlates of learning and memory (Lüscher and Malenka 2012). The induction of LTP requires the simultaneous activity of the pre- and postsynaptic compartments and a stimulus sufficient to activate NMDA receptors. The resulting Ca^{2+} influx into the postsynapse together with secondary messenger cascades alters synaptic strength. The molecular signalling cascades that lead to postsynaptic adaptations in response to different patterns of stimulation have been widely studied. However, the importance of presynaptic changes is non-negligible. Alterations in synaptic vesicle pool size and in the number of Ca_V2 channels in the active zone are crucial determinants of the presynaptic response (Sheng *et al.* 2012). At the perforant pathway in the hippocampus for example, the recruitment of $Ca_V2.2$ channels was shown to play a crucial role for the induction and maintenance of NMDA receptor-dependent LTP (Ahmed and Siegelbaum 2009). This study was the first to directly show the involvement of $Ca_V2.2$ channels in Hebbian synaptic plasticity. The regulation of $Ca_V2.2$ channel distribution or activity is an efficient mechanism to alter presynaptic vesicle release. $Ca_V2.2$ channels have been shown to interact with a myriad of presynaptic proteins, many of which have been implicated in LTP and LTP (Khanna *et al.* 2007; Muller *et al.* 2010). Furthermore, $Ca_V2.2$ channels are more prone to G-protein inhibition or relief thereof, respectively, making them suitable for contributing to synaptic strength adaptations (Sakaba and Neher 2003).

Notably, Ca_V subunits $\alpha_2\delta$-1 and $\alpha_2\delta$-2 were also reported to enhance glutamatergic excitatory neurotransmission by a direct interaction with postsynaptic NMDA receptors in the spinal cord and auditory system, respectively (Chen *et al.* 2018; Fell *et al.* 2016). This interaction was shown to be with the intracellular part of $\alpha_2\delta$-1 which is cleaved off in the ER when the GPI anchor is added, therefore the interaction with NMDA receptors must occur in the ER only (Chen *et al.* 2018). Moreover, a direct interaction of $\alpha_2\delta$-1 with AMPA receptors was shown, affecting the subunit composition of AMPA receptors and thereby corticostriatal LTP (Zhou *et al.* 2018). Additionally, $\alpha_2\delta$-1 may regulate presynaptic function via neurexin1α (Brockhaus *et al.* 2018). These findings all indicate a potential role of $\alpha_2\delta$ subunits for transsynaptic alignment of pre- and postsynaptic regions during normal synaptic functioning and during plastic remodelling. The latter includes both synaptic remodelling during learning and memory, but also pathological adaptations such as neuropathic pain.

1.4.2.1.2. Role of $Ca_V2.2$ channels during HSP

HSP mechanisms interplay with LTP and LTD, maintaining neuronal firing rates within an optimal range (Turrigiano 2008; Turrigiano 2011). This interplay was demonstrated in the hippocampus, for example, where LTP at Schaffer collaterals (SC) was enhanced after prolonged blockade of neuronal activity by voltage-gated sodium channel inhibitor TTX, resulting in elevated levels of AMPA and NMDA receptors on the postsynaptic membrane together with the appearance of new silent synapses (Arendt *et al.* 2013). There is an array of homeostatic negative feedback mechanisms that allow neurons and circuits to sense their activity and in turn adjust their excitability. For this, neurons can either directly regulate the strength of synapses by mediating excitatory and inhibitory synaptic inputs (synaptic scaling) or alter their intrinsic excitability, mediated by voltage-gated ion channels (intrinsic homeostasis) (Frank 2014). Modulation of components of the active zone of the presynaptic terminal is emerging as an important regulatory site for adaptations during HSP (Fig. 1.12). Chronic silencing of neuronal activity results in

restructuring of the active zone including a recruitment of active zone proteins such as Ca_V2 channels (Glebov *et al.* 2017; Lazarevic *et al.* 2011). During synaptic scaling, both post- and presynaptic changes alter synaptic inputs (Fernandes and Carvalho 2016).

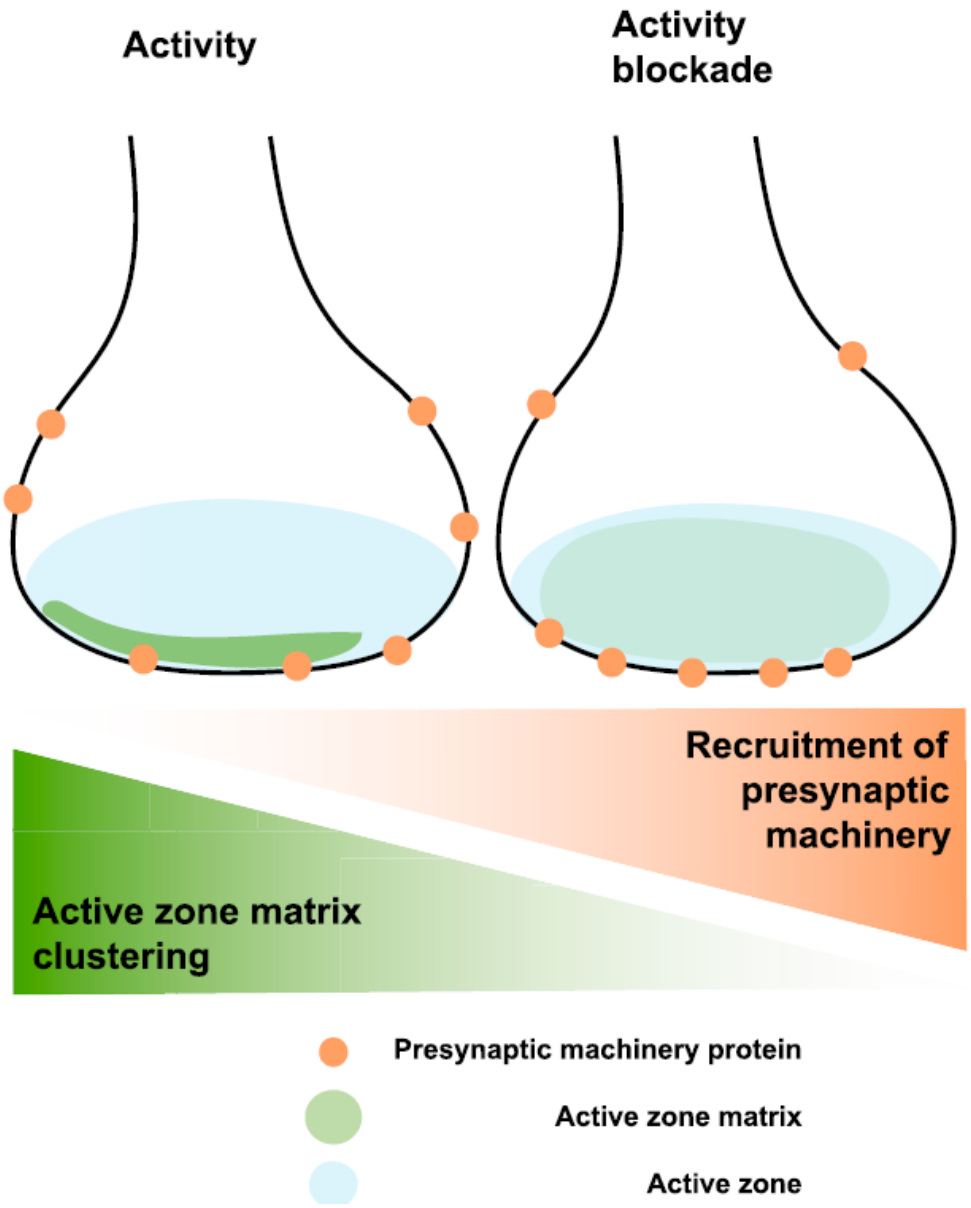

Figure 1. 12. HSP mechanisms at the presynapse involve changes of the active zone.

HSP after increased (left) or decreased (right) neuronal activity leads to a reorganisation of the active zone matrix and of proteins of the presynaptic machinery, including Ca_V2 channels. From (Glebov *et al.* 2017).

Postsynaptic changes rely on altering the composition and abundance of AMPA receptors, whereas presynaptic changes are mediated by alterations of presynaptic Ca^{2+} influx and modulation of the RRP of synaptic vesicles. At mammalian central synapses, multiple presynaptic modifications have been found to underly adaptations of hippocampal neurons in response to neuronal inactivity.

To elucidate the role of presynaptic Ca_V channels during presynaptic adaptation, a recent study expressed Ca^{2+} indicator SyGCaMP2 in hippocampal neurons and revealed increases in AP-triggered Ca^{2+} entry after network silencing which resulted in increased probabilities of synaptic vesicle fusion (Zhao *et al.* 2011). Moreover, one of the mechanisms by which $GABA_B$ receptors control homeostatic augmentation of synaptic strength is via removing inhibition of $Ca_V2.2$ channels, shown in TTX-treated hippocampal neurons (Vertkin *et al.* 2015). Additionally, loss of CDK5 was identified as a key step in presynaptic neurotransmitter release in response to chronic suppression of activity in rat hippocampal neurons (Kim and Ryan 2010). Later, it was shown that the modulation of enzymatic CDK5/calcineurin activity controls $Ca_V2.2$ channels and thereby synaptic function, with inhibition of CDK5 specifically potentiating Ca^{2+} flux via $Ca_V2.2$ (Kim and Ryan 2013). Contrary to this, some studies suggest homeostatic presynaptic plasticity to be exclusively mediated by $Ca_V2.1$ channels (Jeans *et al.* 2017; Glebov *et al.* 2017). Notably, contribution of pre- and postsynaptic adaptations seem to depend on the developmental stage of the organism, with HSP being exclusively postsynaptic at young cortical and hippocampal synapses (> days *in vitro* (DIV) 14), but shifting more to a presynaptic locus of expression as synapses mature (< DIV 18) (Wierenga *et al.* 2006).

Intrinsic homeostasis encompasses all homeostatic changes in intrinsic neuronal excitability, expressed upon prolonged and destabilizing alteration in neuronal activity. This form of HSP relies on altering excitability via changes in distribution and biophysical properties of voltage-gated ion channels (Turrigiano 2011). Neuronal circuits utilize a complex mix of synaptic and intrinsic mechanisms to optimize their activity and adapt to

a changing brain environment. The hierarchy of synaptic and intrinsic mechanisms remains unclear, it is possible they act independently, sequentially or simultaneously (Desai 2003). After blocking hippocampal activity *in vivo*, CA1 hyperexcitability was accompanied by both synaptic and intrinsic changes in the young animals, whereas in older animals intrinsic changes were exclusively observed (Echegoyen *et al.* 2007). Furthermore, studies in organotypic hippocampal slices revealed that upon manipulation of network activity, both synaptic and intrinsic homeostatic were activated in parallel. However, intrinsic changes preceded synaptic changes, decreasing the probability of excitation/inhibition imbalance (Karmarkar and Buonomano 2006).

1.5. Aim of this work

Modulation of presynaptic Ca^{2+} flux through Ca_V2 channels allows fast changes in neurotransmitter release and is therefore crucial for dynamic synaptic function at central synapses. Recent advances in synaptic imaging have improved our ability to identify molecular components of the synaptic vesicle release machinery, including presynaptic $Ca_V2.2$ channels. However, the distinct distribution of $Ca_V2.2$ channels at different synapses remains to be fully elucidated. The aim of this thesis is to determine the role of $Ca_V2.2$ channels at central synapses and changes that may occur as neurons mature and undergo plastic activity-dependent changes.

The maturation of synapses is accompanied by alterations in their complement of proteins. The first part of the thesis will assess how $Ca_V2.2$ channel distribution varies at various developmental stages in different brain regions. For this, gene expression studies are performed and matched by protein studies, using exofacially tagged $Ca_V2.2\_HA^{KI/KI}$ mice to visualise endogenous $Ca_V2.2$ channels.

To then reveal if the extensive remodelling of the active zone that was observed during homeostatic synaptic plasticity (Glebov *et al.* 2017; Lazarevic *et al.* 2011) involves presynaptic $Ca_V2.2$ channels, plasticity will be induced in hippocampal neurons at different ages *in vitro*. Using live cell Ca^{2+} imaging and Western blotting, presynaptic potentiation and changes in $Ca_V2.2$ channel function and abundance will be investigated.

Finally, the role of the $\alpha_2\delta$-1 subunit, crucial for $Ca_V2.2$ channel function but also involved in synaptic organisation (Schöpf *et al.* 2021), will be examined in the context of homeostatic synaptic plasticity using live cell Ca^{2+} imaging and immunoblots of biotinylated hippocampal neurons.

Chapter 2. Material and Methods

2.1. Generation of $Ca_V2.2\_HA^{KI/KI}$ mice

$Ca_V2.2$_HA knockin mice ($Ca_V2.2\_HA^{KI/KI}$) expressing an exofacial tandem haemagglutinin (HA) in the second extracellular loop of domain II loop of the α_1B subunit were generated by homologous recombination (HR) by TaconicArtemis. The targeting vector was constructed including the genomic region around exon 13 of *Cacna1b* from clones of a C57BL/6J RPCIB-731 BAC library into which the sequence coding for the tandem HA tag was cloned (Fig. 2.1 A).

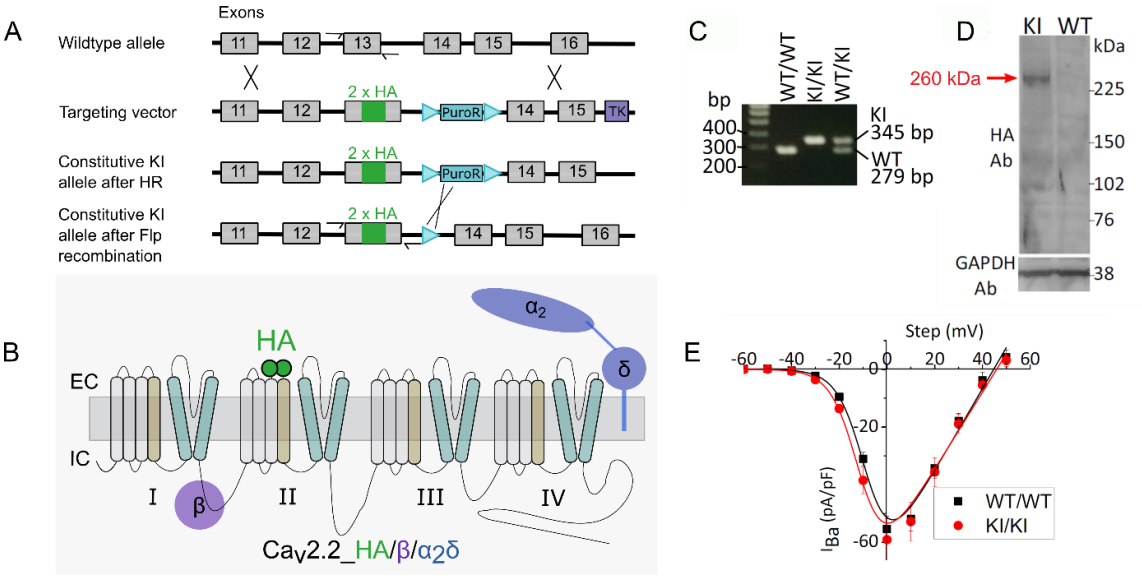

Figure 2. 1. Generation and validation of $Ca_V2.2\_HA^{KI/KI}$ mice.

(A) Schematic diagram of the exon 11-16 of the $Ca_V2.2$ gene and the targeting vector strategy used to generate $Ca_V2.2$_HA knockin mice by HR (adapted from (Nieto-Rostro *et al.* 2018) blue triangles = flipper recombination sites. **(B)** Overview of $Ca_V2.2$ with the tandem HA tag inserted into the second extracellular loop of domain II of α_1B and with its auxiliary subunits $\alpha_2\delta$ and β1 (adapted from Dolphin, 2003). EC = extracellular IC = intracellular. **(C)** PCR showing the presence of the HA tag at 345 bp exclusively in DNA from homozygous $Ca_V2.2\_HA^{KI/KI}$ and heterozygous $Ca_V2.2\_HA^{KI/WT}$ mice. **(D)** Synaptosomes from spinal cord revealed by western blotting show a band at approximately 260 kDa visualised using anti-HA antibodies (Abs) in the $Ca_V2.2\_HA^{KI/KI}$ mouse, but not in the wildtype. **(E)** Current-voltage relationships from $Ca_V2.2\_HA^{KI/KI}$ and wild type dorsal root ganglia neurons show no alterations in Ba^{2+} currents. Figure C, D and E from (Nieto-Rostro *et al.* 2018).

This vector furthermore contained a puromycin resistance gene in intron 13 embedded between two Flipper recombination sites and negative selection marker thymidine kinase outside the homologous regions. The linearized construct was transfected into mouse embryonic stem cells. After selection, homologous recombinant clones were injected into blastocysts from BALB/c mice. Chimeric mice were bred with C57BL/6 mice and germ line transmission confirmed by black offspring. Mice of the first generation were subsequently crossed with Flp deleter transgenic mice to remove the positive selection marker. Finally, backcrossing with C57BL/6 mice allowed selecting Flipper negative and 2x HA tag positive knockin mice. The presence of 2x HA in exon 13 was confirmed by PCR using forward primers 5′-CACACCAGCATACATGCTCG-3′ and reverse primers 5′-TCCAGCCTCACATGCTGC-3′ (Fig. 2.1 C). $Ca_V2.2\_HA^{KI/KI}$ mice are viable, normal in size and weight, reproduce normally and display no obvious behavioural abnormalities (Nieto-Rostro *et al.* 2018). Mice were housed in plastic cages with a 12h/12h light/dark cycle with food and water *ad libitum*, and in a maximum group size of five. The $Ca_V2.2\_HA$ tag was detected in synaptosomes of $Ca_V2.2\_HA^{KI/KI}$ mice (Fig. 2.1 D) and the tagged $Ca_V2.2\_HA$ channel was fully functional (Fig. 2.1 E). All experimental procedures were performed according to the Scientific Procedures Act 1986, UK.

2.2. Reverse Transcriptase quantitative PCR (RT-qPCR)

For gene expression studies, postnatal (P) 0/1, P7 and 12 weeks old mice were sacrificed via cervical dislocation, brains removed and separated into cortex, hippocampus, cerebellum and brain stem. To ensure sufficient amounts of RNA at timepoint P0/1 and P7, brains from 2 mice were pooled. Tissue samples were disrupted using a rotor-stator homogeniser (Disperser T10, IKA, Staufen, Germany). Total RNA was extracted using RNeasy lipid tissue mini kit according to manufacturer's instructions. RNA concentrations were photometrically measured to reversely transcribe 5 µg RNA from each sample into complementary DNA (cDNA) using High-Capacity RNA-to-cDNA kit (1 hour (hr) at 37 °C, 5 minutes (min) at 95 °C). For the 40 cycle qPCR (2 holding

stages of 50 °C 2 min and then 95 °C 10 min, followed by 40 cycles of 95 °C for 15 sec (denaturation) and 60 °C for 1 min (probe binding and amplification)), triplicates from each sample (three different mice for each timepoint) were loaded into a 96-well plate with TaqMan Universal PCR Master Mix (Applied Biosystems) and the following TaqMan probes used (gene name: assay ID): Hypoxanthine-phosphoribosyltransferase 1 (*Hprt1*): Mm00446968m1; glyceraldehyde 3-phosphate dehydrogenase (*Gapdh*): Mm99999915_g1; *Cacna1b*: Mm01333678m1. The *Cacna1b* probe targets exon 1 and will detect all splice variants of $Ca_V2.2$ channels.

A standard curve using different dilutions of *Cacna1b* and *Hprt* TaqMan probes (in ng/µl: 0.8, 4, 20 and 100) was generated by Dr Ramgoolam (unpublished) in order to determine the efficiency of the α_1B and *hprt* probes (Fig. 2.2). Optimal threshold values were defined automatically as 0.1 by 7500 Real-Time PCR software (Applied Biosystems) and used to determine the cycle threshold number (C_T). C_T values were then plotted against the logarithm of the amount of standard material used as input. Based on the resulting slope, efficiencies for each probe were calculated using $(10^{(-1/slope)}) -1) * 100$. The calculated efficiency for the α_1B (*Cacna1b*) probe was 93% and for the *Hprt* probe 96% (from thesis Dr Ramgoolam, unpublished).

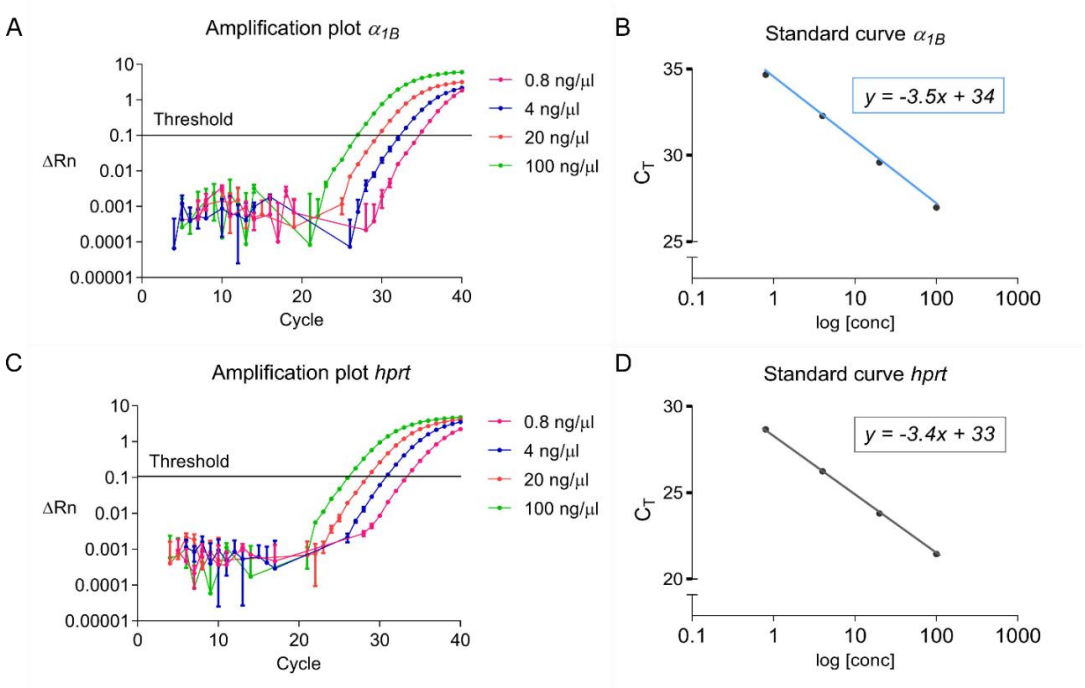

Figure 2. 2. Amplification plots and standard curves for the α$_1$B and Hprt probes.

(A) and **(B)** Different amounts of cDNA were amplified with the α$_1$B probe to create a standard curve. **(C and D)** Different amounts of cDNA amplified with the Hprt probe to create a standard curve. Efficiencies for both probes were close to 100% (from UCL thesis Dr K Ramgoolam, 2020, unpublished).

Results are expressed as fold change in $Ca_V2.2$ mRNA expression, given as mean ± SEM. To compare changes in expression during neonatal development into adulthood in certain brain regions, fold changes were calculated with respect to P0/1. Data were normalised to expression levels of housekeeping gene *Hprt* and analysed using the $2^{-\Delta\Delta CT}$ method (Livak and Schmittgen 2001). For this, mean C_T values for *α$_1$B* and *Hprt* of the three replicates were calculated for each region at each age. Afterwards ΔC_T was calculated using ($C_{T\ \alpha 1B}$ - $C_{T\ Hprt}$). To calculate $\Delta\Delta C_T$, $(\Delta C_{T\ \alpha 1B})_{\text{timepoint x}} - (\Delta C_{T\ \alpha 1B})_{\text{P1}}$ was used. Timepoint x would be either P0/1, P7 or 12 weeks. Finally, fold change expression was calculated using $2^{-\Delta\Delta CT}$. To compare differences in $Ca_V2.2$ mRNA expression levels between distinct brain regions at a certain age, $(\Delta C_{T\ \alpha 1B})_{\text{region x}} - (\Delta C_{T\ \alpha 1B})_{\text{cortex}}$ was used to calculate $\Delta\Delta C_T$, using cortical values as baseline. Here region x would either be cortex, hippocampus, cerebellum or brain stem. For each region at each age, three independent

RNA extractions were performed and were run on the same plate. In all experiments housekeeping gene *Hprt* was included to ensure the availability of stable control values.

2.3. Quantitative immunoblotting

2.3.1. Subcellular fractionation of mouse brains

For subcellular fractionation, brains from P0/1, P7 and 12 weeks old $Ca_V2.2\_HA^{KI/KI}$ mice were dissected in buffer I containing 0.32 M sucrose, 3 mM HEPES, pH 7.4, 0.25 mM dithiothreitol and protease cocktail inhibitor and separated into cortex, hippocampus, brain stem and cerebellum. Synaptosomes were prepared following (Kato *et al.* 2007; Ferron *et al.* 2014). Tissue was homogenised with 10 strokes in a glass potter in ice-cold buffer I and the homogenate centrifuged at 1000 x g for 10 min at 4 °C producing pellet P1 and supernatant S1 (Figure 2.3). Pellet P1, containing the crude nuclear fraction was resuspended in buffer I, centrifuged and the supernatant S1' added to S1. The sample was then centrifuged at 12,000 x g for 15 min producing pellet P2. P2 was resuspended in Buffer I and centrifuged at 13,000 x g for 15 min. The resulting pellet contained crude synaptosomes (P2') which were solubilized in radioimmunoprecipitation assay buffer (50 mM Tris, pH 8, 150 mM NaCl, 1 % Igepal, 0.5 % Na deoxycholate, 0.1 % sodium dodecyl sulphate (SDS), 1 Complete protease inhibitor tablet) (Ferron *et al.* 2008) and incubated on ice for 30 min.

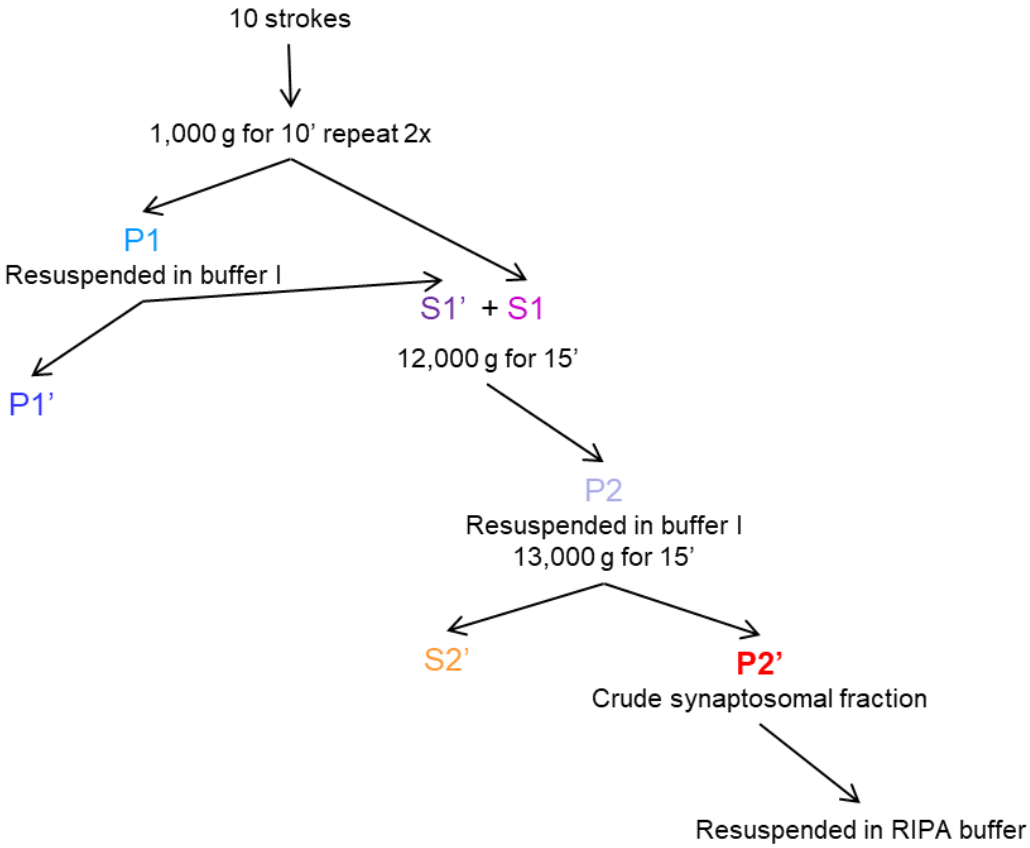

Figure 2. 3. Workflow synaptosome preparation.

Centrifugation for 30 min at 13,000 x g produced a supernatant containing the synaptosomal fraction that was subject to western blotting. The protein concentration in the supernatant was determined using the Bradford protein assay method (BioRad). Samples were adjusted to the same concentration of 1 µg protein /µl and denaturated with 100 mM dithiothreitol reducing agent and Laemmli sample buffer at 55 °C for 10 min. 20 µg of protein were loaded onto a 3-8 % NuPAGE gel and proteins resolved by SDS-polyacrylamide gel electrophoresis (SDS-PAGE) for 1 hr 05 min at 150 V, 50 mA in running buffer (NuPAGE). Separated proteins were transferred from the gel to a polyvinylidene difluoride (PVDF) membrane using a semi-dry transfer blot (BioRad) for 10 min at 25 mV, 1 mA. The membrane was then blocked by incubation with 3 % bovine serum albumin (BSA), 10 mM Tris pH 7.4, 0.5 % Igepal for one hr. Next, membranes were incubated overnight at 4 °C with rat anti-HA, rabbit anti-$Ca_V2.2$ II-II loop, rabbit anti-

synapsin1/2 or mouse anti-GAPDH Abs in blocking buffer. After washing with TBS 0.5 % Igepal, membranes were incubated for one hr at room temperature (RT) with horseradish peroxidase (HRP)-coupled secondary Abs at 1:2000 (all secondary Abs from Biorad, raised in goat, anti-rabbit HRP Cat # 1706515; anti-rat HRP Cat # 5204-2504 and anti-mouse HRP Cat # 1721011). Protein bands were revealed using enhanced chemiluminescence (ECL) reagent with Typhoon 9419 scanner (GE Healthcare) and analysed using ImageJ software as described in (Kadurin *et al.* 2012) . A box was drawn around each band of interest to quantify the mean grey intensity for each band. These values were then normalised to the respective GAPDH values in the same protein lane. For ease of comparison, values were then normalised to cortical protein levels. The molecular weight of $Ca_V2.2$_HA was determined with known molecular weight markers (Fig. 2.4, from UCL thesis Dr K Ramgoolam, 2020, unpublished).

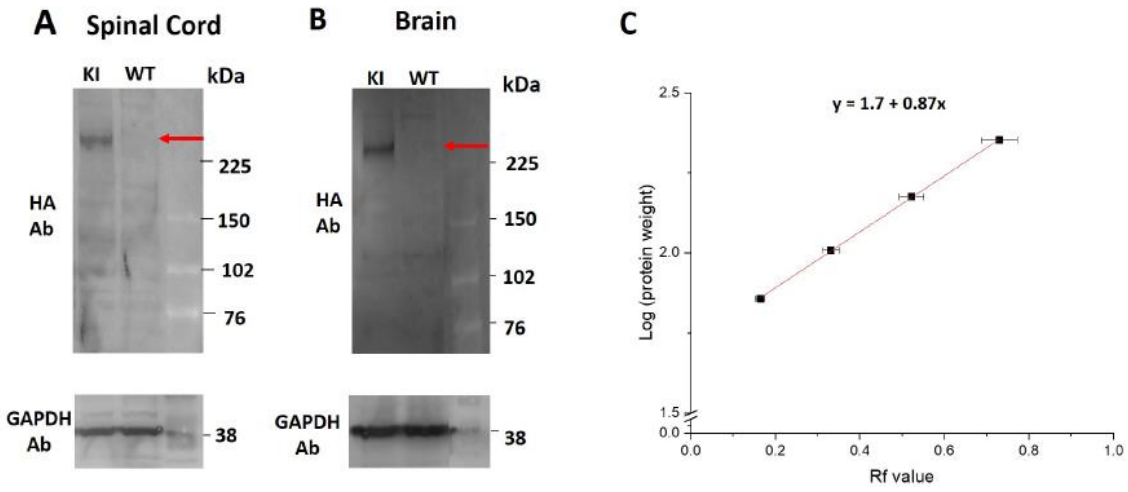

Figure 2. 4. $Ca_V2.2$_HA expression in synaptosomes from $Ca_V2.2$_ $HA^{KI/KI}$ mice.

(A and B) Immunoblot of synaptosomes from spinal cord (A) and brain (B) tissue from $Ca_V2.2$_ $HA^{KI/KI}$ (KI, left lane) and wild type mice (WT, right lane) revealed using anti-HA Abs. GAPDH (bottom) was included as a control for quantification. **(C)** Representative standard curve constructed using known molecular weights of the protein ladder. The molecular mass of $Ca_V2.2$_HA is 261 ± 1.2 kDa. Data from three independent experiments. From UCL thesis Dr K Ramgoolam, 2020, unpublished.

2.3.2. Whole cell lysates of hippocampal neurons

Homeostatic presynaptic plasticity was induced by incubating primary hippocampal neurons (see 2.4) with 1.5 µM tetrodotoxin (TTX) for 48 hr prior to imaging (Zhao *et al.* 2011). Whole-cell lysates (WCL) for immunoblotting were prepared by transferring mouse hippocampal neurons at DIV 18-22 on ice and washing twice with phosphate buffered saline (PBS) containing 1 mM $MgCl_2$ and $CaCl_2$ and then collecting cells by scraping them in $MgCl_2$/$CaCl_2$ PBS containing protease inhibitor. Lysates were cleared by centrifuging at 1000 x g for 10 min at 4 °C and then resuspending the pellet in PBS with 1 % Igepal, 0.1% SDS, 0.5 % sodium deoxycholate and protease inhibitor. After brief sonication and rotation for one hr at 4 °C, cells were spun down at 16,000 x g for 30 min at 4 °C. The protein concentration was determined using Bradford protein assay (Biorad) and proteins were separated and transferred to a PVDF membrane as described above. The membrane was blocked and then incubated overnight at 4 °C with rabbit anti-$Ca_V2.2$ II-III loop (1:500), mouse anti- $\alpha_2\delta$-1 (1:1000) or mouse anti-GAPDH (1:25,000) Abs. After washing with TBS 0.5 % Igepal, membranes were incubated for one hr at RT with respective HRP-coupled secondary Abs at 1:2000. Protein bands were revealed using ECL reagent with a Typhoon 9419 scanner (GE Healthcare) and analysed using ImageJ software as described above. Values were normalised to GAPDH values in the same lane and to control neurons for ease of comparison.

2.3.3. Biotinylation assay of hippocampal neurons

To assess the surface/total levels of $\alpha_2\delta$-1, EZ-Link NHS-LC-Biotin (from now on called biotin) was applied to TTX-treated and untreated control mouse hippocampal neurons aged DIV 18-22. For this, EZ-Link NHS-LC-Biotin was used, binding irreversibly to protein lysines on the cell surfaces. Biotin was diluted to a final concentration of 1 mg/ml in HBSS supplemented with 1 mM $MgCl_2$ and $CaCl_2$ and applied to cells at RT for 30 min to avoid protein endocytosis. After quenching with 200 mM glycine and two washes in HBSS, cells were centrifuged at 1000 x g for 10 min at 4 °C and frozen until sufficient

numbers of samples were collected for pooling. Afterwards, cells were lysed in lysis buffer containing 1 % Igepal, 0.1% SDS, 0.5 % sodium deoxycholate and protease inhibitor in HBSS, sonicated and rotated for one hr at 4 °C. Subsequently, protein concentrations were determined using the Bradford method as described above. Streptavidin beads were then added to a fraction of the cells while keeping some of the sample as a whole cell lysate to run on the same western blot. Streptavidin-treated samples were left on the roller at 4 °C overnight and were then loaded onto a gel as described in section 2.3.2. Protein band were analysed in ImageJ as described above. Values were normalised to GAPDH values of the WCL band for control and TTX conditions, respectively, and to control neuron values for ease of comparison.

2.4. Neuronal cell culture and transfection

Primary neuronal cultures were prepared from hippocampi of mixed sex P0/1 mouse or rat pups. After neck dislocation, hippocampi were dissected in ice-cold dissection medium (Hanks Balanced Salt Solution (HBSS), HEPES 1 M, 1% w/v glucose) and dissociated in enzyme solution containing Papain solution (HBSS, 2 mg/ml L-Cysteine, 2 mg/ml BSA 50 mg/ml Glucose), Papain (70 U/ml) and DNase I (1200 U/ml) in HBSS. After digestion at 37 °C for 40 min, the enzyme solution was aspirated and prewarmed inactivation medium (minimum essential media (MEM) without glutamine or phenol, 5 % v/v foetal bovine serum (FBS), 0.38 % w/v Glucose, 0.25 % w/v BSA) added. Hippocampi were then triturated with a P1000 pipette with polypropylene plastic tips and cells centrifuged at RT at 1000 rpm for 10 min in serum medium (MEM, 5 % v/v FBS, 1.38 % w/v glucose). After cell pellet resuspension, cells were counted and plated at a concentration of 6800 cells/mm^2 on 22 mm^2 cover slips. Prior to plating, coverslips were treated with Histoclear for one hr, followed by washing in 100 % v/v ethanol for 1.5 h. Afterwards, coverslips were thoroughly washed in water, dried overnight and autoclaved. Coverslip surfaces were precoated with poly-D-Lysine (50 µg/ml) and cells covered with serum-free neuronal plating medium comprising Neurobasal medium, supplemented

with B27™ and GlutaMAX™ supplement and kept at 37 °C in 5 % CO_2 with a medium change every 3-4 days.

At DIV 7 cells were transfected using Lipofectamine 2000 Transfection reagent according to manufacturer's instructions. Briefly, 2 hr prior to transfection, half of the cell media was replaced with fresh media and fresh media was added to the previously removed media to obtain conditioned media. Transfection mixes for one 22 mm^2 coverslip typically contained 4 µg DNA (in pCAGGS vector) in 50 µl OptiMEM and 2 µl Lipofectamine in 50 µl OptiMEM. The latter was added to the cDNA mix after a 5 min incubation period, followed by a 20 min incubation of the cDNA-Lipofectamine mix in the dark. After, 100 µl of the mix were added dropwise to each dish and the cells returned to the incubator for 2 hr. Finally, media was replaced with the conditioned media that was prepared at the beginning. All constructs used were in pCAGGS vector and transfection mixes were as follows.

For immunocytochemistry experiments:

(1) For detection of $Ca_V2.2$_HA: GFP_$Ca_V2.2$_HA and $\alpha_2\delta$-1 and β1b at 2:1:1 ratio.
(2) For detection of $Ca_V2.2$_HA: $Ca_V2.2$_HA, $\alpha_2\delta$-1, β1b and mCherry at 3:2:2:0.5 ratio.
(3) For detection of $\alpha_2\delta$-1_HA: $\alpha_2\delta$-1_HA to mCherry to empty vector (EV): 2:1:1 and for EV control experiments, mCherry to EV at 1:3 ratio was used.

For live cell Ca^{2+} imaging experiments:

(4) Synaptophysin-green fluorescent protein-calmodulin protein (Sy-GCaMP6f, (Kadurin *et al.* 2016)) and vesicle associated membrane protein mOrange2 (VAMP-mOr2) at a ratio of 3:1.
(5) For experiments with $\alpha_2\delta$-1 overexpression: Sy-GCaMPf6, VAMP-mOr2 and either $\alpha_2\delta$-1 or EV at a ratio of 2:1:1.

2.5. Immunolabelling

2.5.1. Immunohistochemistry

Immunohistochemical experiments were performed using $Ca_V2.2\_HA^{KI/KI}$ and wild type mice of 12 weeks age. Mice were anaesthetized with an intraperitoneal injection of pentobarbitone (Euthatal, Merial Animal Health, Harlow, UK; 600 mg / kg), transcardially perfused with saline containing heparin (0.1 M) followed by perfusion with 4 % w/v paraformaldehyde (PFA) in 0.1 M phosphate buffer (pH 7.4) at a flow rate of 2.5 ml/min for 5 min. Following perfusion, brains were postfixed in 4 % PFA for two hrs and immersed in cryoprotective 20 % sucrose overnight. Subsequently, brains were mounted in optimal cutting temperature compound and sliced into 20 µm thick coronal sections using a cryostat and then stored at -80 °C. Slices were blocked and permeabilised for one hr at RT in 10 % v/v goat serum (GS) and 0.2 % v/v Triton-X 100 in PBS and then further blocked by applying unconjugated goat F(ab) anti-mouse IgG (1:100) for 1 hr at RT to prevent unspecific binding. Subsequently, primary Abs (see table 2.1) were applied diluted in 5 % v/v GS, 0.2 % v/v Triton-X 100 and 0.005 % v/v NaN_3. After 2 days at 4 °C, 4 % PFA was reapplied for 30 min at RT to ensure stabilisation of the protein-Ab complex. Sections were then incubated with secondary Abs (table 2.2) for 2 days at 4 °C, washed and mounted in Vectashield Antifade Mounting Medium. Images were taken using a LSM 780 confocal microscope (Zeiss) with a x20 objective (89 µm optical section, pixel dwell 2.05 µs, zoom 1.8) or x63 in super resolution mode. After acquisition, super resolution images underwent Airyscan processing and tile stitching using Zen software (Zeiss).

2.5.2. Immunocytochemistry

Hippocampal neurons were fixed with 4 % w/v PFA/ 4 % w/v sucrose in PBS for 5 min followed by washes in PBS. Next, neurons were blocked and permeabilised for at least one hr at RT in 20 % v/v GS, 0.3 % v/v Triton X100. Subsequently, cultures were

incubated overnight at 4 °C with primary Abs diluted in in 10 % v/v GS, 0.3 % v/v Triton X-100 (Ab solution; see table 2.1). Next, cells were washed with PBS and respective Alexa Fluor488 secondary Abs applied for one hr diluted at 1:500. Following washes in PBS and application of nuclear marker 4,6-diamidino-2- phenylindole (DAPI) at 500 nM, cells were mounted in Vectashield and examined using Confocal or super resolution Airyscan mode imaging on a LSM 780 confocal microscopes (Zeiss) with a x20 or x63 objective.

Antigen	Species	Clone	Dilution	Cat #	Source
$\alpha_2\delta$-1	Mouse	Polyclonal	1:1000	C5105	Roche
$Ca_V2.2$ II-III loop	Rabbit	Polyclonal	1:500	ACC002	Alomone
GAPDH	Mouse	Polyclonal	1:25000	AM4300	Ambion
GFAP	Chicken	Polyclonal	1:500	Ab4674	Abcam
GFP	Rabbit	Polyclonal	1:500	ab6556	Abcam
HA	Rat	Monoclonal	1:100	11867423001	Roche
Homer1	Rabbit	Polyclonal	1:500	AF1000	Frontier Institute
MAP2	Chicken	Polyclonal	1:500	Ab5392	Abcam
RFP	Guinea-pig	Polyclonal	1:500	390004	Synaptic Systems
RIM1/2	Rabbit	Polyclonal	1:500	140 203	Synaptic Systems
Synapsin I/II	Rabbit	Polyclonal	1:500	106002	Synaptic Systems
vGAT	Rabbit	Polyclonal	1:500	131003	Synaptic Systems
vGluT1	Guinea-pig	Polyclonal	1:1000	135304	Synaptic Systems

Table 2. 1. Primary Abs used for immunocytochemistry, immunohistochemistry and Western blotting.

Specificity	Conjugation	Species	Dilution	Cat #	Source
Chicken IgG	Alexa Fluor® 647	Goat	1:500	103-605-155	Jackson ImmunoResearch
Guinea-pig IgG	Alexa Fluor® 633	Goat	1:500	106-605-003	Jackson ImmunoResearch
Rabbit IgG	Alexa Fluor® 488	Goat	1:500	111-545-144	Jackson ImmunoResearch
Rabbit IgG	Alexa Fluor® 594	Goat	1:500	111-585-144	Jackson ImmunoResearch
Rat IgG	Alexa Fluor® 488	Goat	1:500	112-545-003	Jackson ImmunoResearch
Rat IgG	Alexa Fluor® 594	Goat	1:500	112-585-167	Jackson ImmunoResearch

Table 2. 2. Secondary Abs used for immunocytochemistry and immunohistochemistry.

2.6. Imaging and image analysis

2.6.2. Confocal and super resolution imaging

Immunostainings were visualised with an LSM 780 AxioObserver (Zeiss) confocal microscope equipped with a Plan-Achromat 63x/1.4 oil or 40x/1.3 oil objective lens in 8 or 16-bit mode. All images revealed in super resolution Airyscan mode were taken in x1.8 zoom. Settings were kept constant within experiments and images analysed in ImageJ (National Institutes of Health).

2.6.2.1. Imaging of hippocampal neuron structures

All images taken of rat and mouse hippocampal neurons are maximum intensity projections of z-stacks with optical sections ranging from 0.144 – 0.512 µm and pixel dwell of 0.55 – 2.05 µs.

2.6.2.2. Imaging of $Ca_V2.2$_HA channels

All images taken of $Ca_V2.2$_HA channels in rat and mouse hippocampal neurons are maximum intensity projections of z-stacks. Rat hippocampal neurons transfected with $Ca_V2.2$_HA and mCherry were imaged as z-stacks in confocal mode with 0.066 µm

optical sections and 1.02 µs pixel dwell (Fig. 4.3). Mouse transfected neurons were imaged as a 4 x 4 tile and imaged in confocal model with 0.281 µm optical sections and 2.05 µs pixel dwell (Fig. 4.9). Endogenous $Ca_V2.2$_HA channels were imaged in super resolution mode with 0.17 µm optical sections and 2.05 µm pixel dwell (Fig. 4.10-12).

2.6.2.3. Imaging of $\alpha_2\delta$-1_HA

Images of $\alpha_2\delta$-1_HA and EV- transfected neurons were taken as 4 x 4 tile and z-stacks in confocal mode with 0.279 µm optical sections and 2.05 µs pixel dwell (Fig. 4.15).

2.6.2.4. Brain slice imaging and analysis

The overview tile scan of the $Ca_V2.2\_HA^{KI/KI}$ hippocampus (Fig. 3.6 A) was taken in super resolution mode at x20 with a pixel dwell of 2.64 µs. Images of the CA1 area were taken at x20 in confocal mode (Fig. 3.6 B and E). Fig. 3.6 C, D, F and G were taken as z-stacks in super resolution mode with 0.197 µm optical sections and 2.38 µs pixel dwell. Images for analysis were taken in super resolution mode with a pixel dwell of 2.05 µs at x63 magnification (Fig. 3.8-3.10). The $Ca_V2.2$_HA fluorescence was quantified using manual tracing of cells with the freehand brush tool in ImageJ (selection line width of 14). $Ca_V2.2$_HA fluorescence was measured using the freehand line tool and manually tracing the surface of the cell. Cells were identified by DAPI staining. The value of the mean pixel intensity was measured and data was normalised to values from the CA1 area or from values from P0/1 mice, respectively. Statistical analysis was performed using individual cells from two or three different brain slices.

2.7. Live cell Ca^{2+} imaging

Ca^{2+} imaging experiments were performed as described in a previous paper (Ferron *et al.* 2020b). Plated cells on 22 mm^2 coverslips were transferred to a laminar-flow perfusion and stimulation chamber (Imaging chamber with field stimulation series 20, multichannel systems) and mounted on an epifluorescence microscope (Axiovert 200 M, Zeiss) under continuous perfusion at 23 °C at 0.5 ml/min^{-1} with Ca^{2+} perfusion buffer containing (in

mM) 119 NaCl, 2.5 KCl, 2 $CaCl_2$, 2 $MgCl_2$, 25 HEPES (buffered to pH 7.4) and 30 glucose. In order to suppress postsynaptic activity, 10 µM 6-cyano-7-nitroquinoxaline-2,3-dione (CNQX, Sigma) and 50 µM D, L-2-amino-5-phosphonovaleric acid (AP5, Sigma) were included. For some experiments, irreversible $Ca_V2.2$ channel inhibitor ω-conotoxin GVIA (ConTx; 1 µM) was applied for 2 minutes before stimulation under continuous perfusion. Before imaging, cells were incubated in Ca^{2+} perfusion buffer for 20 min to wash out TTX. Images were acquired with an Andor iXon+ (model DU-897U-CS0-BV) back-illuminated EMCCD camera using OptoMorph software (Cairn Research, UK) with LEDs as light sources (Cairn Research, UK). Fluorescence excitation and collection was done through a 40 x 1.3 NA Fluar Zeiss objective using 450/50 nm excitation and 510/50 nm emission and 480 nm dichroic filters (for Sy-GCaMP6f) and a 572/35 nm excitation and low-pass 590 nm emission and 580 nm dichroic filters (for VAMP-mOr2). APs were evoked by passing 1 ms current pulses via platinum electrodes. Transfected boutons were selected for imaging by stimulating neurons with trains of 6 APs at 33 Hz using Digitimer D4030 and DS2 isolated voltage stimulator (Digitimer Ltd.). To measure calcium responses, neurons were stimulated with a single AP (repeated at least 5 times with 30 seconds time intervals to improve signal-to noise ratio) and then with 10 APs at 10 Hz to identify boutons for analysis. Synaptic boutons were identified by VAMP-mOr2 expression and defined as functional based on responsiveness to 200 APs stimulation at 10 Hz (here images were acquired at 2 Hz with 50 ms exposure). From each coverslip, a maximum of three fields of views were recorded. When ConTx was applied, only one field of view was imaged. Images were acquired at 100 Hz over a 512 x 266 pixel area in frame transfer mode (7 ms exposure time) and up to 75 putative synaptic boutons within the image field were selected for analysis using a 2 µm region of interest (ROI) and analysed in ImageJ (http://www.rsb.info.nih.gov/ij) using a custom-written plugin (http://www.rsb.info.nih.gov/ij/plugins/time-series.html) (Figure 2.5). In order to correct for background following 1 AP stimulation, the averaged fluorescence of

5 ROIs placed in non-transfected and non-responding areas was calculated (red box Fig 2.5). The corresponding averaged background fluorescence value was then subtracted from selected (up to 75) responding ROIs of the equivalent frame. *ΔF* was determined by subtracting the average of 6 points of the baseline fluorescence before stimulation (as described in (Kadurin *et al.* 2016)). To obtain *ΔF/F0*, *ΔF* was divided by the average of 6 points of the baseline fluorescence before stimulation. To improve the signal-to-noise ratio 1 AP recordings were repeated 5-8 times and values for each ROI were averaged from each recording. For presentational purposes, images were adjusted for brightness and contrast.

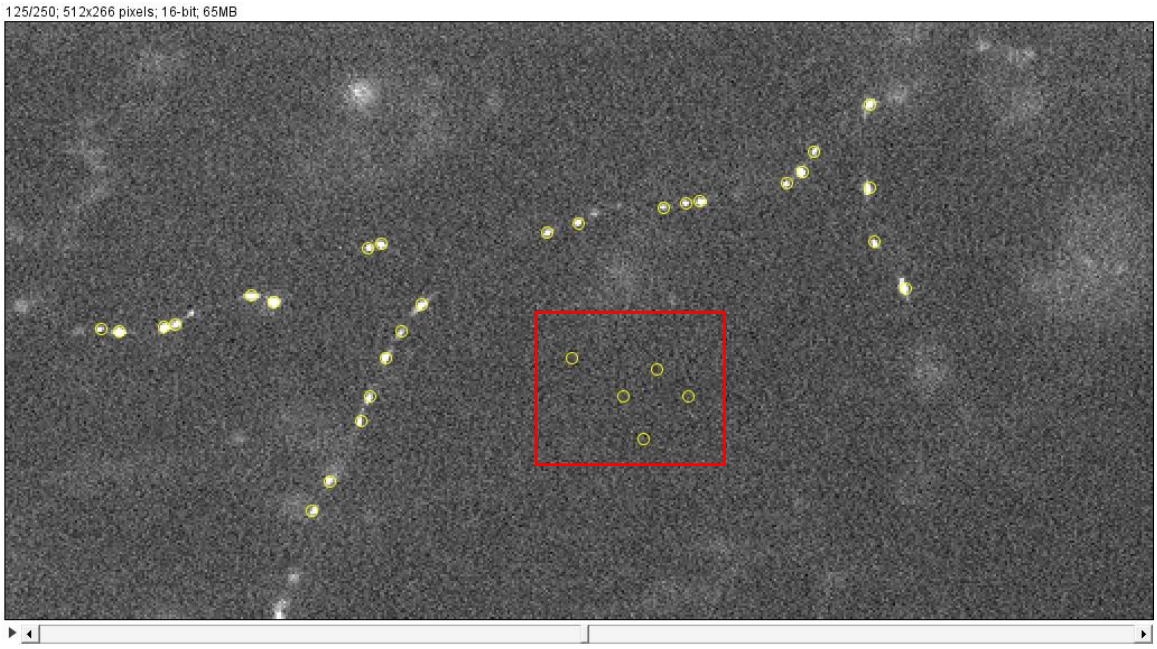

Figure 2. 5. Live cell imaging analysis. Up to 75 ROIs were selected based on their response to 10 AP stimulation in one field of view. Data was background adjusted by placing 5 ROIs in non-transfected areas (red box) of the field of view and subtracting the nonspecific background from the 75 ROIs. Changes in fluorescence were calculated as change of fluorescence intensity over baseline fluorescence before stimulation (*ΔF/F0).*

2.8. Sample numbers and statistical analysis

N numbers correspond to individual experiments and are stated with each figure. Statistical analysis was performed using t-tests, one-way ANOVA and 2way ANOVA in GraphPad Prism9 with suitable post-hoc analysis stated in each figure. Normality tests performed were Anderson-Darling test, D'Agostino & Pearson test, Shapiro-Wilk test and Kolmogorov-Smirnov test. Results were considered significant with a *P* value < 0.05. All data are shown as mean ± standard error of the mean (SEM). Biological replicates in Ca^{2+} imaging experiments refer to all fields of view from one hippocampal culture.

Material	Manufacturer	Cat #
AP5	Sigma-Aldrich	A5282
B27 Supplement	Gibco	17504044
Bovine serum albumin	First Link UK ltd	41-00-410
$CaCl_2$	Sigma-Aldrich	C1016
CNQX	Sigma-Aldrich	C239
DAPI	Molecular probes	Nl5995050
DNase I	Sigma-Aldrich	DN5025
DTT	Melford	MB1015
FBS	Invitrogen	16000044
Glucose	Sigma-Aldrich	G7528
GlutaMAX	Invitrogen	35050061
Glycine	Sigma-Aldrich	G8898
Goat serum	Invitrogen	16210-072
HBSS	Invitrogen	14175-053
HEPES	Invitrogen	15630-056
High-Capacity RNA-to-cDNA kit	Applied Biosystems	4387506
Igepal	Sigma-Aldrich	I3021
KCl	Sigma-Aldrich	P9333
L-Cysteine	Sigma-Aldrich	C7755
Lipofectamine 2000	Invitrogen	1168-027
MEM	Invitrogen	51200-046
$MgCl_2$	Sigma-Aldrich	M1028
NaCl	Sigma-Aldrich	S7653

Neurobasal A Media	Invitrogen	10888-022
Opti-MEM	Thermo Fisher	41965-039
Papain	Sigma-Aldrich	P4762
PBS	Sigma-Aldrich	P4417
PFA	Sigma-Aldrich	158127
Pierce High-Capacity Streptavidin Agarose	Thermo Fisher	20347
Poly-D-Lysine	Sigma-Aldrich	P6407
Premium Grade EZ-link Sulfo-NHS-LC-Biotin	Thermo Fisher	21335
Protease Inhibitors	Roche	11697498001
PVDF	Biorad	1620177
RNeasy lipid tissue mini kit	QIAGEN	74804
SDS	VWR	444062F
SDS -polyacrylamide gel electrophoresis	Invitrogen	EA0375
TaqMan Gene Expression Master Mix	Thermo Fisher	4331182
TritonX100	Thermo Fisher	28314
TTX citrate	Alomone	T-550
Vectashield	Vector Laboratories	H1000-10
ω-conotoxin GVIA	Alomone	SNX-124

Table 2. 3. Materials used.

Chapter 3. $Ca_V2.2$ channels during brain development

3.1. Introduction

Presynaptic Ca_V2 channels play pivotal roles for synaptic transmission by mediating fast neurotransmitter exocytosis via influx of Ca^{2+} into the active zone. In addition, Ca^{2+} influx via $Ca_V2.2$ channels may be important for neuronal development, contributing to neuronal migration and outgrowth (Kater and Mills 1991; Komuro and Rakic 1996; Komuro and Rakic 1992; Sann *et al.* 2008) as well as synaptogenesis (Nishimune *et al.* 2004).

The two main presynaptic Ca^{2+} channels at fast synapses, $Ca_V2.1$ and $Ca_V2.2$, exhibit different coupling properties to Ca^{2+} sensors (nanodomain and microdomain coupling, respectively), which is one of the key determinants of synaptic signalling (Eggermann *et al.* 2011). Therefore, the distribution of both subtypes is likely to be dynamic and dependent on synaptic requirements (Dolphin and Lee 2020). However, the study of the distribution of $Ca_V2.2$ channels at different synapse types, brain regions and developmental stages remains incomplete. This is largely due to the unavailability of reliable antibodies targeting functional cell surface $Ca_V2.2$ channels. In addition, it has been difficult to develop functional exofacially tagged $Ca_V2.2$ channels without altering its function (Altier *et al.* 2006). Finally, low endogenous expression levels of $Ca_V2.2$ channels at the synapse have also complicated their study.

Ca_V channel subtypes can be distinguished pharmacologically by their distinct susceptibility to inhibitors such as ω-conotoxin GVIA ($Ca_V2.2$) and ω-agatoxin IVA ($Ca_V2.1$). Based on findings utilizing these toxins combined with electrophysiological recordings, there is evidence for a developmental switch during the neonatal period mediating the transition from predominant $Ca_V2.2$ channels at the immature synapse to a dominance of $Ca_V2.1$ channels at many adult synapses (Scholz and Miller 1995; Miki *et al.* 2013). This has been shown at the mouse and rat calyx of Held in the brain stem, where synaptic transmission before hearing onset relies on loosely coupled $Ca_V2.2$ channels but requires $Ca_V2.1$ channels, tightly coupled to the exocytic release machinery

for rapid firing at the mature synapse (Iwasaki and Takahashi 1998; Fedchyshyn and Wang 2005). A similar developmental adaptation has also been described in neocortical (Bornschein *et al.* 2019) and hippocampal (Scholz and Miller 1995; Scholz and Miller 1996) cell culture systems, where a mixed population of both $Ca_V2.1$ and $Ca_V2.2$ channels was found at young synapses with a shift to predominant Ca^{2+} influx via $Ca_V2.1$ nanodomains in more mature synapses. Other studies in mouse hippocampal culture systems reported an equal contribution of both $Ca_V2.1$ and $Ca_V2.2$ channels to presynaptic Ca^{2+} transients (Brockhaus *et al.* 2019; Cao and Tsien 2010). Most synapses in the brain are likely to have a repertoire of $Ca_V2.1$, $Ca_V2.2$ and, to a lesser extent, $Ca_V2.3$ channel subtypes, enabling the diversification of Ca^{2+} influx to match distinct presynaptic responses to variations in activity and modulation (Ricoy and Frerking 2014).

The overall distribution of $Ca_V2.2$ channels at the different synapse types in the brain is still poorly understood. In the present study, qPCR and synaptosomal fractionation immunoblotting were used to study the mRNA expression and protein distribution of $Ca_V2.2$ channels, respectively, in four different brain regions of newborn (P0/1), young (P7) and adult mice (12 weeks). Additionally, the transgenic $Ca_V2.2\_HA^{KI/KI}$ mouse model with an exofacial HA-tag on the extracellular loop of $Ca_V2.2$ was used to study the distribution of $Ca_V2.2$ channels in the hippocampus at different ages using immunohistochemistry and super resolution microscopy.

3.2. $Ca_V2.2$ mRNA expression studies during postnatal brain development

3.2.1. Brain maturation is associated with a reduction of $Ca_V2.2$ channel mRNA

mRNA expression of $Ca_V2.2$ channels has previously been reported to be the highest in embryonic tissue from mouse cortex and hippocampus with levels decreasing as the brain matures (Schlick *et al.* 2010). To confirm these findings and expand on brain regions, this study analysed $Ca_V2.2$ mRNA expression from cortex (cx), hippocampus (hc), cerebellum (cb) and brain stem (bs) tissue, from mice aged P0/1, P7 and 12 weeks. The probe used to detect $Ca_V2.2$ mRNA targets all known $Ca_V2.2$ splice variants.

Figure 3.1 shows a similar decrease of $Ca_V2.2$ mRNA expression across all four brain areas as the brain matures with similar levels at P0/1 and P7 and low levels observed in the adult brain. In the cortex, levels of $Ca_V2.2$ mRNA in the adult were decreased by 60 ± 0.2 % compared to P0/1 (1 ± 0.4 at P0/1 vs 0.4 ± 0.2 in the adult; one-way ANOVA $P = 0.001$; Fig. 3.1 A). Adult hippocampal $Ca_V2.2$ levels were 42 ± 0.08 % lower compared tissue from P0/P1 (1 ± 0.1 at P0/1 vs 0.58 ± 0.08 in the adult, one-way ANOVA $P = 0.01$; Fig. 3.1 B). In cerebellum and brain stem, $Ca_V2.2$ mRNA levels were decreased by 74 ± 0.02 % and 81 ± 0.02 %, respectively, compared to levels in newborn mice (1 ± 0.12 and 1 ± 0.17 at P0/1 versus 0.26 ± 0.03 and 0.19 ± 0.02 in the adult in cerebellum and brain stem, one-way ANOVA with $P = 0.002$ and $P = 0.01$, respectively; Fig. 3.1 C and D). Values were normalised to internal control gene hypoxanthine-guanine phosphoribosyl transferase (HPRT). These results confirm previous findings of a decrease in $Ca_V2.2$ mRNA expression in all regions as the brain develops (Schlick *et al.* 2010).

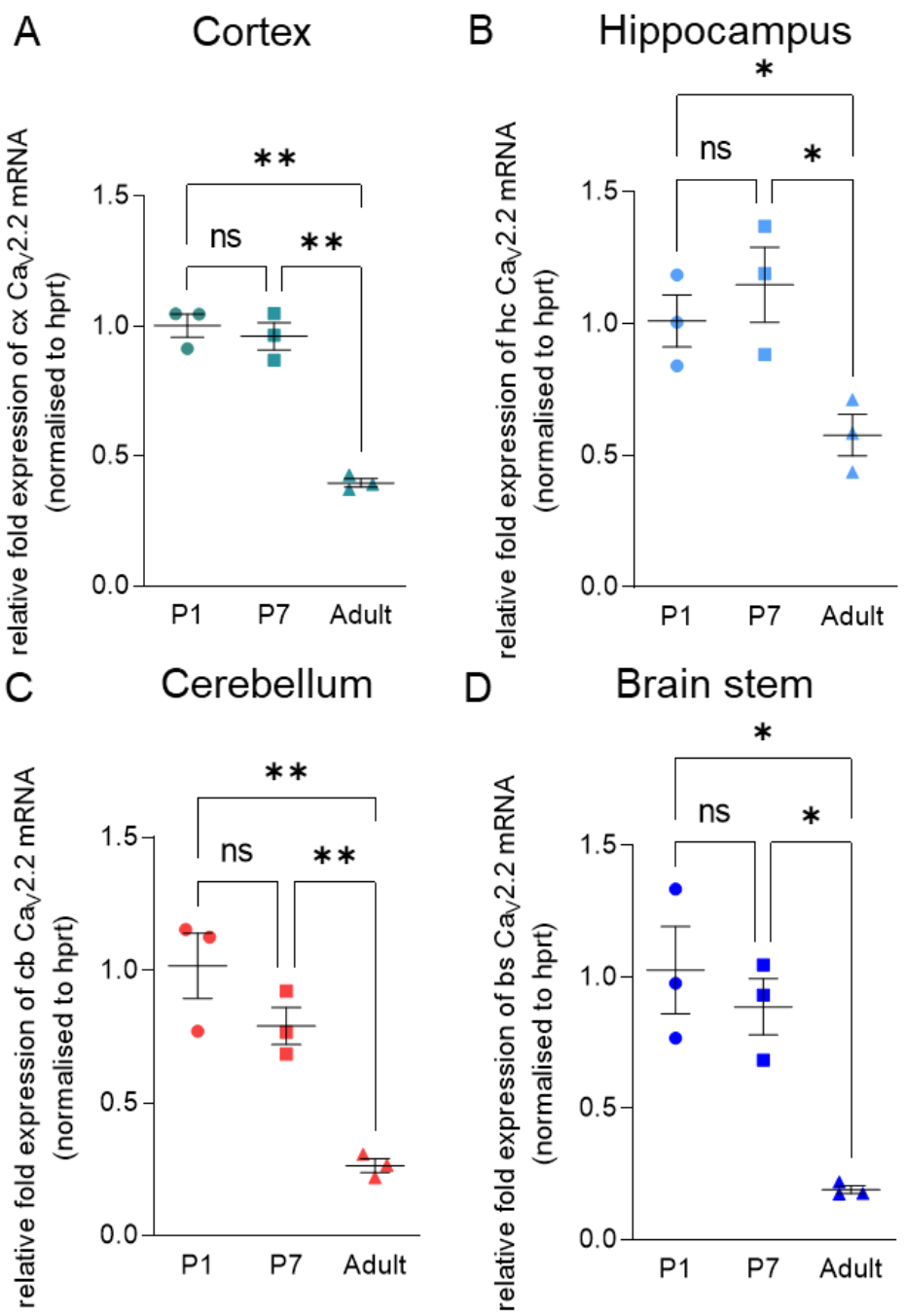

Figure 3. 1. $Ca_V2.2$ mRNA expression decreases as the brain matures.

(A-D) qPCR analysis of $Ca_V2.2$ mRNA in cortex (A), hippocampus (B), cerebellum (C) and brain stem (D) tissue of P0/1 and P7 immature brains and adult brains showed a significant decrease in $Ca_V2.2$ mRNA levels in the adult, n = 3 biological replicates, for P0/1 and P7 timepoints 2 brains were pooled, each n was assayed in triplicates. Data are shown as mean ± SEM. One-way ANOVA, Bonferroni post-hoc * = $P < 0.05$ ** = $P < 0.005$. ns = not significant.

3.2.2. Differential expression of $Ca_V2.2$ mRNA across different brain regions

To assess how $Ca_V2.2$ mRNA expression levels differ between the four regions at each timepoint during development, data were re-analysed and normalised to cortex values at P0/1, P7 and 12 weeks, respectively (Fig. 3.2). At P0/1, levels of $Ca_V2.2$ mRNA were similar across cortex, hippocampus, cerebellum and brain stem (Fig. 3.2 A). At P7, however, $Ca_V2.2$ levels were similar between cortex, hippocampus, and cerebellum, but there was a reduction of 38 % of the mRNA levels in the brain stem compared to cortical expression levels (1 ± 0.04 in cortex vs 0.62 ± 0.06 in brain stem, one-way ANOVA, P = 0.02; Fig. 3.2 B). In the mature brain, there was a stark difference between anterior and posterior area with highest levels of $Ca_V2.2$ mRNA expression in the cortex and hippocampus. In contrast, in the cerebellum and brain stem, mRNA levels were reduced by 40 ± 0.1 % and 65 ± 0.03 %, respectively (one-way ANOVA, Fig. 3.2 C).

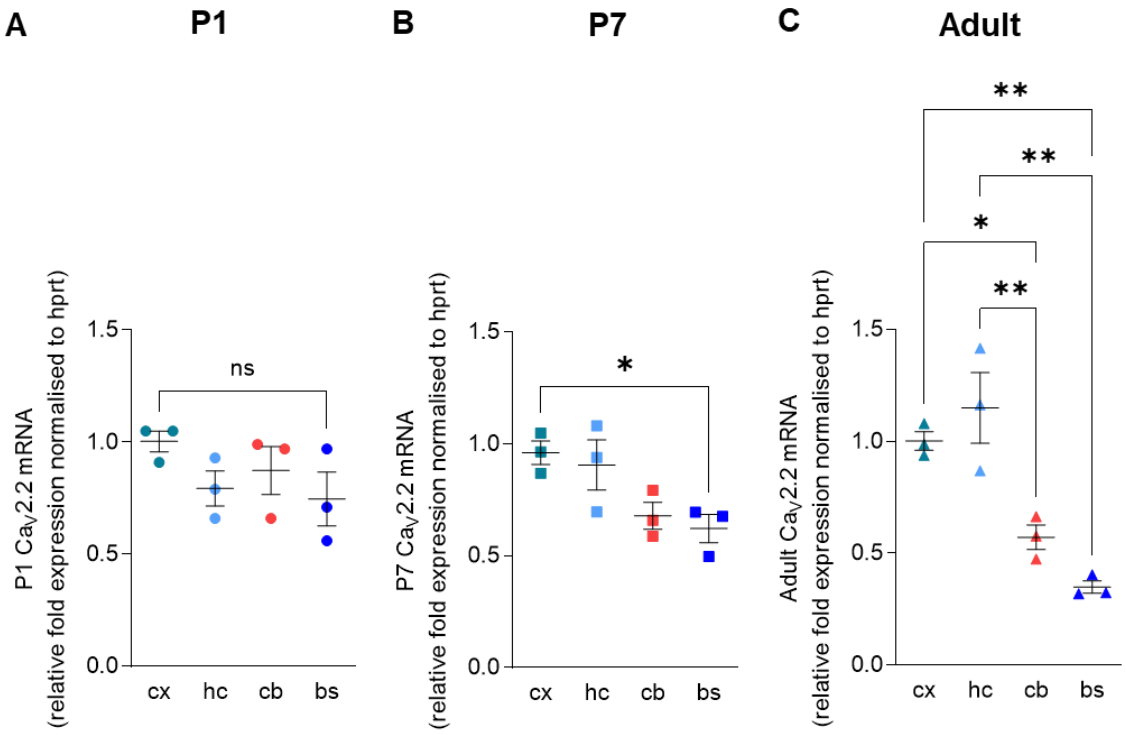

Figure 3. 2. Differential expression of $Ca_V2.2$ mRNA levels in different brain regions with most $Ca_V2.2$ mRNA in the adult cortex and hippocampus.

(A and B). At P0/1 and P7, mRNA levels of $Ca_V2.2$ were similar in all four brain regions, except for higher levels in the cortex compared to brain stem at P7. **(C)** In adult brains, $Ca_V2.2$ mRNA levels were significantly reduced in cerebellum (cb) and brain stem (bs) compared to cortex (cx) and hippocampus (hc). n = 3 biological replicates with 1 brain used per experiment, except for P0/1 and P7, for which 2 brains were pooled. Each experiment was assayed in triplicates. Data are shown as mean ± SEM and normalized to respective cortex values. One-way ANOVA, Bonferroni post-hoc * = $P < 0.05$ ** = $P < 0.005$. ns = not significant.

3.3. Subcellular analysis of $Ca_V2.2$ channel distribution

3.3.1. Brain synaptosome preparations to study distribution of synaptic proteins

Next, this study sought to examine the distribution and localisation of $Ca_V2.2$ channels during brain development of the same four brain regions used for qPCR experiments shown above. For this, tissue from mouse cortex, hippocampus, cerebellum and brain stem were used to study synaptic proteins using subcellular fractionation and western blotting.

First, the presence of the two isoforms of synaptic protein synapsin 1 and 2 was revealed to establish the successful purification of synapses (Fig. 3.3).

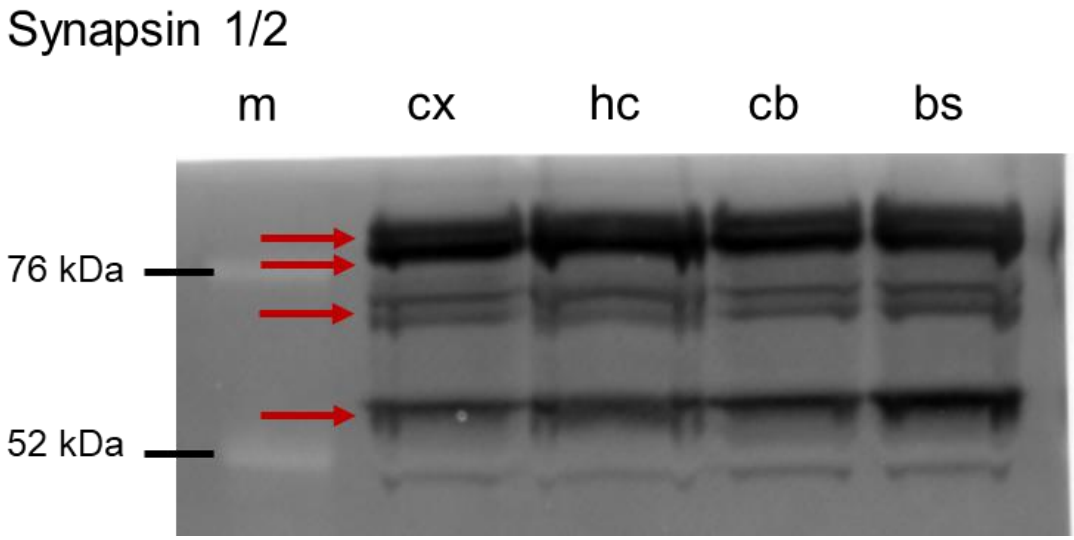

Figure 3. 3. Detection of synapsin 1/2 in synaptosome immunoblots.
Anti-synapsin 1/2 primary Abs were used to reveal the presence of synapses in tissue from cortex (cx), hippocampus (hc), cerebellum (cb) and brain stem (bs) at P0/1. Brains from 8 P0/1 mice were pooled to obtain sufficient protein concentrations. Four isoforms of synapsin 1 and 2 are shown at approximately 80, 86, 74 and 55 kDa (red arrows), m = molecular marker.

3.3.2. High abundance of $Ca_V2.2$_HA channels in the cortex and hippocampus of adult mice

Next, this approach was used to decipher the distribution of $Ca_V2.2$ channels at the synapses of the different brain regions. For this, tissue was extracted from $Ca_V2.2\_HA^{KI/KI}$ mice and synaptosomes were purified. Fig. 3.4 A and D show the protein levels of $Ca_V2.2$_HA in brain tissue at P0/1. At this age, levels of $Ca_V2.2$_HA were similar in all regions, though levels were slightly higher in the brain stem compared to the cortex (1.34 ± 0.02 in the brain stem compared to 1 in cortex, one-way ANOVA, $P = 0.03$; Fig. 3.4 A). In line with this, at P7 there was also an even protein distribution of $Ca_V2.2$_HA throughout the different brain regions (Fig. 3.4 B and E, one-way ANOVA). Strikingly, in the adult tissue, cortex and hippocampus revealed the highest amount of $Ca_V2.2$_HA channels. In contrast, levels of $Ca_V2.2$ channels in the cerebellum and brain stem were decreased by 90 ± 0.04 % and 89 ± 0.06 %, respectively, compared to cortical levels (1 in cortex, 0.89 ± 0.1 in hippocampus, 0.09 ± 0.04 in cerebellum and 0.14 ± 0.06 % in brain stem, one-way ANOVA, cortex vs hippocampus $P < 0.1$; cortex vs cerebellum $P = 0.001$; cortex vs brain stem $P = 0.004$; Fig. 3.4 C and D).

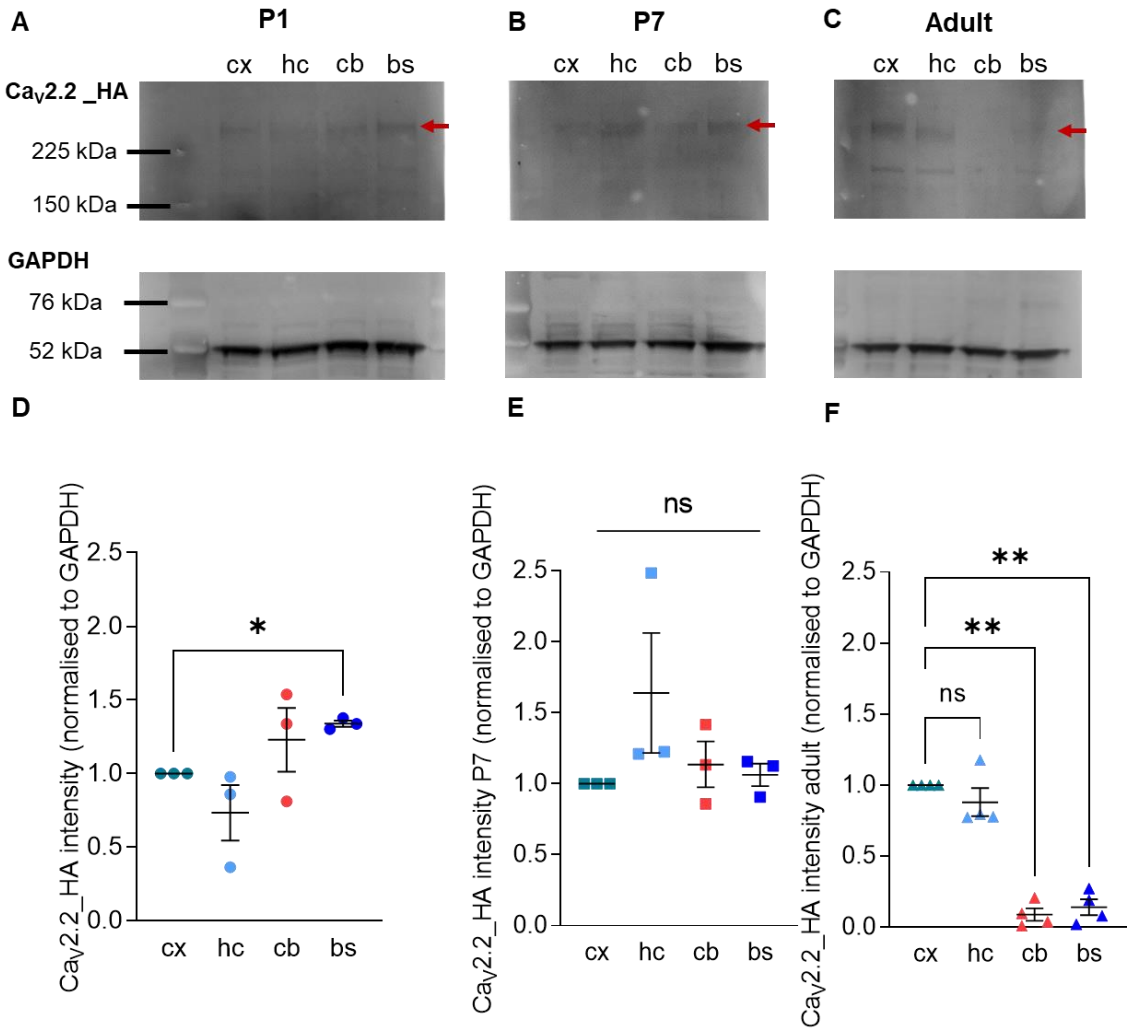

Figure 3. 4. High abundance of $Ca_V2.2$_HA channels in the adult cortex and hippocampus, whereas young mice have a more even distribution of $Ca_V2.2$ channels across the four brain regions.

(A-C) Immunoblots of synaptosomes from $Ca_V2.2$_$HA^{KI/KI}$ mice showing the expression of $Ca_V2.2$_HA (red arrow) (top) and GAPDH (bottom) for P0/1 (A), P7 (B) and adult mice (C). The molecular mass of $Ca_V2.2$_HA is 261 ± 1.2 kDa as determined by molecular weight markers. **(D)** Similar levels of $Ca_V2.2$ _HA in cortex (cx), hippocampus (hc), cerebellum (cb) and brain stem (bs) from P0/1 $Ca_V2.2$_$HA^{KI/KI}$ mice. Graphs show values from three biological replicates with 8 mice pooled for each set. Values are normalised to GAPDH values on the same gel. Data are shown as mean ± SEM. One-way ANOVA, Bonferroni multiple comparisons post-hoc test, cortex versus brain stem $P = 0.01$ **(E)** Similar levels of $Ca_V2.2$_HA in cortex, hippocampus, cerebellum and brain stem from P7 $Ca_V2.2$_$HA^{KI/KI}$ mice. Graphs show values from three biological replicates with 4

mice pooled for each set. Values are normalised to GAPDH values on the same gel. One-way ANOVA, Bonferroni multiple comparisons post-hoc test. **(F)** In adult mice, $Ca_V2.2$_HA levels were higher in the cortex and hippocampus compared to cerebellum and brain stem. Graphs show values from four biological replicates. Values are normalised to GAPDH values on the same gel. One-way ANOVA, Bonferroni multiple comparisons post-hoc test, cortex vs hippocampus $P = 0.67$; cortex vs cerebellum $P = 0.001$; cortex vs brain stem $P = 0.002$.

To confirm the protein band revealed with anti-HA antibody, an antibody targeting the intracellular epitope between loop II and III of $Ca_V2.2$ channels ($Ca_V2.2$ II-III loop Ab) was used on the same samples and is shown in Figure 3.5.

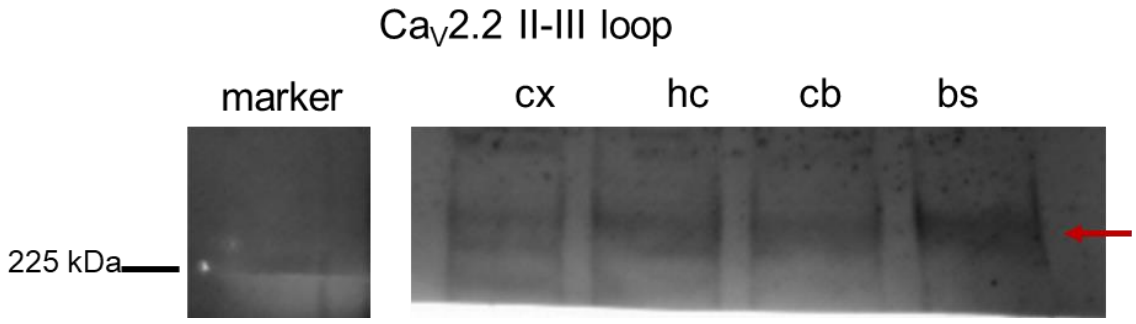

Figure 3. 5. $Ca_V2.2$ channels detected with intracellular $Ca_V2.2$ II-III loop Abs. Immunoblots of synaptosomes from $Ca_V2.2$_$HA^{KI/KI}$ mice showing the expression of $Ca_V2.2$ channels (red arrow) at P7 in the four brain regions cortex (cx), hippocampus (hc), cerebellum (cb) and brain stem (bs) revealed with $Ca_V2.2$ II-III loop Ab. The white hole is at the 225 kDa marker position (left side of blot).

3.4. Pilot experiments: Visualisation of $Ca_V2.2$_HA channels in the hippocampus of $Ca_V2.2$_$HA^{KI/KI}$ mice

Based on results from qPCR and subcellular fractionation studies showing relatively high levels of $Ca_V2.2$ channels in the hippocampus, this study next sought to analyse the distribution of $Ca_V2.2$ in hippocampal neurons. The generation of the $Ca_V2.2$_$HA^{KI/KI}$ with an extracellular HA tag on $Ca_V2.2$ channels allows for the first time to visualise $Ca_V2.2$ channels in brain tissue. Based on findings shown above, the hippocampus was chosen as a region of interest as high levels of $Ca_V2.2$ channels were detected in the adult mouse

hippocampus, compared to cerebellum and brain stem. Moreover, the well-established cell types and neuronal circuits of the hippocampus facilitated the study of $Ca_V2.2$ channel distribution in this brain area.

3.4.1. $Ca_V2.2$_HA channel distribution in the hippocampus of $Ca_V2.2$_HA$^{KI/KI}$ mice

To study the expression of $Ca_V2.2$_HA in the hippocampus, brain slices from the $Ca_V2.2$_HA$^{KI/KI}$ knock-in mice were stained using anti-HA antibodies and subsequently super resolution images were acquired (Fig. 3.6). This revealed $Ca_V2.2$_HA channels in the *stratum pyramidale* of the CA1 and CA3 region of the hippocampus (Fig. 3.6 A and B (CA1)). Shown in Fig. 3.6 C and D are CA1 pyramidal neurons at high magnification revealing the colocalization of $Ca_V2.2$_HA with presynaptic inhibitory marker vesicular GABA transporter (vGAT). As expected, in control tissue from wild type mice with untagged $Ca_V2.2$ channels, no HA signal could be detected, whereas the vGAT staining was similar to stainings from $Ca_V2.2$_HA$^{KI/KI}$ mice (Fig. 3.6 E-G).

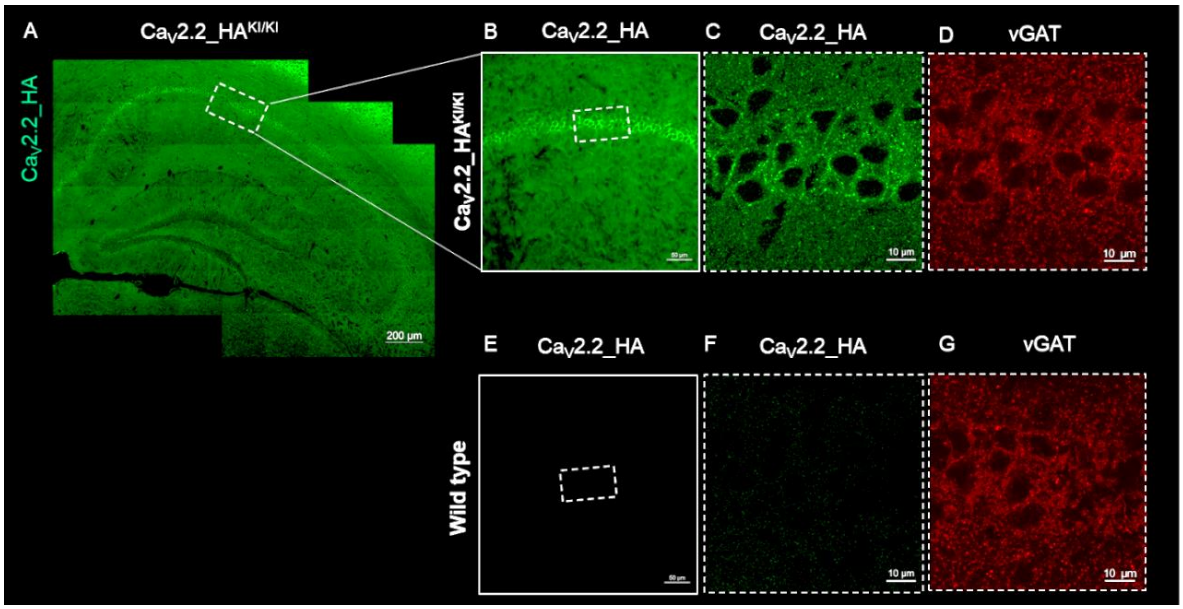

Figure 3. 6. Visualisation of $Ca_V2.2$_HA channels in pyramidal neurons of the CA1 region in the adult hippocampus of $Ca_V2.2$_HA$^{KI/KI}$ mice.

(A) $Ca_V2.2$_HA channels in the hippocampus of adult $Ca_V2.2$_HA$^{KI/KI}$ mice visualised using anti-HA antibodies (green). x20 super resolution tile scan. Scale bar = 200 µm. **(B)** $Ca_V2.2$_HA (green) signal in CA1 area of $Ca_V2.2$_HA$^{KI/KI}$ mice

x20 confocal imaging, scale bar = 50 µm. **(C)** $Ca_V2.2$_HA (green) x63 of CA1 somata of $Ca_V2.2$_$HA^{KI/KI}$ mice in super resolution, maximum intensity projection of z-stack with 0.197 µm optical sections, scale bar = 10 µm. **(D)** vGAT signal shown in red in CA1 in super resolution, maximum intensity projection of z-stack with 0.197 µm optical sections, scale bar = 10 µm. **(E-G)** Wild-type control images of $Ca_V2.2$_HA and vGAT at x20 confocal, scale bar = 50 µm (E) and x63 super resolution, maximum intensity projection of z-stack, scale bar = 10 µm (F and G).

3.4.2. Highest levels of $Ca_V2.2$ immunoreactivity in the adult CA1 region

To quantify the $Ca_V2.2$_HA signal in the hippocampus, the cell body layers of CA1, CA3 and DG were chosen as areas of interest (Fig. 3.7 A). Lines were drawn around cell bodies in these areas and their fluorescence intensity analysed using ImageJ (Fig. 3.7 B).

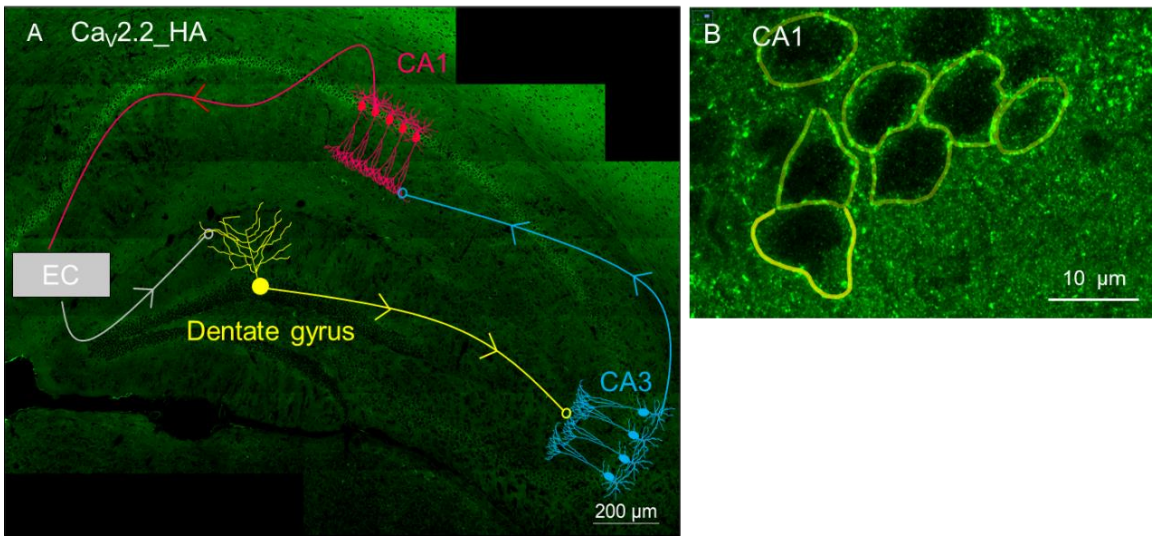

Figure 3. 7. CA1, CA3 and DG from the hippocampal trisynaptic circuit were chosen to analyse the distribution of $Ca_V2.2$_HA channels.

(A) The trisynaptic circuit in the hippocampus is a well-studied relay of synaptic transmission. Briefly, granule cells of the DG (yellow) receive input from the entorhinal cortex (grey, EC), the DG synapses onto pyramidal cells of the CA3 region (blue), which synapses to pyramidal cells of CA1 (red). Coronal section of 12 weeks old $Ca_V2.2\_HA^{KI/KI}$ mouse brain at x20 magnification imaged in super resolution mode. Scale bar = 200 µm. **(B)** An example image showing the analysis method. To analyse the intensity of the $Ca_V2.2$_HA signal around somata in the three regions, lines were drawn around cells onto the image (here shown as yellow lines) and their intensity was measured with ImageJ. Scale bar = 10 µm.

In hippocampi from mice at P0/1, immunostainings revealed the highest levels of $Ca_V2.2$_HA fluorescence in CA3 and the lowest in the DG (CA1 100 ± 1.13 % versus CA3 117.5 ± 1.90 versus DG 88.18 ± 1.70 %, one-way ANOVA, $P < 0.0001$; Fig. 3.8 A). Notably, due to their small size, animals were not transcardially perfused at P0/1, brains were only immersed in 4 % PFA/sucrose for two hrs before slicing into coronal sections of 20 µm thickness.

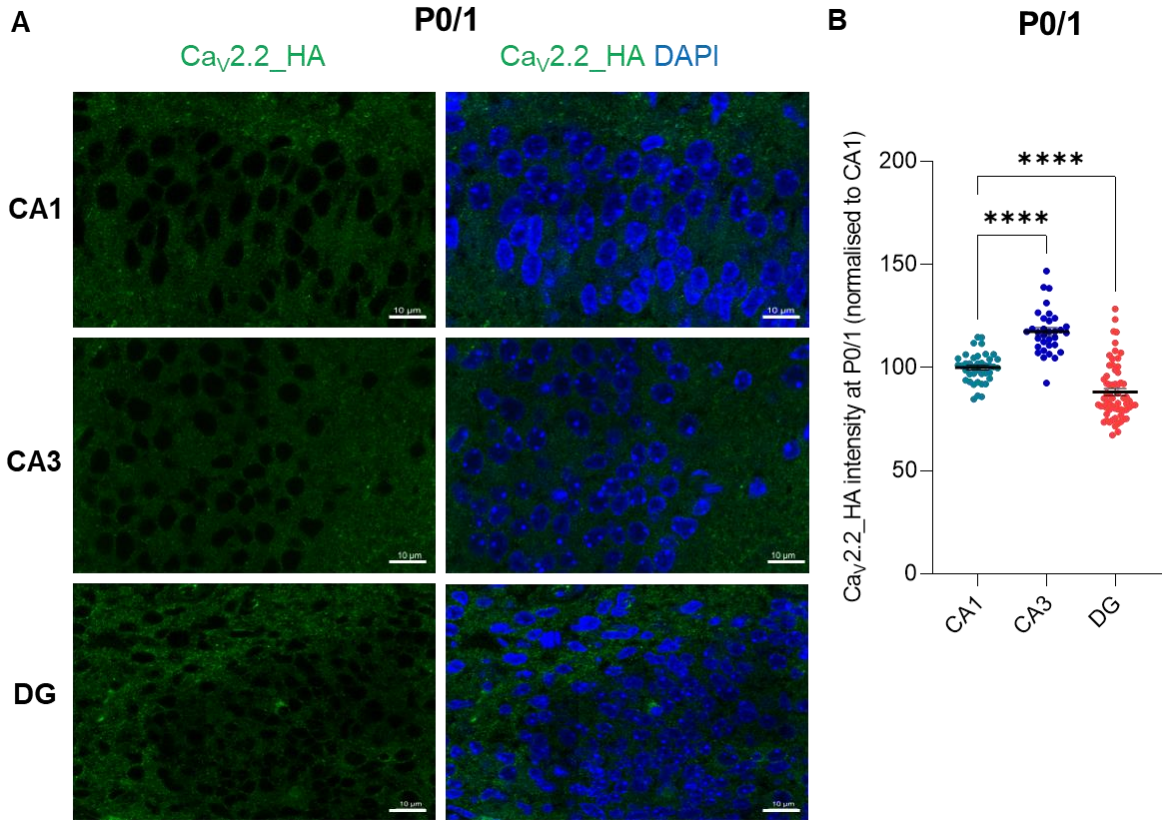

Figure 3. 8. Highest $Ca_V2.2$_HA channel fluorescence in hippocampal CA3 in neonatal brains.

(A) Images of the $Ca_V2.2$ _HA signal (green) and DAPI (blue) in CA1 (top row), CA3 (middle row) and DG (bottom row) in brains from P0/1 $Ca_V2.2\_HA^{KI/KI}$ mice. Scale bar = 10 µm, x63 tile scan in using super resolution mode. **(B)** The fluorescence intensity of $Ca_V2.2$_HA was the highest in the CA3 region and the lowest in DG. One-way ANOVA, Dunnett's multiple comparisons post-hoc test, $P < 0.0001$, n for CA1 = 40 neurons; n for CA3 = 33 neurons, n for DG = 64 neurons. Values were normalised to the average intensity of neurons in CA1 and shown as mean ± SEM. Neurons analysed were from two brain slices from one brain, for CA3 only one brain slice was included.

Analysis of the different hippocampal areas at P7 revealed levels of $Ca_V2.2$_HA fluorescence intensity similar to P0/1. Compared to CA1, $Ca_V2.2$_HA fluorescence was the highest in CA3 and lowest in the DG (CA1 100 ± 1.13 % versus CA3 110.6 ± 1.87 versus DG 62.62 ± 1.02 %, one-way ANOVA, $P < 0.0001$; Fig. 3.9 B).

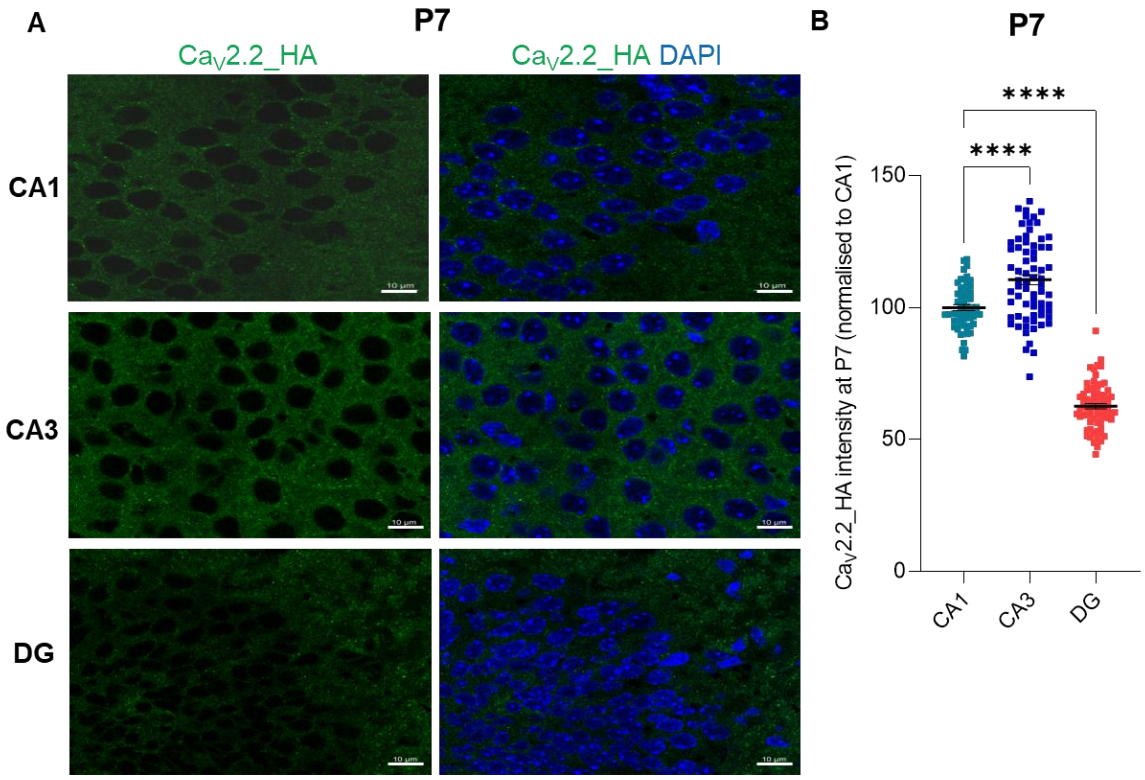

Figure 3. 9. Stronger $Ca_V2.2$_HA fluorescence intensity in CA1 and CA3 compared to cells in the DG at P7.

(A). Example images of the $Ca_V2.2$ _HA signal (green) and DAPI (blue) in CA1 (top row), CA3 (middle row) and DG (bottom row) in brains from P7 $Ca_V2.2$_$HA^{KI/KI}$ mice. Scale bar = 10 µm, x63 tile scan imaged in super resolution mode. **(B)** The fluorescence intensity of $Ca_V2.2$_HA was strongest in the CA3 area and significantly lower in the DG. One-way ANOVA, Dunnett's multiple comparisons post-hoc test, $P < 0.0001$, n for CA1 = 56 neurons; n for CA3 = 69 neurons, n for DG = 71 neurons. Values were normalised to the average intensity of neurons in CA1 and shown as mean ± SEM. Neurons analysed were from two brain slices from one brain.

In older mice aged 12 weeks, the signal of $Ca_V2.2$_HA in pyramidal cells of the CA1 region was significantly higher than in CA3 and DG (CA1 100 ± 2.70 % versus CA3 80.94 ± 3.46 versus DG 52.09 ± 1.08 %, one-way ANOVA, $P < 0.0001$; Fig. 3.10).

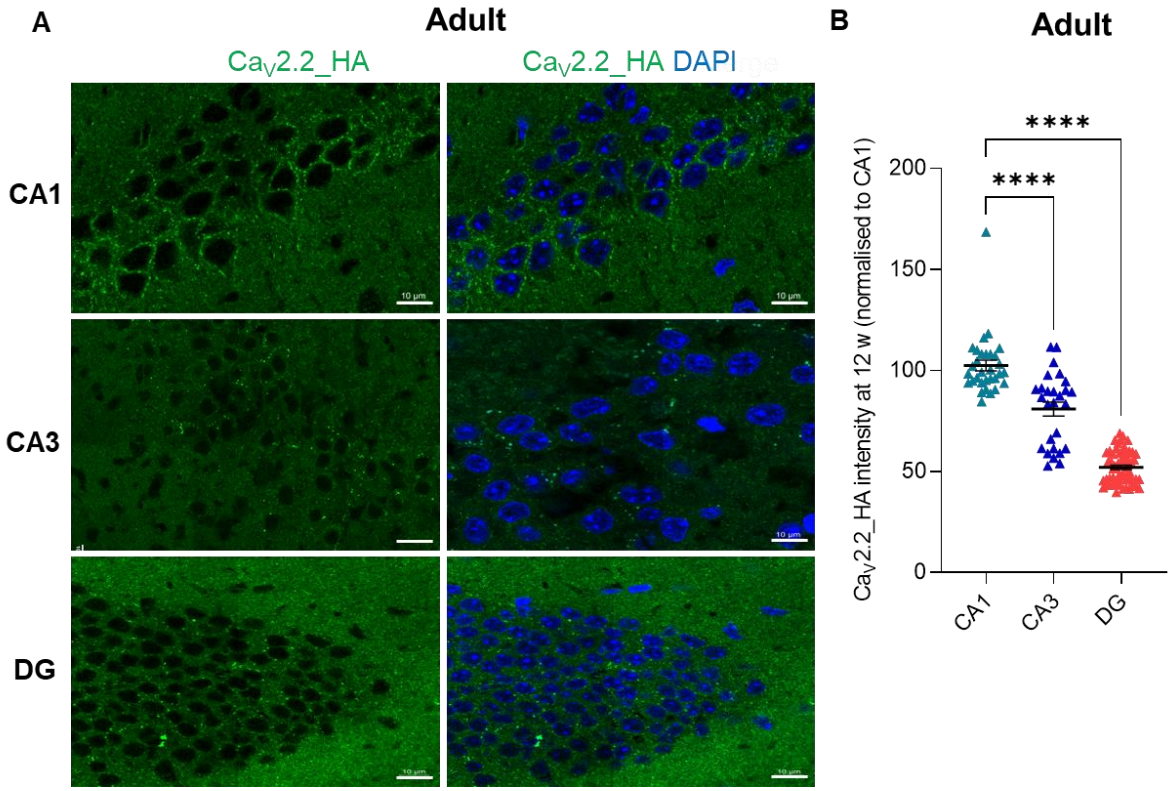

Figure 3. 10. $Ca_V2.2$_HA channel abundance highest in pyramidal cells of CA1 in the adult hippocampus.

(A) Images of the $Ca_V2.2$_HA signal (green) and DAPI (blue) in CA1 (top row), CA3 (middle row) and DG (bottom row) in brains from 12 weeks old $Ca_V2.2\_HA^{KI/KI}$ mice. Scale bar = 10 µm, x63 tile scan in super resolution mode. **(B)** The fluorescence intensity of $Ca_V2.2$_HA was strongest in the CA1 area and lowest in cells of the DG. One-way ANOVA, Dunnett's multiple comparisons post-hoc test, $P < 0.0001$, n for CA1 = 31 neurons; n for CA3 = 27 neurons, n for DG = 56 neurons. Values were normalised to the average intensity of neurons in CA1 and shown as mean ± SEM. Neurons analysed were from two brain slices from one brain.

Comparison of the fluorescence intensity of $Ca_V2.2$_HA channels across the ages for each region revealed increasing levels of $Ca_V2.2$_HA channel fluorescence intensity as the brain matures, with highest levels in CA1 and DG at 12 weeks and in CA3 at P7 and 12 weeks. There was a striking difference between the high levels of $Ca_V2.2$_HA channel abundance in the pyramidal cell layer of the CA1 region of adult mice compared to relatively low levels in mice at P0/1 (100 ± 1.13 % at P0/1 vs 227.10 ± 2.76 % at P7 versus 276.8 ± 5.61 % at 12 weeks, one-way ANOVA, $P < 0.001$; Fig. 3.11 A). Likewise, the levels of $Ca_V2.2$_HA channel fluorescence in CA3 were lowest at P0/1, peaked at P7 and remained at these levels in adult brains (100 ± 1.6 % at P0/1 vs 208.6 ± 3.53 % at P7 and 194.48 ± 8.3 % at 12 weeks, one-way ANOVA, $P < 0.001$; Fig. 3.11 B). In the DG, levels of $Ca_V2.2$_HA channels were highest at 12 weeks, decreased at P7 and reached the lowest point at P0/1 (100 ± 1.83 % at P0/1 vs 157.70 ± 2.56 % at P7 and 167.00 ± 3.45 % at 12 weeks, one-way ANOVA, $P < 0.001$; Fig. 3.11 C).

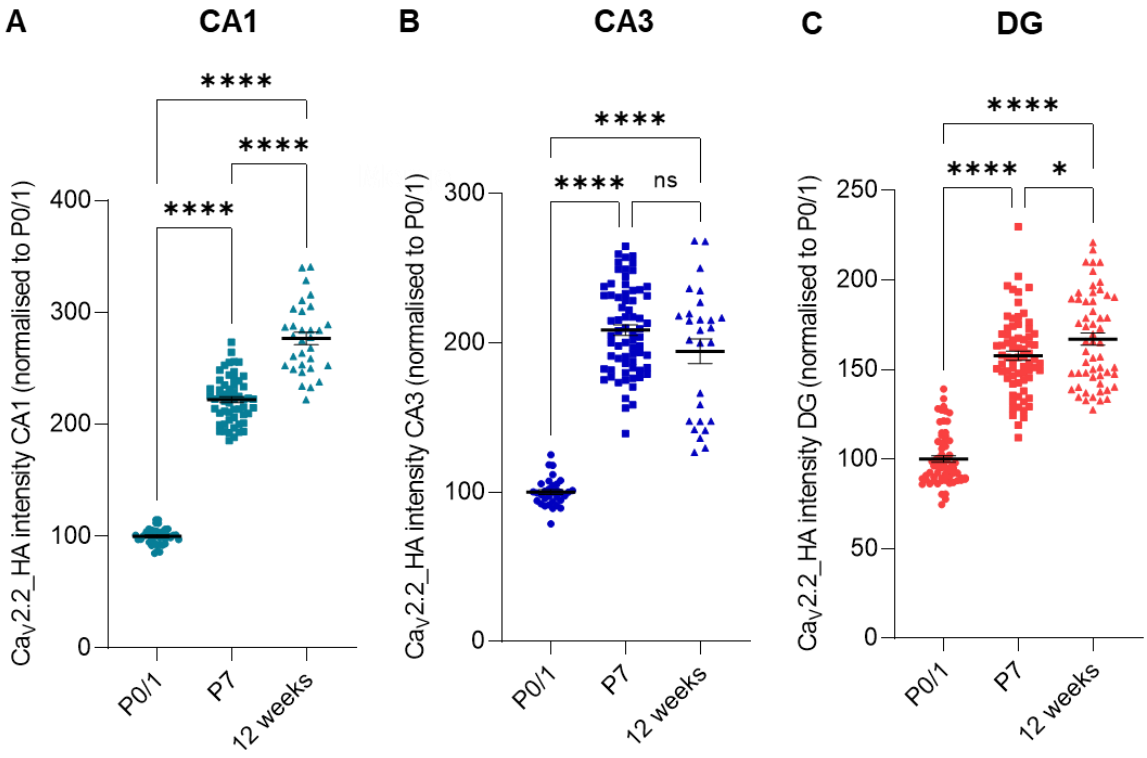

Figure 3. 11. $Ca_V2.2$_HA channel abundance in the hippocampus increases as the brain matures.

(A) $Ca_V2.2$_HA intensity in CA1 increased as the brain matures with the strongest fluorescence intensity at 12 weeks, one-way ANOVA, Tukey's post hoc, $P < 0.001$, n for P0/1 = 40 neurons; n for P7 = 56 neurons; n for 12 weeks = 31 neurons. **(B)** $Ca_V2.2$_HA intensity in CA3 increased as the brain matures. One-way ANOVA, Tukey's post hoc, $P < 0.001$, n for P0/1 = 33 neurons, n for P7 = 69 neurons; n for 12 weeks = 27 neurons. **(C)** Highest levels of $Ca_V2.2$_HA channels in the DG at 12 weeks compared to P0/1. One-way ANOVA, Tukey's multiple comparisons post-hoc test, $P < 0.0001$, n for P0/1 = 65 neurons; n for P7 = 71 neurons, n for 12 weeks = 56 neurons. Values were normalised to the average intensity of neurons at P0/1 and shown as mean ± SEM. Neurons analysed were from two brain slices from one brain. ns = not significant.

3.5. Summary and Discussion

In the present study the expression and distribution of presynaptic $Ca_V2.2$ channels in different brain regions at different ages was assessed.

First, using qPCR, a decrement in relative $Ca_V2.2$ mRNA expression from the immature new-born brain to the mature brain was shown. mRNA was extracted from cortex, hippocampus, cerebellum and brain stem of mice at different ages and expression patterns of $Ca_V2.2$ mRNA revealed by normalising CT values to those of internal control gene HPRT, shown to yield efficiency levels of 90 % (see Materials and Methods section). Here, it was shown that the $Ca_V2.2$ mRNA expression was the lowest in brain tissue from adult mice when compared to younger developmental stages. This decrease during brain maturation is in line with previous reports on gene expression of the different Ca_Vs and their subunits (Schlick *et al.* 2010). Furthermore, a decrease is unsurprising as one would not assume a high turnover of $Ca_V2.2$ channels at the mature synapse, where the expression of proteins of the active zone is more stable compared to young synapses (Südhof 2018). In contrast, the brain at P0/P1 is still immature and is likely to require an abundance of mRNAs of various synaptic proteins during maturation of synapses and circuits. These data also support the hypothesis that during a developmental switch, $Ca_V2.2$ channels are downregulated and potentially replaced by $Ca_V2.1$ as the predominant presynaptic Ca^{2+} channel. It is interesting, that when comparing $Ca_V2.2$ mRNA levels between different brain regions of the same age, that in the adult murine brain the expression level is higher in cortex and hippocampus than in cerebellum and brain stem. This finding suggests a developmental regulation of $Ca_V2.2$ channels that may be dependent on the brain region.

Findings on mRNA expression levels do not necessarily correspond to translated protein levels in the cell or their expression levels at the plasma membrane. Therefore, this work next sought to reveal the distribution of $Ca_V2.2$ channel proteins in the same brain regions at different maturity stages. To measure protein levels, a subcellular

fractionation technique was used which allows the purification of crude synaptosomes from brain tissue using differential centrifugation steps (Kato *et al.* 2007). To detect endogenous $Ca_V2.2$ channels, brains from the $Ca_V2.2\_HA^{KI/KI}$ mice with an exofacial HA tag on $Ca_V2.2$ channels were used. The validity of this mouse model has been presented in (Nieto-Rostro *et al.* 2018) and the successful purification of synaptosomes is shown by the immunoblots of synapsin 1/2 (Fig 3.3). Moreover, the specificity of the HA signal was confirmed using anti $Ca_V2.2$ II-III loop antibody (Ferron *et al.* 2014), which revealed bands of the same size as the HA antibodies targeting $Ca_V2.2\_HA$. In immunoblots of brain tissue from cortex, hippocampus, cerebellum and brain stem in younger mice, at P0/1 and P7, the distribution of $Ca_V2.2\_HA$ channels appeared similar across the different regions, with higher levels in the brain stem compared to the cortex at P7. However, in adult mouse brains, there were strikingly higher levels of $Ca_V2.2\_HA$ channels in the cortex and hippocampus compared to the posterior brain.

These relatively high levels of $Ca_V2.2$ channels in the mature versus immature hippocampus were partially confirmed performing immunohistochemical stainings and super resolution Airyscan imaging in different areas of the hippocampus. For this, the exofacially tagged $Ca_V2.2\_HA^{KI/KI}$ mice were used at different ages and revealed $Ca_V2.2\_HA$ tagged channels in the hippocampus, whereas in the wild-type control brain slices no signal was detected using the anti-HA antibody. Analysis of the fluorescence intensity of $Ca_V2.2\_HA$ in pyramidal cells in the CA1 and CA3 area and of granule cells in the DG revealed the highest $Ca_V2.2\_HA$ channel abundance in CA1 (12 weeks) and CA3 (P7 and P0/1). When comparing the $Ca_V2.2\_HA$ channel signal from each region across ages, it became apparent that $Ca_V2.2\_HA$ channel abundance increases at the brain matures, as levels at 12 weeks were the highest in all regions. Notably, more experiments with different biological replicates need to be performed in order to obtain reliable data from these experiments. Moreover, using identical protocols for studying aspects of brain development is often challenging as brains usually have different sizes

and tissue properties at different maturity stages. For example, due to limitations on anaesthetic procedures in P0/1 mice, they could not be transcardially perfused and their brains were fixed by immersion in 4 % PFA/sucrose for two hours. This might have had an impact on the $Ca_V2.2$_HA channel staining. Moreover, one cannot clearly conclude from these immunostainings if the detected $Ca_V2.2$_HA signal is on the cell surface of the somata of the pyramidal or granule cells, respectively, or if the signal is from neurons that synapse onto the respective soma. To further elucidate this, excitatory or inhibitory synapse markers should be included with $Ca_V2.2$_HA labelling in future stainings.

The findings presented here are exciting for several reasons. First, data from synaptosome experiments and immunohistochemistry data correlate with results from qPCR experiments where $Ca_V2.2$ mRNA expression levels were relatively similar in brains from younger mice, but in adult mice the expression of $Ca_V2.2$ mRNA was higher in cortex and hippocampus compared to cerebellum and brain stem. Second, the combination of gene expression and protein level studies suggest an important role of $Ca_V2.2$ channels in cortical and hippocampal brain regions in the adult brain, whereas $Ca_V2.2$ channels may be of less importance for synaptic transmission in adult cerebellum and brain stem (Fedchyshyn and Wang 2005; Iwasaki *et al.* 2000). Third, this work presents the first visualisation of endogenous $Ca_V2.2$ channels in brain slices using the $Ca_V2.2\_HA^{KI/KI}$ mouse model, which requires more data acquisition for reliable quantification.

Presynaptic Ca_V2 channels are organised in micro-or nanodomains around a vesicle site which implies tight or loose coupling to the synaptic vesicle release machinery, respectively. Both $Ca_V2.1$ and $Ca_V2.2$ channels have been reported to be loosely coupled, whereas only $Ca_V2.1$ channels support nanodomain coupling (Kusch *et al.* 2018). During synaptic maturation coupling distance undergoes substantial tightening, as $Ca_V2.1$ nanocoupling becomes the predominant Ca^{2+} channel in the cerebellum (Forsythe *et al.* 1998; Iwasaki *et al.* 2000; Fedchyshyn and Wang 2005;

Kusch *et al.* 2018), and neocortex (Bornschein *et al.* 2019). In the cerebellum, this developmental transition was shown to be mediated by Munc13-3, as its deletion abolished the nanopositioning of $Ca_V2.1$ channels at the rat postnatal synapse (Kusch *et al.* 2018). This transition from an initial microdomain coupling supported by both $Ca_V2.1$ and $Ca_V2.2$ channels to tighter nanodomain coupling at the mature synapse, exclusively supported by $Ca_V2.1$ channels, remains to be demonstrated in regions other than the cerebellum, brain stem and neocortex.

The data presented here show $Ca_V2.2$ channels at hippocampal and cortical synapses, as previously reported (Luebke *et al.* 1993; Wheeler *et al.* 1996; Cao and Tsien 2010; Brockhaus *et al.* 2019; Ferron *et al.* 2020a; Iwasaki *et al.* 2000). It is likely that certain mature synapses use nanodomain coupling whereas others rely on a mix of both subtypes in a circuit and pathway-specific matter (Eggermann *et al.* 2011; Dolphin and Lee 2020). For example, PV^+ interneurons signalling onto hippocampal cells exhibit tight coupling, whereas CCK^+ interneurons synapsing onto the same hippocampal cells exhibit lose coupling (Hefft and Jonas 2005; Bucurenciu *et al.* 2008). More diversified Ca^{2+} signalling at the presynapse may allow more dynamic synaptic adaptations as required during Hebbian or homeostatic synaptic plasticity. In addition to their different coupling distances, $Ca_V2.1$ and $Ca_V2.2$ channels are also subject to different regulation, for example by G-proteins (Brody and Yue 2000; Scheuber *et al.* 2004; Dolphin 2003b).

Together, these data support the notion that during development, $Ca_V2.2$ channels become less prominent at the presynapse. However, findings presented here limit this developmental adaptation to the cerebellum and brain stem area of the brain, as no decrease was detected in the adult cortex and hippocampus. In contrast, $Ca_V2.2$ protein levels were found to be the highest in the cortex and hippocampus, with a strong signal in the pyramidal cell layers of the CA1 and CA3 area in the hippocampus from pilot immunohistochemical experiments. As hippocampal neurons are known to be highly plastic, enabling learning and memory processes, $Ca_V2.2$ channels likely contribute to

Ca^{2+} flux at all developmental stages. A combination of different presynaptic Ca_V2 channels with different coupling properties, activity-dependent facilitation and G-protein mediated inhibition likely cooperatively contributes to Ca^{2+} flux allowing dynamic changes in synaptic output depending on synaptic activity.

Chapter 4. $Ca_V2.2$ channels in hippocampal cultures and live cell Ca^{2+} imaging

4.1. Introduction

Presynaptic Ca_V2 channels mediate Ca^{2+} influx into the presynaptic terminal, triggering neurotransmitter release and synaptic transmission. $Ca_V2.1$ and $Ca_V2.2$ are the two main channel types controlling Ca^{2+} flux at the presynapse in the mammalian brain (Dolphin and Lee 2020). The precise distribution of both channel types at different synapses and in different contexts, such as during brain development and plasticity, remains to be fully understood. Here, cell culture systems from rat and mouse hippocampal neurons were used to visualise transfected $Ca_V2.2$ channels. In addition, endogenous $Ca_V2.2$ channels were visualised in hippocampal neurons from the transgenic $Ca_V2.2\_HA^{KI/KI}$ mouse. Neurons were also transfected with Sy-GCaMP6f, a fast genetically encoded Ca^{2+} indicator which reports changes in Ca^{2+} flux after electrical stimulation with APs (Chen *et al.* 2013; Ferron *et al.* 2020a) (Fig. 4.1).

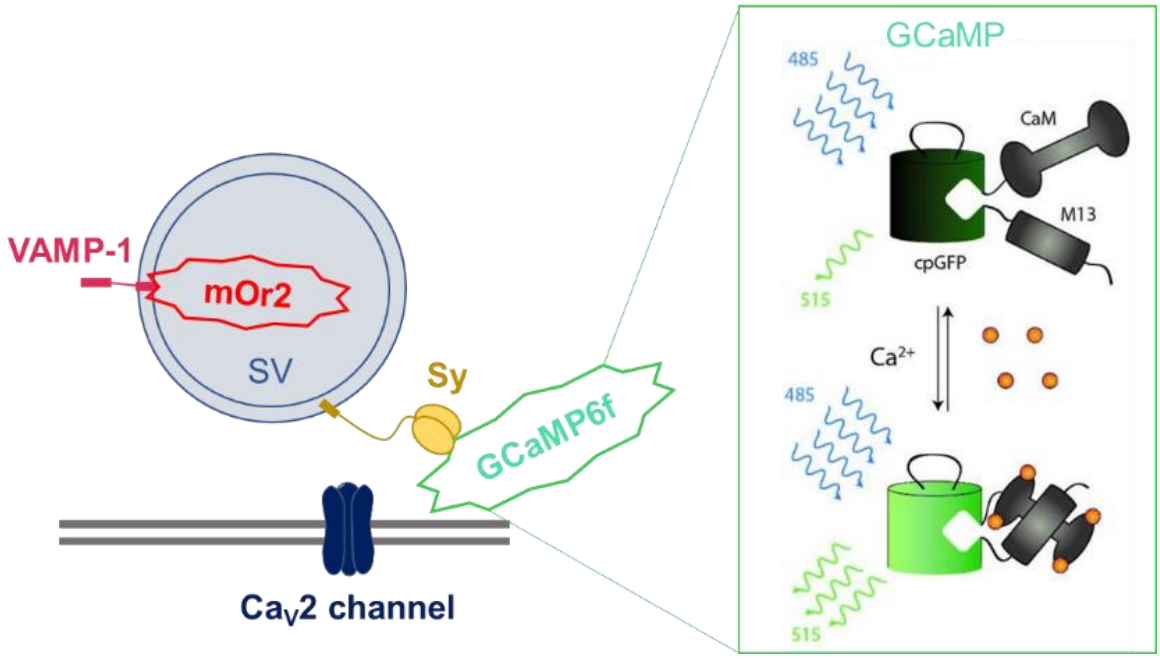

Figure 4. 1. Sy-GCaMP6f and VAMP-mOr2 as functional presynaptic markers for live cell Ca^{2+} imaging experiments.

Sy-GCaMP6f changes fluorescence upon Ca^{2+} binding to CaM which is measured as $\Delta F/F_0$. Changes in VAMP-mOr2 fluorescence indicate which boutons release synaptic vesicles. SV = synaptic vesicle, Sy = synaptophysin, cpGFP = circularly permuted green fluorescent protein. From (Broussard *et al.* 2014).

GCaMP6f consists of modified green fluorescent protein (GFP), Ca^{2+} chelator CaM and CaM-interacting M13 peptide. Ca^{2+} binding to CaM causes a conformational change in GCaMP6f, resulting in increased in GFP fluorescence, measured as change in fluorescence (ΔF). In the absence of Ca^{2+} flux, GFP is kept in a low-fluorescent conformation.

Here, GCaMP6f coupled to presynaptic protein synaptophysin was used to ensure the presynaptic localisation of the Ca^{2+} reporter, associated with synaptic vesicles (Dreosti *et al.* 2009). Moreover, cells were transfected with the preysynaptic protein VAMP tagged with pH-sensitive mOr2, which fluoresces after synaptic vesicle exocytosis, thereby allowing the distinction between neurotransmitter-releasing and non-releasing boutons (Ferron *et al.* 2020a). The contribution of $Ca_V2.2$ channels to Ca^{2+} flux was determined by application of $Ca_V2.2$-specific inhibitor ConTx. Using this system, Ca^{2+} flux in mouse and rat hippocampal neurons was examined in less mature neurons at day *in vitro* (DIV) 14-17 and in more mature neurons at DIV 18-22.

4.2. Rat hippocampal cultures

To study $Ca_V2.2$ channels and presynaptic Ca^{2+} transients in central synapses, hippocampal cultures were used as they recapitulate major features of neural network development (Dotti, 1988). Initially, hippocampal cell cultures from newborn rats were characterized using immunocytochemistry. To visualise the presence of both neurons and astrocytes in primary cultures from P0/1 rat hippocampi, antibodies targeting neuronal microtubule associated protein 2 (MAP2) and astrocytic glial fibrillary acidic protein (GFAP) were applied (Fig. 4.2). Additionally, antibodies against excitatory presynaptic marker vesicular Glutamate transporter 1 (vGluT1) and postsynaptic marker Homer revealed the presence of synapses in these cultures (Fig. 4.3).

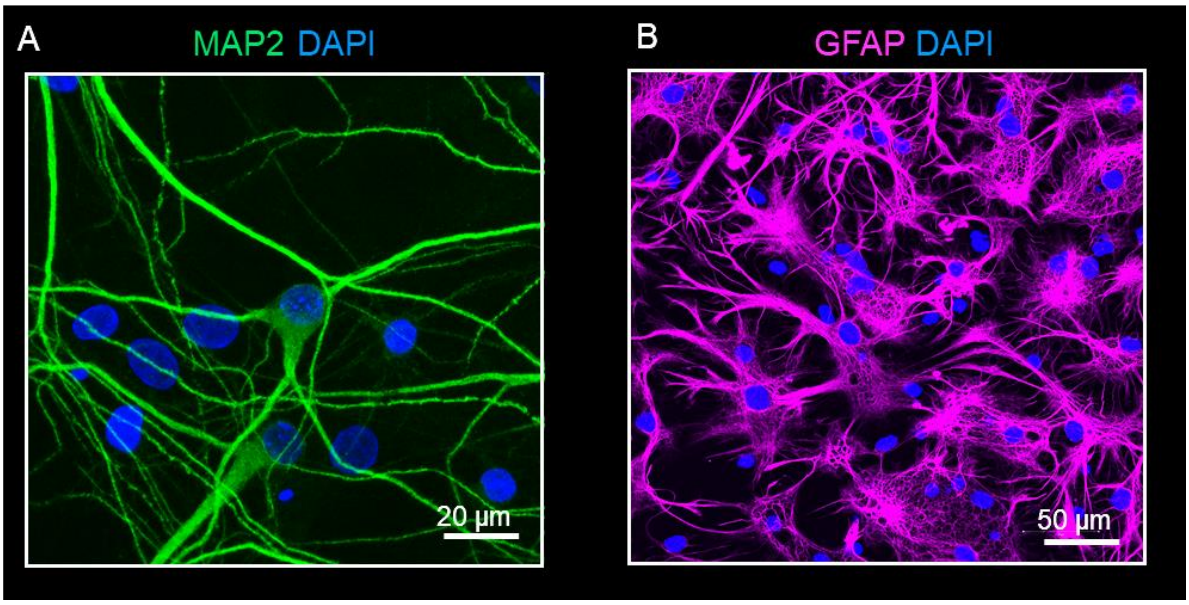

Figure 4. 2. Visualisation of rat hippocampal neurons and astrocytes *in vitro*. **(A)** Neuronal staining using MAP2 antibodies (green) and nuclear marker DAPI (blue) at DIV 19. x63, maximum intensity projection of z-stack. Scale bar = 20 µm. **(B)** Glial fibrillary acidic protein (GFAP) antibodies reveal the presence of astrocytes (magenta) and DAPI (blue) at DIV 14. Super resolution mode, x20, maximum intensity projection of z-stack and tile scan. Scale bar = 50 µm.

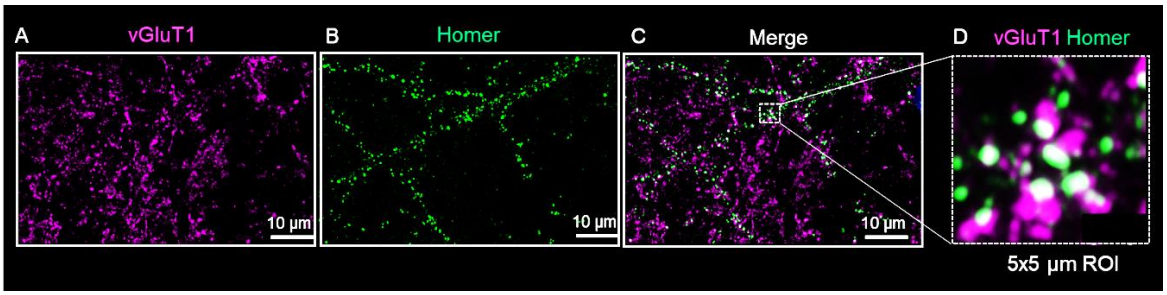

Figure 4. 3. Pre- and postsynaptic structures in cultured hippocampal neurons.

(A-C) Excitatory presynaptic marker vGluT1 (magenta, A) and postsynaptic marker Homer (green, B) and merged (C) at DIV 14. Super resolution x63, maximum intensity projection of z-stack; scale bar = 10 µm. **(D)** 5x5 µm subset ROI reveals the close proximity between vGluT1 and Homer at a putative synapse.

4.2.1. Visualisation of transfected $Ca_V2.2$ channels in hippocampal neurons

Overexpression of wild type or genetically modified proteins is a common technique to study their expression and distribution in cells. This is especially useful when there is a lack of viable antibodies against the endogenous protein, as it is the case for $Ca_V2.2$ channels. Hippocampal cells were transfected with cDNA of $Ca_V2.2$ channels with an extracellular tandem HA tag ($Ca_V2.2$_HA, (Cassidy *et al.* 2014)) in order to visualise channels *in vitro*. Additionally, auxiliary subunits $\alpha_2\delta$-1 and β1b were included in the transfection mix, as they are both required for trafficking and correct functioning of $Ca_V2.2$ channels at the synapse (Cassidy *et al.* 2014; Kadurin *et al.* 2016; Waithe *et al.* 2011). Transfection marker mCherry was used for selection of transfected neurons. Fig. 4.4 shows transfected $Ca_V2.2$_HA channels in the soma and along the processes of a mCherry-positive neuron at DIV 19.

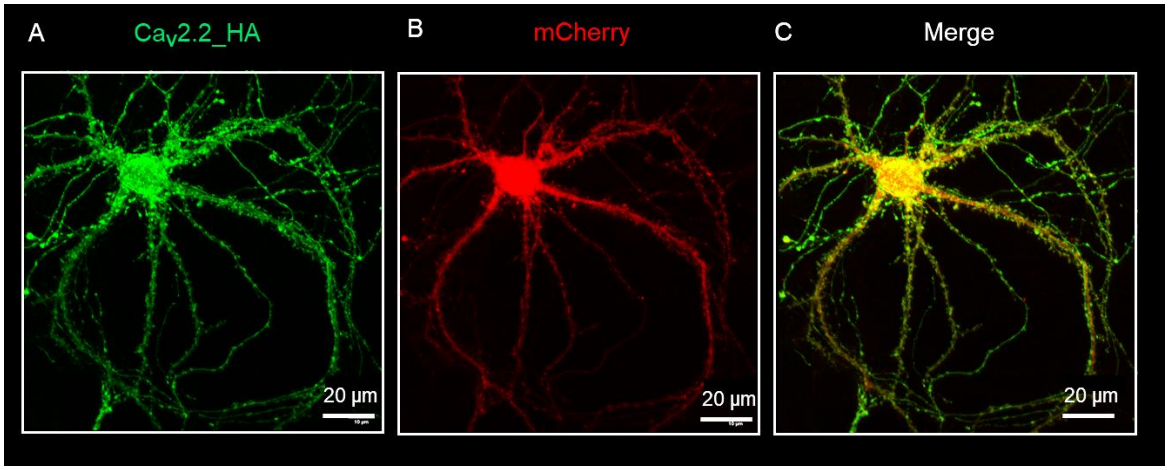

Figure 4. 4. Transfected $Ca_V2.2$_HA channels in hippocampal neurons.
(A) Anti-HA antibodies were used to detect $Ca_V2.2$_HA (green) in neurons transfected with $Ca_V2.2$_HA, $\alpha_2\delta$-1, β1b in permeabilised conditions at DIV 19. **(B)** As a transfection marker, mCherry was used (red). **(C)** Merge image of $Ca_V2.2$_HA and mCherry signal. x63, maximum intensity projection of z-stack. Confocal mode, scale bar = 20 µm.

4.2.2. Sy-GCaMP6f live cell Ca^{2+} imaging and VAMP-mOr2 vesicular release imaging in rat hippocampal neurons

To study Ca^{2+} dynamics and the role of $Ca_V2.2$ channels at presynaptic boutons, rat hippocampal neurons were transfected with fast presynaptic Ca^{2+} indicator Sy-GCaMP6f (Fig. 4.5). The pH-sensitive mOr2 coupled to presynaptic VAMP was also co-transfected, with changes in its fluorescence over F_0 (Fig. 4.5 D and G) correlating to changes in pH due to the fusion of synaptic vesicles with the plasma membrane. Cells were stimulated with different stimulation protocols, which included stimulation with 1 AP. Averaging 5-8 repeats of 1 AP stimulation was applied to improve signal-to-noise ratio (Fig. 4.5 B and E). Stimulation with 10 APs was used to identify responding boutons for placement of ROIs (Fig. 4.5 C and F) and boutons were categorized into neurotransmitter-releasing (Fog 4.5. G orange line) and non-releasing (Fig. 4.5. D black line) based on the VAMP-mOr2 signal after stimulation with 200 APs at 10 Hz (Fig. 4.5 D and G). Unless stated otherwise, all subsequent datasets show values from functionally-releasing presynaptic terminals only.

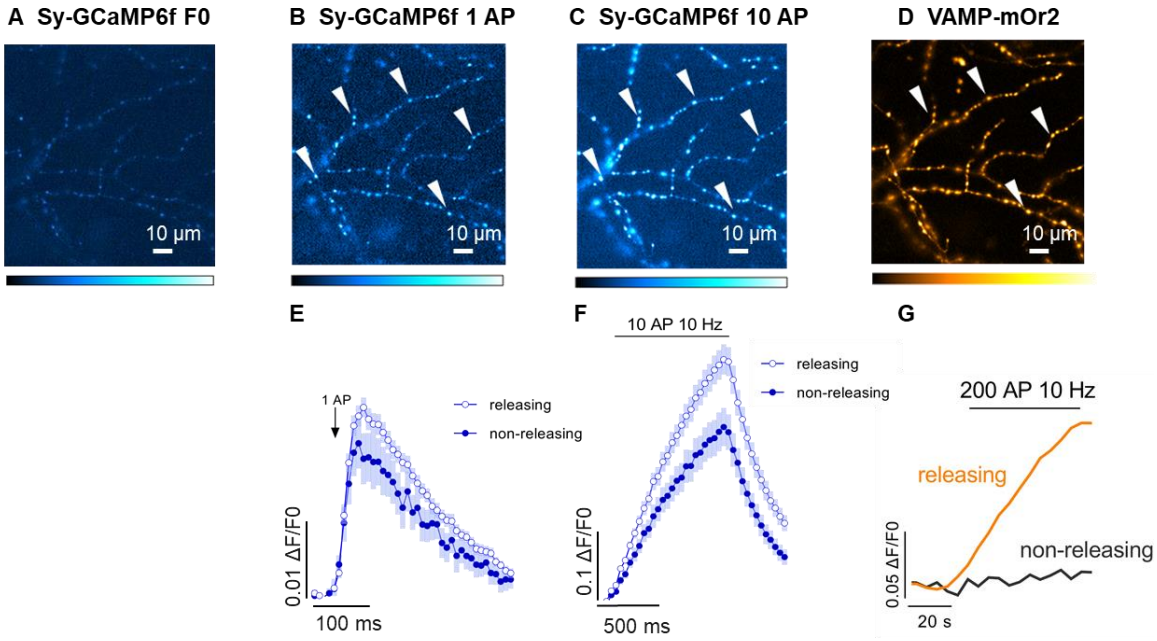

Figure 4. 5. Monitoring presynaptic Ca^{2+} transients and vesicular release in hippocampal neurons with Sy-GCaMP6f and VAMP-mOr2.

(A) Image showing field of view of hippocampal processes showing Sy-GCaMP6f fluorescence variations in boutons (arrow heads) before electrical stimulation. **(B and C)** Image showing the expression of Sy-GCaMP6f in putative boutons during stimulation with 1 (B) and 10 AP (C; arrowheads). **(D)** VAMP-mOr2 fluorescence after stimulation with 200 APs at 10 Hz was used to identify functional vesicle-releasing synapses based on an increase in fluorescence following the increase in pH to which it is exposed during vesicle fusion. **(E)** Up to 75 ROIs were selected per field of view to show changes in fluorescence over baseline fluorescence ($\Delta F/F_0$) of averages of 5-8 repeats of 1 AP stimulation. Responses from releasing (blue open circles) and non-releasing (blue filled circles) were distinguished based on VAMP-mOr2 responses. **(F)** Responses from releasing (blue open circles) and non-releasing (blue filled circles) after stimulation with 10 APs. **(G)** Increases in VAMP-mOr2 fluorescence (orange line) after stimulation with 200 APs was used to identify releasing boutons (orange line). Based on this, responses to 1 AP were categorized into releasing and non-releasing boutons.

4.2.3. *In vitro* maturation does not affect Ca^{2+} transient amplitudes of presynaptic terminals of rat hippocampal neurons

As Ca^{2+} transients may vary at different maturity states of the synapse, changes in Sy-GCaMP6f fluorescence from functionally-releasing presynaptic terminals were compared between the two different ages (Fig. 4.6). Synapses at DIV 14-17 revealed Ca^{2+} transients similar to more mature synapses at DIV 18-22 after stimulation with 1 AP (Fig. 4.6 A and B, $\Delta F/F_0$ 0.036 ± 0.004 and $\Delta F/F_0$ 0.028 ± 0.002, respectively; unpaired t-test P = 0.1).

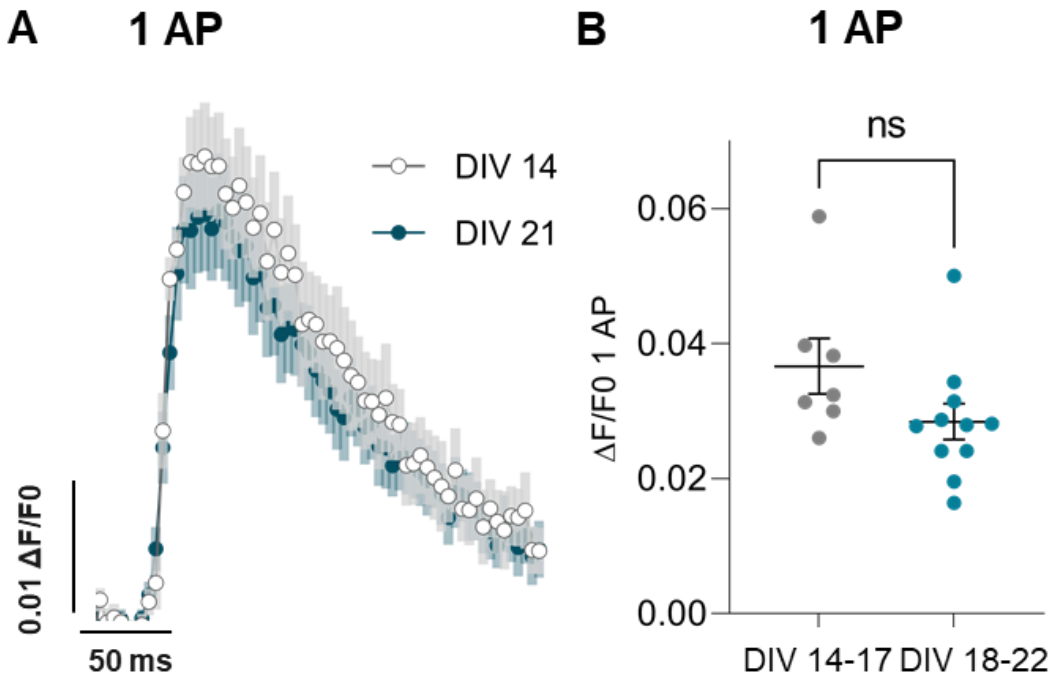

Figure 4. 6. Ca^{2+} transient amplitude is not affected by maturation *in vitro* in rat hippocampal neurons.

(A) Fluorescence changes in Sy-GCaMP6f expressing boutons over time in neurons at DIV 14-17 (grey) and DIV 18-22 (blue) after stimulation with 1 AP. Averaged traces of 5-8 repeats of electrical stimulation with 1 AP. For each field of view, 10-75 ROIs were chosen for analysis of change in fluorescence over baseline fluorescence ($\Delta F/F_0$). n for DIV 14-17 = 7 and n for DIV 18-22 = 11 biological replicates. **(B)** At DIV 14-17 (grey data points), synaptic Ca^{2+} transients are similar to DIV 18-22 (blue data points); n for DIV 14-17 = 7 and n for DIV 18-22 = 11 biological replicates, unpaired t-test P = 0.1. Data are shown as mean ± SEM.

4.3. Mouse hippocampal cultures

Because it was intended to eventually use $Ca_V2.2$_HA knock-in mice, experiments were repeated in hippocampal cultures from newborn mice. As this was the first time mouse hippocampal cultures were used in the laboratory, initial experiments were performed to reveal different cell types and synaptic proteins. Figure 4.8 shows neurons (Fig. 4.7 A) and astrocytes (Fig. 4.7 B) from mouse hippocampal cultures, stained using anti-MAP2 and anti-GFAP antibodies. To detect synapses, antibodies targeting presynaptic excitatory marker vGluT1 and postsynaptic Homer were applied (Fig. 4.8 A-D). 5x5 µm ROI of the merged image shows the apposed position of vGluT1 and homer along the process of a neuron (Fig. 4.8 D). In addition, inhibitory marker vGAT is shown in Figure 4.8 E-H, where both inhibitory and excitatory synapses were detected around the neuronal soma.

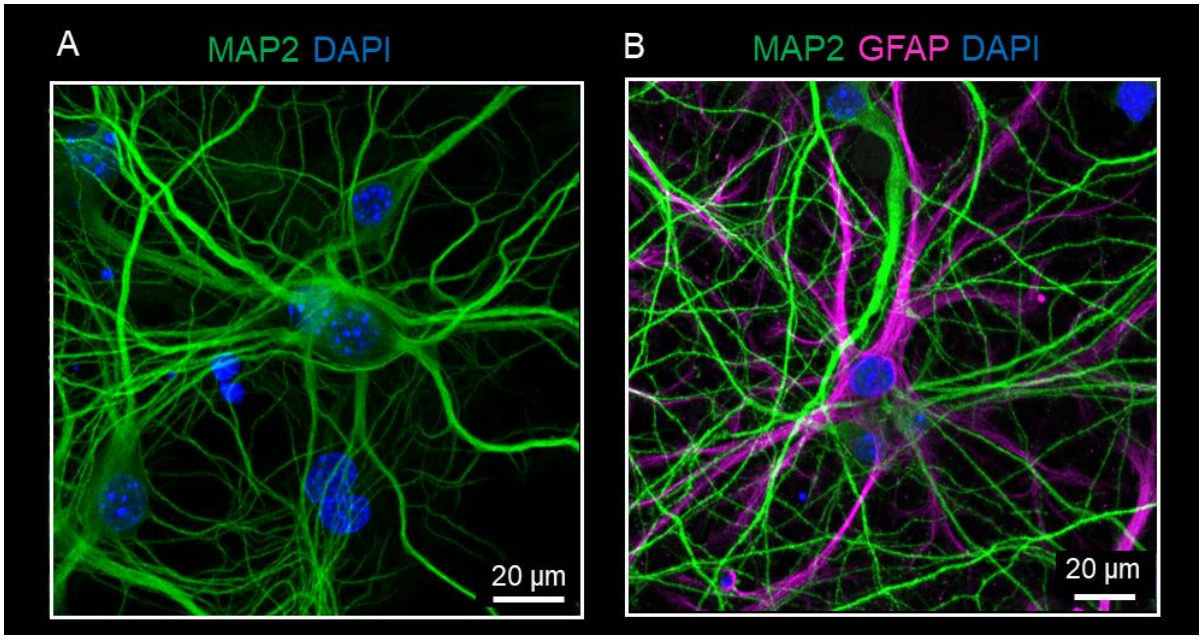

Figure 4. 7. Visualisation of hippocampal cells from mice.

(A) Neuronal staining using anti-MAP2 antibodies (green) and nuclear marker DAPI (blue) at DIV 14. x63 z-stack tile scan. Scale bar = 20 µm. **(B)** Anti-GFAP antibodies reveal the presence of astrocytes (magenta) and anti-MAP2 antibodies show neurons (green) at DIV 14. DAPI is shown in blue. Confocal x63 z-stack tile scan. Scale bar = 20 µm.

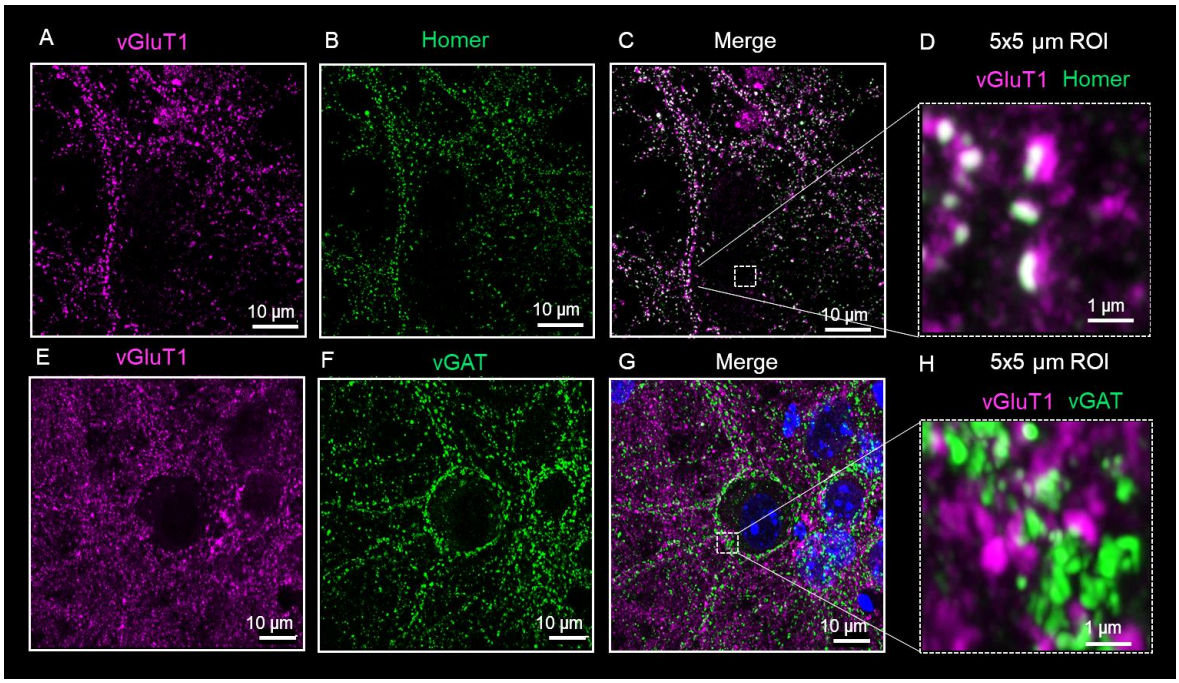

Figure 4. 8. Synaptic structures revealed in mouse hippocampal cultures. **(A-C)** Excitatory presynaptic marker vGluT1 (magenta, A) and postsynaptic marker Homer (green, B) and merged (C) at DIV 14. **(D)** 5x5 µm subset ROI reveals the apposed position of vGluT1 and Homer at the synapse. Scale bar = 1 µm. **(E)** vGluT1 in magenta at DIV 14. **(F)** Inhibitory synapse marker vGAT is shown in green. **(G)** Merge of vGluT1 and vGAT with DAPI. Super resolution x63. Scale bar = 10 µm. **(H)** 5x5 µm subset ROI shows the presence of both vGAT and vGluT positive puncta around the soma. Scale bar = 1 µm.

4.3.1. Visualisation of $Ca_V2.2$_HA channels in transfected mouse hippocampal neurons

$Ca_V2.2$ with an extracellular tandem HA tag and an intracellular N-terminal GFP tag (GFP_$Ca_V2.2$_HA) was transfected into mouse hippocampal cells. This genetic modification allowed the visualisation of the distribution of exogenous $Ca_V2.2$ channels in mouse hippocampal neurons (Fig. 4.9). The overall distribution of Cav2.2_HA is visible in permeabilised conditions (green, Fig. 4.9 A and C), together with intracellular marker GFP (red, Fig. 4.9 B). In order to specifically detect $Ca_V2.2$_HA channels on the plasma membrane of neurons, anti-HA antibodies were applied to non-permeabilised cells where only epitopes on the cell surface were available for antibody binding. Figure 4.9 D and F show cell surface $Ca_V2.2$_HA channels, in a typical ring-like structure around the cell surface of a neuronal soma and along several processes. In Figure 4.9 E, the intracellular expression of $Ca_V2.2$_HA channels was revealed by antibodies targeting GFP coupled to the intracellular N-terminal of $Ca_V2.2$.

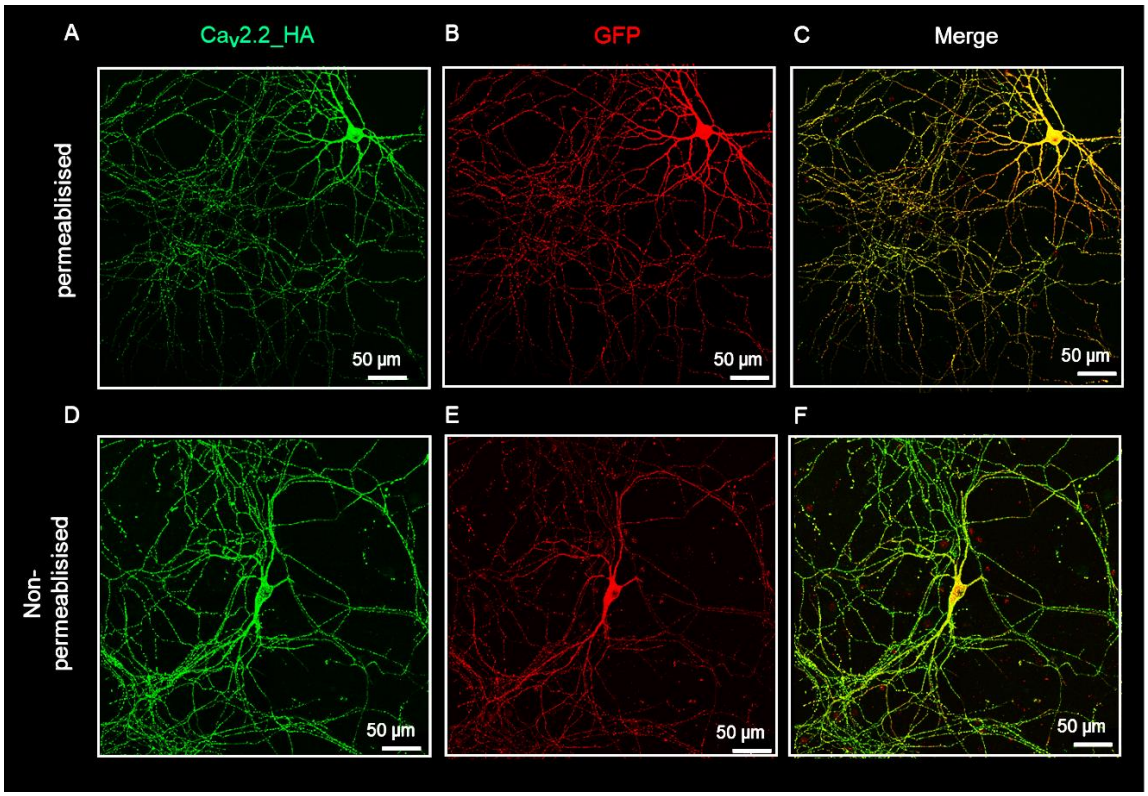

Figure 4. 9. Detection of total and surface GFP_Ca_V2.2_HA channels in transfected mouse hippocampal neurons.

(A) Anti-HA antibodies were used to detect Ca_V2.2_HA channels (green) in permeabilised neurons transfected with GFP_Ca_V2.2_HA, $\alpha_2\delta$-1 and β1b. **(B)** As transfection marker, GFP coupled to intracellular Ca_V2.2 channels was used (red). **(C)** Merge of Ca_V2.2_HA and GFP signal. Confocal x63 z-stack, 0.066 µm optical sections. Scale bar = 50 µm. **(D)** Anti-HA antibodies were used to detect surface Ca_V2.2_HA channels (green) in non-permeabilised neurons transfected with GFP_Ca_V2.2_HA, $\alpha_2\delta$-1 and β1b. **(E)** The GFP of GFP_Ca_V2.2_HA was revealed with anti-GFP Abs (red). **(F)** Merge of Ca_V2.2_HA and GFP signal. Confocal x63 z-stack. Scale bar = 50 µm. Cultures were fixed at DIV 18. Colours were changed in ImageJ so that Ca_V2.2_HA would be consistently shown in green.

4.3.2. Visualisation of endogenous $Ca_V2.2$_HA channels in hippocampal cultures

Numerous studies of protein localisation using microscopy rely on the overexpression of genetically modified proteins for fluorescent detection. However, this is known to influence the trafficking and function of the protein of interest as well as interacting proteins, which might ultimately impair the overall function of the cell. Therefore, neurons from the transgenic $Ca_V2.2\_HA^{KI/KI}$ mouse model available in our laboratory were used to study endogenous $Ca_V2.2$_HA channels using super resolution imaging. Figure 4.10 shows endogenous $Ca_V2.2$_HA channels (green, Fig. 4.10 A and C) in hippocampal neurons from $Ca_V2.2\_HA^{KI/KI}$ mice at DIV 14. As a postsynaptic marker, Homer was used (red, Fig. 4.10 B and C). ROIs with synaptic dimensions of 2x2 µm were chosen (Fig. 4.10 D), where the close proximity of presynaptic $Ca_V2.2$_HA channels to postsynaptic Homer was revealed. In the negative control, no specific synaptic staining was visible (Fig. 4.10 E-G).

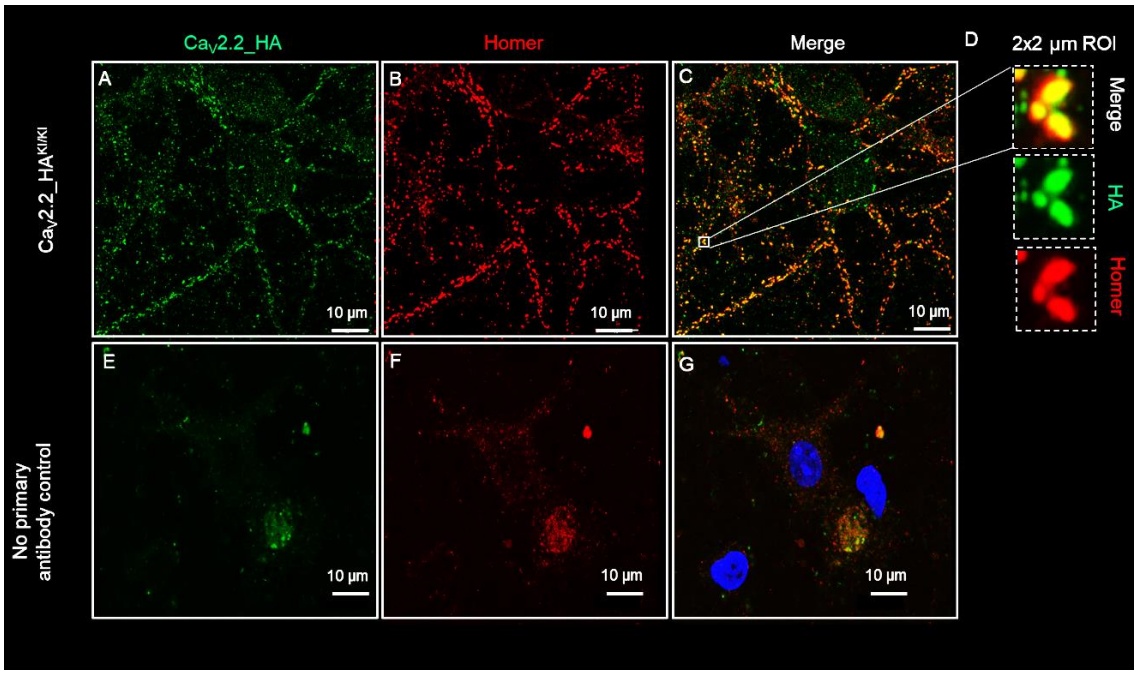

Figure 4. 10. Endogenous $Ca_V2.2$_HA channels opposite postsynaptic Homer in mouse hippocampal neurons.

(A) Anti-HA antibodies were used to detect $Ca_V2.2$_HA (green) along the processes of neurons from $Ca_V2.2$_$HA^{KI/KI}$ mice at DIV 14. **(B)** Homer (red) was used to visualise the postsynapse. **(C)** Merge of $Ca_V2.2$_HA and Homer. **(D)** 2x2 µm subset image showing $Ca_V2.2$_HA channels in green and Homer in red at a putative synapse. **(E-G)** For the negative control, only secondary antibodies were applied. All images were taken at x63 in super resolution mode. Scale bar = 10 µm.

Presynaptic RIM 1/2 is an important protein at the active zone that binds directly to $Ca_V2.2$ channels (Kaeser *et al.* 2011). In the immunostaining of $Ca_V2.2$_HA and RIM 1/2 in hippocampal neurons from $Ca_V2.2$_$HA^{KI/KI}$ shown in Figure 4.11, both proteins were observed co-localising around neuronal somata and along processes (Fig. 4.11 A-D). In wild type neurons the RIM1/2 signal was similar to neurons from $Ca_V2.2$_$HA^{KI/KI}$ mice (Fig. 4.11 F). However, the unspecific background signal from rat anti-HA antibodies was high, making it difficult to discern true HA signal from $Ca_V2.2$_$HA^{KI/KI}$ neurons (Fig. 4.11 E). In negative-control neurons, the staining for both markers was absent (Fig. 4.11 H-J).

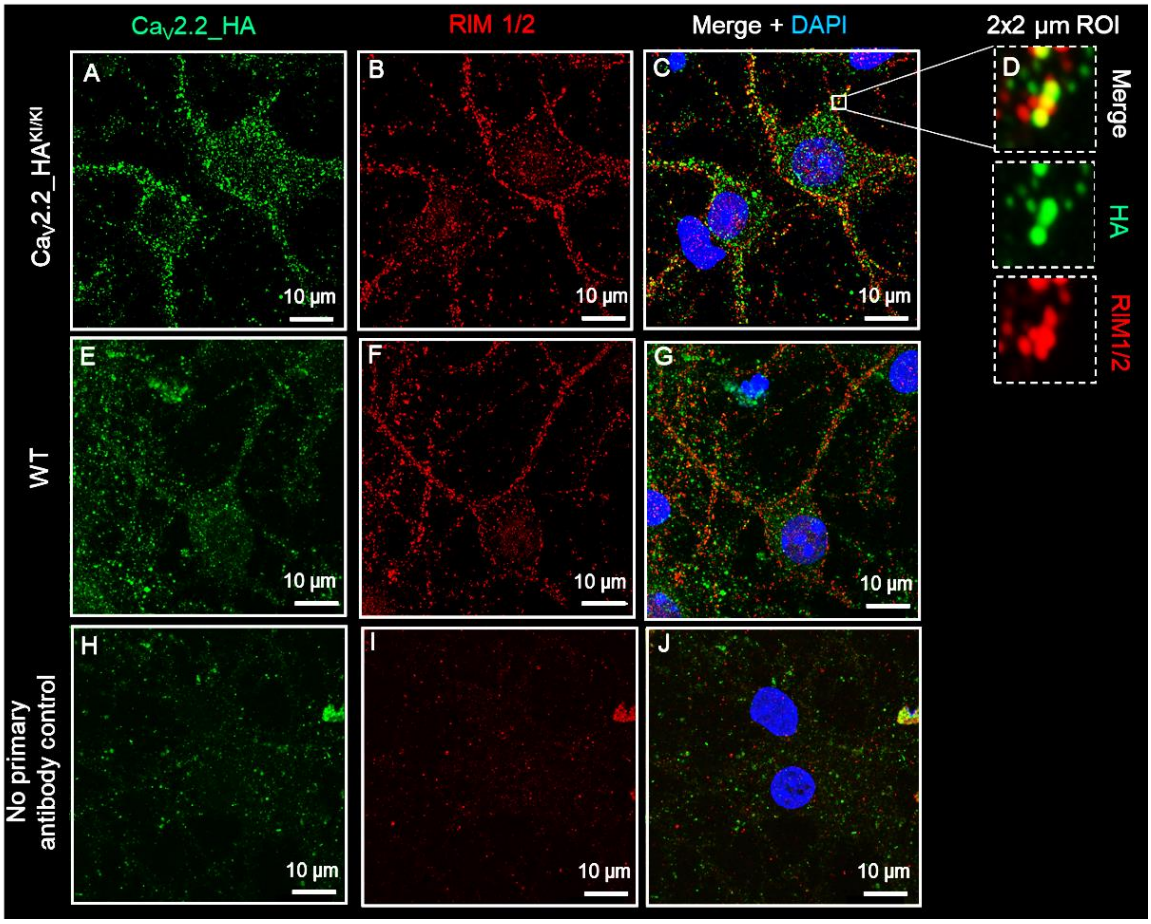

Figure 4. 11. Visualisation of endogenous $Ca_V2.2$_HA channels and RIM 1/2 in mouse hippocampal neurons.

(A) Anti-HA antibodies were used for detection of $Ca_V2.2$_HA channels (green) along the processes and around the somata of $Ca_V2.2\_HA^{KI/KI}$ neurons at DIV 21. **(B)** Anti-RIM 1/2 (red) antibodies were used as presynaptic marker. **(C)** Merge of $Ca_V2.2$_HA and RIM 1/2 with DAPI. **(D)** Subset image of 2 x 2 µm, showing the colocalization of $Ca_V2.2$_HA (green) with RIM1/2 (red). **(E)** Anti-HA antibodies in WT neurons were used as a control. **(F)** RIM1/2 signal in WT neurons. **(G)** Merge of HA and RIM 1/2 with DAPI. **(H-J)** Negative control neurons without any primary Abs applied. All images taken at x63 in super resolution mode. Scale bar = 10 µm.

Finally, Figure 4.12 shows $Ca_V2.2$_HA channels in super resolution from $Ca_V2.2\_HA^{KI/KI}$ mouse neurons at DIV 21, together with presynaptic vGluT1 and postsynaptic Homer. The 2x2 µm ROI reveals all three proteins at a putative synapse (Fig. 4.12 E).

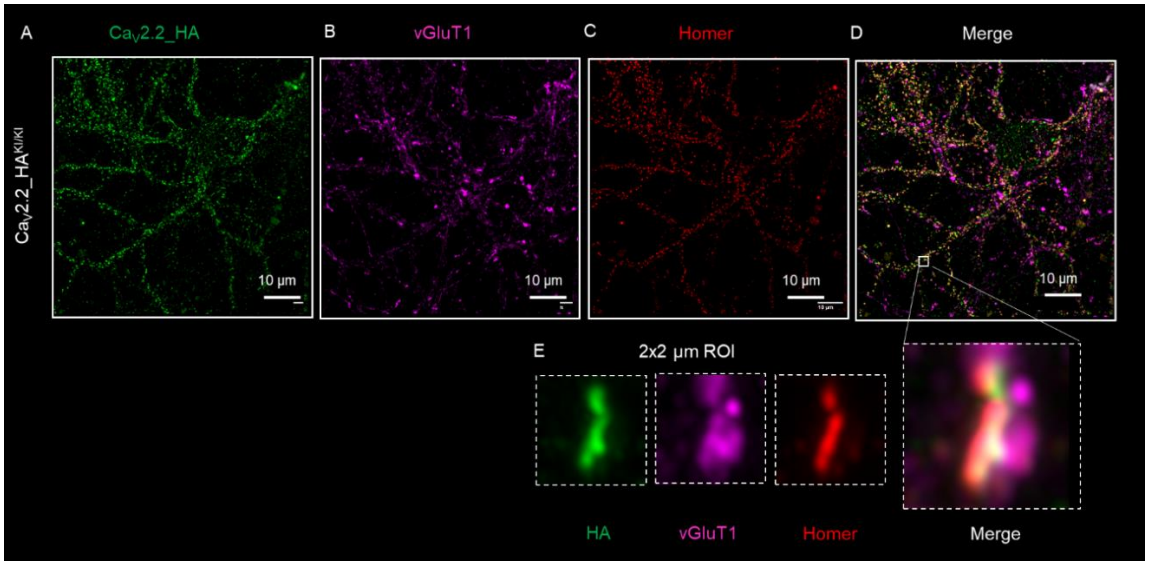

Figure 4. 12. Detection of endogenous $Ca_V2.2$_HA channels colocalizing with excitatory synapse marker vGluT1 and Homer in mouse hippocampal neurons.

(A) Anti-HA antibodies were used to detect $Ca_V2.2$_HA channels (green) along the processes and around the somata of neurons from $Ca_V2.2\_HA^{KI/KI}$ neurons at DIV 21. **(B)** Anti-vGluT1 (magenta) antibodies were used to visualise the excitatory presynapse. **(C)** Postsynaptic Homer is shown in red. **(D)** Merge of $Ca_V2.2$_HA, vGluT1 and homer with DAPI. Scale bar = 10 µm. **(E)** 2x2 µm subset image showing $Ca_V2.2$_HA channels (green), opposed to vGluT1 (magenta) and Homer (red). All images were taken at x63 in super resolution mode.

4.3.3. In less mature presynaptic boutons, Ca^{2+} transients are larger than in more mature neurons

It has previously been shown that there is substantial restructuring of the presynaptic active zone as synapses mature (Südhof 2018). Consequently, the aim of this study was to further investigate whether Ca^{2+} dynamics would differ between mouse hippocampal neurons aged DIV 14-17 and DIV 18-22. For this, neurons were stimulated with 1 AP and changes in Sy-GCaMP6f fluorescence measured from functionally-releasing presynaptic terminals (Fig. 4.13 A and B). This revealed a reduction of 30 % of transient peak amplitudes at DIV 18-22 compared to neuron terminals at DIV 14-17 (0.024 ± 0.002 versus 0.032 ± 0.003, respectively, unpaired t-test P = 0.03).

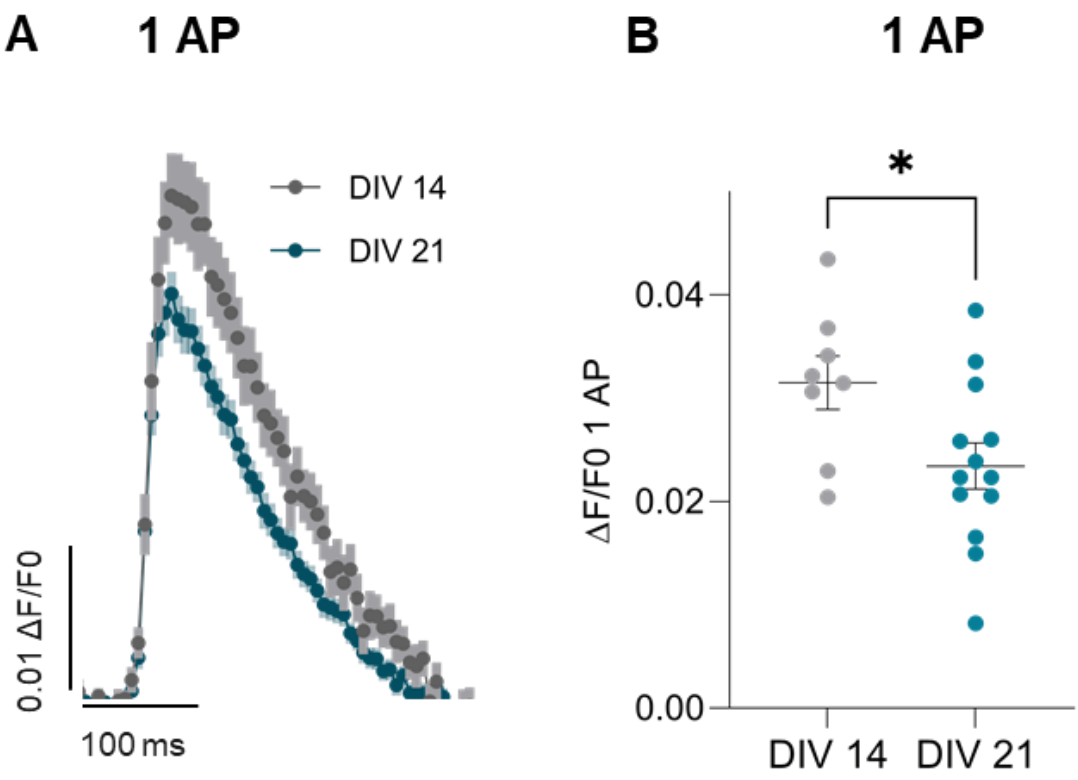

Figure 4. 13. Effect of *in vitro* maturation on Ca^{2+} transient amplitudes.
(A) Larger fluorescence changes in Sy-GCaMP6f expressing VAMP-mOr2-positive boutons over time in younger neurons at DIV 14-17 (grey) after stimulation with 1 AP compared to neurons at DIV 18-22 (blue). Averaged traces of 5-8 repeats of electrical stimulation with 1 AP. For each field of view, 10-75 ROIs were chosen for analysis of change in fluorescence over baseline fluorescence ($\Delta F/F_0$). n for

DIV 14-17 = 8 biological replicates and n for DIV 18-22 = 13. **(B)** At DIV 14-17 (grey, 0.032 ± 0.003), Ca^{2+} transients are larger than at DIV 18-22 (blue, 0.025 ± 0.001); n for DIV 14-17 = 8 biological replicates and n for DIV 18-22 = 13. Unpaired t-test, *P* = 0.03.

4.3.4. Similar contribution of $Ca_V2.2$ channels to Ca^{2+} transients in both maturity stages

To gain an insight into the specific contribution of $Ca_V2.2$ channels to Ca^{2+} flux at different ages, $Ca_V2.2$ channel blocker ConTx was applied to cells for two minutes. Initially, to ascertain whether any observed reduction in fluorescence was due to the incubation period or due to bleaching during re-stimulation, control experiments were performed with normal imaging medium applied for two minutes instead of ConTx and cells re-stimulated (Fig. 4.14). This resulted in a reduction of 8.8 ± 9.0 % during 1 AP stimulation (Fig. 4.14). All values shown in Figure 4.17, and all other subsequent figures with ConTx treatment, have been adjusted for this reduction (8.8 % subtracted for 1 AP values).

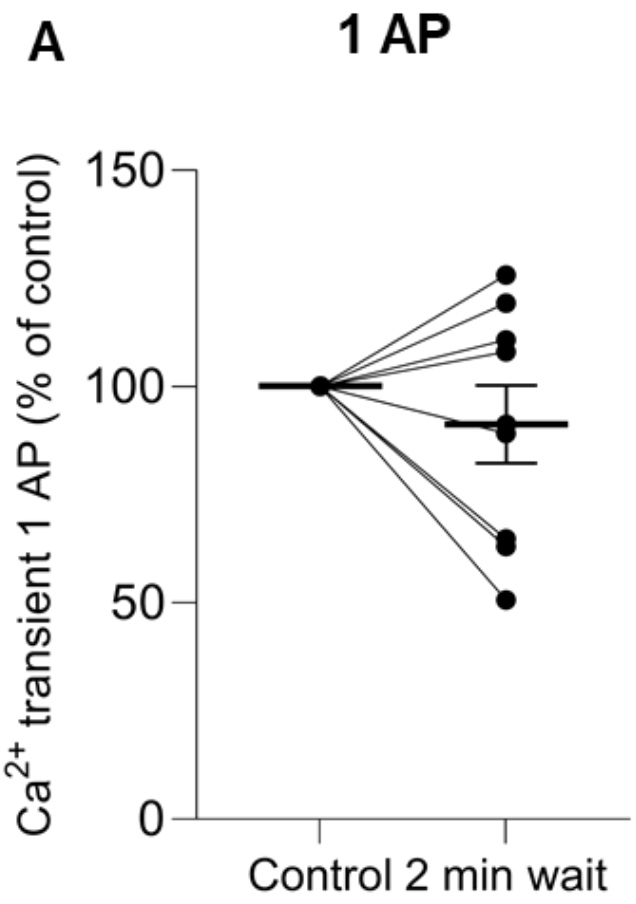

Figure 4. 14. Control run-down in Ca^{2+} transient amplitudes during 2 minutes without application of ConTx during 1 AP stimulation in mouse hippocampal neurons.

A two minute rest after stimulation with 1 AP resulted in decreased responses when stimulating again with a 8.8 ± 9.0 % reduction. Average Ca^{2+} transients were normalised to their respective control before the two-minute rest; n = 9 fields of view from 4 biological replicates.

Following control experiments, the $Ca_V2.2$ channel blocker ConTx was applied to cells to assess the resistant synaptic Ca^{2+} transients (Fig. 4.15). ConTx incubation resulted in a reduction of Ca^{2+} transients during 1 AP stimulation at both DIV 14-17 and DIV 18-22. During 1 AP stimulation, 31.4 ± 7.4 % and 28.6 ± 8.4 % of Ca^{2+} transients are mediated by $Ca_V2.2$ channels at DIV 14-17 and at DIV 18-22, respectively (paired t-test, P = 0.8, Fig. 4.15).

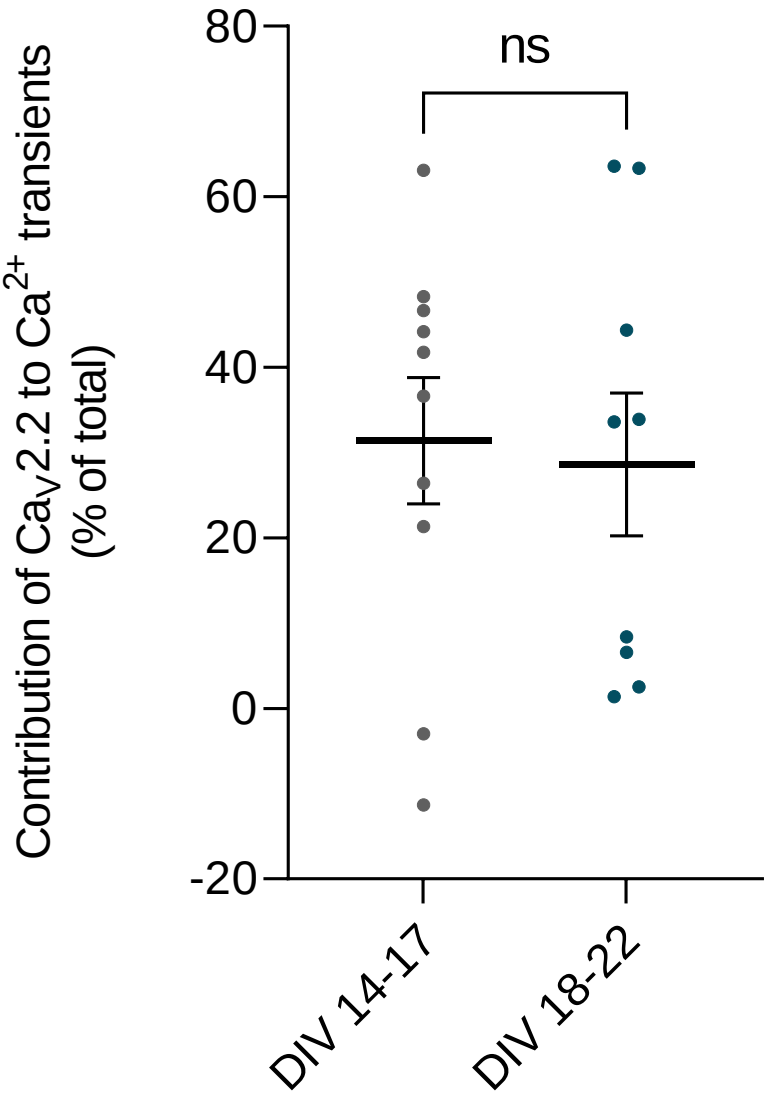

Figure 4. 15. $Ca_V2.2$ channel contribution to presynaptic Ca^{2+} transients in mouse hippocampal neurons is not affected by neuronal maturation.

(A) At DIV 14-17, contribution of $Ca_V2.2$ channels to Ca^{2+} transients after electrical stimulation with 1 AP was 31.4 ± 7.4 % (grey) at DIV 14-17 and 28.6 ± 8.4 % (blue) at DIV 18-22. Average Ca^{2+} transients were normalised to their respective "no toxin" control before ConTx application. Paired t-test, *P* = 0.8; n for DIV 14-17 = 9 fields of view and n for DIV 18-22 = 8 fields of view. All values have been corrected subtracting the control reduction shown above in Fig. 4.14 for mouse neurons.

4.4 Comparison of presynaptic Ca^{2+} transients from rat and mouse hippocampal neurons

Both rats and mice are widely used model organisms for the study of presynaptic Ca_V2 channels. In order to assess the size of Ca^{2+} transients and the contribution of $Ca_V2.2$ channels in neurons from both organisms, data from rat and mouse hippocampal neurons were compared (Fig. 4.16). Figure 4.16 A shows that changes in fluorescence after stimulation with 1 AP were similar in mouse and rat hippocampal neurons at DIV 14-17 and at DIV 18-22 (2way ANOVA, mouse DIV 14-17 vs rat DIV 14-17, $P = 0.45$ and mouse DIV 18-22 vs rat DIV 18-22 $P = 0.31$).

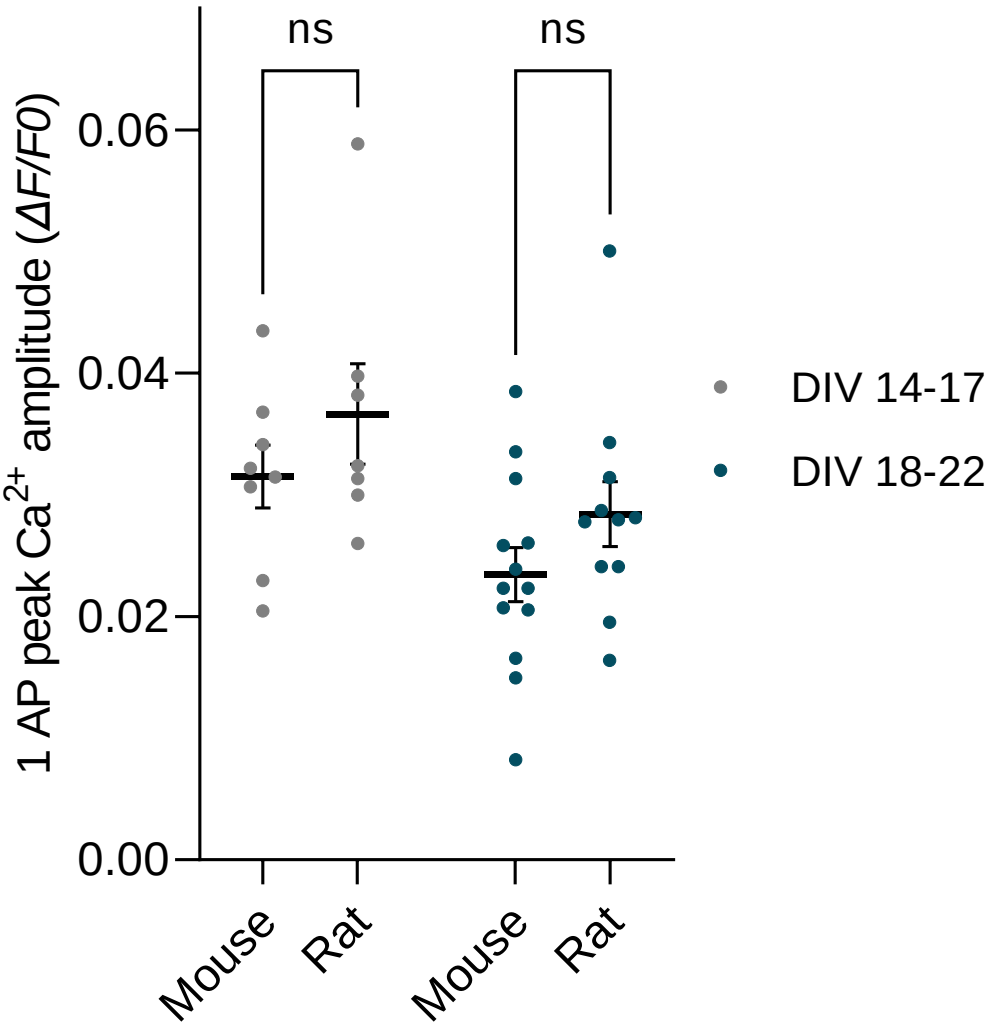

Figure 4. 16. Ca^{2+} transients are similar in mouse and rat neurons.
Stimulation with 1 AP elicits similar Ca^{2+} transients in hippocampal neurons from mice and rats at different ages *in vitro*; n for mouse DIV 14-17 = 8 biological replicates; n for DIV 18-22 = 13 biological replicates; n for rat DIV 14-17 = 7 biological replicates; n for DIV 18-22 = 11 biological replicates. 2way ANOVA, Sidak's multiple comparisons test, DIV 14-17 *P* = 0.45 and DIV 18-22 *P* = 0.31; interaction *P* = 0.98.

Comparing the effect of ConTx on Ca^{2+} flux in mouse and rat hippocampal neurons confirms a much higher proportion of $Ca_V2.2$ channel contribution in rat neurons after stimulation with 1 AP at DIV 18-22 (unpaired t-test *P* = 0.02, Fig. 4.17). In Sy-GCaMP6f

transfected neurons, $Ca_V2.2$ channels contributed to 28.4 ± 8.4 % (mouse) and 53.3 ± 5.5 % (rat) of total Ca^{2+} transients.

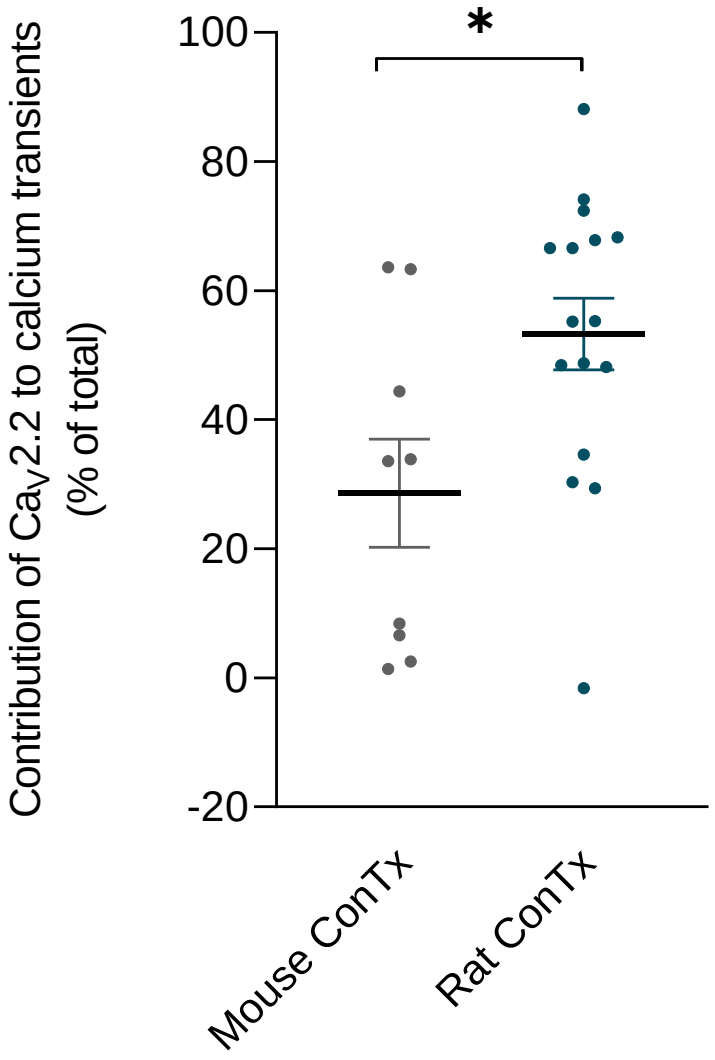

Figure 4. 17. $Ca_V2.2$ channels contribute more to Ca^{2+} transients in rat neurons than in mouse neurons.

Contribution of $Ca_V2.2$ channels to Ca^{2+} transients after electrical stimulation with 1 AP was 28.4 ± 8.4 % for mouse neurons (grey) and 53.3 ± 5.5 % for rat neurons (blue). Average Ca^{2+} transients were normalised to their respective "no toxin" control before ConTx application. Unpaired t-test *P* = 0.02; n for mouse = 9 fields of view and n for rat = 16 fields of view. Data are shown as mean ± SEM. All values have been corrected subtracting the control reduction shown above in Fig. 4.14 and 5.2.

4.5. Summary and Discussion

In vitro culture systems are widely used to study cells and proteins at a cellular and sub-cellular level. An advantage of this experimental approach is the accessibility of neuronal and glial cells to fluorescently labelled antibodies for microscopy. Moreover, cells *in vitro* can be genetically modified, allowing for a multitude of biological questions to be studied.

This study sought to establish viable neuronal cultures from rat and mouse hippocampi to study the distribution and role of $Ca_V2.2$ channels. Thus far, most studies on synaptic ion channels have relied on rat hippocampal neurons, therefore, initial experiments presented here were also performed using rat cultures. Immunocytochemistry experiments showed neurons and astrocytes and the presence of synaptic markers, indicating that synapses have formed *in vitro*. Rat hippocampal neurons were transfected with cDNA of genetically modified $Ca_V2.2$_HA, allowing to visualise these channels using anti-HA antibodies and to later compare this to staining of endogenous $Ca_V2.2$_HA channels in mouse cultures. Stainings of transfected $Ca_V2.2$_HA channels revealed an ubiquitous distribution of channels along neuronal processes and on the soma of neurons positive for transfection marker mCherry. Following this, the distribution of $Ca_V2.2$ channels in mouse hippocampal cultures was assessed. Using the same protocol as for rat neurons, we found that cultured mouse neurons formed excitatory and inhibitory synapses *in vitro*, demonstrated using different antibodies in immunocytochemistry stainings. Protein overexpression was used to visualise the distribution of $Ca_V2.2$_HA channels, revealing high levels of $Ca_V2.2$_HA channels in and on the soma and along the processes in permeabilised immunostaining conditions, similar to findings from transfected rat cells. In non-permeabilised conditions, where only surface $Ca_V2.2$ epitopes are accessible for the anti-HA antibody, a ring-like structure was observed around the soma, indicating specific surface channel labelling. As GFP coupled to the intracellular part of $Ca_V2.2$_HA was used as a control, one can conclude that the $Ca_V2.2$_HA fluorescence is from channels expressed on the soma of

the imaged neuron. However, it is known that endogenous expression levels of $Ca_V2.2$ channels are relatively low, so one can assume that transfecting cells with $Ca_V2.2$ channels will result in very high, non-physiological expression levels which will also affect the subcellular distribution. Moreover, it is not known how increased levels of $Ca_V2.2$ channels affect other proteins and the overall function of the cell, therefore providing only a limited insight into the physiological distribution of $Ca_V2.2$ channels.

Hence, the $Ca_V2.2\_HA^{KI/KI}$ mouse model was used to study endogenous $Ca_V2.2$ channels, thus far hindered by the lack of viable anti-$Ca_V2.2$ antibodies and the low distribution of endogenous channel levels at the presynapse. Hippocampal neurons from $Ca_V2.2\_HA^{KI/KI}$ mice revealed the presence of HA-tagged $Ca_V2.2$ channels around somata and along neuronal processes. The $Ca_V2.2$_HA staining was absent from wild-type neurons. Combining anti-HA antibodies with presynaptic protein RIM1/2 showed a co-localisation of the two components of putative presynaptic active zones. Moreover, $Ca_V2.2$_HA channels were shown to be in close proximity to excitatory synapse marker vGluT1 and apposed to postsynaptic marker Homer, in a typical half-moon shape that was also observed in a co-culture system of DRG and spinal cord cells from $Ca_V2.2\_HA^{KI/KI}$ mice (thesis UCL Dr K Ramgoolam, 2020). Levels of non-specific background from anti-rat antibodies (required for detection of rat-anti HA primary Abs) on mouse neurons require future optimisation of the staining protocol, such as changing the PFA concentration during fixation or the blocking buffer used to prevent unspecific antibody binding. Due to the background staining, the fluorescence signal of $Ca_V2.2$_HA from $Ca_V2.2\_HA^{KI/KI}$ neurons was not used for quantification. Nonetheless, this is the first time that endogenous $Ca_V2.2$_HA channels in hippocampal neurons were visualised *in vitro*, which will enable numerous ways of studying $Ca_V2.2$ channels in detail in the future.

A relatively novel way of studying Ca_V function is by genetically encoded Ca^{2+} indicators, allowing determination of synaptic Ca^{2+} flux based on fluorescence changes (Nakai *et al.* 2001). Following a strong 200 Hz stimulation to measure VAMP-mOr2

fluorescence, boutons were differentiated into neurotransmitter-releasing and non-releasing boutons. Here, we only considered neurotransmitter-releasing presynaptic boutons for analysis as we cannot be certain that non-releasing boutons were indeed presynaptic terminals.

Data from electrical stimulations with 1 AP show that presynaptic Ca^{2+} flux in rat neurons that were aged 14-17 DIV was similar to Ca^{2+} flux in neurons aged DIV 18-22. As discussed above, as synapses mature, a developmentally-regulated tightening of coupling at the presynapse had been reported, from microdomain coupling in younger synapses to more defined nanodomain coupling of Ca_V2 channels to the synaptic vesicle release machine. Hence, in this study one would have expected larger and more diffuse Ca^{2+} transients in less mature neurons and smaller, more precise Ca^{2+} flux at the mature synapse. However, our findings of similar Ca^{2+} flux at both ages do not fully rule out the possibility of a transition from micro- to nanodomain coupling. If neurons younger than DIV 14 had been included in the present study, this effect might have been detectable. This was not possible, as cells were transfected at DIV 7 and needed sufficient time to fully express Sy-GCaMP6f and VAMP-mOr2. Moreover, synapses younger than DIV 14 are not fully functional yet (Moutin *et al.* 2020).

Using a combination of two presynaptic functional markers (Sy-GCaMP6f and VAMP-mOr2) with the specific $Ca_V2.2$ channel inhibitor ConTx allowed to study Ca^{2+} transients of neurotransmitter-releasing presynaptic boutons and $Ca_V2.2$ channel contribution simultaneously across many individual boutons of mouse hippocampal neurons. In less mature cultures from mouse neurons at DIV 14-17, larger Ca^{2+} transients were observed compared to more mature neurons. This has not been studied before and would be in line with the maturation of the synapses and their transition from more diffuse microdomains to tighter nanodomains. Changes in coupling properties and differential contributions of $Ca_V2.2$ and $Ca_V2.1$ channels could be studied further by assessing presynaptic vesicular release.

For an insight into the specific role of $Ca_V2.2$ channels for presynaptic Ca^{2+} flux at different ages, ConTx was applied and Sy-GCaMP6f fluorescence changes measured after stimulation. This showed similar levels of $Ca_V2.2$ channel contribution to overall Ca^{2+} flux at DIV 14-17 and at DIV 18-22. During 1 AP stimulation $Ca_V2.2$ channels contributed approximately 30 % of total Ca^{2+} transient. In a similar study using GCaMP6f in mouse hippocampal neurons at DIV 17-21, levels of $Ca_V2.2$ channel contribution were estimated to be about 40 % (Brockhaus *et al.* 2019) and about 50 % in mouse neurons aged DIV 12-18, revealed using patch clamp techniques (Cao and Tsien 2010). Findings presented in this study do not suggest a developmental downregulation of $Ca_V2.2$ channels but support the notion that hippocampal transmission is partially mediated by $Ca_V2.2$ channels. The remaining Ca^{2+} flux is likely mediated by joint activity of $Ca_V2.1$ and, to lesser extent, $Ca_V2.3$ channels. This diverse Ca_V2 channel composition at the presynapse might be crucial for dynamic changes in presynaptic strength in response to alterations in synaptic activity.

Finally, this study found differences in the levels of $Ca_V2.2$ channel contribution to Ca^{2+} transients between rat and mouse hippocampal neurons. In rat hippocampal neurons, $Ca_V2.2$ channels mediated more than half of total Ca^{2+} flux, whereas in mouse neurons only approximately one third was found to be via $Ca_V2.2$ channels. This suggests differences between the two species with important implications for the choice of model organism when studying Ca_V2 channels.

In conclusion, this chapter presented different ways of visualising $Ca_V2.2$ channels in hippocampal neurons. As the immunostaining of endogenous $Ca_V2.2$_HA requires more optimisation, studies on $Ca_V2.2$ channels were performed with genetically encoded Ca^{2+} indicator and vesicular release reporter. Using these, this work revealed that in younger mouse hippocampal neurons, presynaptic Ca^{2+} transients from functionally-releasing presynaptic terminals were larger than in more mature terminals, despite similar levels of $Ca_V2.2$ channel contribution to total Ca^{2+} flux.

Chapter 5. $Ca_V2.2$ channels, $\alpha_2\delta$-1 and homeostatic synaptic plasticity

5.1. Introduction

Homeostatic synaptic adaptations involve synaptic mechanisms that prevent hyper- or hypoactivity after changes in neuronal networks. In *in vitro* systems, this form of plasticity is often studied by either chronically overexciting neurons or by chronic silencing of neuronal activity. For the latter, the voltage-gated sodium channel inhibitor TTX is applied to neurons, which results, after a delay, in pre- and postsynaptic adaptive changes to maintain stable networks (Turrigiano 2011). Incubation of neurons with TTX caused increased presynaptic Ca^{2+} influx (Zhao *et al.* 2011), increased vesicle release probability (Vitureira *et al.* 2011) and induced restructuring of the active zone involving multiple presynaptic proteins (Glebov *et al.* 2017). Among those, presynaptic Ca^{2+} channels have been of interest as they mediate Ca^{2+} influx required for neurotransmitter release. In a study using rat hippocampal cells, an upregulation of $Ca_V2.1$ channels was observed after network silencing with TTX (Jeans *et al.* 2017; Glebov *et al.* 2017). A role for $Ca_V2.2$ channels in the induction of homeostatic synaptic plasticity (HSP) has also been proposed, as the channel was found enriched at the presynaptic active zone upon TTX treatment in rat hippocampal neurons (Glebov *et al.* 2017).

$\alpha_2\delta$ subunits are of particular interest in the context of compensatory synaptic changes because of their direct regulation of Ca_V2 channels, serving as a checkpoint for trafficking and activation of Ca_V channels (Hoppa *et al.* 2012; Kadurin *et al.* 2016). In addition to their importance for Ca_V2 channel function, $\alpha_2\delta$-1 has been shown to be involved in trans-synaptic organisation of the excitatory synapse, independent from their role as a Ca_V channel subunit (Eroglu *et al.* 2009; Chen *et al.* 2018; Zhou *et al.* 2018; Bikbaev *et al.* 2020; Schöpf *et al.* 2021). This might have important implications for $\alpha_2\delta$-1 during non-Hebbian, adaptational forms of plasticity.

Here, TTX was applied to cultured mouse and rat hippocampal neurons of different ages to study compensatory changes at the synapse. Ca^{2+} flux was then monitored with live cell Ca^{2+} imaging using Sy-GCaMP6f and vesicular release was

monitored with VAMP-mOr2. To assess compensatory plasticity at different maturity stages of the neurons, cells were either imaged at DIV 14-17 (less mature) or at DIV 18-22 (more mature). To establish the role of $Ca_V2.2$ channels for presynaptic homeostatic potentiation, the specific $Ca_V2.2$ channel inhibitor ConTx was applied to cells. Levels of $Ca_V2.2$ channels after TTX treatment were also determined using Western blotting of whole cell lysates. In addition, the effect of TTX on endogenous surface and total $\alpha_2\delta$-1 was explored using biotinylation assays. Finally, the impact of $\alpha_2\delta$-1-overexpression on adaptational plasticity and Ca^{2+} transients via $Ca_V2.2$ channels were assessed.

5.2. Homeostatic synaptic plasticity in rat hippocampal neurons

The involvement of $Ca_V2.2$ channels in homeostatic adaptations at the presynapse remains to be fully elucidated. To establish whether there is a role for $Ca_V2.2$ channels in mediating increased presynaptic Ca^{2+} transients upon network silencing, AP-evoked Ca^{2+} transients were measured in presynaptic terminals of neuronal rat cultures, transfected with presynaptic Ca^{2+} indicator Sy-GCaMP6f and with VAMP-mOr2, a reporter of presynaptic exocytosis. Cells were treated with TTX for 48 hrs to induce HSP. Afterwards, neurons were stimulated and Ca^{2+} transients measured as described in Chapters 2 and 4.

5.2.1. Elevated Ca^{2+} transients during homeostatic synaptic plasticity

Hippocampal neurons of different ages were treated with TTX, and Ca^{2+} transient amplitudes at putative synaptic boutons were compared to untreated control neurons. In neurons aged 14-17 DIV, presynaptic Ca^{2+} transient amplitudes from functionally-releasing presynaptic terminals were similar in both conditions after stimulation with 1 AP (Fig. 5.1, $\Delta F/F_0$ 0.037 ± 0.004 in control; $\Delta F/F_0$ 0.041 ± 0.01 in TTX-treated neurons, 2way ANOVA, P = 0.9). However, when neurons were cultured for 18-22 days, network silencing with TTX resulted in Ca^{2+} transient amplitudes approximately 45 % larger than

control neurons (Fig. 5.1, TTX-treated 0.05 ± 0.009; control neurons $\Delta F/F_0$ 0.028 ± 0.003, 2way ANOVA, P = 0.02).

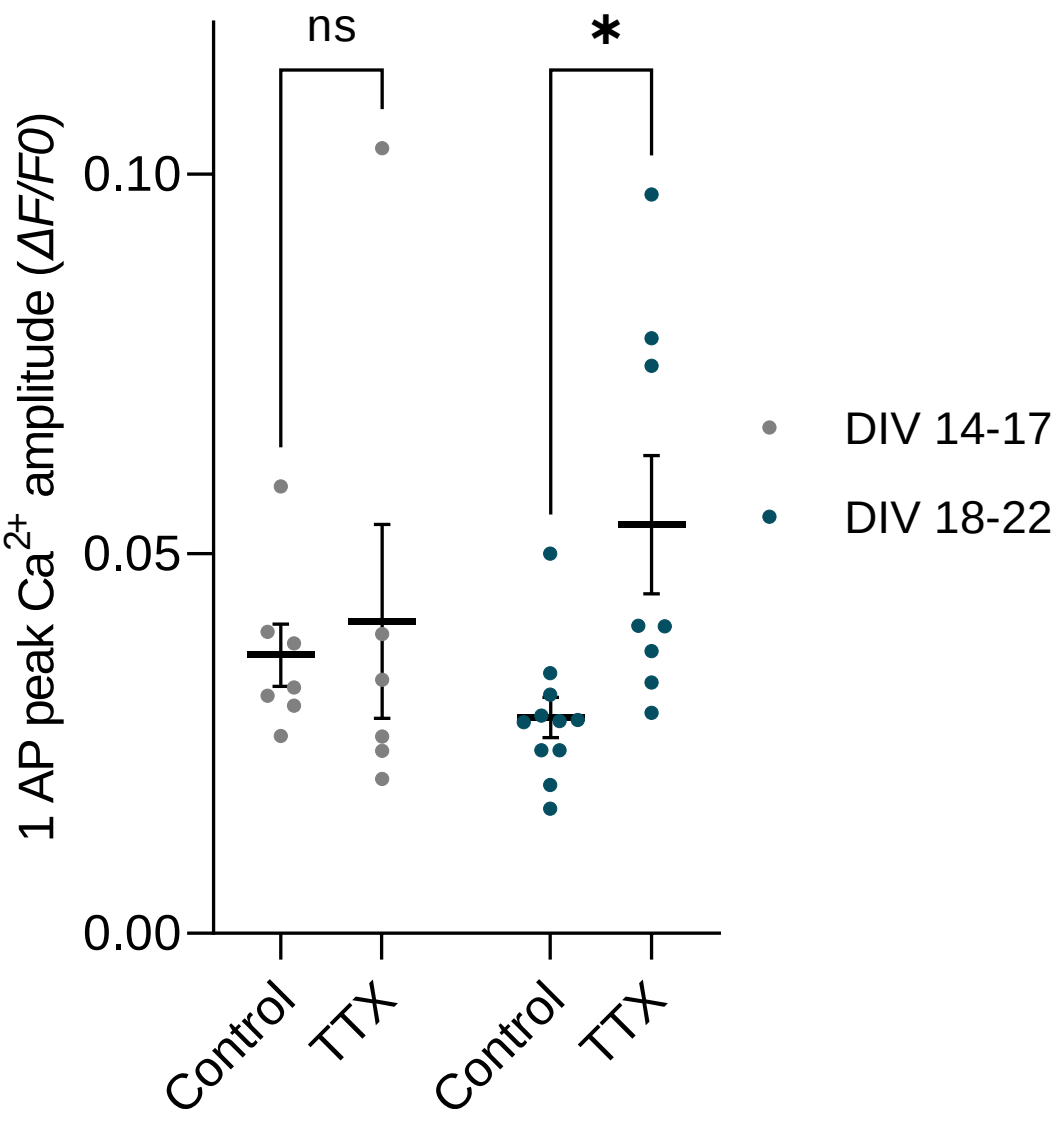

Figure 5. 1. TTX treatment effect on presynaptic boutons at different days *in vitro*.

At DIV 14-17 (grey data points), no significant differences were observed between control and TTX-treated Ca^{2+} transient amplitudes, n = 7 biological replicates. 2way ANOVA, P = 0.9, Sidak's multiple comparisons test. At DIV 18-22 (blue data points), TTX treatment induced a larger increase in Ca^{2+} transient amplitudes compared to control boutons. n = 11 biological replicates. 2way ANOVA, P = 0.02, Sidak's multiple comparisons test, interaction factor P = 0.15; values are shown as mean ± SEM. ns = not significant.

5.2.3. Compensatory changes in rat hippocampal neurons do not lead to increased $Ca_V2.2$ channel contribution to Ca^{2+} transients

Data presented above confirmed that neuronal activity blockade induced by TTX treatment results in larger presynaptic Ca^{2+} currents from functionally-releasing presynaptic rat terminals at 18-22 DIV. To determine whether $Ca_V2.2$ channels contribute to increased levels of Ca^{2+} flux, the $Ca_V2.2$ channel-specific inhibitor ConTx was applied to cultures during the stimulation protocol. Beforehand, however, two imaging sequences with 1 AP stimulation, separated by two minutes, were performed with normal perfusion medium in order to take into account any potential variations of fluorescence due to run-down or run-up (Fig. 5.2). Indeed, similar to findings in mouse neurons (Chapter 4, Fig. 4.14), Ca^{2+} transient amplitudes after 1 AP re-stimulation were reduced by 7.6 ± 8.4 % without adding any toxin (Fig. 5.5). All values shown below and above have been adjusted for this reduction (7.6 % subtracted for 1 AP values).

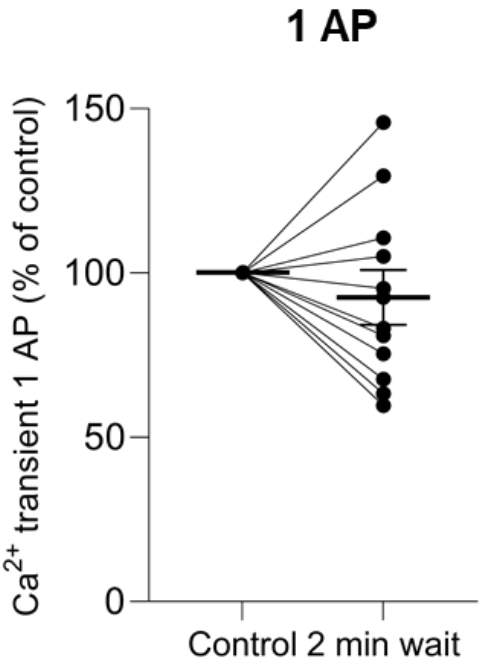

Figure 5. 2. Control run-down in presynaptic Ca^{2+} transient amplitudes during 2 minutes without application of ConTx during 1 AP in rat hippocampal terminals.
Two-minute wait after stimulation with 1 AP resulted in decreased Sy-GCaMP6f fluorescence changes from releasing presynaptic terminals during re-stimulation. n = 11 fields of view from 3 biological replicates.

Figure 5.3 depicts the contribution of $Ca_V2.2$ channels to presynaptic Ca^{2+} transients in functionally-releasing presynaptic terminals during 1 AP stimulation. In control boutons during 1 AP stimulation, 53.3 ± 5.5 % of presynaptic Ca^{2+} flux was via $Ca_V2.2$ channels (Fig. 5.3). TTX-treatment did not significantly alter $Ca_V2.2$ contribution as ConTx treatment revealed they make up 62.2 ± 5.7 % of total Ca^{2+} transients (unpaired t-test, *P* = 0.7; Fig. 5.3).

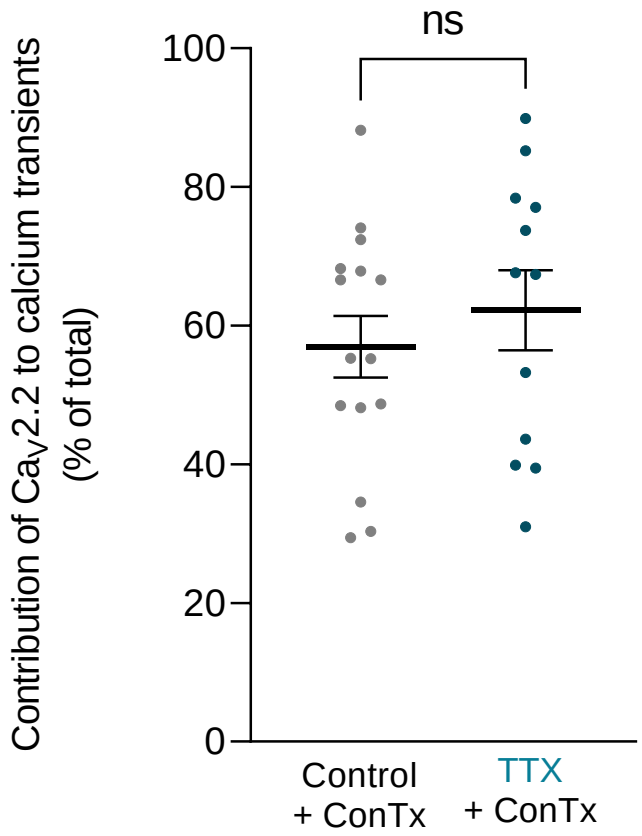

Figure 5. 3. Similar levels of $Ca_V2.2$ channel contribution to presynaptic Ca^{2+} flux at rat hippocampal terminals.

At DIV 18-22, $Ca_V2.2$ channels show a similar contribution to total Ca^{2+} flux at the presynapse after 1 AP stimulation in control (grey data points) and TTX-treated boutons (blue data points). Average Ca^{2+} transients were normalised to their respective "no toxin" peak before ConTx application. Unpaired t-test *P* = 0.7, n for control = 16 fields of view and n for TTX = 12 fields of view, n corresponds to fields of view from 3 independent experiments and is shown as mean ± SEM. The control data is the same data shown in Fig. 4.17. All values have been corrected subtracting the control reduction shown above in Fig. 5.2.

5.3. Elevated Ca^{2+} transients during homeostatic synaptic plasticity in mouse hippocampal neurons

Following confirmation that TTX potentiated presynaptic Ca^{2+} transients in rat neurons, Sy-GCaMP6f and VAMP-mOr2 experiments were repeated in mouse hippocampal terminals. As most studies on HSP in primary cells were thus far conducted in rat neuronal cultures, there is currently a lack of data regarding the effect of TTX on mouse neurons.

5.3.1. Increased presynaptic Ca^{2+} currents during homeostatic synaptic plasticity at DIV 18-22

First, presynaptic terminals expressing Sy-GCaMP6f and VAMP-mOr2 were stimulated with 1 AP at age 14-17 DIV and 18-22 DIV in untreated or TTX-treated conditions as described for rat neurons above. Fig. 5.4 shows that presynaptic Ca^{2+} transient amplitudes in functionally-releasing presynaptic terminals were similar in control and TTX conditions at DIV 14-17 (Fig. 5.7, DIV 14-17 control $\Delta F/F_0$ 0.032 ± 0.003 versus TTX-treated $\Delta F/F_0$ 0.04 ± 0.005, 2way ANOVA, P = 0.18). When leaving neurons in culture for longer, however, TTX treatment resulted in an increase of 40 % in presynaptic Ca^{2+} transient amplitudes in releasing boutons during stimulation with 1 AP ($\Delta F/F_0$ 0.038 ± 0.002 in TTX neurons; $\Delta F/F_0$ 0.024 ± 0.002 in control neurons, 2way ANOVA, P = 0.003).

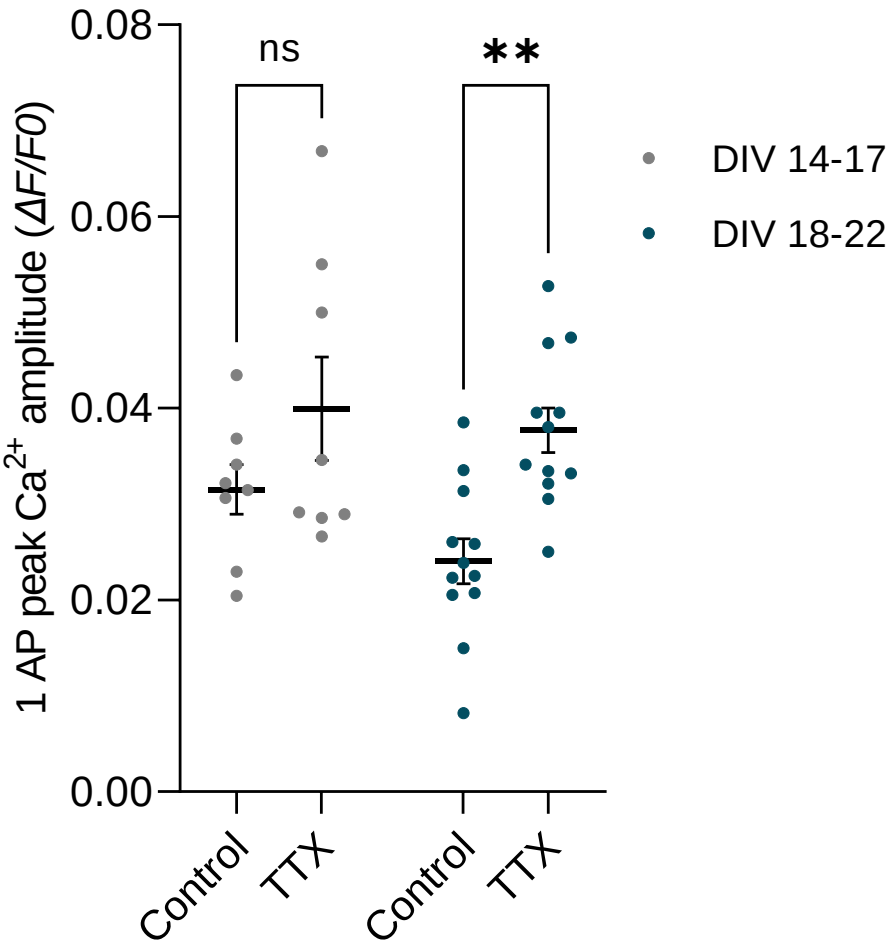

Figure 5. 4. TTX treatment effect on presynaptic Ca^{2+} transient amplitudes in hippocampal boutons at DIV 14-17 and at DIV 18-22.

At DIV 14-17, no significant differences were observed between presynaptic Ca^{2+} transients in control (grey data points) and TTX-treated (magenta data points) boutons, n = 8 biological replicates, 2way ANOVA, Sidak's multiple comparisons, *P* = 0.18. n corresponds to independent experiments and data are shown as mean ± SEM. At DIV 18-22, TTX treatment (blue data points) induced an increase in presynaptic Ca^{2+} transients compared to control boutons (grey data points), n = 12 biological replicates, 2way ANOVA, Sidak's multiple comparisons, *P* = 0.003. Interaction *P* = 0.41; n corresponds to independent experiments and data are shown as mean ± SEM.

5.3.2. Increased Ca^{2+} transients during homeostatic synaptic adaptations are mediated by $Ca_V2.2$ channels

Next, this study aimed to reveal if there was an increase of $Ca_V2.2$ channel contribution at presynaptic active zones to mediate the elevated Ca^{2+} transient amplitudes observed during compensatory adaptations at the synapse. For this, neurons were stimulated with 1 AP after a two-minute application of ConTx and Ca^{2+} transients were measured from functionally-releasing presynaptic terminals. Fig. 5.5 shows similar levels of $Ca_V2.2$ channel contribution to total Ca^{2+} flux in control and TTX-treated boutons at DIV 14-17. At this age, $Ca_V2.2$ channels mediated 31.4 ± 7.4 % (control) and 46.8 ± 5.9 % (TTX-treated) of all Ca^{2+} transients (2way ANOVA, *P* = 0.18; Fig. 5.5). However, at DIV 18-22 a significant increase in $Ca_V2.2$ channel contribution was observed after the induction of HSP with TTX. In control conditions, $Ca_V2.2$ channels made up 28.6 ± 8.4 % of all channels contributing to Ca^{2+} transients during 1 AP stimulation (Fig. 5.5). This contribution rose to 55.3 ± 4.3 % during homeostatic synaptic potentiation (2way ANOVA, *P* = 0.01; Fig. 5.5).

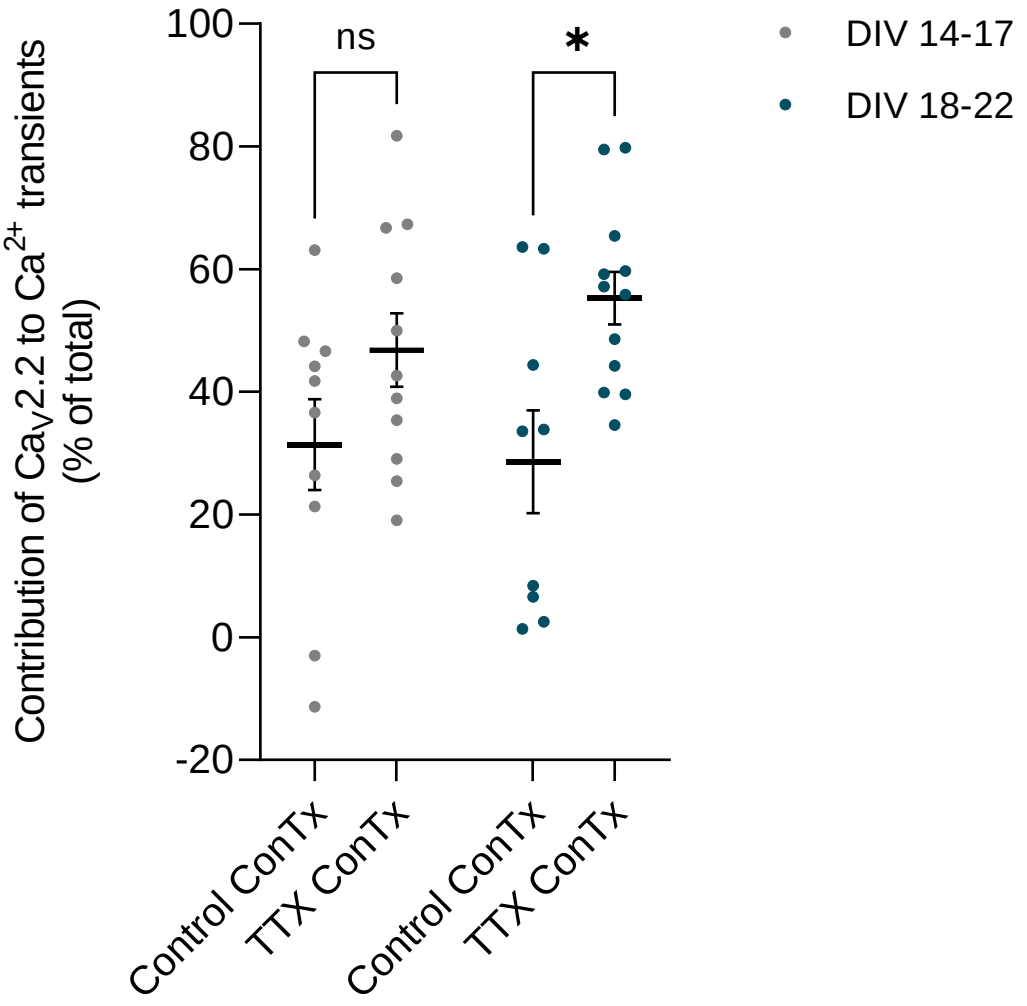

Figure 5. 5. $Ca_V2.2$ channels mediate increased Ca^{2+} transients during presynaptic potentiation at DIV 18-22.

(A) At DIV 14-17, contribution of $Ca_V2.2$ channels to total Ca^{2+} transients after 1 AP stimulation was similar in control (grey) and TTX-treated (orange) presynaptic terminals, averaged Ca^{2+} transients were normalised to their respective "no toxin" peaks (before ConTx application). 2way ANOVA, Sidak's multiple comparisons, *P* = 0.18, n for control = 10 fields of view from 3 biological replicates and n for TTX = 11 fields of view from 3 biological replicates; data are shown as mean ± SEM. **(B)** At DIV 18-22, $Ca_V2.2$ channels had a larger contribution to overall Ca^{2+} flux in TTX treated terminals (orange) than compared to control, untreated terminals (grey). Averaged Ca^{2+} transients were normalised to their respective "no toxin" peaks (before ConTx application). 2way ANOVA, Sidak's multiple comparisons, *P* = 0.01, n for control = 9 fields of view from 3 biological replicates and for TTX = 12 fields

of view from 3 biological replicates, interaction *P* = 0.39; data are shown as mean ± SEM. ns = not significant.

5.3.3. $Ca_V2.2$ channel levels increase during homeostatic adaptations, whereas $\alpha_2\delta$-1 levels decrease

To confirm the increase in $Ca_V2.2$ channel levels after induction of adaptational changes, immunoblotting experiments were performed. For this, whole cell lysates of neurons aged 18-22 DIV, untreated or TTX-treated, were purified and $Ca_V2.2$ channel levels revealed with anti-$Ca_V2.2$ channel II-III loop Abs by western blotting. Moreover, surface and total levels of the Ca_V subunit $\alpha_2\delta$-1 were studied, as this subunit is an important regulator of pre-and postsynaptic organisation. Figure 5.6 A and B show that during non-Hebbian plastic adaptations, overall levels of $Ca_V2.2$ channels were increased by 36.7 ± 0.02 %, paired t-test, *P* = 0.02), in line with findings from Ca^{2+} imaging experiments presented above. $Ca_V2.2$ channel levels were normalised to internal levels of GAPDH for each condition. To assess changes after TTX treatment, values were normalised to $Ca_V2.2$ levels in control samples. Next, cell surface biotinylation assays were performed to assess if the surface fraction of total levels of $\alpha_2\delta$-1 change after treatment with TTX. The hippocampal neurons potentiated with TTX revealed a decrease of surface (biotinylated fraction) and total $\alpha_2\delta$-1 (WCL fraction) (decrease to 88.61 ± 0.01 % and to 86.8 ± 0.04 %, respectively). Both values were normalised to WCL GAPDH signals from respective control and TTX conditions (Fig. 5.6 C and D). This finding may have important implications for the role of $\alpha_2\delta$-1 in regulating both $Ca_V2.2$ channels and other mechanisms involved in HSP.

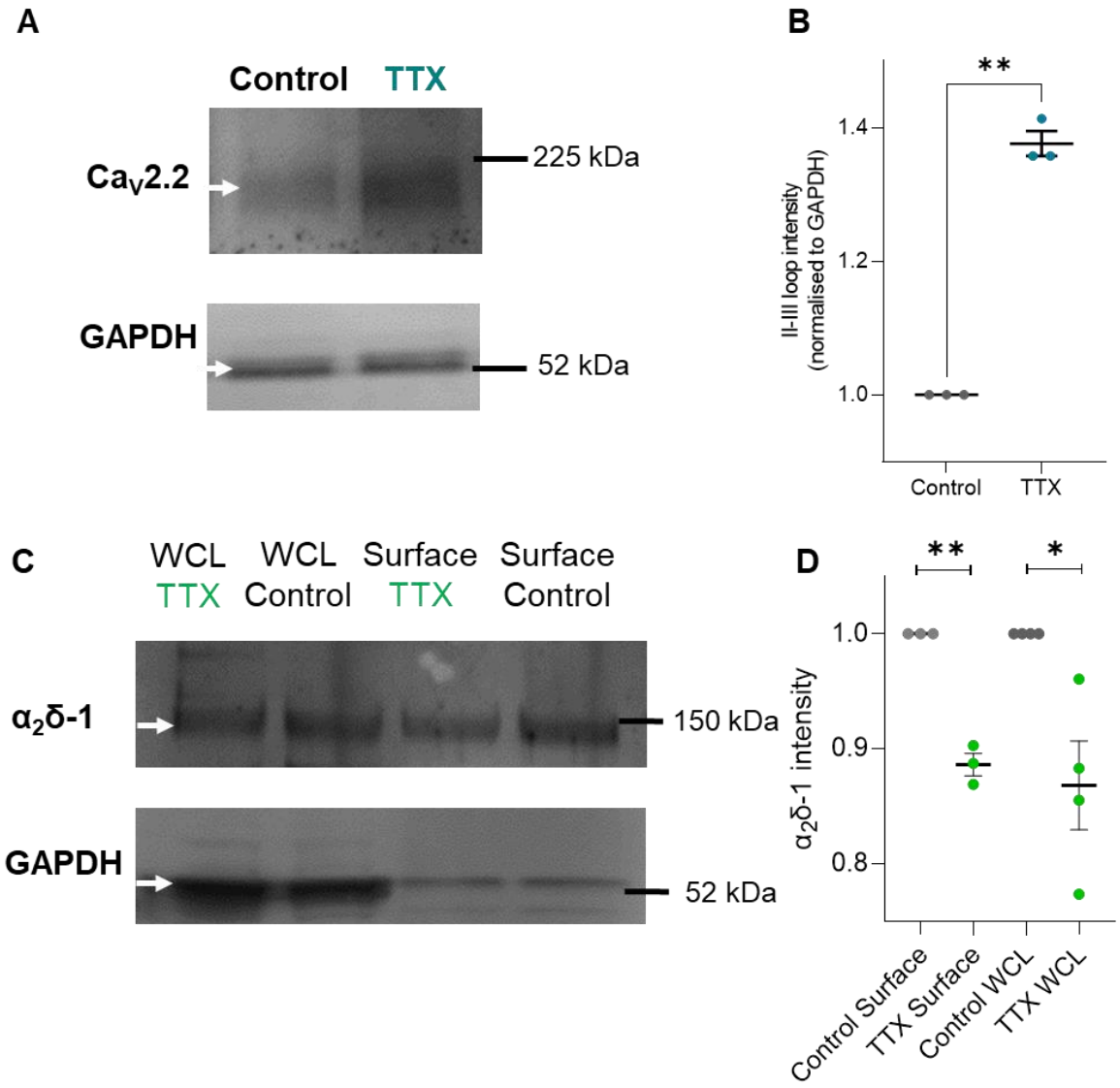

Figure 5. 6. During HSP, overall $Ca_V2.2$ channel levels increase whereas surface and overall abundance of $\alpha_2\delta$-1 decreases.

(A) Representative immunoblots showing the signal of antibodies against the II-III loop of $Ca_V2.2$ channels in whole-cell lysates (WCL) of control neurons and TTX-treated neurons (white arrowhead, top gel) at DIV 18-22. Values were normalised to the intensity of GAPDH antibodies for control and TTX neurons, respectively (white arrow heads, bottom gel). **(B)** Quantification of the intensity of $Ca_V2.2$ II-III loop Ab bands of three independent experiments reveal a stronger band after the induction of HSP with TTX (blue column) compared to control, untreated neurons (grey column). Paired t-test, P = 0.02, n = 3 biological replicates, averaged duplicates for each experiment. **(C)** Biotinylation experiments of control and TTX-treated hippocampal neurons showing the total amount of $\alpha_2\delta$-1 (WCL) and surface fractions, respectively (top gel, white arrow). Bands for GAPDH are shown in the

bottom gel (white arrow). **(D)** Values for $\alpha_2\delta$-1 were normalised to GAPDH (WCL) control bands for both TTX WCL and TTX surface values. n WCL = 4 biological replicates, n surface = 3 biological replicates. Paired t-test WCL *P* = 0.04; surface *P* = 0.007.

5.3.4. $\alpha_2\delta$-1 overexpression does not change basal Ca^{2+} flux but prevents Ca^{2+} transient increase during homeostatic adaptations

The observed downregulation of $\alpha_2\delta$-1 during adaptational plasticity after chronic TTX application led to the question of how $\alpha_2\delta$-1 may be involved in presynaptic remodelling. Therefore, the effect of overexpression of $\alpha_2\delta$-1 on basal Ca^{2+} transients and $Ca_V2.2$ channel contribution was investigated. For this, cells were co-transfected with Sy-GCaMP6f and VAMP-mOr2 and with $\alpha_2\delta$-1 or EV plasmids as a control (Fig. 5.7). The over-expression of $\alpha_2\delta$-1_HA in neurons is shown in Figure 5.7 A using anti-HA Abs targeting HA-tagged $\alpha_2\delta$-1_HA. As expected, no staining is visible in control neurons. Comparison of Ca^{2+} transient amplitudes in functionally-releasing presynaptic terminals during 1 AP stimulation showed similar Sy-GCaMP6f fluorescence values in the EV control ($\Delta F/F_0$ 0.025 ± 0.002) and in the $\alpha_2\delta$-1 overexpressing boutons ($\Delta F/F_0$ 0.028 ± 0.002, Fig. 5.7 B). Notably, ConTx application had a smaller effect on Ca^{2+} transients in $\alpha_2\delta$-1 overexpressing neurons. Here, the overall contribution of $Ca_V2.2$ channels to Ca^{2+} flux was decreased to 28.1 ± 5.8 % compared to 42.5 ± 6.4 % in control neurons (Fig. 5.7 C).

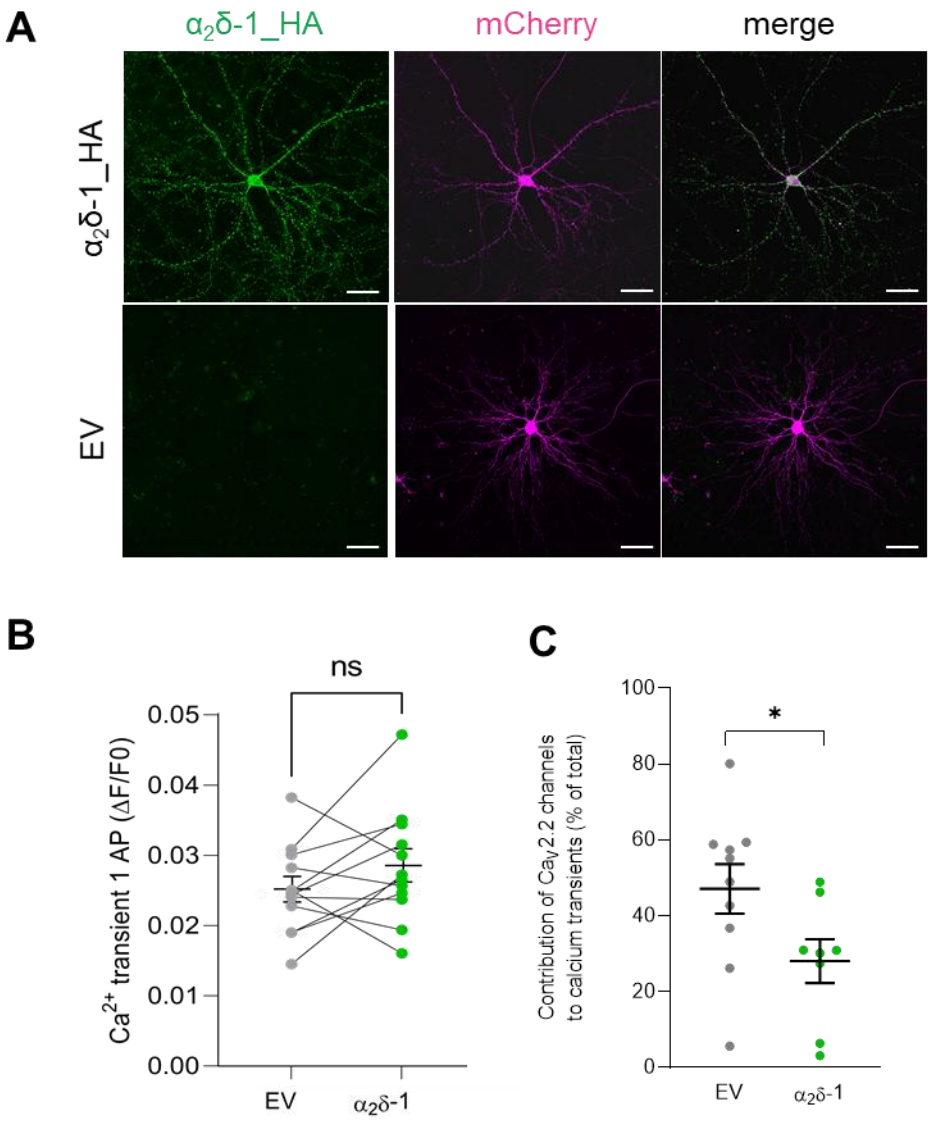

Figure 5. 7. The overexpression of α₂δ-1 does not change basal Ca^{2+} transient amplitudes but decreases the contribution of $Ca_V2.2$ channels to overall Ca^{2+} flux.

(A) Confocal images of immunostaining for α₂δ-1_HA in α₂δ-1 overexpressing neurons (top row) and control, EV-transfected neurons (bottom row). α₂δ-1_HA is shown in green and transfection marker mCherry in magenta, the staining was amplified with anti-RFP Abs. Maximum intensity projection of z-stacks and tile scan, optical section 0.279 µm, confocal mode x40, scale bar = 50 µm. **(B)** Ca^{2+} transient amplitudes after stimulation with 1 AP were similar in EV (grey) and α₂δ-1-overexpressing (green) neurons, n = 12 biological replicates, paired t-test *P* = 0.18. n corresponds to independent experiments and data are shown as mean ± SEM **(C)** Contribution of $Ca_V2.2$ channels to Ca^{2+} transients after stimulation with 1 AP was 42.5 ± 6.4 % (grey) in EV neurons and 28.1 ± 5.8 % (green) in neurons

overexpressing $\alpha_2\delta$-1, n for EV control = 9 fields of view and n for $\alpha_2\delta$-1 = 8 fields of view. Unpaired t-test, $P = 0.05$. Average Ca^{2+} transients were normalised to their respective “no toxin” peaks before ConTx application, n corresponds to fields of view from 5 independent experiments and is shown as mean ± SEM.

The expression of HSP, here measured as elevated presynaptic Ca^{2+} flux, was examined in presynaptic boutons overexpressing $\alpha_2\delta$-1 (Fig. 5.8). The effect of TTX on increased Ca^{2+} flux in functionally-releasing presynaptic terminals was abolished in neurons overexpressing $\alpha_2\delta$-1 ($\Delta F/F_0$ 0.027 ± 0.001 in $\alpha_2\delta$-1 overexpressing neurons and $\Delta F/F_0$ 0.029 ± 0.003 in TTX-treated $\alpha_2\delta$-1 overexpressing neurons, 2way ANOVA, $P = 0.99$), whereas control (EV) neurons were still potentiated by TTX ($\Delta F/F_0$ 0.023 ± 0.001 in EV-transfected neurons and $\Delta F/F_0$ 0.043 ± 0.005 in TTX treated EV-transfected neurons, 2way ANOVA, $P = 0.0002$).

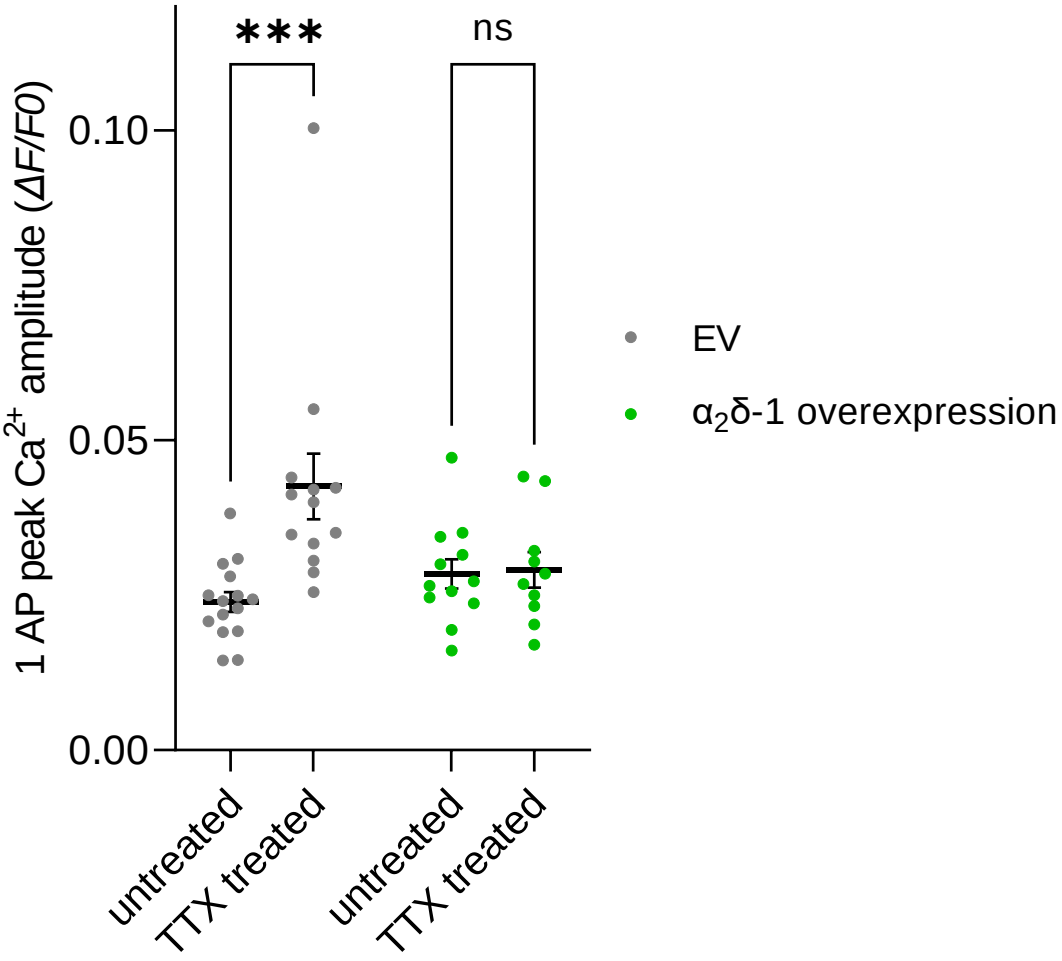

Figure 5. 8. Prevention of Ca^{2+} transient increase during compensatory adaptations in presynaptic terminals overexpressing $\alpha_2\delta$-1.

Ca^{2+} transient amplitudes after stimulation with 1 AP were larger in TTX-treated EV control conditions (P = 0.002) but similar in $\alpha_2\delta$-1 overexpressing neurons with and without TTX (P = 0.99), 2way ANOVA, Sidak's multiple comparisons post-hoc test, interaction P = 0.01; n corresponds to biological replicates and data are shown as mean ± SEM; n for EV = 15 biological replicates and EV + TTX = 13 biological replicates; n for $\alpha_2\delta$-1-overexpressing neurons = 12 biological replicates and n $\alpha_2\delta$-1-overexpressing neurons + TTX = 10 biological replicates. ns = not significant.

5.4. Summary and Discussion

This work sought to elucidate the impact of presynaptic potentiation during HSP on Ca^{2+} flux, vesicular release, presynaptic $Ca_V2.2$ channels and $\alpha_2\delta$-1 in hippocampal neurons. Numerous studies have shown that silencing neuronal network activity by applying Na_V inhibitor TTX results in both pre- and postsynaptic remodelling (Turrigiano 2011). As presynaptic Ca_V2 channels mediate synaptic transmission, an increase or decrease in channel activity or levels would be a direct way to modulate neurotransmitter release. Indeed, it was observed that adaptive changes during HSP result in increased presynaptic Ca^{2+} flux (Jeans *et al.* 2017; Zhao *et al.* 2011) and release probability (Jeans *et al.* 2017; Vitureira *et al.* 2011; Murthy *et al.* 2001). This has been shown to be at least partially mediated by a recruitment of $Ca_V2.1$ channels to the active zone facilitating increased Ca^{2+} transients after the induction of HSP with TTX (Jeans *et al.* 2017; Glebov *et al.* 2017).

In the first part of this chapter, the presynaptic potentiation of Ca^{2+} flux was visualised by changes in Sy-GCaMP6f fluorescence from neurotransmitter-releasing presynaptic boutons of rat hippocampal cells. As most studies thus far have used hippocampal or cortical cultures from rat embryos or new born rats, this study initially used hippocampal rat neurons as well. The potentiating effect of TTX on Ca^{2+} transient amplitudes was found only in more mature rat hippocampal neurons at DIV 18-22 with 1 AP stimulation. In less mature neurons, TTX treatment did not have a discernible effect on levels of Ca^{2+} transient amplitudes in functionally-releasing presynaptic boutons during 1 AP stimulation, contradicting findings from a previous study (Jeans *et al.* 2017). Including VAMP-mOr2 as a reporter of presynaptic exocytosis allowed identification of active, neurotransmitter-releasing boutons and non-releasing boutons. Only Ca^{2+} transients from releasing boutons were used to analyse changes after TTX treatment, as only in these boutons one can assume that Ca^{2+} flux was at functional synapses.

The application of ConTx to hippocampal rat neurons revealed similar levels of $Ca_V2.2$ channel contribution to total Ca^{2+} flux in control and TTX-potentiated presynaptic

terminals. Ca^{2+} flux during 1 AP stimulation was mainly via $Ca_V2.2$ channels, mediating more than half of the Ca^{2+} transients during 1 AP. This was slightly higher than reported in previous studies (Ferron *et al.* 2020a) and may be due to differences in experimental setup or protocol design. As Ca^{2+} transients increased after TTX treatment and the contribution of $Ca_V2.2$ channels remained similar compared to control neurons, $Ca_V2.2$ channels abundance at the presynapse can be assumed to have increased. This was likely accompanied by a simultaneous upregulation of $Ca_V2.1$, and $Ca_V2.3$ to a lesser extent. Data from a study that performed Ca^{2+} live cell imaging experiments in rat hippocampal neurons aged 14-18 DIV suggests that the Ca^{2+} influx after TTX application is $Ca_V2.2$ channel-independent and that it relies solely on $Ca_V2.1$ channels (Jeans *et al.* 2017). Another study, however, observed a recruitment of $Ca_V2.2$ channels to the TTX-treated active zone in rat neurons at DIV 16-21 using STORM super resolution imaging (Glebov *et al.* 2017). They did not include ConTx in Ca^{2+} imaging experiments to confirm a potential upregulation during their stimulation protocol with 10 AP as their work focused on $Ca_V2.1$ channels. The application of $Ca_V2.1$ channel inhibitor ω-agatoxin IVA presented in their work, did not completely block the increase induced by TTX treatment, indicating a potential additional involvement of $Ca_V2.2$ or $Ca_V2.3$ channels.

Moreover, some studies found a temporal regulation of the expression locus of HSP. In younger neurons, a predominantly postsynaptic remodelling was described, whereas in more mature neurons both pre- and postsynaptic adaptations were observed (Han and Stevens 2009; Wierenga *et al.* 2006). The classification of hippocampal neurons into less (DIV 14-17) and more mature (DIV 18-22) in this study allowed confirmation of the involvement of presynaptic Ca^{2+} flux during HSP in more mature neurons exclusively. This age-dependent effect of TTX on presynaptic Ca_V2 channels is especially interesting as there might be a developmental regulation of Ca_V2 channel distribution.

Because of the relative sparsity of Ca^{2+} imaging experiments performed in mouse neurons together with the availability of the novel $Ca_V2.2\_HA^{KI/KI}$ mouse model in our

laboratory, HSP experiments with Ca^{2+} indicator Sy-GCaMP6f were expanded to include mouse hippocampal neurons. Similar to the described effect of TTX on rat neurons, the application of TTX to mouse hippocampal neurons resulted in an increase of Ca^{2+} flux due to compensatory changes at the synapse. This was exclusively observed in more mature mouse cultures aged 18-22 DIV, whereas levels of Ca^{2+} flux in younger neurons at DIV 14-17 seemed unaffected by incubation with TTX. Together these data indicate that presynaptic potentiation is only induced in more mature neurons at DIV 18-22, further supporting the notion of a presynaptic expression of HSP in older neurons (Han and Stevens 2009; Wierenga *et al.* 2006).

The application of ConTx revealed that in less mature presynaptic terminals, $Ca_V2.2$ channels are responsible for about a third of the total Ca^{2+} transient after stimulation with 1 AP. Whereas levels of $Ca_V2.2$ channel contribution to baseline Ca^{2+} flux were similar in neurons aged DIV 14-17 and DIV 18-22, the application of TTX resulted in a significant increase of 25 % of $Ca_V2.2$ channel contribution to the total Ca^{2+} flux in response to 1 AP in more mature neurons. $Ca_V2.2$ channels therefore play an important role during presynaptic homeostatic adaptations. The discrepancy between rat and mouse neurons in terms of $Ca_V2.2$ channel contribution to presynaptic Ca^{2+} flux provides further evidence for distinct synaptic properties in neurons of the two different animal models.

After having established that TTX treatment induces increased presynaptic Ca^{2+} transients via $Ca_V2.2$ channels in functionally-releasing terminals at 18-22 DIV, western blotting experiments were performed which confirmed findings from live cell imaging experiments. Immunoblots of whole cell lysates from control and TTX-treated neurons revealed an increase of total $Ca_V2.2$ channels of approximately 30 % after TTX treatment, and thereby confirmed the increase detected with ConTx in live neurons. Further studies should assess if the increased $Ca_V2.2$ channels are mostly located on the cell surface or if it is an overall increase of membrane and intracellular $Ca_V2.2$ channels being trafficked to the active zone. However, biotinylation studies aiming to analyse surface $Ca_V2.2$

channel levels were unsuccessful, potentially due to the number of channels being below detection levels via western blotting or because the few extracellular lysines that are biotinylatable were occluded by auxiliary $\alpha_2\delta$ subunits or other interaction partners (Cassidy *et al.* 2014).

$\alpha_2\delta$-1 subunits are an important parameter for synaptic transmission as they regulate Ca_V2 channel abundance on the presynaptic membrane (Hoppa *et al.* 2012). In addition, $\alpha_2\delta$-1 acts independently from Ca_V channels to interact with other proteins and to modulate synaptic activity (Schöpf *et al.* 2021; Dolphin 2013). Therefore, this study sought to determine changes in surface $\alpha_2\delta$-1 during compensatory changes at the synapse following chronic TTX treatment by biotinylation and immunoblotting. This revealed lower levels of $\alpha_2\delta$-1 both in whole cell lysates and specifically on the surface of neurons after the induction of HSP with TTX, indicating a downregulation of $\alpha_2\delta$-1. Intrigued to further elucidate the role of $\alpha_2\delta$-1 during HSP, neurons were transfected with $\alpha_2\delta$-1 and Ca^{2+} flux was analysed with Sy-GCaMP6f and VAMP-mOr2. There were no changes in basal presynaptic Ca^{2+} transient amplitudes in terminals overexpressing $\alpha_2\delta$-1, contrary to previous findings in which $\alpha_2\delta$-1 overexpression led to a reduction in Ca^{2+} flux (Hoppa *et al.* 2012). However, ConTx treatment revealed a reduced contribution of $Ca_V2.2$ channels to total Ca^{2+} flux in $\alpha_2\delta$-1 overexpressing neurons. Finally, data indicate that the $\alpha_2\delta$-1 overexpression prevents elevated presynaptic Ca^{2+} transients observed after TTX treatment. A recent study investigated the effect of $\alpha_2\delta$-1 overexpression on the developmental of neuronal networks *in vitro* and discovered that neurons overexpressing $\alpha_2\delta$-1 exhibit spontaneous neuronal activity and increased presynaptic glutamate release (Bikbaev *et al.* 2020). This finding might indicate that neuronal network activity in $\alpha_2\delta$-1 overexpressing neurons was already increased, therefore the application of TTX did not have a potentiating effect. This increased neuronal activity might also explain the downregulation of $Ca_V2.2$ channels.

Generally, the amount of $\alpha_2\delta$ proteins is likely to vary in different synapses, but levels are usually thought to be higher than those of Ca_V2 channels (Muller *et al.* 2010). It was shown that the complex between $\alpha_2\delta$ and Ca_V2 channels is in an equilibrium (Muller *et al.* 2010), hence the more $\alpha_2\delta$ is present, the more Ca_V2 channels will be in complex with $\alpha_2\delta$. $\alpha_2\delta$-1 is present in lipids rafts, small microdomains within the plasma membrane, high in cholesterol and sphingolipids (Pani and Singh 2009). Notably, $\alpha_2\delta$-1 also mediates the partitioning of $Ca_V2.2$ channels into these specialised lipid-rich membrane domains (Robinson *et al.* 2010), resulting in reduced Ca^{2+} currents (Ronzitti *et al.* 2014; Davies *et al.* 2006). Increasing the abundance of $\alpha_2\delta$-1 in presynaptic terminals during overexpression, may lead to increased levels of $Ca_V2.2$ channels in lipid rafts, decreasing their mobility and their contribution to Ca^{2+} flux. The fact that basal Ca^{2+} transients did not change in $\alpha_2\delta$-1-overexpressing terminals may be due to compensatory $Ca_V2.1$ or $Ca_V2.3$ channel upregulation, ensuring stable Ca^{2+} transients. Chronic silencing of neuronal activity caused an increase in Ca^{2+} transients due to greater $Ca_V2.2$ channel contribution and increased $Ca_V2.2$ protein levels, while levels of $\alpha_2\delta$-1 decreased. This decrease of $\alpha_2\delta$-1 may be required to allow increased mobility of $Ca_V2.2$ channels, necessary for presynaptic potentiation. Overexpression of $\alpha_2\delta$-1 potentially prevents the elevation of presynaptic Ca^{2+} transients after TTX treatment by “clamping” $Ca_V2.2$ channels in lipid domains.

Further work is needed to evaluate the interaction between $\alpha_2\delta$-1 and Ca_V2 channels at the different compartments of the active zone. Together, these findings show an involvement of $Ca_V2.2$ channels in HSP and demand further examination into the role of $\alpha_2\delta$ subtypes, as major regulators of homeostatic processes at the synapse.

Chapter 6. General Discussion and Outlook

6.1. Distribution of presynaptic $Ca_V2.2$ channels in the brain

Presynaptic $Ca_V2.2$ channels have an important role in the release of neurotransmitters, both in the central and peripheral nervous system. Due to this vital role of $Ca_V2.2$ channels in synaptic transmission, many studies have focussed on deciphering their biophysical properties, interaction partners and distribution. As $Ca_V2.2$ channels in the nociceptive pathway are also a therapeutic target to alleviate neuropathic pain, understanding their contribution to Ca^{2+} release at different synapses is crucial.

At most central synapses, Ca^{2+} release is mediated cooperatively by $Ca_V2.1$, $Ca_V2.2$ and, to a lesser extent, $Ca_V2.3$ channels. The number and type of presynaptic Ca_V2 channels is an important determinant for vesicle exocytosis. However, only few generalities can be made regarding the distribution of each subtype at different synapses in the brain. In the large Calyx of Held synapse in the brain stem, synaptic transmission in neonates is mediated by loosely coupled $Ca_V2.1$ and $Ca_V2.2$ channels, whereas in the mature synapse Ca^{2+} flux is predominantly mediated by tightly coupled $Ca_V2.1$ channels (Iwasaki and Takahashi 1998; Iwasaki *et al.* 2000; Fedchyshyn and Wang 2005). This developmental shift from $Ca_V2.2$ to $Ca_V2.1$ channels has also been described in other brain regions (Bornschein *et al.* 2019; Scholz and Miller 1995; Miki *et al.* 2013) and is partially confirmed by findings presented in Chapter 4. Whereas at neonatal ages, $Ca_V2.2$ channel mRNA and protein levels were similar across the different brain regions, in adult brains, levels of $Ca_V2.2$ were much higher in cortex and hippocampus compared to brain stem and cerebellum (Fig 3.2 and Fig 3.4). This suggests that $Ca_V2.2$ channels may be less relevant for synaptic transmission in the adult brain stem and cerebellum, compared to new-born mice. In the cortex and hippocampus in contrast, $Ca_V2.2$ channels seem to remain important at the presynapse at all ages. The availability of the three Ca_V2 channels for Ca^{2+} influx may allow for more diverse Ca^{2+} transients and faster modulation of synaptic release (Dolphin and Lee 2020).

Functional surface $Ca_V2.2$ channels have mostly been studied through electrophysiological and pharmacological means. Though this provides insight into channel physiology and regulation, information on the spatial organisation of $Ca_V2.2$ channels at the active zone requires immunocytochemistry approaches with specific antibodies. Visualisation of $Ca_V2.2$ channels, especially in their functional state at the plasma membrane, had been hindered by the availability of appropriate tools, such as specific antibodies. Here, super resolution imaging of $Ca_V2.2\_HA^{KI/KI}$ brain slices revealed $Ca_V2.2$_HA channels in the brain for the first time (Fig 3.6-3.10). Previous work has confirmed the validity of the mouse model and showed the distribution of $Ca_V2.2$_HA channels in spinal cord and DRG neurons (Nieto-Rostro *et al.* 2018). In chapter 3, I reveal $Ca_V2.2$_HA channels around somata of pyramidal neurons of the hippocampal CA1, CA3 and granule cells of the DG area, with higher levels in adult brains compared to neonates (Fig 3.11). Although it is not possible to conclude if channels were expressed on the somatic surface of the neurons or if they were from neurons synapsing onto the pyramidal cells, these findings show the importance of $Ca_V2.2$ channels for synaptic transmission in the hippocampus, likely involved in the formation of memory. Indeed, in a $Ca_V2.2$ knock-out mouse model, impairments in long-term memory were observed (Nakagawasai *et al.* 2010).

Immunostaining of hippocampal neurons from $Ca_V2.2\_HA^{KI/KI}$ mice in Chapter 4 show the subcellular distribution of endogenous $Ca_V2.2$ channels on the soma and along neurites (Fig 4.10-4.12), similar to findings in a spinal cord-DRG coculture system of the same mouse model (thesis UCL K Ramgoolam, 2020). The background non-specific signal detected in wild type control hippocampal neurons, however, made the analysis of $Ca_V2.2$_HA from $Ca_V2.2\_HA^{KI/KI}$ neurons puncta challenging. It would be difficult to ascertain true $Ca_V2.2$_HA puncta with masking techniques using ImageJ for example, as similar levels of HA puncta might be visible in wild type and $Ca_V2.2\_HA^{KI/KI}$ neurons.

Therefore, the stainings of endogenous $Ca_V2.2$_HA channels in central synapses require optimization for analysis of fluorescent puncta.

Using the $Ca_V2.2$ channel inhibitor ConTx revealed similar $Ca_V2.2$ channel levels in mouse hippocampal neurons at two maturity stages (Fig 4.15), contradicting earlier reports on a downregulation of $Ca_V2.2$ channels in more mature hippocampal cultures (Scholz and Miller 1995). Notably, larger Ca^{2+} transients at the less mature timepoint indicate less tight coupling of Ca_V2 channels to the vesicle release machinery (Fig 4.6). This may be due to predominant microdomain coupling at a younger timepoint *in vitro*, at which higher levels of Ca^{2+} influx are required for vesicle exocytosis. Although, live cell Ca^{2+} imaging provides specific insights into Ca^{2+} transients at presynaptic boutons, recordings of one field of view always involve several (up to 75) ROIs, therefore the values obtained represent an average of many boutons. Moreover, both excitatory and inhibitory synapses are present in hippocampal cultures and transfecting with Sy-GCaMP6f does not discriminate between the two types. Therefore, differences in Ca^{2+} signalling and Ca_V2 channel abundance between different types of boutons cannot be detected and will require another experimental approach to be revealed.

Results from Chapter 3 and 4 highlight the role of $Ca_V2.2$ channels in the mouse hippocampus at different stages of maturity, where channels contribute to Ca^{2+} influx and synaptic vesicle release.

6.2. Role of $Ca_V2.2$ during homeostatic synaptic plasticity

Homeostatic synaptic plasticity involves compensatory synaptic mechanisms to prevent neuronal hyper- or hypoactivity, often in response to plastic changes such as Hebbian plasticity or pathological network alterations (Turrigiano 2008; Pozo and Goda 2010). At the presynapse, it was shown that compensatory changes after activity blockade results in unclustering of the active zone matrix and the recruitment of proteins of the vesicle release machinery, such as Ca_V2 channels (Glebov *et al.* 2017). Although most studies of non-Hebbian plasticity in TTX-treated hippocampal neurons have thus far focussed on $Ca_V2.1$ channels (Jeans *et al.* 2017; Glebov *et al.* 2017), super resolution imaging also revealed an enrichment of $Ca_V2.2$ and $Ca_V2.3$ channels at the active zone (Glebov *et al.* 2017). Data presented in chapter 5 shows the involvement of $Ca_V2.2$ channels in compensatory adaptation, as their contribution to Ca^{2+} transients to 1 AP stimulation increased by 30 % after chronic activity blockade (Fig 5.5). The increase in Ca^{2+} transients and the elevated $Ca_V2.2$ channel contribution was, however, only observed in cultures at DIV 18-22. In younger cultures, TTX did not induce a consistent potentiation of Ca^{2+} flux or an increase in $Ca_V2.2$ channels (Fig 5.4 and Fig 5.5). When taking a close look at individual data points, the responses of boutons to electrical stimulation seem more variable compared to responses in older cultures. This might indicate more diverse synaptic populations in less mature neurons, that become more refined as neurons mature.

HSP is not mediated by the bidirectional up-or downregulation of a single protein, but involves diverse processes acting simultaneously on different levels to stabilise neuronal networks (Lee *et al.* 2014). Therefore, further work is required to study $Ca_V2.2$ channels at different synapse and neuron types and to identify interaction partners of $Ca_V2.2$ channels that might support their enrichment or increase their function at the active zone of the presynaptic terminal.

6.3. $\alpha_2\delta$-1 and homeostatic synaptic plasticity

The $\alpha_2\delta$ subunits are crucial for trafficking and functioning of Ca_V2 channels but beyond this, they are also essential for synaptic function (Schöpf *et al.* 2021; Dolphin 2013). Their newly emerging role in synaptic plasticity (Brennan *et al.* 2021; Wang *et al.* 2016) has implications for clinical applications, as $\alpha_2\delta$-1 is an important target of analgesics (Field *et al.* 2006). However, very little is known about the effects of $\alpha_2\delta$-1 in brain plasticity. Data presented in chapter 5 show that surface and total levels of $\alpha_2\delta$-1 decrease after the application of TTX (Fig 5.7), while in neurons that overexpress $\alpha_2\delta$-1, the effect of TTX on potentiating presynaptic Ca^{2+} currents was abolished (Fig. 5.8). This suggests that the downregulation of $\alpha_2\delta$-1 might be required to facilitate compensatory changes at the synapse with $\alpha_2\delta$-1 as a checkpoint for changes to the presynapse. $\alpha_2\delta$-1 subunits play an important part during neuronal development and synaptogenesis, hence overexpressing $\alpha_2\delta$-1 from DIV 7 on will influence neuronal networks formed *in vitro*. Recently, a study revealed increased levels of spontaneous neuronal network activity in rat hippocampal neurons overexpressing $\alpha_2\delta$-1 together with a higher density of excitatory synaptic connections (Bikbaev *et al.* 2020). This elevated baseline activity itself might have induced some form of compensatory HSP mechanisms and might explain why $Ca_V2.2$ channels were downregulated and why TTX did not potentiate Ca^{2+} transients further. Notably, baseline levels of Ca^{2+} transients were similar in control and $\alpha_2\delta$-1-overexpressing boutons. This contradicts previous reports which showed that increased levels of $\alpha_2\delta$-1 result in increased levels of $Ca_V2.2$ channels, but variations in experimental conditions, eg rat versus mouse cultures, synaptic density and stimulation protocols, might explain the observed differences.

6.4. Future work

6.4.1. $Ca_V2.2$ channel distribution at different synapse types

The distribution of $Ca_V2.2$ channels is heterogenous and most synapses likely contain different presynaptic Ca_V2 channels, providing a way of terminal-specific modulation of synaptic function. Numerous questions regarding the subcellular distribution and surface expression of $Ca_V2.2$ channels remain unanswered. To shed light on this, super resolution microscopy could be used on cultured hippocampal neurons from the $Ca_V2.2\_HA^{KI/KI}$ mouse. The extracellular HA tag would allow the visualisation of functional $Ca_V2.2$ channels at single active zones, previously inaccessible due to a lack of suitable antibodies. These studies should be complemented by specific excitatory and inhibitory synapse markers to establish the distribution of $Ca_V2.2$ channels at different synapses at different time points in culture. To overcome some *in vitro* limitations, such as neuronal networks that only recapitulate some features of brain circuits together with potential changes in cell surface expression of proteins during enzymatic dissociation of cells, organotypic slices from the same mouse model could be used to confirm the distribution of $Ca_V2.2\_HA$ channels observed *in vitro*. Organotypic slices of brains of different ages would reveal *in vivo* how the distribution of $Ca_V2.2$ channels changes as the brain matures.

6.4.2. $Ca_V2.2$ channel trafficking

Regulating the amount of $Ca_V2.2$ channel trafficking and insertion into the plasma membrane of the presynaptic terminal is an important modulator of synaptic function. To assess $Ca_V2.2$ channel trafficking and mobility in different neuronal compartments, quantum dot nanoparticles could be used, which allow tracking the mobility of surface proteins in real time over extended periods of time. Quantum dots consist of core nanocrystals, an inorganic shell and an organic shell enabling the coupling to proteins, such as antibodies that can be used for direct binding of the quantum dot to the target of

interest. Due to their small size of approximately 5 nm, their high brightness and low photobleaching, they can be used to track molecules in various membrane compartments, including confined spaces, such as the active zone of the presynaptic terminal. Targeting the extracellular epitope of $Ca_V2.2$ channels in neurons from $Ca_V2.2\_HA^{KI/KI}$ mice, dynamics of endogenous channels could be tracked for the first time. This could help establish different mobility patterns of $Ca_V2.2$_HA channels at different ages and after the induction of HSP with TTX for example. Combining Sy-GCaMP6f experiments with quantum dots would reveal the effect of electrical stimulation on surface $Ca_V2.2$ channels, which would contribute to our understanding of presynaptic zone dynamics during synaptic activity.

6.4.3. $Ca_V2.2$ channels and their interaction with $\alpha_2\delta$-1 and $\alpha_2\delta$-3

$\alpha_2\delta$-1 proteins are present in lipid rafts (Davies *et al.* 2006) and might mediate the partitioning of $Ca_V2.2$ channels into these microdomains to modulate their function. Lipid rafts could be disrupted by cholesterol depleting agents such as β-cyclodextrin to investigate if this affects the observed downregulation of $Ca_V2.2$ channels in hippocampal neurons that overexpress $\alpha_2\delta$-1. Whereas $\alpha_2\delta$-1 overexpression was shown to result in increased spontaneous neuronal activity and increased excitatory synapse levels, $\alpha_2\delta$-3 was shown to promote inhibitory spinogenesis in hippocampal cultures (Bikbaev *et al.* 2020). The effect of $\alpha_2\delta$-3 overexpression for $Ca_V2.2$ channel function, would be exciting to decipher, for example in the context of synaptic plasticity.

6.4.5. $Ca_V2.2$ channels and homeostatic synaptic remodelling

Synapses are highly dynamic and can adjust their molecular composition of proteins depending on synaptic needs. $Ca_V2.2$ channels are crucial for vesicle exocytosis at most central synapses. Therefore, modulation of their abundance or their activity provides a powerful means to increase or decrease synaptic activity, for example during synaptic plasticity. Here, we showed the increase of $Ca_V2.2$ channels during HSP after chronic

neuronal activity blockade. Next, the effect of chronically increased neuronal activity, for example by blocking neuronal inhibition with $GABA_A$ receptor antagonist gabazine, could be studied. This might reveal novel roles of $Ca_V2.2$ channels in regulation of firing rates in neuronal networks. Moreover, neurons from double transgenic $Ca_V2.2\_HA^{KI/KI}$ $\alpha_2\delta$-$1^{KO/KO}$ mice (Nieto-Rostro *et al.* 2018) could be used to study the effect of the lack of $\alpha_2\delta$-1 subunits on $Ca_V2.2$ channels during HSP. The HSP experiments in hippocampal cultures could be complemented by *in vivo* studies of hippocampal HSP and $Ca_V2.2$ channels in organotypic hippocampal slices (Kim and Tsien 2008). Live cell Ca^{2+} imaging and immunohistochemistry studies would reveal changes in Ca^{2+} transients and distribution of $Ca_V2.2\_HA$ after chronic activity silencing with TTX.

6.5. Conclusion

Data presented here reveals the importance of presynaptic $Ca_V2.2$ channels in the mouse brain at different stages of development, with a focus on hippocampal neurons. Moreover, novel functions of $Ca_V2.2$ as well as $\alpha_2\delta$-1 during synaptic plasticity were revealed.

In Chapter 3, the abundance of $Ca_V2.2$ channels in cortex, hippocampus, cerebellum and brain stem is shown on a genetic and protein level. Whereas levels of $Ca_V2.2$ decrease in brain stem and cerebellum as the mouse brain matures, levels in the cortex and hippocampus remain high in adult brains. Hippocampal slices from $Ca_V2.2\_HA^{KI/KI}$ mice allow the visualisation of $Ca_V2.2$ channels in the trisynaptic loop for the first time.

Chapter 4 introduces hippocampal cultures form rats and mice to further investigate the role of $Ca_V2.2$ channels in the hippocampus. Immunostainings of neurons from $Ca_V2.2\_HA^{KI/KI}$ mice reveal endogenous channels in different neuronal compartments. Additionally, Sy-GCaMP6f transfected cells were used to study the contribution of $Ca_V2.2$ channels to presynaptic Ca^{2+} dynamics, which revealed larger transients in less mature neurons.

Finally, chapter 5 shows an increased contribution of $Ca_V2.2$ channels to elevated Ca^{2+} transients during HSP in more mature cultures. Whereas levels of $Ca_V2.2$ channels increased after TTX treatment, surface and total levels of $\alpha_2\delta$-1 decreased. Furthermore, the overexpression of $\alpha_2\delta$-1 prevented the potentiation of Ca^{2+} transients and resulted in decreased contribution of $Ca_V2.2$ channels to overall presynaptic Ca^{2+} flux.

Overall, this work shows the importance of $Ca_V2.2$ channels at different maturity stages of the brain. Especially in hippocampal neurons, $Ca_V2.2$ channels are crucial for synaptic function and a critical feature of homeostatic synaptic plasticity processes at the presynapse. Moreover, data presented here reveal novels role for $\alpha_2\delta$-1 during synaptic remodelling.

Bibliography

Ablinger C., Geisler S. M., Stanika R. I., Klein C. T., Obermair G. J. (2020) Neuronal α2δ proteins and brain disorders. *Pflugers Arch.* **472**, 845–863.

Ahmed M. S., Siegelbaum S. A. (2009) Recruitment of N-Type Ca(2+) channels during LTP enhances low release efficacy of hippocampal CA1 perforant path synapses. *Neuron* **63**, 372–385.

Ali A. B., Nelson C. (2006) Distinct Ca2+ channels mediate transmitter release at excitatory synapses displaying different dynamic properties in rat neocortex. *Cereb. Cortex* **16**, 386–393.

Altier C., Dale C. S., Kisilevsky A. E., Chapman K., Castiglioni A. J., Matthews E. A., Evans R. M., et al. (2007) Differential role of N-type calcium channel splice isoforms in pain. *J. Neurosci.* **27**, 6363–6373.

Altier C., Garcia-Caballero A., Simms B., You H., Chen L., Walcher J., Tedford H. W., Hermosilla T., Zamponi G. W. (2011) The Cavbeta subunit prevents RFP2-mediated ubiquitination and proteasomal degradation of L-type channels. *Nat. Neurosci.* **14**, 173–180.

Altier C., Khosravani H., Evans R. M., Hameed S., Peloquin J. B., Vartian B. A., Chen L., et al. (2006) ORL1 receptor-mediated internalization of N-type calcium channels. *Nat. Neurosci.* **9**, 31–40.

Andrade A., Denome S., Jiang Y.-Q., Marangoudakis S., Lipscombe D. (2010) Opioid inhibition of N-type Ca2+ channels and spinal analgesia couple to alternative splicing. *Nat. Neurosci.* **13**, 1249–1256.

Arendt K. L., Sarti F., Chen L. (2013) Chronic inactivation of a neural circuit enhances LTP by inducing silent synapse formation. *J. Neurosci.* **33**, 2087–2096.

Ariel P., Hoppa M. B., Ryan T. A. (2012) Intrinsic variability in Pv, RRP size, Ca(2+) channel repertoire, and presynaptic potentiation in individual synaptic boutons. *Front. Synaptic Neurosci.* **4**, 9.

Arimura N., Ménager C., Kawano Y., Yoshimura T., Kawabata S., Hattori A., Fukata Y., et al. (2005) Phosphorylation by Rho kinase regulates CRMP-2 activity in growth cones. *Mol. Cell. Biol.* **25**, 9973–9984.

Barclay J., Balaguero N., Mione M., Ackerman S. L., Letts V. A., Brodbeck J., Canti C., et al. (2001) Ducky mouse phenotype of epilepsy and ataxia is associated with mutations in the Cacna2d2 gene and decreased calcium channel current in cerebellar Purkinje cells. *J. Neurosci.* **21**, 6095–6104.

Bear M. F., Connors B. W., Paradiso M. A. (2007) *Neuroscience: Exploring the brain, 3rd ed.* Lippincott Williams & Wilkins Publishers, Philadelphia, PA, US.

Bell T. J., Thaler C., Castiglioni A. J., Helton T. D., Lipscombe D. (2004) Cell-specific alternative splicing increases calcium channel current density in the pain pathway. *Neuron* **41**, 127–138.

Beuckmann C. T., Sinton C. M., Miyamoto N., Ino M., Yanagisawa M. (2003) N-type calcium channel alpha1B subunit (Cav2.2) knock-out mice display hyperactivity and vigilance state differences. *J. Neurosci.* **23**, 6793–6797.

Biederer T., Südhof T. C. (2000) Mints as adaptors. Direct binding to neurexins and recruitment of munc18. *J. Biol. Chem.* **275**, 39803–39806.

Bikbaev A., Ciuraszkiewicz A., Heck J., Klatt O., Freund R., Mitlöhner J., Lacalle S. E., et al. (2020) Auxiliary α2δ1 and α2δ3 subunits of calcium channels drive excitatory and inhibitory neuronal network development. *J. Neurosci.*, JN-RM-1707-19.

Bleakman D., Bowman D., Bath C. P., Brust P. F., Johnson E. C., Deal C. R., Miller R. J., Ellis S. B., Harpold M. M., Hans M. (1995) Characteristics of a human N-type

calcium channel expressed in HEK293 cells. *Neuropharmacology* **34**, 753–765.

Bornschein G., Eilers J., Schmidt H. (2019) Neocortical High Probability Release Sites Are Formed by Distinct Ca2+ Channel-to-Release Sensor Topographies during Development. *Cell Rep.*

Brennan F. H., Noble B. T., Wang Y., Guan Z., Davis H., Mo X., Harris C., Eroglu C., Ferguson A. R., Popovich P. G. (2021) Acute post-injury blockade of α2δ-1 calcium channel subunits prevents pathological autonomic plasticity after spinal cord injury. *Cell Rep.* **34**, 108667.

Brockhaus J., Brüggen B., Missler M. (2019) *Imaging and Analysis of Presynaptic Calcium Influx in Cultured Neurons Using synGCaMP6f* .

Brockhaus J., Schreitmuller M., Repetto D., Klatt O., Reissner C., Elmslie K., Heine M., Missler M. (2018) alpha-Neurexins Together with alpha2delta-1 Auxiliary Subunits Regulate Ca(2+) Influx through Cav2.1 Channels. *J. Neurosci.* **38**, 8277–8294.

Brodie C., Bak A., Shainberg A., Sampson S. R. (1987) Role of Na-K ATPase in regulation of resting membrane potential of cultured rat skeletal myotubes. *J. Cell. Physiol.* **130**, 191–198.

Brody D. L., Yue D. T. (2000) Relief of G-protein inhibition of calcium channels and short-term synaptic facilitation in cultured hippocampal neurons. *J. Neurosci.* **20**, 889–898.

Broussard G. J., Liang R., Tian L. (2014) Monitoring activity in neural circuits with genetically encoded indicators. *Front. Mol. Neurosci.* **7**, 97.

Brown S. P., Safo P. K., Regehr W. G. (2004) Endocannabinoids inhibit transmission at granule cell to Purkinje cell synapses by modulating three types of presynaptic calcium channels. *J. Neurosci.* **24**, 5623–5631.

Brunger A. T., Choi U. B., Lai Y., Leitz J., White K. I., Zhou Q. (2019) The pre-synaptic fusion machinery. *Curr. Opin. Struct. Biol.* **54**, 179–188.

Bucurenciu I., Bischofberger J., Jonas P. (2010) A small number of open Ca2+ channels trigger transmitter release at a central GABAergic synapse. *Nat. Neurosci.* **13**, 19–21.

Bucurenciu I., Kulik A., Schwaller B., Frotscher M., Jonas P. (2008) Nanodomain coupling between Ca2+ channels and Ca2+ sensors promotes fast and efficient transmitter release at a cortical GABAergic synapse. *Neuron* **57**, 536–545.

Bunda A., LaCarubba B., Bertolino M., Akiki M., Bath K., Lopez-Soto J., Lipscombe D., Andrade A. (2019) Cacna1b alternative splicing impacts excitatory neurotransmission and is linked to behavioral responses to aversive stimuli. *Mol. Brain* **12**, 81.

Cantí C., Nieto-Rostro M., Foucault I., Heblich F., Wratten J., Richards M. W., Hendrich J., et al. (2005) The metal-ion-dependent adhesion site in the Von Willebrand factor-A domain of α2δ subunits is key to trafficking voltage-gated Ca^{2}+ channels. *Proc. Natl. Acad. Sci. U. S. A.* **102**, 11230 LP – 11235.

Canti C., Page K. M., Stephens G. J., Dolphin A. C. (1999) Identification of residues in the N terminus of alpha1B critical for inhibition of the voltage-dependent calcium channel by Gbeta gamma. *J. Neurosci.* **19**, 6855–6864.

Cao Y.-Q., Tsien R. W. (2010) Different relationship of N- and P/Q-type Ca2+ channels to channel-interacting slots in controlling neurotransmission at cultured hippocampal synapses. *J. Neurosci.* **30**, 4536–4546.

Cassidy J. S., Ferron L., Kadurin I., Pratt W. S., Dolphin A. C. (2014) Functional exofacially tagged N-type calcium channels elucidate the interaction with auxiliary alpha2delta-1 subunits. *Proc. Natl. Acad. Sci. U. S. A.* **111**, 8979–8984.

Castiglioni A. J., Raingo J., Lipscombe D. (2006) Alternative splicing in the C-terminus of CaV2.2 controls expression and gating of N-type calcium channels. *J. Physiol.* **576**, 119–134.

Castillo J. del, Katz B. (1954) Quantal components of the end-plate potential. *J. Physiol.* **124**, 560–573.

Castro H., Bermeo K., Arenas I., Garcia D. E. (2020) Maintenance of CaV2.2 channel-current by PIP2 unveiled by neomycin in sympathetic neurons of the rat. *Arch. Biochem. Biophys.* **682**, 108261.

Catterall W. A. (2010) Ion channel voltage sensors: structure, function, and pathophysiology. *Neuron* **67**, 915–928.

Catterall W. A. (2011) Voltage-gated calcium channels. *Cold Spring Harb. Perspect. Biol.* **3**, a003947.

Catterall W. A., Few A. P. (2008) Calcium channel regulation and presynaptic plasticity. *Neuron* **59**, 882–901.

Catterall W. A., Leal K., Nanou E. (2013) Calcium channels and short-term synaptic plasticity. *J. Biol. Chem.* **288**, 10742–10749.

Chen J., Li L., Chen S.-R., Chen H., Xie J.-D., Sirrieh R. E., MacLean D. M., et al. (2018) The alpha2delta-1-NMDA Receptor Complex Is Critically Involved in Neuropathic Pain Development and Gabapentin Therapeutic Actions. *Cell Rep.* **22**, 2307–2321.

Chen T.-W., Wardill T. J., Sun Y., Pulver S. R., Renninger S. L., Baohan A., Schreiter E. R., et al. (2013) Ultrasensitive fluorescent proteins for imaging neuronal activity. *Nature* **499**, 295–300.

Chen X., Wu X., Wu H., Zhang M. (2020) Phase separation at the synapse. *Nat. Neurosci.* **23**, 301–310.

Chi X. X., Schmutzler B. S., Brittain J. M., Wang Y., Hingtgen C. M., Nicol G. D., Khanna R. (2009) Regulation of N-type voltage-gated calcium channels (Cav2.2) and transmitter release by collapsin response mediator protein-2 (CRMP-2) in sensory neurons. *J. Cell Sci.* **122**, 4351–4362.

Cole R. L., Lechner S. M., Williams M. E., Prodanovich P., Bleicher L., Varney M. A., Gu G. (2005) Differential distribution of voltage-gated calcium channel alpha-2 delta (alpha2delta) subunit mRNA-containing cells in the rat central nervous system and the dorsal root ganglia. *J. Comp. Neurol.* **491**, 246–269.

Currie K. P. M. (2010) G protein modulation of CaV2 voltage-gated calcium channels. *Channels (Austin).* **4**, 497–509.

Dahimene S., Page K. M., Kadurin I., Ferron L., Ho D. Y., Powell G. T., Pratt W. S., Wilson S. W., Dolphin A. C. (2018) The α(2)δ-like Protein Cachd1 Increases N-type Calcium Currents and Cell Surface Expression and Competes with α(2)δ-1. *Cell Rep.* **25**, 1610-1621.e5.

Davies A., Douglas L., Hendrich J., Wratten J., Tran Van Minh A., Foucault I., Koch D., Pratt W. S., Saibil H. R., Dolphin A. C. (2006) The calcium channel alpha2delta-2 subunit partitions with CaV2.1 into lipid rafts in cerebellum: implications for localization and function. *J. Neurosci.* **26**, 8748–8757.

Desai N. S. (2003) Homeostatic plasticity in the CNS: synaptic and intrinsic forms. *J. Physiol. Paris* **97**, 391–402.

Dick I. E., Tadross M. R., Liang H., Tay L. H., Yang W., Yue D. T. (2008) A modular switch for spatial Ca2+ selectivity in the calmodulin regulation of CaV channels. *Nature* **451**, 830–834.

Dickman D. K., Kurshan P. T., Schwarz T. L. (2008) Mutations in a Drosophila alpha2delta voltage-gated calcium channel subunit reveal a crucial synaptic

function. *J. Neurosci.* **28**, 31–38.

Dittman J. S., Ryan T. A. (2019) The control of release probability at nerve terminals. *Nat. Rev. Neurosci.* **20**, 177–186.

Doering C. J., Kisilevsky A. E., Feng Z.-P., Arnot M. I., Peloquin J., Hamid J., Barr W., et al. (2004) A single Gbeta subunit locus controls cross-talk between protein kinase C and G protein regulation of N-type calcium channels. *J. Biol. Chem.* **279**, 29709–29717.

Dolphin A. C. (2003a) Beta subunits of voltage-gated calcium channels. *J. Bioenerg. Biomembr.* **35**, 599–620.

Dolphin A. C. (2003b) G protein modulation of voltage-gated calcium channels. *Pharmacol. Rev.* **55**, 607–627.

Dolphin A. C. (2012) Calcium channel auxiliary alpha2delta and beta subunits: trafficking and one step beyond. *Nat. Rev. Neurosci.* **13**, 542–555.

Dolphin A. C. (2013) The α2δ subunits of voltage-gated calcium channels. *Biochim. Biophys. Acta - Biomembr.* **1828**, 1541–1549.

Dolphin A. C. (2016) Voltage-gated calcium channels and their auxiliary subunits: physiology and pathophysiology and pharmacology. *J. Physiol.* **594**, 5369–5390.

Dolphin A. C., Lee A. (2020) Presynaptic calcium channels: specialized control of synaptic neurotransmitter release. *Nat. Rev. Neurosci.* **21**, 213–229.

Dooley D. J., Lupp A., Hertting G., Osswald H. (1988) Omega-conotoxin GVIA and pharmacological modulation of hippocampal noradrenaline release. *Eur. J. Pharmacol.* **148**, 261–267.

Dreosti E., Odermatt B., Dorostkar M. M., Lagnado L. (2009) A genetically encoded reporter of synaptic activity in vivo. *Nat. Methods* **6**, 883–889.

Echegoyen J., Neu A., Graber K. D., Soltesz I. (2007) Homeostatic plasticity studied using in vivo hippocampal activity-blockade: synaptic scaling, intrinsic plasticity and age-dependence. *PLoS One* **2**, e700.

Eggermann E., Bucurenciu I., Goswami S. P., Jonas P. (2011) Nanodomain coupling between Ca(2)(+) channels and sensors of exocytosis at fast mammalian synapses. *Nat. Rev. Neurosci.* **13**, 7–21.

Ellinor P. T., Yang J., Sather W. A., Zhang J. F., Tsien R. W. (1995) Ca2+ channel selectivity at a single locus for high-affinity Ca2+ interactions. *Neuron* **15**, 1121–1132.

Ellinor P. T., Zhang J. F., Horne W. A., Tsien R. W. (1994) Structural determinants of the blockade of N-type calcium channels by a peptide neurotoxin. *Nature* **372**, 272–275.

Eroglu C., Allen N. J., Susman M. W., O'Rourke N. A., Park C. Y., Ozkan E., Chakraborty C., et al. (2009) Gabapentin receptor alpha2delta-1 is a neuronal thrombospondin receptor responsible for excitatory CNS synaptogenesis. *Cell* **139**, 380–392.

Faas G. C., Raghavachari S., Lisman J. E., Mody I. (2011) Calmodulin as a direct detector of Ca2+ signals. *Nat. Neurosci.* **14**, 301–304.

Falk T., Muller Y. L., Yool A. J. (1999) Differential expression of three classes of voltage-gated Ca2+ channels during maturation of the rat cerebellum in vitro. *Dev. Brain Res.* **115**, 161–170.

Fatt P., Katz B. (1952) Spontaneous subthreshold activity at motor nerve endings. *J. Physiol.* **117**, 109–128.

Fedchyshyn M. J., Wang L.-Y. (2005) Developmental transformation of the release modality at the calyx of Held synapse. *J. Neurosci.* **25**, 4131–4140.

Fell B., Eckrich S., Blum K., Eckrich T., Hecker D., Obermair G. J., Münkner S., et al. (2016) alpha2delta2 Controls the Function and Trans-Synaptic Coupling of Cav1.3 Channels in Mouse Inner Hair Cells and Is Essential for Normal Hearing. *J. Neurosci.* **36**, 11024–11036.

Fernandes D., Carvalho A. L. (2016) Mechanisms of homeostatic plasticity in the excitatory synapse. *J. Neurochem.* **139**, 973–996.

Ferron L., Davies A., Page K. M., Cox D. J., Leroy J., Waithe D., Butcher A. J., et al. (2008) The stargazin-related protein gamma 7 interacts with the mRNA-binding protein heterogeneous nuclear ribonucleoprotein A2 and regulates the stability of specific mRNAs, including CaV2.2. *J. Neurosci.* **28**, 10604–10617.

Ferron L., Kadurin I., Dolphin A. C. (2018) Proteolytic maturation of α2δ controls the probability of synaptic vesicular release. *Elife* **7**.

Ferron L., Nieto-Rostro M., Cassidy J. S., Dolphin A. C. (2014) Fragile X mental retardation protein controls synaptic vesicle exocytosis by modulating N-type calcium channel density. *Nat. Commun.* **5**, 3628.

Ferron L., Novazzi C. G., Pilch K. S., Moreno C., Ramgoolam K., Dolphin A. C. (2020a) FMRP regulates presynaptic localization of neuronal voltage gated calcium channels. *Neurobiol. Dis.* **138**, 104779.

Ferron L., Novazzi C. G., Pilch K. S., Moreno C., Ramgoolam K., Dolphin A. C. (2020b) FMRP regulates presynaptic localization of neuronal voltage gated calcium channels. *Neurobiol. Dis.* **138**.

Few A. P. (2009) *Presynaptic calcium channel regulation and short-term synaptic plasticity.*

Field M. J., Cox P. J., Stott E., Melrose H., Offord J., Su T.-Z., Bramwell S., et al. (2006) Identification of the alpha2-delta-1 subunit of voltage-dependent calcium channels

as a molecular target for pain mediating the analgesic actions of pregabalin. *Proc. Natl. Acad. Sci. U. S. A.* **103**, 17537–17542.

Finkel L., Koh S. (2013) N-type calcium channel antibody-mediated autoimmune encephalitis: An unlikely cause of a common presentation. *Epilepsy Behav. case reports* **1**, 92–96.

Foehring R. C. (1996) Serotonin modulates N- and P-type calcium currents in neocortical pyramidal neurons via a membrane-delimited pathway. *J. Neurophysiol.* **75**, 648–659.

Forsythe I. D., Tsujimoto T., Barnes-Davies M., Cuttle M. F., Takahashi T. (1998) Inactivation of presynaptic calcium current contributes to synaptic depression at a fast central synapse. *Neuron* **20**, 797–807.

Frank C. A. (2014) How voltage-gated calcium channels gate forms of homeostatic synaptic plasticity. *Front. Cell. Neurosci.* **8**, 40.

Gao S., Yao X., Yan N. (2021) Structure of human Ca(v)2.2 channel blocked by the painkiller ziconotide. *Nature* **596**, 143–147.

Glebov O. O., Jackson R. E., Winterflood C. M., Owen D. M., Barker E. A., Doherty P., Ewers H., Burrone J. (2017) Nanoscale Structural Plasticity of the Active Zone Matrix Modulates Presynaptic Function. *Cell Rep.* **18**, 2715–2728.

Goldman D. E. (1943) POTENTIAL, IMPEDANCE, AND RECTIFICATION IN MEMBRANES. *J. Gen. Physiol.* **27**, 37–60.

Gorman K. M., Meyer E., Grozeva D., Spinelli E., McTague A., Sanchis-Juan A., Carss K. J., et al. (2019) Bi-allelic Loss-of-Function CACNA1B Mutations in Progressive Epilepsy-Dyskinesia. *Am. J. Hum. Genet.* **104**, 948–956.

Goswami S. P., Bucurenciu I., Jonas P. (2012) Miniature IPSCs in hippocampal granule

cells are triggered by voltage-gated Ca2+ channels via microdomain coupling. *J. Neurosci.* **32**, 14294–14304.

Groen J. L., Andrade A., Ritz K., Jalalzadeh H., Haagmans M., Bradley T. E. J., Jongejan A., et al. (2015) CACNA1B mutation is linked to unique myoclonus-dystonia syndrome. *Hum. Mol. Genet.* **24**, 987–993.

Hammond C. (2015) Cellular and Molecular Neurophysiology: Fourth Edition. 1–433.

Han E. B., Stevens C. F. (2009) Development regulates a switch between post- and presynaptic strengthening in response to activity deprivation. *Proc. Natl. Acad. Sci. U. S. A.* **106**, 10817–10822.

Han Y., Kaeser P. S., Sudhof T. C., Schneggenburger R. (2011) RIM determines Ca(2)+ channel density and vesicle docking at the presynaptic active zone. *Neuron* **69**, 304–316.

Hanson P. I., Heuser J. E., Jahn R. (1997) Neurotransmitter release - four years of SNARE complexes. *Curr. Opin. Neurobiol.* **7**, 310–315.

Hata Y., Slaughter C. A., Südhof T. C. (1993) Synaptic vesicle fusion complex contains unc-18 homologue bound to syntaxin. *Nature* **366**, 347–351.

Hatakeyama S., Wakamori M., Ino M., Miyamoto N., Takahashi E., Yoshinaga T., Sawada K., et al. (2001) Differential nociceptive responses in mice lacking the alpha(1B) subunit of N-type Ca(2+) channels. *Neuroreport* **12**, 2423–2427.

Hefft S., Jonas P. (2005) Asynchronous GABA release generates long-lasting inhibition at a hippocampal interneuron-principal neuron synapse. *Nat. Neurosci.* **8**, 1319–1328.

Heinke B., Gingl E., Sandkuhler J. (2011) Multiple targets of mu-opioid receptor-mediated presynaptic inhibition at primary afferent Adelta- and C-fibers. *J. Neurosci.*

31, 1313–1322.

Held R. G., Liu C., Ma K., Ramsey A. M., Tarr T. B., Nola G. De, Wang S. S. H., et al. (2020) Synapse and Active Zone Assembly in the Absence of Presynaptic Ca2+ Channels and Ca2+ Entry. *Neuron* **107**, 667-683.e9.

Hendrich J., Minh A. T. Van, Heblich F., Nieto-Rostro M., Watschinger K., Striessnig J., Wratten J., Davies A., Dolphin A. C. (2008) Pharmacological disruption of calcium channel trafficking by the alpha2delta ligand gabapentin. *Proc. Natl. Acad. Sci. U. S. A.* **105**, 3628–3633.

Herdon H., Nahorski S. R. (1989) Investigations of the roles of dihydropyridine and omega-conotoxin-sensitive calcium channels in mediating depolarisation-evoked endogenous dopamine release from striatal slices. *Naunyn. Schmiedebergs. Arch. Pharmacol.* **340**, 36–40.

Herlitze S., Garcia D. E., Mackie K., Hille B., Scheuer T., Catterall W. A. (1996) Modulation of Ca2+ channels by G-protein beta gamma subunits. *Nature* **380**, 258–262.

Hirning L. D., Fox A. P., McCleskey E. W., Olivera B. M., Thayer S. A., Miller R. J., Tsien R. W. (1988) Dominant role of N-type Ca2+ channels in evoked release of norepinephrine from sympathetic neurons. *Science* **239**, 57–61.

Hodgkin A. L., Huxley A. F. (1945) Resting and action potentials in single nerve fibres. *J. Physiol.* **104**, 176–195.

Hodgkin A. L., Huxley A. F. (1952a) The dual effect of membrane potential on sodium conductance in the giant axon of Loligo. *J. Physiol.* **116**, 497–506.

Hodgkin A. L., Huxley A. F. (1952b) Currents carried by sodium and potassium ions through the membrane of the giant axon of Loligo. *J. Physiol.* **116**, 449–472.

Hodgkin A. L., Huxley A. F. (1952c) The components of membrane conductance in the giant axon of Loligo. *J. Physiol.* **116**, 473–496.

Hodgkin A. L., Huxley A. F. (1952d) A quantitative description of membrane current and its application to conduction and excitation in nerve. *J. Physiol.* **117**, 500–544.

Hodgkin A. L., Keynes R. D. (1955) The potassium permeability of a giant nerve fibre. *J. Physiol.* **128**, 61–88.

Hoover K. M., Gratz S. J., Qi N., Herrmann K. A., Liu Y., Perry-Richardson J. J., Vanderzalm P. J., O'Connor-Giles K. M., Broihier H. T. (2019) The calcium channel subunit α2δ-3 organizes synapses via an activity-dependent and autocrine BMP signaling pathway. *Nat. Commun.* **10**, 5575.

Hoppa M. B., Lana B., Margas W., Dolphin A. C., Ryan T. A. (2012) alpha2delta expression sets presynaptic calcium channel abundance and release probability. *Nature* **486**, 122–125.

Horne A. L., Kemp J. A. (1991) The effect of omega-conotoxin GVIA on synaptic transmission within the nucleus accumbens and hippocampus of the rat in vitro. *Br. J. Pharmacol.* **103**, 1733–1739.

Huynh T. G., Cuny H., Slesinger P. A., Adams D. J. (2015) Novel mechanism of voltage-gated N-type (Cav2.2) calcium channel inhibition revealed through alpha-conotoxin Vc1.1 activation of the GABA(B) receptor. *Mol. Pharmacol.* **87**, 240–250.

Ikeda S. R. (1996) Voltage-dependent modulation of N-type calcium channels by G-protein beta gamma subunits. *Nature* **380**, 255–258.

Inchauspe C. G., Martini F. J., Forsythe I. D., Uchitel O. D. (2004) Functional compensation of P/Q by N-type channels blocks short-term plasticity at the calyx of Held presynaptic terminal. *J. Neurosci.* **24**, 10379–10383.

Iwasaki S., Momiyama A., Uchitel O. D., Takahashi T. (2000) Developmental changes in calcium channel types mediating central synaptic transmission. *J. Neurosci.* **20**, 59–65.

Iwasaki S., Takahashi T. (1998) Developmental changes in calcium channel types mediating synaptic transmission in rat auditory brainstem. *J. Physiol.* **509 (Pt 2**, 419–423.

Jeans A. F., Heusden F. C. van, Al-Mubarak B., Padamsey Z., Emptage N. J. (2017) Homeostatic Presynaptic Plasticity Is Specifically Regulated by P/Q-type Ca(2+) Channels at Mammalian Hippocampal Synapses. *Cell Rep.* **21**, 341–350.

Kadurin I., Alvarez-Laviada A., Ng S. F. J., Walker-Gray R., D'Arco M., Fadel M. G., Pratt W. S., Dolphin A. C. (2012) Calcium currents are enhanced by α2δ-1 lacking its membrane anchor. *J. Biol. Chem.* **287**, 33554–33566.

Kadurin I., Ferron L., Rothwell S. W., Meyer J. O., Douglas L. R., Bauer C. S., Lana B., et al. (2016) Proteolytic maturation of α2δ represents a checkpoint for activation and neuronal trafficking of latent calcium channels. *Elife* **5**.

Kaeser P. S., Deng L., Wang Y., Dulubova I., Liu X., Rizo J., Sudhof T. C. (2011) RIM proteins tether Ca2+ channels to presynaptic active zones via a direct PDZ-domain interaction. *Cell* **144**, 282–295.

Karmarkar U. R., Buonomano D. V (2006) Different forms of homeostatic plasticity are engaged with distinct temporal profiles. *Eur. J. Neurosci.* **23**, 1575–1584.

Kater S. B., Mills L. R. (1991) Regulation of growth cone behavior by calcium. *J. Neurosci.* **11**, 891 LP – 899.

Kato A. S., Zhou W., Milstein A. D., Knierman M. D., Siuda E. R., Dotzlaf J. E., Yu H., et al. (2007) New transmembrane AMPA receptor regulatory protein isoform, gamma-7, differentially regulates AMPA receptors. *J. Neurosci.* **27**, 4969–4977.

Khanna R., Zougman A., Stanley E. F. (2007) A proteomic screen for presynaptic terminal N-type calcium channel (CaV2.2) binding partners. *J. Biochem. Mol. Biol.* **40**, 302–314.

Kim C., Jun K., Lee T., Kim S. S., McEnery M. W., Chin H., Kim H. L., et al. (2001) Altered nociceptive response in mice deficient in the alpha(1B) subunit of the voltage-dependent calcium channel. *Mol. Cell. Neurosci.* **18**, 235–245.

Kim J., Tsien R. W. (2008) Synapse-specific adaptations to inactivity in hippocampal circuits achieve homeostatic gain control while dampening network reverberation. *Neuron* **58**, 925–937.

Kim, Ryan T. A. (2010) CDK5 serves as a major control point in neurotransmitter release. *Neuron* **67**, 797–809.

Kim, Ryan T. A. (2013) Balance of calcineurin Aalpha and CDK5 activities sets release probability at nerve terminals. *J. Neurosci.* **33**, 8937–8950.

Kimpinski K., Iodice V., Vernino S., Sandroni P., Low P. A. (2009) Association of N-type calcium channel autoimmunity in patients with autoimmune autonomic ganglionopathy. *Auton. Neurosci.* **150**, 136–139.

Kisilevsky A. E., Mulligan S. J., Altier C., Iftinca M. C., Varela D., Tai C., Chen L., et al. (2008) D1 receptors physically interact with N-type calcium channels to regulate channel distribution and dendritic calcium entry. *Neuron* **58**, 557–570.

Kiyonaka S., Nakajima H., Takada Y., Hida Y., Yoshioka T., Hagiwara A., Kitajima I., Mori Y., Ohtsuka T. (2012) Physical and functional interaction of the active zone protein CAST/ERC2 and the beta-subunit of the voltage-dependent Ca(2+) channel. *J. Biochem.* **152**, 149–159.

Kiyonaka S., Wakamori M., Miki T., Uriu Y., Nonaka M., Bito H., Beedle A. M., et al. (2007) RIM1 confers sustained activity and neurotransmitter vesicle anchoring to

presynaptic Ca2+ channels. *Nat. Neurosci.* **10**, 691–701.

Klugbauer N., Lacinová L., Marais E., Hobom M., Hofmann F. (1999) Molecular Diversity of the Calcium Channel α2δ Subunit. *J. Neurosci.* **19**, 684 LP – 691.

Ko J., Humbert S., Bronson R. T., Takahashi S., Kulkarni A. B., Li E., Tsai L. H. (2001) p35 and p39 are essential for cyclin-dependent kinase 5 function during neurodevelopment. *J. Neurosci.* **21**, 6758–6771.

Komuro H., Rakic P. (1992) Selective role of N-type calcium channels in neuronal migration. *Science* **257**, 806–809.

Komuro H., Rakic P. (1996) Intracellular Ca2+ fluctuations modulate the rate of neuronal migration. *Neuron* **17**, 275–285.

Kurshan P. T., Oztan A., Schwarz T. L. (2009) Presynaptic alpha2delta-3 is required for synaptic morphogenesis independent of its Ca2+-channel functions. *Nat. Neurosci.* **12**, 1415–1423.

Kusch V., Bornschein G., Loreth D., Bank J., Jordan J., Baur D., Watanabe M., et al. (2018) Munc13-3 Is Required for the Developmental Localization of Ca2+ Channels to Active Zones and the Nanopositioning of Cav2.1 Near Release Sensors. *Cell Rep.* **22**, 1965–1973.

Lazarevic V., Schöne C., Heine M., Gundelfinger E. D., Fejtova A. (2011) Extensive Remodeling of the Presynaptic Cytomatrix upon Homeostatic Adaptation to Network Activity Silencing. *J. Neurosci.* **31**, 10189 LP – 10200.

Lee K. F. H., Soares C., Béïque J.-C. (2014) Tuning into diversity of homeostatic synaptic plasticity. *Neuropharmacology* **78**, 31–37.

Li L., Bischofberger J., Jonas P. (2007) Differential gating and recruitment of P/Q-, N-, and R-type Ca2+ channels in hippocampal mossy fiber boutons. *J. Neurosci.* **27**,

13420–13429.

Lipscombe D., Andrade A., Allen S. E. (2013) Alternative splicing: functional diversity among voltage-gated calcium channels and behavioral consequences. *Biochim. Biophys. Acta* **1828**, 1522–1529.

Lipscombe D., Raingo J. (2007) Alternative splicing matters: N-type calcium channels in nociceptors. *Channels (Austin).* **1**, 225–227.

Liu, Papa A., Katchman A. N., Zakharov S. I., Roybal D., Hennessey J. A., Kushner J., et al. (2020) Mechanism of adrenergic CaV1.2 stimulation revealed by proximity proteomics. *Nature* **577**, 695–700.

Liu X., Yang P. S., Yang W., Yue D. T. (2010) Enzyme-inhibitor-like tuning of Ca(2+) channel connectivity with calmodulin. *Nature* **463**, 968–972.

Livak K. J., Schmittgen T. D. (2001) Analysis of relative gene expression data using real-time quantitative PCR and the 2(-Delta Delta C(T)) Method. *Methods* **25**, 402–8.

Luebke J. I., Dunlap K., Turner T. J. (1993) Multiple calcium channel types control glutamatergic synaptic transmission in the hippocampus. *Neuron* **11**, 895–902.

Lüscher C., Malenka R. C. (2012) NMDA receptor-dependent long-term potentiation and long-term depression (LTP/LTD). *Cold Spring Harb. Perspect. Biol.* **4**, a005710.

Macabuag N., Dolphin A. C. (2015) Alternative Splicing in Ca(V)2.2 Regulates Neuronal Trafficking via Adaptor Protein Complex-1 Adaptor Protein Motifs. *J. Neurosci.* **35**, 14636–14652.

Marangoudakis S., Andrade A., Helton T. D., Denome S., Castiglioni A. J., Lipscombe D. (2012) Differential ubiquitination and proteasome regulation of Ca(V)2.2 N-type channel splice isoforms. *J. Neurosci.* **32**, 10365–10369.

Maximov A., Bezprozvanny I. (2002) Synaptic targeting of N-type calcium channels in

hippocampal neurons. *J. Neurosci.* **22**, 6939–6952.

Maximov A., Südhof T. C., Bezprozvanny I. (1999) Association of neuronal calcium channels with modular adaptor proteins. *J. Biol. Chem.* **274**, 24453–24456.

McCarthy C. I., Chou-Freed C., Rodriguez S. S., Yaneff A., Davio C., Raingo J. (2020) Constitutive activity of dopamine receptor type 1 (D1R) increases CaV2.2 currents in PFC neurons. *J. Gen. Physiol.* **152**.

McGivern J. G. (2007) Ziconotide: a review of its pharmacology and use in the treatment of pain. *Neuropsychiatr. Dis. Treat.* **3**, 69–85.

Meir A., Bell D. C., Stephens G. J., Page K. M., Dolphin A. C. (2000) Calcium channel beta subunit promotes voltage-dependent modulation of alpha 1 B by G beta gamma. *Biophys. J.* **79**, 731–746.

Mencacci N. E., R'bibo L., Bandres-Ciga S., Carecchio M., Zorzi G., Nardocci N., Garavaglia B., et al. (2015) The CACNA1B R1389H variant is not associated with myoclonus-dystonia in a large European multicentric cohort. *Hum. Mol. Genet.* **24**, 5326–5329.

Meyer J. O., Dahimene S., Page K. M., Ferron L., Kadurin I., Ellaway J. I. J., Zhao P., et al. (2019) Disruption of the Key Ca(2+) Binding Site in the Selectivity Filter of Neuronal Voltage-Gated Calcium Channels Inhibits Channel Trafficking. *Cell Rep.* **29**, 22-33.e5.

Meyer J. O., Dolphin A. C. (2021) Rab11-dependent recycling of calcium channels is mediated by auxiliary subunit α(2)δ-1 but not α(2)δ-3. *Sci. Rep.* **11**, 10256.

Miki T., Hirai H., Takahashi T. (2013) Activity-dependent neurotrophin signaling underlies developmental switch of Ca2+ channel subtypes mediating neurotransmitter release. *J. Neurosci.* **33**, 18755–18763.

Mintz I. M., Sabatini B. L., Regehr W. G. (1995) Calcium control of transmitter release at a cerebellar synapse. *Neuron* **15**, 675–688.

Mochida S. (2019) Presynaptic Calcium Channels. *Int. J. Mol. Sci.* **20**, 2217.

Mochida S., Few A. P., Scheuer T., Catterall W. A. (2008) Regulation of presynaptic Ca(V)2.1 channels by Ca2+ sensor proteins mediates short-term synaptic plasticity. *Neuron* **57**, 210–216.

Momiyama T. (2003) Parallel decrease in omega-conotoxin-sensitive transmission and dopamine-induced inhibition at the striatal synapse of developing rats. *J. Physiol.* **546**, 483–490.

Moutin E., Hemonnot A.-L., Seube V., Linck N., Rassendren F., Perroy J., Compan V. (2020) Procedures for Culturing and Genetically Manipulating Murine Hippocampal Postnatal Neurons. *Front. Synaptic Neurosci.* **12**.

Muller C. S., Haupt A., Bildl W., Schindler J., Knaus H.-G., Meissner M., Rammner B., et al. (2010) Quantitative proteomics of the Cav2 channel nano-environments in the mammalian brain. *Proc. Natl. Acad. Sci.* **107**, 14950–14957.

Murakami M., Suzuki T., Nakagawasai O., Murakami H., Murakami S., Esashi A., Taniguchi R., et al. (2001) Distribution of various calcium channel alpha(1) subunits in murine DRG neurons and antinociceptive effect of omega-conotoxin SVIB in mice. *Brain Res.* **903**, 231–236.

Murthy V. N., Schikorski T., Stevens C. F., Zhu Y. (2001) Inactivity produces increases in neurotransmitter release and synapse size. *Neuron* **32**, 673–682.

Nakagawasai O., Onogi H., Mitazaki S., Sato A., Watanabe K., Saito H., Murai S., et al. (2010) Behavioral and neurochemical characterization of mice deficient in the N-type Ca2+ channel alpha1B subunit. *Behav. Brain Res.* **208**, 224–230.

Nakai J., Ohkura M., Imoto K. (2001) A high signal-to-noise Ca2+ probe composed of a single green fluorescent protein. *Nat. Biotechnol.* **19**, 137–141.

Nakamura Y., Harada H., Kamasawa N., Matsui K., Rothman J. S., Shigemoto R., Silver R. A., DiGregorio D. A., Takahashi T. (2015) Nanoscale distribution of presynaptic Ca(2+) channels and its impact on vesicular release during development. *Neuron* **85**, 145–158.

Nanou E., Sullivan J. M., Scheuer T., Catterall W. A. (2016) Calcium sensor regulation of the Ca_V2.1 Ca²⁺ channel contributes to short-term synaptic plasticity in hippocampal neurons. *Proc. Natl. Acad. Sci.* **113**, 1062 LP – 1067.

Narahashi T., Moore J. W., Scott W. R. (1964) Tetrodotoxin blockage of sodium conductance incrase in lobster giant axons. *J. Gen. Physiol.* **47**, 965–974.

Newton P. M., Orr C. J., Wallace M. J., Kim C., Shin H.-S., Messing R. O. (2004) Deletion of N-type calcium channels alters ethanol reward and reduces ethanol consumption in mice. *J. Neurosci.* **24**, 9862–9869.

Nieto-Rostro M., Ramgoolam K., Pratt W. S., Kulik A., Dolphin A. C. (2018) Ablation of α2d1 inhibits cell-surface trafficking of endogenous N-type calcium channels in the pain pathway in vivo. *Proc. Natl. Acad. Sci.* **115**, E12043 LP-E12052.

Nimmervoll B., Flucher B. E., Obermair G. J. (2013) Dominance of P/Q-type calcium channels in depolarization-induced presynaptic FM dye release in cultured hippocampal neurons. *Neuroscience* **253**, 330–340.

Nishimune H., Sanes J. R., Carlson S. S. (2004) A synaptic laminin-calcium channel interaction organizes active zones in motor nerve terminals. *Nature* **432**, 580–587.

Nowycky M. C., Fox A. P., Tsien R. W. (1985) Three types of neuronal calcium channel with different calcium agonist sensitivity. *Nature* **316**, 440–443.

O'Rourke N. A., Weiler N. C., Micheva K. D., Smith S. J. (2012) Deep molecular diversity of mammalian synapses: why it matters and how to measure it. *Nat. Rev. Neurosci.* **13**, 365–379.

Page K. M., Canti C., Stephens G. J., Berrow N. S., Dolphin A. C. (1998) Identification of the amino terminus of neuronal Ca2+ channel alpha1 subunits alpha1B and alpha1E as an essential determinant of G-protein modulation. *J. Neurosci.* **18**, 4815–4824.

Pani B., Singh B. B. (2009) Lipid rafts/caveolae as microdomains of calcium signaling. *Cell Calcium* **45**, 625–633.

Potier B., Dutar P., Lamour Y. (1993) Different effects of $ω$-conotoxin GVIA at excitatory and inhibitory synapses in rat CA1 hippocampal neurons. *Brain Res.* **616**, 236–241.

Pozo K., Goda Y. (2010) Unraveling mechanisms of homeostatic synaptic plasticity. *Neuron* **66**, 337–351.

Pragnell M., Waard M. De, Mori Y., Tanabe T., Snutch T. P., Campbell K. P. (1994) Calcium channel beta-subunit binds to a conserved motif in the I-II cytoplasmic linker of the alpha 1-subunit. *Nature* **368**, 67–70.

Raingo J., Castiglioni A. J., Lipscombe D. (2007) Alternative splicing controls G protein-dependent inhibition of N-type calcium channels in nociceptors. *Nat. Neurosci.* **10**, 285–292.

Rebola N., Reva M., Kirizs T., Szoboszlay M., Lőrincz A., Moneron G., Nusser Z., DiGregorio D. A. (2019) Distinct Nanoscale Calcium Channel and Synaptic Vesicle Topographies Contribute to the Diversity of Synaptic Function. *Neuron* **104**, 693-710.e9.

Reid C. A., Bekkers J. M., Clements J. D. (2003) Presynaptic Ca2+ channels: a functional

patchwork. *Trends Neurosci.* **26**, 683–687.

Reynolds I. J., Wagner J. A., Snyder S. H., Thayer S. A., Olivera B. M., Miller R. J. (1986) Brain voltage-sensitive calcium channel subtypes differentiated by omega-conotoxin fraction GVIA. *Proc. Natl. Acad. Sci. U. S. A.* **83**, 8804–8807.

Ricoy U. M., Frerking M. E. (2014) Distinct roles for Cav2.1–2.3 in activity-dependent synaptic dynamics. *J. Neurophysiol.* **111**, 2404–2413.

Risher W. C., Kim N., Koh S., Choi J.-E., Mitev P., Spence E. F., Pilaz L.-J., et al. (2018) Thrombospondin receptor α2δ-1 promotes synaptogenesis and spinogenesis via postsynaptic Rac1. *J. Cell Biol.*, jcb.201802057.

Robinson P., Etheridge S., Song L., Armenise P., Jones O. T., Fitzgerald E. M. (2010) Formation of N-type (Cav2.2) voltage-gated calcium channel membrane microdomains: Lipid raft association and clustering. *Cell Calcium* **48**, 183–194.

Ronzitti G., Bucci G., Emanuele M., Leo D., Sotnikova T. D., Mus L. V, Soubrane C. H., et al. (2014) Exogenous α-synuclein decreases raft partitioning of Cav2.2 channels inducing dopamine release. *J. Neurosci.* **34**, 10603–10615.

Ruth P., Rohrkasten A., Biel M., Bosse E., Regulla S., Meyer H. E., Flockerzi V., Hofmann F. (1989) Primary structure of the beta subunit of the DHP-sensitive calcium channel from skeletal muscle. *Science (80-.).* **245**, 1115 LP – 1118.

Saegusa H., Kurihara T., Zong S., Kazuno A., Matsuda Y., Nonaka T., Han W., Toriyama H., Tanabe T. (2001) Suppression of inflammatory and neuropathic pain symptoms in mice lacking the N-type Ca2+ channel. *EMBO J.* **20**, 2349–2356.

Sakaba T., Neher E. (2003) Direct modulation of synaptic vesicle priming by GABAB receptor activation at a glutamatergic synapse. *Nature* **424**, 775–778.

Sann S. B., Xu L., Nishimune H., Sanes J. R., Spitzer N. C. (2008) Neurite Outgrowth

and In VivoSensory Innervation Mediated by a CaV2.2–Laminin β2 Stop Signal. *J. Neurosci.* **28**, 2366 LP – 2374.

Scheiffele P. (2003) Cell-cell signalling during synapse formation in the CNS. *Annu. Rev. Neurosci.* **26**, 485–508.

Scheiffele P., Fan J., Choih J., Fetter R., Serafini T. (2000) Neuroligin expressed in nonneuronal cells triggers presynaptic development in contacting axons. *Cell* **101**, 657–669.

Scheuber A., Miles R., Poncer J. C. (2004) Presynaptic Cav2.1 and Cav2.2 differentially influence release dynamics at hippocampal excitatory synapses. *J. Neurosci.* **24**, 10402–10409.

Schlick B., Flucher B. E., Obermair G. J. (2010) Voltage-activated calcium channel expression profiles in mouse brain and cultured hippocampal neurons. *Neuroscience* **167**, 786–798.

Schlüter O. M., Basu J., Südhof T. C., Rosenmund C. (2006) Rab3 Superprimes Synaptic Vesicles for Release: Implications for Short-Term Synaptic Plasticity. *J. Neurosci.* **26**, 1239 LP – 1246.

Scholz K. P., Miller R. J. (1995) Developmental changes in presynaptic calcium channels coupled to glutamate release in cultured rat hippocampal neurons. *J. Neurosci.* **15**, 4612–4617.

Scholz K. P., Miller R. J. (1996) Presynaptic inhibition at excitatory hippocampal synapses: development and role of presynaptic Ca2+ channels. *J. Neurophysiol.* **76**, 39–46.

Schöpf C. L., Ablinger C., Geisler S. M., Stanika R. I., Campiglio M., Kaufmann W. A., Nimmervoll B., et al. (2021) Presynaptic α2δ subunits are key organizers of glutamatergic synapses. *Proc. Natl. Acad. Sci.* **118**, e1920827118.

Sheng J., He L., Zheng H., Xue L., Luo F., Shin W., Sun T., Kuner T., Yue D. T., Wu L.-G. (2012) Calcium-channel number critically influences synaptic strength and plasticity at the active zone. *Nat. Neurosci.* **15**, 998–1006.

Sidorov M. S., Auerbach B. D., Bear M. F. (2013) Fragile X mental retardation protein and synaptic plasticity. *Mol. Brain* **6**, 15.

Simms B. A., Zamponi G. W. (2014) Neuronal voltage-gated calcium channels: structure, function, and dysfunction. *Neuron* **82**, 24–45.

Söllner T., Whiteheart S. W., Brunner M., Erdjument-Bromage H., Geromanos S., Tempst P., Rothman J. E. (1993) SNAP receptors implicated in vesicle targeting and fusion. *Nature* **362**, 318–324.

Stotz S. C., Hamid J., Spaetgens R. L., Jarvis S. E., Zamponi G. W. (2000) Fast inactivation of voltage-dependent calcium channels. A hinged-lid mechanism? *J. Biol. Chem.* **275**, 24575–24582.

Stotz S. C., Jarvis S. E., Zamponi G. W. (2004) Functional roles of cytoplasmic loops and pore lining transmembrane helices in the voltage-dependent inactivation of HVA calcium channels. *J. Physiol.* **554**, 263–273.

Su S. C., Seo J., Pan J. Q., Samuels B. A., Rudenko A., Ericsson M., Neve R. L., Yue D. T., Tsai L.-H. (2012) Regulation of N-type voltage-gated calcium channels and presynaptic function by cyclin-dependent kinase 5. *Neuron* **75**, 675–687.

Südhof T. C. (2013) Neurotransmitter release: the last millisecond in the life of a synaptic vesicle. *Neuron* **80**, 675–690.

Südhof T. C. (2018) Towards an Understanding of Synapse Formation. *Neuron* **100**, 276–293.

Szabo G. G., Lenkey N., Holderith N., Andrasi T., Nusser Z., Hajos N. (2014) Presynaptic

calcium channel inhibition underlies CB(1) cannabinoid receptor-mediated suppression of GABA release. *J. Neurosci.* **34**, 7958–7963.

Takahashi T., Momiyama A. (1993) Different types of calcium channels mediate central synaptic transmission. *Nature* **366**, 156–158.

Tang L., Gamal El-Din T. M., Payandeh J., Martinez G. Q., Heard T. M., Scheuer T., Zheng N., Catterall W. A. (2014) Structural basis for Ca2+ selectivity of a voltage-gated calcium channel. *Nature* **505**, 56–61.

Tedeschi A., Dupraz S., Laskowski C. J., Xue J., Ulas T., Beyer M., Schultze J. L., Bradke F. (2016) The Calcium Channel Subunit Alpha2delta2 Suppresses Axon Regeneration in the Adult CNS. *Neuron* **92**, 419–434.

Tomizawa K., Ohta J., Matsushita M., Moriwaki A., Li S.-T., Takei K., Matsui H. (2002) Cdk5/p35 regulates neurotransmitter release through phosphorylation and downregulation of P/Q-type voltage-dependent calcium channel activity. *J. Neurosci.* **22**, 2590–2597.

Tran-Van-Minh A., Dolphin A. C. (2010) The alpha2delta ligand gabapentin inhibits the Rab11-dependent recycling of the calcium channel subunit alpha2delta-2. *J. Neurosci.* **30**, 12856–12867.

Turner T. J., Adams M. E., Dunlap K. (1993) Multiple Ca2+ channel types coexist to regulate synaptosomal neurotransmitter release. *Proc. Natl. Acad. Sci. U. S. A.* **90**, 9518–9522.

Turrigiano (2008) The self-tuning neuron: synaptic scaling of excitatory synapses. *Cell* **135**, 422–435.

Turrigiano (2011) Too many cooks? Intrinsic and synaptic homeostatic mechanisms in cortical circuit refinement. *Annu. Rev. Neurosci.* **34**, 89–103.

Vertkin I., Styr B., Slomowitz E., Ofir N., Shapira I., Berner D., Fedorova T., et al. (2015) GABAB receptor deficiency causes failure of neuronal homeostasis in hippocampal networks. *Proc. Natl. Acad. Sci. U. S. A.*

Vitureira N., Letellier M., White I. J., Goda Y. (2011) Differential control of presynaptic efficacy by postsynaptic N-cadherin and β-catenin. *Nat. Neurosci.* **15**, 81–89.

Vivas O., Castro H., Arenas I., Elias-Vinas D., Garcia D. E. (2013) PIP(2) hydrolysis is responsible for voltage independent inhibition of CaV2.2 channels in sympathetic neurons. *Biochem. Biophys. Res. Commun.* **432**, 275–280.

Vyleta N. P., Jonas P. (2014) Loose Coupling Between Ca2+ Channels and Release Sensors at a Plastic Hippocampal Synapse. *Science (80-.).* **343**, 665 LP – 670.

Waithe D., Ferron L., Page K. M., Chaggar K., Dolphin A. C. (2011) Beta-subunits promote the expression of Ca(V)2.2 channels by reducing their proteasomal degradation. *J. Biol. Chem.* **286**, 9598–9611.

Wang T., Jones R. T., Whippen J. M., Davis G. W. (2016) α2δ-3 Is Required for Rapid Transsynaptic Homeostatic Signaling. *Cell Rep.* **16**, 2875–2888.

Weber A. M., Wong F. K., Tufford A. R., Schlichter L. C., Matveev V., Stanley E. F. (2010) N-type Ca2+ channels carry the largest current: implications for nanodomains and transmitter release. *Nat. Neurosci.* **13**, 1348–1350.

Wessler I., Dooley D. J., Werhand J., Schlemmer F. (1990) Differential effects of calcium channel antagonists (omega-conotoxin GVIA, nifedipine, verapamil) on the electrically-evoked release of [3H]acetylcholine from the myenteric plexus, phrenic nerve and neocortex of rats. *Naunyn. Schmiedebergs. Arch. Pharmacol.* **341**, 288–294.

Westenbroek R. E., Hell J. W., Warner C., Dubel S. J., Snutch T. P., Catterall W. A. (1992) Biochemical properties and subcellular distribution of an N-type calcium

channel alpha 1 subunit. *Neuron* **9**, 1099–1115.

Weyrer C., Turecek J., Niday Z., Liu P. W., Nanou E., Catterall W. A., Bean B. P., Regehr W. G. (2019) The Role of Ca(V)2.1 Channel Facilitation in Synaptic Facilitation. *Cell Rep.* **26**, 2289-2297.e3.

Wheeler D. B., Randall A., Tsien R. W. (1996) Changes in action potential duration alter reliance of excitatory synaptic transmission on multiple types of Ca2+ channels in rat hippocampus. *J. Neurosci.* **16**, 2226–2237.

Wierenga C. J., Walsh M. F., Turrigiano G. G. (2006) Temporal regulation of the expression locus of homeostatic plasticity. *J. Neurophysiol.* **96**, 2127–2133.

Woodward J. J., Rezazadeh S. M., Leslie S. W. (1988) Differential sensitivity of synaptosomal calcium entry and endogenous dopamine release to omega-conotoxin. *Brain Res.* **475**, 141–145.

Wu J., Yan Z., Li Z., Qian X., Lu S., Dong M., Zhou Q., Yan N. (2016) Structure of the voltage-gated calcium channel Ca(v)1.1 at 3.6 A resolution. *Nature* **537**, 191–196.

Wu X., Cai Q., Shen Z., Chen X., Zeng M., Du S., Zhang M. (2019) RIM and RIM-BP Form Presynaptic Active-Zone-like Condensates via Phase Separation. *Mol. Cell* **73**, 971-984.e5.

Wycisk K. A., Zeitz C., Feil S., Wittmer M., Forster U., Neidhardt J., Wissinger B., et al. (2006) Mutation in the auxiliary calcium-channel subunit CACNA2D4 causes autosomal recessive cone dystrophy. *Am. J. Hum. Genet.* **79**, 973–977.

Yamamoto K., Kobayashi M. (2018) Opposite Roles in Short-Term Plasticity for N-Type and P/Q-Type Voltage-Dependent Calcium Channels in GABAergic Neuronal Connections in the Rat Cerebral Cortex. *J. Neurosci.* **38**, 9814–9828.

Zamponi, Bourinet E., Nelson D., Nargeot J., Snutch T. P. (1997) Crosstalk between G

proteins and protein kinase C mediated by the calcium channel alpha1 subunit. *Nature* **385**, 442–446.

Zamponi G. W., Striessnig J., Koschak A., Dolphin A. C. (2015) The Physiology, Pathology, and Pharmacology of Voltage-Gated Calcium Channels and Their Future Therapeutic Potential. *Pharmacol. Rev.* **67**, 821–870.

Zhang Y., Helm J. S., Senatore A., Spafford J. D., Kaczmarek L. K., Jonas E. A. (2008) PKC-induced intracellular trafficking of Ca(V)2 precedes its rapid recruitment to the plasma membrane. *J. Neurosci.* **28**, 2601–2612.

Zhao C., Dreosti E., Lagnado L. (2011) Homeostatic synaptic plasticity through changes in presynaptic calcium influx. *J. Neurosci.* **31**, 7492–7496.

Zhou J.-J., Li D.-P., Chen S.-R., Luo Y., Pan H.-L. (2018) The α2δ-1-NMDA receptor coupling is essential for corticostriatal long-term potentiation and is involved in learning and memory. *J. Biol. Chem.* **293**, 19354–19364.

Zhou Q., Zhou P., Wang A. L., Wu D., Zhao M., Südhof T. C., Brunger A. T. (2017) The primed SNARE-complexin-synaptotagmin complex for neuronal exocytosis. *Nature* **548**, 420–425.

Zhu Y., Ikeda S. R. (1994) Modulation of Ca(2+)-channel currents by protein kinase C in adult rat sympathetic neurons. *J. Neurophysiol.* **72**, 1549–1560.

Zucker R. S., Regehr W. G. (2002) Short-Term Synaptic Plasticity. *Annu. Rev. Physiol.*